DEVELOPMENT OF BI- AND MULTICOMPONENT FIBRES FOR TISSUE ENGINEERING BY ELECTROSPINNING

Olubayọde Ọladiran Ero-Phillips

[redacted]

A thesis submitted to

the University of Birmingham

for the degree of Doctor of Philosophy in

Metallurgy & Materials

School of Metallurgy & Materials,

University of Birmingham

February 2012

Acknowledgements

First and foremost, I wish to express my sincere thanks to Dr. Artemis Stamboulis for giving me the opportunity to conduct this research under her supervision. Her many constructive comments were invaluable over the course of this research. My appreciation also goes to Dr. Mike Jenkins for his constructive feedback at various points during the duration of this project.

I would also like to thank the following individuals for the various roles they played in making this project a success: Dr. Julie Gough and Dr. Louise Carney, our collaborators on the biocompatibility studies (School of Materials, University of Manchester); Dr. James Bowen (School of Chemical Engineering, University of Birmingham) for help with interferometry and tensile tests; Theresa Morris (School of Metallurgy & Materials, University of Birmingham) for help with microscopy; Frank Biddlestone (School of Metallurgy & Materials, Unviersity of Birmingham) for help with DSC and FTIR and Loung Nguyen (NUSNNI, National University of Singapore) for teaching me the basics of cell culture. I also acknowledge the kindness of Professor Seeram Ramakrishna in accepting me to work in his laboratory as a Universitas 21 scholar.

Certain events without which I would never have started the research or completed it successfully are also worth mentioning: (i) A casual statement from my Dad over twelve years ago that I could study for a PhD degree; (ii) Overseas Research Students scholarship and School of Metallurgy & Materials, University of Birmingham scholarship award; and (iii) University of Birmingham Universitas 21 scholarship to the National University of Singapore.

My parents and siblings are deeply appreciated for their prayers and support and belief in me all these years.

Finally and most importantly, I wish to express my profound gratitude to my darling wife for her patience and support. She was my patient sounding board, and I promise that all my chatter about crystallinity, degradation and electrospinning shall cease henceforth.

Dedication

To God Almighty, Creator of heaven and earth, the Source of all wisdom and the Infinite Mind behind all the discoveries of science

And

Ekemeien, my darling wife, for her patience, support, and constant encouragement.

Abstract

The aims of this research project were: (i) to investigate the possibility of tailoring the crystallinity of electrospun fibres by controlling the electrospinning parameters (also referred to as crystallinity studies); (ii) to study the degradation behaviour of PLLA and PLLA-HA electrospun scaffolds; and (iii) to fabricate bi- and multicomponent scaffolds based on PLLA by electrospinning.

During the crystallinity studies, the effects of various electrospinning process parameters on the crystallinity of the electrospun poly(L-lactic acid) (PLLA) fibres were investigated. Thermal analysis of the fibres revealed that they exhibited crystallinities ranging from 23 to 46% while that for the as-received granule was approximately 37%, suggesting that the crystallinity of electrospun PLLA fibres can be controlled by optimizing the electrospinning process. The results of this work showed that the degree of crystallinity of the electrospun fibres decreased with increasing the polymer solution concentration. Furthermore, an optimum electrospinning voltage at which the maximum degree of crystallinity can be obtained was observed. At voltages higher or lower than the optimum electrospinning voltage, the degree of crystallinity will decrease or increase, respectively. The effect of the needle tip to collector distance (NTCD) on the degree of crystallinity followed no predictable and consistent pattern.

In order to study the degradation behaviour of poly(L-lactic acid) (PLLA) and composite PLLA-hydroxyapatite (HA) scaffolds, PLLA and PLLA-HA scaffolds were fabricated by electrospinning. The average fibre diameters of the scaffolds were 781 nm and 316 nm, respectively. The small diameters of the PLLA-HA electrospun fibres resulted in a high

surface area to volume ratio (SVR) and therefore faster degradation rate in comparison to the PLLA electrospun fibres.

Finally, bi-component scaffolds based on PLLA and gelatin were fabricated by electrospinning. Multicomponent scaffolds based on PLLA and gelatin and hydroxyapatite were fabricated by electrospinning followed by electrospraying of the HA phase. Blending gelatin with PLLA resulted in an approximate 50% decrease in fibre diameter compared with PLLA electrospun fibres. Hydrogen bonds between the carbonyl group of PLLA and the amino group of gelatin were formed as confirmed by FTIR and DSC. Hydrogen bonding between PLLA and gelatin resulted in an improvement in tensile strength and tensile stiffness, respectively. A 49-day degradation study of the PLLA, PLLAGel and PLLAGel-HA scaffolds showed that the scaffolds retained their integrity, although some of the gelatin was leached out of the blend-based scaffolds as indicated by FTIR analysis. Biocompatibility studies with adult human osteoblasts (HOBs) revealed that the scaffolds permitted cell attachment and spreading with best results for PLLAGel-HA scaffolds after 1.5, 4 and 24 hours of cell culture. Similarly, the PLLAGel-HA showed significantly higher mineralisation in comparison to the PLLA and PLLAGel scaffolds. These observations were attributed to the presence of exposed hydroxyapatite particles on the surface of the PLLAGel-HA scaffolds which promoted better binding with integrins for osteoconductivity, and acted as a chelating agent for the mineralisation of HOBs.

List of Figures

List of Tables

List of Abbreviations

PLLA – Poly(L-lactic acid)

PDLLA – Poly(D,L-lactic acid)

PGA – Poly(glycolic acid)

PLGA – Poly(lactic-*co*-glycolic acid)

PCL – Poly(ε-caprolactone)

POM – Polyoxymethylene

DCM – Dichloromethane

DMF – N,N-Dimethylformamide

TFE – 2,2,2-trifluoroethanol

HA – Hydroxyapatite

DSC – Differential scanning calorimetry

ALP – Alkaline phosphatase

NTCD – Needle-tip-to-collector distance (cm)

PS - Polystyrene

Poly(DTE-carbonate) – Poly(desaminotyrosyl-tyrosine ethyl ester-carbonate)

PVA – Poly(vinyl alcohol)

THF - Tetrahydrofuran

PAN – Polyacrylonitrile

PLCL – Poly(L-lactide-*co*-ε-caprolactone)

PLACL – Poly(L-lactic acid)-*co*-poly(ε-caprolactone)

MWCNT – Multiwalled carbon nanotubes

HSA - 12-hydroxy-stearic acid

SD – Standard deviation

M_w – Weight-average molecular weight

M_n – Number-average molecular weight

SEM – Scanning electron microscope

ESEM – Environmental scanning electron microscope

EDS – Energy dispersive X-ray spectroscopy

HOBs – Adult human osteoblasts

EDTA - Ethylenediaminetetraacetic acid

DMEM - Dulbecco's modified eagle medium

HMDS – Hexamethyldisilazan

DAPI - 4',6-diamidino-2-phenylindole

CTS – Chitosan

T_g – Glass-transition temperature

T_m – Melting temperature

ECM – Extra-cellular matrix

PFA – Paraformaldehyde

cSt – Centistokes

ΔH_m – Heat of fusion ($J.g^{-1}$)

ΔH_c – Heat of crystallisation ($J.g^{-1}$)

HCN – Hydrogen cyanide

WAXD – Wide angle X-ray diffraction

WAXS – Wide angle X-ray scattering

mRNA – Messenger ribonucleic acid

hFob – Human fetal osteoblast

β-TCP – Beta-tricalcium phosphate

BMSC – Bone-marrow stromal cell

Table of Contents

1.0 Literature Review

1.1 Tissue Engineering - Introduction

The beginning of tissue engineering as an area of research is not clearly defined (Vacanti and Vacanti, 2007), however, it is generally believed that it was the *Science* review article titled 'Tissue Engineering' by Professors Robert Langer and Joseph Vacanti in 1993 that created a general awareness of this field of research (Lal et al., 2003). Since that time however, interest in this field of research has grown tremendously with various fields such as cell biology, basic medical sciences, biomaterials, and biomedical engineering contributing immensely to its growth (Jagur-Grodzinski, 2006; Lal et al., 2003; Vacanti and Vacanti, 2007). The reasons for this exponential growth in tissue engineering research are varied.

One of this is due to the fact that in spite of revolutionary advances in technology which have made it possible for patients with diseased organs to have organ transplants, many people still die each year because of unavailability of donor organs or even organ substitutes (Thomson et al., 1995). Organ/tissue loss or failure is one of the most frequent, devastating, and costly problems in human health care (Langer and Vacanti, 1993). Statistics show that in 1990, approximately 30,000 deaths resulted from chronic liver disease or cirrhosis but fewer than 3,000 liver donors are available annually (Thomson et al., 1995); similarly, as recently as 2007, there were 92,587 people on transplant waiting lists in the United States (Vacanti and Vacanti, 2007).

Physicians have attempted to restore the mechanical function of hard tissues such as cartilage and bone through the use of implants (Thomson et al., 1995). Additionally, mechanical devices such as kidney dialyzers have been used to treat organ loss or

malfunction (Langer and Vacanti, 1993). However, these are often temporary solutions as implants may cause infections, bone atrophy or even fail (Ishaug-Riley et al., 1997) and mechanical devices cannot perform the whole function of body organs (Langer and Vacanti, 1993), thus creating the need for further treatment, increasing treatment cost and creating more trauma for patients.

It is within this background that tissue engineering has emerged as a possible solution to the complications associated with the existing methods of treating organ malfunction/loss (Mikos and Temenoff, 2000). Tissue engineering applies the principles of engineering and life sciences towards the development of biological substitutes that restore, maintain, or improve tissue function (Langer and Vacanti, 1993). Three strategies have been adopted for the creation of new tissue:

I. Isolated cells or cell substitutes to replace cells that supply the required function (Ma, 2004; Langer and Vacanti, 1993);
II. The delivery of tissue-inducing substances such as growth factors to targeted locations (Ma, 2004; Langer and Vacanti, 1993); and
III. Growing cells in three-dimensional scaffolds (Langer and Vacanti, 1993).

However, the first two approaches are somewhat limited in the sense that they can only be effective in instances where defects being addressed are small. One other limitation of the first method is the possibility that the implanted cells may not fulfil their function(s), or there may even be a case of immune rejection (Langer and Vacanti, 1993). For these reasons, the third method is more preferable and has thus become more increasingly active. The role of scaffolds is paramount in this method because they guide the cells to grow and organize in three dimensions (Mikos and Temenoff, 2000). The scaffolds also serve as a temporary structural support for the cells to attach, grow, differentiate and form extra-

cellular matrix (ECM), which is a molecular complex that consists of molecules (e.g. collagens and hyaluronic acid) that reside outside the cells, molecules that harbour proteins, matrix-degrading enzymes and their inhibitors (Jagur-Grodzinski, 2006; Thomson et al., 1995; Petreaca and Martins-Green, 2007).

There are certain requirements that an ideal 3D tissue engineering scaffold needs to meet (Hutmacher, 2000; Liu and Ma, 2004; Rezwan et al., 2006; Luo et al., 2007; Murphy and Mikos, 2007; Thomson et al., 1995), and the most important ones are listed below.

1) Biocompatibility (Mikos and Temenoff, 2000; Murphy and Mikos, 2007) - Using a substance that is not biocompatible can result in immune rejection.
2) High porosity and proper pore size (Ma, 2004; Murphy and Mikos, 2007) - Since restoration of organ function requires a large number of cells, it is essential that there is a large void volume available to accommodate transplanted cells (Thomson et al., 1995). High porosities (≥90%) and large pore sizes (at least 100 μm) are also required for proper vascularisation and cell penetration (Rezwan et al., 2006).
3) Large surface area-to-volume-ratio (Thomson et al., 1995) – Many cells are anchorage dependent, therefore it is necessary that the scaffold should have a large surface area that can accommodate a large number of cells. It has been recently shown that cells can attach and organize better on nanoscale materials than microscale materials; this is probably due to the fact that nanomaterials possess high surface area to volume ratios (Liao et al., 2008).
4) Mechanical integrity (Murphy and Mikos, 2007) – The material used as a scaffold must be able to mechanically support the tissue during growth without failure (Ma, 2004; Thomson et al., 1995).

5) Surface properties that would encourage cell adhesion, growth and proliferation – As earlier stated, most cells are anchorage-dependent, therefore, it is imperative for scaffolds to have excellent surface properties that would encourage cell adhesion. Most polymers may need to be subjected to surface modification treatments such as plasma irradiation so that the scaffold surfaces are rendered active for interaction with seeded cells (Ma, 2004; Ramakrishna et al., 2005).
6) Biodegradability – As a general requirement, the scaffold material should be biodegradable with a controllable degradation rate to match that of neo-tissue formation (Ma, 2004). However, non-biodegradable materials may also be used as tissue engineering scaffolds (Vacanti and Vacanti, 2007; Jagur-Grodzinski, 2006).
7) It should enhance new tissue formation without formation of scar tissue.
8) It should be easily and cheaply produced to ISO/FDA/CE[1] standards.

These different expectations of a scaffold though simple, quite conflict with one another. For this reason, although many scaffolds have been fabricated by different methods over the past decade, very few hold any special promise (Lannutti et al., 2007). It is therefore not a surprise that to date, only a handful of products incorporating cells together with scaffolds, notably bio-artificial skin grafts and replacement cartilage, have gained regulatory approval, and these have only achieved limited market penetration (Furth and Atala, 2007). The key challenges to industrial development include problems in devising cost-efficient, scalable processes, guaranteeing product viability and satisfying regulatory authorities (Buttery and Bishop, 2005).

[1] ISO – International Organization for Standardization; FDA – United States Food and Drug Administration; CE – Conformité Européenne

In spite of these myriad challenges however, tissue engineering research continues to expand rapidly and research is currently being carried out on engineering various parts of, though not limited to, the cardiovascular, musculoskeletal, nervous and respiratory systems.

1.2 Bone-Tissue Engineering

Improvement in healthcare all over the world in the last several years has resulted in increased life expectancy and an attendant increase in aging population (Thomson et al., 1995; Ramakrishna et al., 2005; Ngiam et al., 2009), however, many people all over the world suffer from bone defects caused by trauma or bone disease, and many die due to the lack of an appropriate treatment e.g., unavailability of an ideal bone substitute (Venugopal et al., 2008d; Venugopal et al., 2010). Bone defects can be treated by implants but there are many limitations to this method such as bone atrophy and stress shielding, infections and even implant failure (Ishaug-Riley et al., 1997; Gupta et al., 2009), thus increasing the cost and time of treatment and causing further trauma for patients. Another method that has been used to treat bone defects is bone grafting – this could be either autogenic or allogeneic; with over 800,000 bone grafts being performed annually worldwide, this treatment has become commonplace (Laurencin et al., 1999). Autogenic bone grafting involves taking a section of bone from the patient's own body (usually the iliac crest) while allogeneic bone grafting involves obtaining a bone section from a cadaver or the patient's relative. Despite the seeming advantages of autogenic bone grafting, there are many drawbacks associated with this procedure, such as, the requirement of a secondary surgery to obtain bone from the patient's body, insufficient bone availability at donor site, chronic pain at donor site and of course, increased operating times. With allogeneic bone grafting,

there is the risk of tissue rejection and infection (Venugopal et al., 2008d; Burg et al., 2000; Thomson et al., 1995; Olivier et al., 2004; Venugopal et al., 2007; Coombes and Meikle, 1994).

Over the last several years, tissue engineering researchers have developed natural and synthetic biomaterials to serve as bone substitutes in order to overcome the limitations of implants and grafts. The aim of bone-tissue engineering is to be able to use a temporary scaffolding material to induce formation of bone from the surrounding tissue or to act as a carrier or template for implanted bone cells or other agents (Burg et al., 2000).

1.3 Bone

Bone is the main supporting system in the human body. Bone is a composite material consisting of three major components (Piekarsk, 1973; Hench, 2005):

I. Living cells such as osteoblasts, osteoclasts, and osteocytes;
II. Non-living organic components (bone matrix) such as collagen and muco-polysaccharides;
III. Non-living inorganic crystals (bone mineral) such as hydroxapatite.

Essentially, bone is a composite consisting of an organic phase (mostly made up of type I collagen fibres) and a mineral phase (mostly made up of hydroxyapatite crystals) (Hench, 2005; Piekarsk, 1973; Yamashita et al., 2002). Osteoblasts are the cells responsible for the synthesis of bone matrix components and they also play an important role in bone mineralisation. They originate from local mesenchymal stem cells, which differentiate into preosteoblasts and then into matutre osteoblasts. A differentiated osteoblast has a size in the range of 20-30 μm with a polyhedral shape. Osteoclasts are highly specialised cells

attached to the bone surface and are thought to originate from haematopoietic stem cells known as ‘granulocyte-macrophage colony-forming units’ (GM-CFU). Osteoclasts are about 100 µm in size and are responsible for the resorption of bone. Osteocytes are terminally differentiated osteoblasts, which have been entrapped within bone matrix before mineralisation (Wozniak and Jel Haj, 2007).

Bone formation can be divided into two steps, namely bone matrix synthesis and mineralisation. In the first step, osteoblasts synthesise, secrete and deposit bone matrix which is mainly made up of collagen type I, with the collagen fibres organised in preferentially orientated layers called lamellae. This matrix is deposited at the rate of 2-3 µm per day until it reaches a width of 20 µm, after which mineralisation begins. Osteoblasts, due to high activity of alkaline phosphatase, also participate in mineralisation stage, during which apatite crystals are formed as slender needles, 20-40 nm in length and 1.5-3 nm in thickness, within and between the collagen fibrils and aligned along the axis of the collagen fibrils (Hench, 2005; Park and Lakes, 1992; Wozniak and Jel Haj, 2007). These mineral-containing fibrils are arranged into lamellar sheets (3-7 µm) that run helically with respect to the long axis of the cylindrical osteons (also called Haversian systems) (Park and Lakes, 1992). The osteon is made up of 4 to 20 lamellae that are arranged in concentric rings around the Haversian canal (Figure 1). The diameter of an osteon is typically between 150-250 µm.

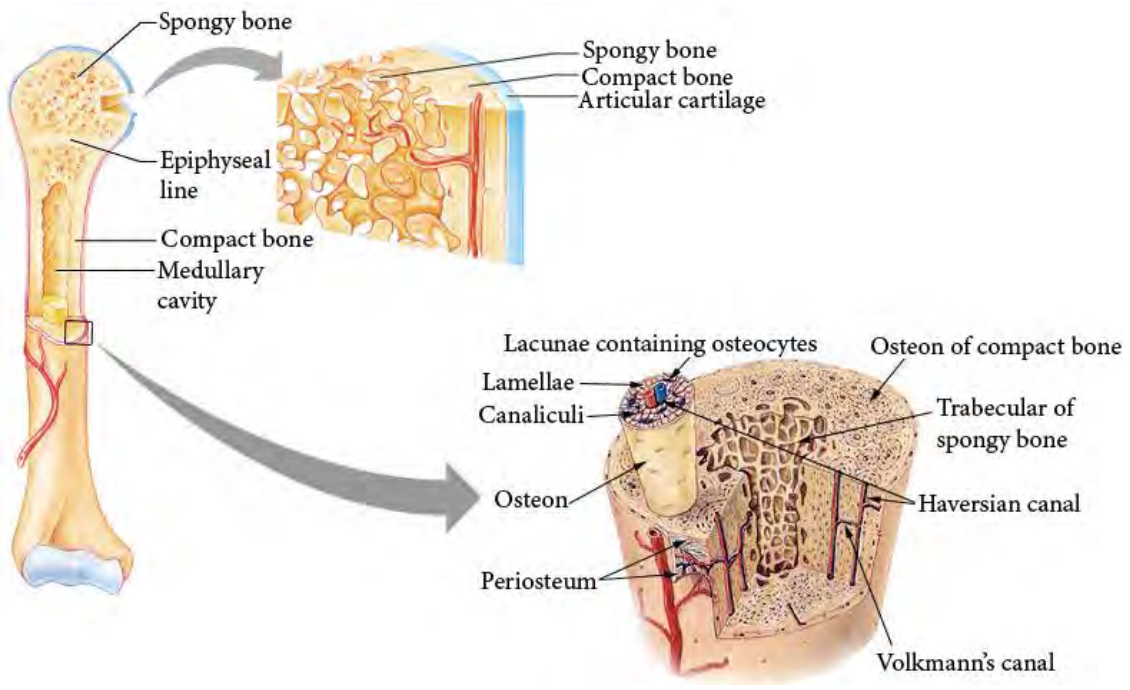

Figure 1: Bone microstructure

The parallel orientation of osteons to the long axis of bone gives rise to the anistropic properties of bone (Hench, 2005). Additionally, because bone is largely made up of collagen, it is also viscoelastic (Hallab et al., 2004). Most polymers exhibit viscoelasticity which makes them exhibit both viscous and elastic characteristics when undergoing deformation (Callister, 2003). The viscoelastic characteristics (i.e., time-dependent strain) of bone can be expressed as: stress relaxation, which is a gradual decrease in stress in a specimen held at constant strain; creep, which is a time-dependent and permanent deformation under constant stress; attenuation of sonic or ultrasonic waves; load-rate dependence of stiffness; or energy dissipation in bone loaded dynamically (Lakes, 2009; Lakes, 2010). A recent study however showed, that the viscoelastic properties of bone may not be due only to the collagen content, but it could also be due to the interactions between collagen, moisture and bone mineral (Yamashita et al., 2002).

In addition to its supportive function, bone has an important function in the regulation of calcium and phosphate blood levels. Also located inside the bone is the bone marrow, where white and red blood cells are produced (van Gaalen et al., 2008).

Macroscopically, there are about 208 bones in the human body, but on a structural level, two types of bone exist: cancellous (also called trabecular or spongy bone) and compact (dense or cortical) bone (van Gaalen et al., 2008; Hench, 2005) (Figure 1). Cancellous bone is the most changing and active part. It is active in growth, calcium homeostasis and hematopoiesis, and its supportive function is mainly in locations with a predominantly compressive loading, such as in vertebral bodies and adjacent to articulating joints (e.g. the knee joint). Compact bone is more static and stronger. Its main locations are the shafts of long bones and peripheral lining of flat bones (van Gaalen et al., 2008).

Microscopically, two major forms of bone can be identified: woven and lamellar bone. Woven bone is the immature unorganized type of bone. It is present abundantly in newborns and in locations where fast bone formation takes place, like in the growth plates and in fracture repair. After woven bone is laid down, it is organized by remodelling to become lamellar bone (van Gaalen et al., 2008).

1.4 Materials Used in Bone-Tissue Engineering

Materials that have been used in bone-tissue engineering include polymers and biocomposites. A description of these materials is given below.

1.4.1 Biodegradable polymers

As a consequence of the advantage of biodegradability that biodegradable polymers offer, they have found increasing use in medical devices (Middleton and Tipton, 2000). Some

commercially available biodegradable medical devices include SmartPins (used for fracture fixation), LactoSorb Screws and Plates (used for craniomaxillofacial fixation), Meniscus Arrow (used for meniscus repair) and Meniscal Stinger (used for meniscus repair) (Middleton and Tipton, 2000). All these devices are polyesters composed of homopolymers or copolymers of glycolide and lactide. Additionally, biodegradable polymers have been widely researched for tissue engineering purposes due to their biocompatibility and the ease with which they can be processed into complex shapes (Thomson et al., 1995; Maquet and Jerome, 1997; Middleton and Tipton, 2000). Biodegradable polymers can be divided into two categories – natural and synthetic.

1.4.1.1 Natural biodegradable polymers

Natural biodegradable polymers were the first to be used as scaffolds for tissue regeneration (Thomson et al., 1995; Gomes and Reis, 2004). Collagen has been used to repair nerve, skin, cartilage and bone while chitosan has been shown to exhibit biostimulating activities in the healing process of various tissues (Maquet and Jerome, 1997; Gomes and Reis, 2004). Natural polymers have the advantage of possessing a highly organized structure at both molecular and macroscopic levels, and exhibiting desirable properties as biomaterials, such as the ability to induce tissue ingrowth. However, natural polymers also have three main disadvantages: (i) antigenicity, this usually leads to adverse tissue reaction and immune rejection; (ii) patient to patient variation in degradation rate due to the fact that the degradation rate of natural polymers is usually reliant on enzymatic processes; and (iii) poor mechanical performance (Maquet and Jerome, 1997; Thomson et al., 1995; Gomes and Reis, 2004). Other natural biodegradable polymers that have been investigated for tissue engineering include, but are not limited to, gelatin (Swetha et al.,

2010; Sisson et al., 2010; Liu et al., 2009; Malafaya et al., 2007), cellulose (Tsioptsias and Panayiotou, 2008; Fang et al., 2009; Zaborowska et al., 2010), alginate (Fan et al., 2005; Malafaya et al., 2007; Drury and Mooney, 2003; Li et al., 2005b; Turco et al., 2009) and hyaluronic acid (Drury and Mooney, 2003; Lee and Mooney, 2001; Kim et al., 2008b).

1.4.1.2 Synthetic biodegradable polymers

Synthetic biodegradable polymers offer greater advantages and versatility over natural polymers because their molecular weight and molecular weight distribution (with varying degrees of accuracy depending on, among other factors, the type of polymerization reaction) can be easily tuned to give a wider range of properties (Gomes and Reis, 2004; Maquet and Jerome, 1997; Thomson et al., 1995; Middleton and Tipton, 2000). These characteristics greatly affect the physico-mechanical properties (such as strength and degradation rate) of the polymer (Maquet and Jerome, 1997; Thomson et al., 1995; Gomes and Reis, 2004). These polymers usually degrade by simple chemical hydrolysis because they are synthesised to have hydrolytically unstable linkages in their backbone (Thomson et al., 1995; Maquet and Jerome, 1997; Middleton and Tipton, 2000). As a result, the degradation rate does not vary from patient to patient (unless there are local pH variations due to inflammation, implant degradation etc) (Gomes and Reis, 2004). A further advantage of synthetic polymers is their easy processibility into porous materials. Copolymerization can be used to alter degradation rates and also impart degradability on a hydrolytically stable polymer (Thomson et al., 1995).

There are different types of synthetic polymers used as tissue engineering scaffolds, these include linear aliphatic polyesters [this class of polymers includes poly(glycolic acid) - PGA, poly(lactic acid) - PLA, poly(lactic-*co*-glycolic acid) - PLGA, and poly(ε-caprolactone) - PCL],

poly(dioxanone), polyethylene oxide, polybutylene terephthalate, poly(propylene fumarate), and poly(amino acids) (Ma, 2004; Gomes and Reis, 2004). Poly(α-hydroxyl acids) especially poly(glycolic acid) and poly(lactic acid) are the most widely investigated and most commonly used synthetic biodegradable polymers in medicine (Gomes and Reis, 2004; Pachence et al., 2007; Gupta et al., 2007; Middleton and Tipton, 2000) based in part on their biocompatibility and their approval by the FDA for human clinical use (Thomson et al., 1995).

1.4.2 Biocomposites

Bone is a composite consisting of an organic phase and a mineral phase (Hench, 2005; Piekarsk, 1973; Yamashita et al., 2002; Rho et al., 1998; Wei and Ma, 2004; Venugopal et al., 2010) as mentioned in Section 1.3. In an effort to closely mimic the composite nature of bone, polymer/calcium phosphate biocomposites have been widely researched using various fabrication techniques (Wei and Ma, 2004; Zhang et al., 2007c; Venugopal et al., 2008c; Venugopal et al., 2010; Ngiam et al., 2009; Zhang and Ma, 1999b; Prabhakaran et al., 2009; Supova, 2009; Kim et al., 2006a; Sui et al., 2007; Kim et al., 2005; Jagur-Grodzinski, 2006). Synthetic biodegradable polymers can be easily processed into porous 3-dimensional (3D) tissue engineering scaffolds, however, their surfaces do not enhance cell adhesion, differentiation and proliferation (Venugopal et al., 2008c; Venugopal et al., 2010). On the contrary, calcium phosphates such as hydroxyapatite and β-TCP have been shown to be osteoconductive (Rezwan et al., 2006). As a result, synthetic biodegradable polymer/calcium phosphate biocomposite scaffolds have been investigated as an improvement on synthetic biodegradable polymer scaffolds. For instance, when cultured with cells, a poly(L-lactic) acid (PLLA)/HA composite scaffold showed new tissue formation throughout the scaffold while

new tissue formation was only observed on the surface layer (<240 μm) of poly(DL-lactic-*co*-glycolic acid) (PLGA) foams (Wei and Ma, 2004). Similarly, Venugopal et al. (2008) observed higher mineral deposition on collagen/HA composite scaffolds when cultured with osteoblasts than on pure collagen scaffolds (Venugopal et al., 2008b).

It has also been suggested, that polymer/calcium phosphate biocomposite scaffolds exhibit improved degradation properties, for instance, by monitoring the pH variations during incubation in phosphate buffered saline (PBS) for 24 weeks, it was found that the pH value of PLLA-HA composite scaffold was more stable than that of pure PLLA scaffold and pure HA scaffold (Zhang and Ma, 1999b).

1.5 Poly(L-Lactic Acid) (PLLA)

1.5.1 Introduction

Poly(lactic acid) is made of building blocks of lactic acid, which is a chiral molecule that exists as two stereo isomers – L-lactic acid and D-lactic acid (Gupta et al., 2007; Bogaert and Coszach, 2000; Lunt, 1998; Gomes and Reis, 2004) (Figure 2). The L-lactic acid rotates the plane of polarized light in a clockwise (*dextro*) direction while the D-lactic acid rotates the plane of polarized light in an anti-clockwise (*laevo*) direction. Only the L and D isomers exhibit any optical activity, while the racemic mixture (i.e. 50% L-lactic acid and 50% D-lactic acid) is optically inactive (Gupta et al., 2007; Lunt, 1998).

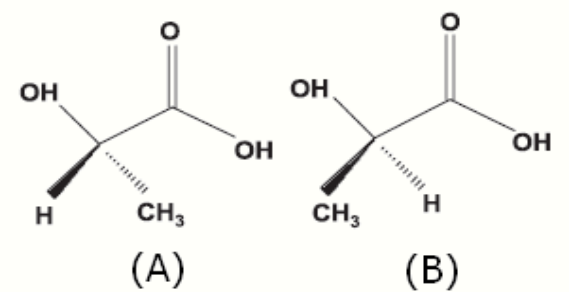

Figure 2: Lactic acid enantiomers: (A) L-lactic acid and (B) D-lactic acid (Gupta et al., 2007)

Lactic acid occurs commonly in nature as the L-isomer, although it also sometimes occurs as the racemic mixture, while the D-isomer is uncommon in nature (Bogaert and Coszach, 2000; Lim et al., 2008; Fukushima et al., 2004).

1.5.2 Synthesis

The two methods used to produce lactic acid are:

1. Petrochemical synthesis – The petrochemical route is shown in Figure 3. This method has been reported to yield the racemic lactide (Gupta et al., 2007; Bogaert and Coszach, 2000; Lunt, 1998); and
2. Fermentation – Bacterial fermentation of molassess, potato starch or dextrose from corn can be used to produce a high yield of lactic acid. It has been reported that the lactic acid produced by this method is exclusively (>99.5%) the L-isomer (Gupta et al., 2007; Lunt, 1998), however, the production of D-lactic acid by bacterial fermentation of rice (Fukushima et al., 2004; Lee, 2007; Lu et al., 2009) and self-fermentation of microalgae (Hirayama and Ueda, 2004) has also been reported.

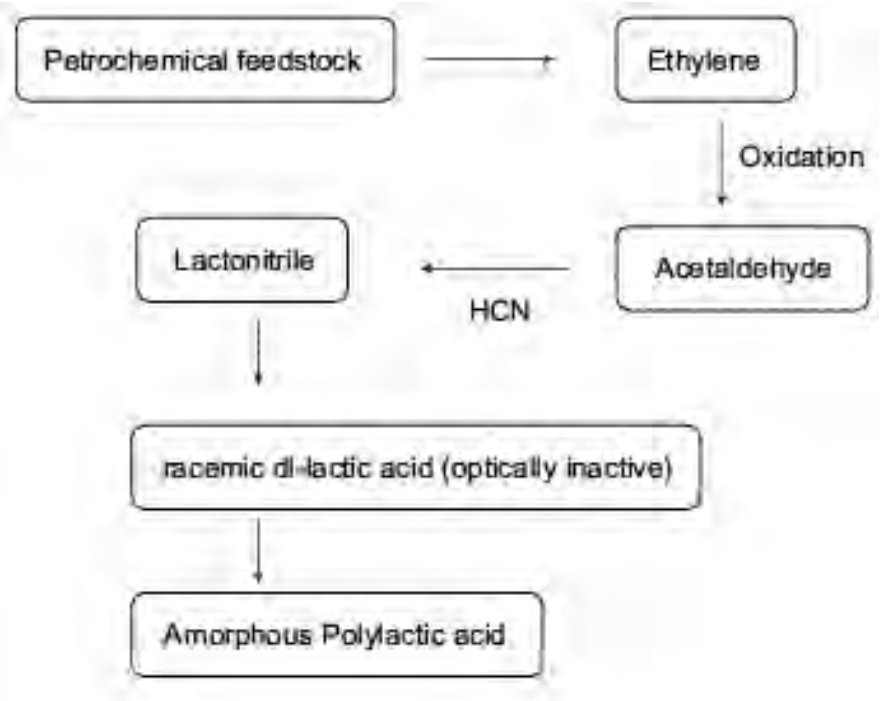

Figure 3: Petrochemical synthesis of lactic acid (Gupta et al., 2007)

The petrochemical route was the more commonly used method until the early 1990s when the more economic fermentation method was developed (Gupta et al., 2007).

The polymerization of lactic acid to yield poly(lactic acid) can be achieved by two different routes.

I. Direct condensation – This is a solvent-based method which produces low to intermediate molecular weight polymer and utilizes azeotropic distillation to continuously remove the water of condensation (Figure 4). The polymer can be used as is, or coupled with isocyanates, epoxides or peroxides to produce a range of molecular weights (Gupta et al., 2007; Lunt, 1998; Drumright et al., 2000).

II. Formation of cyclic dimer of lactic acid (lactide) followed by ring-opening polymerization in the presence of a catalyst – This is a solvent-free method in which a low-molecular weight poly(lactic acid) is produced, followed by controlled depolymerisation to produce a cyclic dimer (lactide). Purification of the lactide by

distillation followed by catalytic ring-opening polymerization results in poly(lactic acid) with controlled molecular weight (Gupta et al., 2007; Lunt, 1998; Bogaert and Coszach, 2000; Drumright et al., 2000) (Figure 4). Tin compounds, especially tin octoate are the most preferred catalysts used in this process; this is due to their solubility in molten lactide, high catalytic activity, and low rate of racemisation of the polymer (Drumright et al., 2000). A coordination-insertion mechanism involving the ring opening of the lactide to add two lactic acid molecules to the growing end of the polymer chain (Figure 5) is generally believed to be the reaction mechanism when tin octoate is used to polymerize lactide (Drumright et al., 2000).

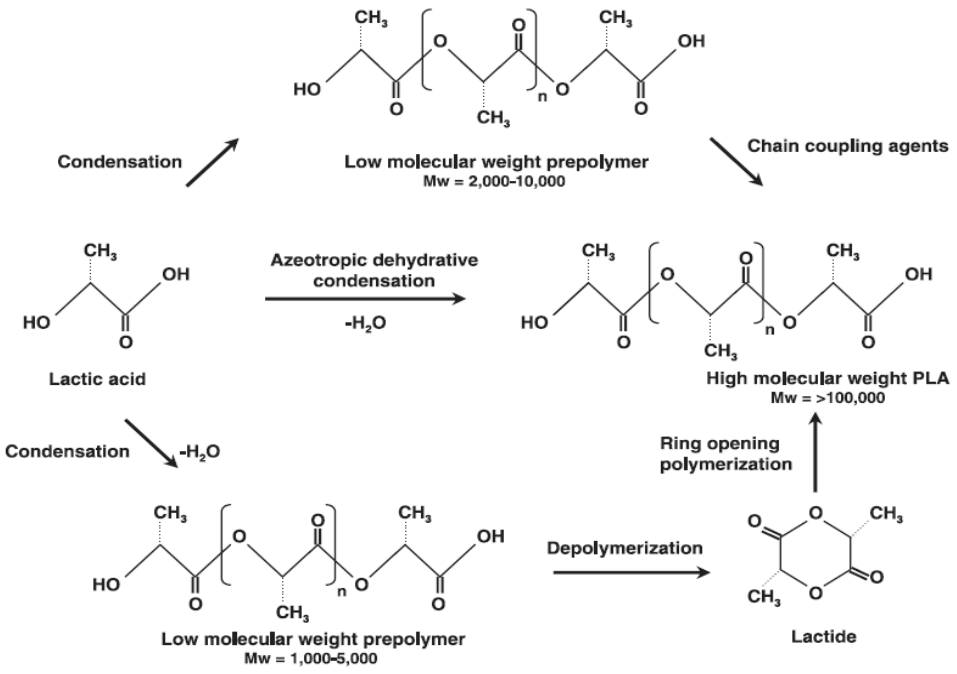

Figure 4: Synthesis of PLA by direct condensation, and catalytic ring-opening of the lactide (Lunt, 1998)

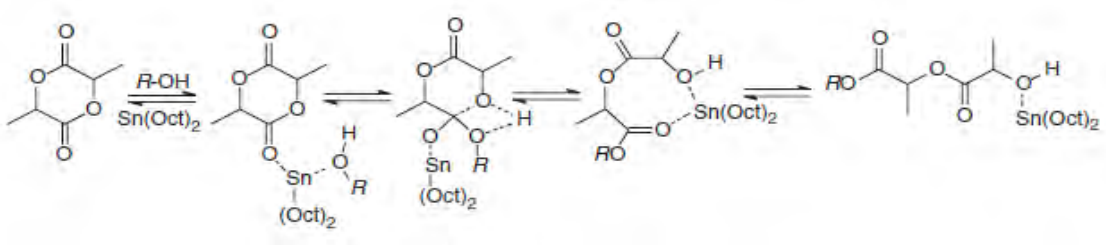

Figure 5: Generalized coordination-insertion chain growth mechanism of lactide to PLA; R = growing polymer chain (Drumright et al., 2000)

To a very large extent, the stereochemistry of the lactide monomer determines the stereochemical composition of the resulting polymer. Similarly, the stereochemical composition of the polymer has a dramatic effect upon the physical properties of the polymer such as the melting point, rate and degree of crystallisation and mechanical strength (Drumright et al., 2000; Bogaert and Coszach, 2000; Lunt, 1998). A high L-lactic acid content in poly(lactic acid) will impart a high degree of crystallinity, high glass transition and melting points and finally, high mechanical strength (Drumright et al., 2000; Lim et al., 2008). Addition of D-lactide or *meso*-lactide to poly(L-lactide) will lower the melting point, rate of crystallisation and degree of crystallisation but will have little effect on the glass transition temperature (Drumright et al., 2000; Lunt, 1998; Lim et al., 2008); in fact, poly(L-lactide) becomes amorphous after the addition of approximately 15% meso-lactide (Drumright et al., 2000).

PLA is the most extensively researched and utilized biodegradable and renewable thermoplastic polyester (Rasal et al., 2010). This is due to its biocompability, biodegradability, relative ease of processibility and energy-efficient production (Rasal et al., 2010). Until recently, PLA had mainly been limited to biomedical applications, owing to its high cost and limited molecular weight, however, with the development of economical production methods capable of producing high molecular weight PLA, it has found

increasing use in other areas (Lim et al., 2008). Its uses include, but are not limited to, packaging material for food and other consumer products (Lim et al., 2008), paper coating (Drumright et al., 2000), personal hygiene products (Bogaert and Coszach, 2000), surgical sutures (Chandra and Rustgi, 1998), implant/bone-fixation devices (Bergsma et al., 1995; Chandra and Rustgi, 1998), drug delivery systems (Chandra and Rustgi, 1998) and tissue engineering scaffolds.

1.5.3 The use of PLLA, its blends and co-polymers as tissue engineering scaffolds

The use of PLLA as a tissue engineering scaffold is predominantly based on its biodegradability and the compatibility of its degradation product (lactic acid) with the human body (Gupta et al., 2007). Lactic acid occurs naturally in the human body and upon formation, it is processed through normal metabolic pathways and ultimately eliminated through the respiratory system as carbon dioxide (Thomson et al., 1995). Furthermore, its mechanical properties make it suitable for use as a scaffold material for both soft and hard tissues.

PLLA has been shown to be a promising tissue engineering scaffold material for regenerating cartilage (Shastri et al., 2000; Freed et al., 1993), liver (Nam et al., 2000), skin (Blackwood et al., 2008; van Dijkhuizen-Radersma et al., 2008) nerve tissue (Corey et al., 2008; Yang et al., 2005) and bone (Chen et al., 2006; van Dijkhuizen-Radersma et al., 2008).

In spite of its biocompatibility and biodegradability, there are some limitations to the use of PLLA as a tissue engineering scaffold; some of these are discussed below.

A. Slow degradation rate – PLLA has a crystallinity of about 37%; it degrades slowly and may take over two years to be completely resorbed (Middleton and Tipton, 2000). The mechanism of PLLA degradation is hydrolysis of the ester bond, although during

in vivo degradation, there is a small but nonetheless significant contribution from enzymatic degradation. The methyl groups in its backbone provide steric hinderance to cleavage of the ester bond, hence the long degradation time (Barnes et al., 2007; Thomson et al., 1995). In order to have greater control over the degradation rate of PLLA, it can be copolymerized with poly(glycolic acid) (PGA) to produce poly(DL-lactic-*co*-glycolic acid) (PLGA). By altering the ratio of lactic acid to glycolic acid in the copolymer, the degradation rate can be tailored to specific requirements (Ma, 2004; Thomson et al., 1995). However, no linear relationship exists between the glycolic acid:lactic acid ratio and the physico-mechanical properties of the corresponding copolymers (Pachence et al., 2007; Gomes and Reis, 2004). Like PLLA, PLGA has been shown to be a promising tissue engineering scaffold material for regenerating bone (Ishaug-Riley et al., 1997; Shea et al., 2000; Ishaug-Riley et al., 1998), skin (Blackwood et al., 2008), nerve (van Dijkhuizen-Radersma et al., 2008), bladder (van Dijkhuizen-Radersma et al., 2008) and liver (van Dijkhuizen-Radersma et al., 2008).

B. Hydrophobicity - PLLA is relatively hydrophobic, with a static water contact angle of approximately 80^{o}, which results in low cell affinity (Rasal et al., 2010). This drawback becomes very significant when considering PLLA for use as a tissue engineering scaffold. Various surface modification treatments have been used to improve the hydrophilicity of PLLA, such as plasma treatment (Chen and Su, 2011; Park et al., 2007; Khorasani et al., 2009), surface hydrolysis (Yang et al., 2003) and electrostatic self-assembly (Liu et al., 2005). Additionally, blending PLLA with natural polymers (Jiao et al., 2007; Li et al., 2009b; Li et al., 2009a) such as collagen (Sato et al., 2004; Schofer et al., 2009) and gelatin (Andric et al., 2010; Kim et al., 2008a) or with inorganic materials such as hydroxyapatite (HA) (Sui et al., 2007; Kim et al.,

2006a; Ma et al., 2001) or a combination of natural polymers and inorganic materials (Prabhakaran et al., 2009) has been reported to improve cell proliferation and differentiation.

It has been suggested, that the simple blending of PLLA with bioactive natural biodegradable polymers may offer a more cost-effective method than bulk surface modification to improve the cell affinity of PLLA (Zhang et al., 2007c).

1.5.4 General degradation mechanism and characteristics of biodegradable polyesters

Degradable polyesters have found increasing use in medical applications because of their biocompatibility (Hakkarainen, 2002). Biodegradable polyesters have been utilized in drug delivery (Martina and Hutmacher, 2007), implant devices (De Jong et al., 2005; MainilVarlet et al., 1997; Bergsma et al., 1995) and surgical sutures (Gilding and Reed, 1979; Reed and Gilding, 1981) owing to their ability to degrade and produce non-toxic by-products.

The degradation of biodegradable polymers is characterised by a chain scissioning process during which the polymer chains are severed/broken to form oligomers and eventually monomers (Gopferich, 1996). Chain scission can occur either by hydrolysis or by the action of enzymes that help to catalyse hydrolysis (Gomes and Reis, 2004; Gopferich, 1996). Hydrolysis occurs after penetration of water into the polymer. During hydrolysis, there is a reaction between water and the functional group containing the unstable bond (Gopferich, 1996). Hence, polymer degradation involves hydrolysis and depends on the absorption of water (St. Pierre and Chiellini, 1986). The degradation rate is influenced by such factors as: the type of chemical bond, pH, copolymer composition and water uptake (Gopferich, 1996). Following degradation, erosion can occur either by bulk erosion (also referred to as homogenous erosion) or surface erosion (also referred to as heterogenous erosion) (Dong et

al., 2009; Gomes and Reis, 2004; Gopferich, 1996; Middleton and Tipton, 2000; van Dijkhuizen-Radersma et al., 2008). Erosion is characterised by loss of material, i.e. weight loss, due to the oligomers and monomers leaching out of the polymer. The mechanism of erosion for a particular polymer is dependent on the balance between the rate of water penetration into the polymer and the rate of conversion of the polymer into water soluble materials (Dong et al., 2009; Gopferich, 1996; van Dijkhuizen-Radersma et al., 2008). It should be noted that both erosion mechanisms are ideal cases only (Gopferich, 1996), that is, most polymers are not sufficiently hydrophobic to prevent water from penetrating the material while allowing the erosion of the surface alone (Tamada and Langer, 1993) and vice versa. During bulk erosion, material is lost uniformly throughout the polymer volume; whereas, during surface erosion, material is lost from the surface of the polymer alone, and the erosion front usually moves from the outside to the inside of the material (Tamada and Langer, 1993). Generally, amorphous and hydrophilic polymers are likely to undergo bulk erosion while hydrophobic polymers with high crystallinities are likely to undergo surface erosion (Dong et al., 2009). Polymer erosion is a complex phenomenon as it depends on many other processes besides degradation, such as morphological changes and characteristics of the oligomers formed (Gopferich, 1996). The erosion and dissolution of polyesters is governed by such factors as: the hydrolysis rate constant of the ester bond, the diffusion coefficient of water within the polymer matrix, the diffusion of chain fragments within the polymer matrix and the solubility of degradation products in the surrounding medium (Vert, 2005).

At the initial stages of polymer degradation, water penetrates the polymer matrix which induces polymer chain scission. Polymer chain scission leads to a decrease in molecular weight and the formation of oligomers (i.e. degradation), which if they possess a molecular

weight that is low enough, will leach out of the polymer matrix and possibly dissolve in the degradation medium (i.e. erosion) (Dong et al., 2009). However, if the size of the polymer device is large (typically, > ≈300 μm), the oligomers formed in the interior of the device will be trapped within the interior of the device (Grizzi et al., 1995; Li et al., 1990) which will result in an increase in the number of carboxylic chain ends in the interior, leading to a drastic change in pH at the interior of the polymer. Consequently, accelerated degradation will be observed at the interior of the polymer device due to autocatalysis; this is usually characterised by the formation of a hollow structure (Dong et al., 2009; Grizzi et al., 1995; Li et al., 1990; Li and McCarthy, 1999a). pH has been shown to affect the rate of the hydrolysis reaction through catalysis, and the rate of the hydrolysis reaction has been specifically shown for PGA and PLGA to be fastest at low and high pH (Gopferich, 1996). The autocatalytic effect has been well documented in the literature for large-sized PLA/GA polymers during both *in vitro* and *in vivo* degradation (Grizzi et al., 1995; Li and McCarthy, 1999a; Therin et al., 1992). However, Grizzi et al. estimated that, below a critical thickness of between 200–300 μm, autocatalysis will not occur because the soluble hydrolytic products can easily diffuse into the degradation medium (Grizzi et al., 1995).

1.6 Gelatin

1.6.1 Introduction

Gelatin is a natural biodegradable polymer derived by thermal denaturation or physical and chemical degradation of collagen (Bigi et al., 1998; Bigi et al., 2001). It consists of 19 amino acids joined by peptide linkages and can be hydrolysed by a variety of proteolytic enzymes to yield its constituent amino acids and peptide components (Chandra and Rustgi, 1998).

The production of gelatin from collagen results in a partially reversible disordering of noncovalent bonds of the triple-helix structure of collagen (Bigi et al., 1998; Bigi et al., 2001).

1.6.2 Synthesis

Under suitable conditions, during a renaturation process, the polymer chains of gelatin can undergo a disorder-order transformation to regain the triple-helix structure of collagen (Zhang et al., 2006). Depending on the pre-treatment method to which collagen is subjected prior to the extraction of gelatin, two types of gelatin exist – acidic (Type A) and alkaline gelatin (Type B) (Zhang et al., 2005); this is because gelatin can be produced by either acidic or alkaline processing of collagen. This pre-treatment process also affects the electrical nature of collagen and thus results in the possibility of producing gelatin with different isoelectric points. Alkaline processing of collagen hydrolyses its amide groups giving the resulting gelatin a high density of carboxyl groups and thus a negative charge and low isoelectric point. In contrast, because the acidic processing of collagen has less effect on its amide groups, the isoelectric point of gelatin produced by this route will be similar to that of collagen (Malafaya et al., 2007).

From hard and soft capsules to vascular prostheses sealant, gelatin has found wide usage in the biomedical and pharmaceutical industries because of its biodegradability, biocompatibility and non-immunogenicity (Malafaya et al., 2007; Bigi et al., 2001; Chandra and Rustgi, 1998; Silva et al., 2010; Tabata and Ikada, 1998). Relative to collagen, it has low antigenicity since it is a denatured collagen (Malafaya et al., 2007). Additionally, it is cheaper and easier to obtain than collagen (Bigi et al., 2001).

1.6.3 Gelatin and its blends as tissue engineering scaffolds

Although synthetic polymers are versatile and possess mechanical properties that make them valuable for as tissue engineering scaffolds, they lack cell recognition sites and thus exhibit poor cell affinity (Zhang et al., 2007c). Natural polymers on the contrary generally exhibit better biocompatibility than synthetic polymers (Giusti et al., 1998). However, natural polymers often have poor mechanical properties, limited processibility (due to the necessity of preserving their biological properties) and high production costs. A review of the literature portrays collagen as the most widely researched natural polymer in tissue engineering. Using 'tissue engineering scaffold' as the keyword for literature searching through the ISI Web of Science®, and further refining the search results by using 'collagen' as a keyword yielded 3003 results[2]. However, the cheap cost of gelatin relative to collagen has made it a favourable alternative to collagen since in fact, gelatin is a denatured form of collagen (Huang et al., 2004; Giusti et al., 1998; Venugopal et al., 2010).

Gelatin has been reported to be a promising tissue scaffolding material for adipose tissue (Hong et al., 2005) and bone (Sisson et al., 2010).

However, the poor mechanical properties of gelatin limit its application as a tissue engineering scaffold. Some of the methods used to overcome this limitation are further discussed below.

A. Cross-linking - Chemical cross-linking (by using chemicals such as glutaraldehyde) and physical cross-linking (by using ultraviolet or gamma irradiation) have been used to overcome this problem (Bigi et al., 1998). Bigi et al. (1998) reported the use of glutaraldehyde to cross-link gelatin films under deformation to obtain films with significantly improved mechanical properties in the direction of deformation; they

[2] Literature search done on April 21, 2011 - Using 'gelatin', 'chitosan', 'hyaluronic acid', and 'alginate' as refining keywords yielded 471, 706, 346 and 425 publications, respectively.

further reported that the mechanical properties of the cross-linked drawn films fell within the range of several connective tissues (Bigi et al., 1998). In another work by the same group of researchers, the authors reported that gelatin films can be cross-linked to yield improved mechanical properties by a relatively low concentration of glutaraldehyde, thus reducing the risk of cytotoxicity posed by glutaraldehyde (Bigi et al., 2001).

Cross-linked gelatin has been shown to be a promising material for tissue engineering of bone (Francis et al., 2010).

B. Blending – The poor mechanical properties of gelatin limit its possible applications as a biomaterial (Bigi et al., 2001). However, by blending gelatin with other polymers (usually synthetic polymers) or with inorganic materials such as hydroxyapatite, it has been shown that its mechanical properties can be improved. Su et al. (2010) reported an increase in breaking strength from 1.86 MPa for electrospun gelatin (8 wt% gelatin) to 3.48 MPa for electrospun PLLA-gelatin (1 wt% gelatin:7 wt% PLLA) blend; the authors attributed this increase in strength to the PLLA component (Su et al., 2010). Similarly, Liu et al. (2009) reported a 75% increase in compressive modulus when bone-like apatite was incorporated onto the surface of 3D-nanofibrous gelatin (Liu et al., 2009)

It has also been suggested, that the blending of gelatin with a synthetic polymer also has the additional advantage of producing a new biomaterial which overcomes the shortcomings of both gelatin and the synthetic polymer (Venugopal et al., 2010).

Gelatin blends have been shown to be promising tissue scaffolding materials for bone (Zhang et al., 2005; Liu et al., 2009; Kim et al., 2005; Francis et al., 2010) and cardiac tissue (Li et al., 2006).

1.7 Hydroxyapatite

1.7.1 Introduction

Hydroxyapatite (HA) is a major mineral component of bone, making up about 60 wt% of bone (Supova, 2009; Venugopal et al., 2010; Rezwan et al., 2006; Hench and Wilson, 1984; Simske et al., 1997). It is a bioactive ceramic and has been used successfully in the clinic as a bone filler material (Jones, 2005). In synthetic form, it has been widely used because of its similarity in composition and Young's modulus to that of bone and also because of its excellent osteoconductivity (Jones, 2005; Venugopal et al., 2010; Wei and Ma, 2004).

1.7.2 Synthesis

Nano-HA (10-100 nm) has recently received a lot of interest in bone-tissue engineering research because of its excellent functional properties, such as improvement in the formation of neo-tissue within a short time due to its ability to promote osteoblast adhesion, differention and proliferation, osteointegration, and deposition of calcium-containing minerals on its surface (Supova, 2009).

Various methods of synthesizing nano-HA powders have been reported in the literature, these include: solid-phase reaction (Ota et al., 1998); pH shock wave (Koumoulidis et al., 2001); hydrothermal processes (Ioku et al., 2002; Zhang and Gonsalves, 1997); hydrothermal microemulsion (Lin et al., 2007); sol-gel methods (Kuriakose et al., 2004; Bigi et al., 2004); wet chemical precipitation methods (Murugan and Ramakrishna, 2005; Orlovskii et al., 2002; Pramanik et al., 2007; Tas, 2000); precipitation accompanied by microwave processing (Siddharthan et al., 2004); and mechano-chemical processes (Yeong et al., 2001). The crystallinity, Ca/P ratio, particle size, size distribution and agglomeration of

the synthesised powder will depend on the preparation method used, and varies from method to method (Supova, 2009).

1.7.3 The use of hydroxyapatite and its blends as tissue engineering scaffolds

Porous HA can be colonized by bone tissue; however, a problem with porous ceramics is that they generally possess low compressive strength. The strength of the scaffold depends on the thickness and strength of the struts or pore walls (Jones, 2005) and generally, HA scaffolds are not ideal tissue engineering scaffolds because they are brittle and inelastic, and therefore cannot be used in load-bearing sites (Rezwan et al., 2006; Olivier et al., 2004; Wei and Ma, 2004; Coombes and Meikle, 1994). While HA is still considered as a bone replacement material rather than a regenerative material, silicon-substituted HA scaffolds are being considered as potential materials for bone-tissue engineering (Jones, 2005). Furthermore, its inherent brittleness and difficulty of processing limit the use of HA as a scaffold material (Wei and Ma, 2004). For these reasons, HA is rarely used as a stand-alone tissue engineering scaffold material, as such, there is very limited report in the literature on pure HA scaffolds. In order to overcome the difficulty of processing HA into tissue engineering scaffolds, and also to overcome its brittleness, it is usually combined with biodegradable polymers either by mixing or biomimetic methods. Polymer/HA scaffolds have been reported to show improved osteoconductive properties (Venugopal et al., 2010) and degradation properties (Zhang and Ma, 1999b) over pure HA scaffolds.

1.8 Methods of Producing Bone-Tissue Engineering Scaffolds

A variety of methods have been used to develop bone-tissue engineering scaffolds; such methods include solvent casting and particulate leaching (Murphy et al., 2002; Shea et al.,

2000; Cao and Kuboyama, 2010; Laurencin et al., 1999; Liu and Ma, 2004; Murphy and Mikos, 2007), thermally-induced phase separation (Boccaccini et al., 2006; Maquet et al., 2003; Maquet et al., 2004; Wei and Ma, 2004; Zhang and Ma, 1999b; Hutmacher, 2000; Liu and Ma, 2004; Murphy and Mikos, 2007), solid freeform fabrication techniques (also called rapid prototyping) (Leong et al., 2003; Hutmacher, 2000; Das et al., 2003; Liu and Ma, 2004; Murphy and Mikos, 2007), microsphere sintering (Laurencin et al., 1999), fibre bonding (Gomes et al., 2003; Murphy and Mikos, 2007), self assembly (Hartgerink et al., 2001; Hosseinkhani et al., 2006; Murphy and Mikos, 2007) and electrospinning (Ngiam et al., 2009; Gupta et al., 2009; Prabhakaran et al., 2009; Venugopal et al., 2008a; Zhang et al., 2008; Venugopal et al., 2007; Liao et al., 2008; Yoshimoto et al., 2003; Sui et al., 2007; Liu and Ma, 2004; Zhang and Lim, 2008; Murphy and Mikos, 2007). The production route for a polymer scaffold is mainly determined by the properties of the polymer and its intended use (Thomson et al., 1995; Murphy and Mikos, 2007).

Polymers used as tissue engineering scaffolds are processed based on two general techniques (Maquet and Jerome, 1997):

a) Melt Processing – This technique depends on the viscosity of the polymer in molten state, and would usually involve heating the polymer above its glass transition temperature (T_g) or above its melting temperature (T_m); and

b) Solvent Processing – This depends on the solubility of the polymer and volatility of the solvent used.

1.8.1 Solvent casting and particulate leaching

In this method, a water-soluble salt is used as a porogen. The polymer to be used as a scaffold is first dissolved in a solvent, for instance, PLLA or PGA would be dissolved in

chloroform and then the solution is poured out into a petri dish containing particles of a water soluble salt such as sodium chloride. After this, the solvent is allowed to evaporate, and the residual amounts of the solvent can be removed by vacuum drying, then the resulting polymer/salt composite is soaked in de-ionized water to leach out the salt particles leaving pores in the spaces the particles once occupied. Finally, the membrane is dried. It is essential that the salt used should be insoluble in the solvent used to dissolve the polymer (Ma, 2004; Thomson et al., 1995; Mikos and Temenoff, 2000; Maquet and Jerome, 1997).

Shastri et al. (2000) reported an alternative form of this method in which waxy hydrocarbons were used as the porogen. The porogen and the polymer were mixed into a paste which was then packed in a Teflon mould. The mould was immersed in a hydrocarbon solvent to dissolve the waxy porogen leaving the polymer unaffected. Finally, the polymer membrane was vacuum-dried for several days to remove any residual solvents. The authors further reported that these scaffolds exhibited porosities as high as 87% with surface areas of 20 m^2/g (Shastri et al., 2000).

The pore size and porosity of the scaffold can be controlled by varying the porogen particle size and the amount of porogen respectively. Ishaug-Riley et al. (1997) reported the fabrication of PLGA scaffold foams using a sodium chloride (NaCl) porogen, with pore sizes ranging from 150 µm to 700 µm. Furthermore, it was reported, that when these scaffolds were seeded with rat marrow stromal cells and implanted into rat mesentery, mineralized bone-like tissue formation was observed within 7 days post-implantation (Ishaug-Riley et al., 1997).

One of the disadvantages of this technique is the use of organic solvents which make it impossible to add pharmacological agents to the membrane during production (Mikos and Temenoff, 2000). Also, in its simplest form it can only be used to produce thin wafers of

approximately 2 mm thickness (Thomson et al., 1995), although Shastri et al. (2000) reported thicknesses of approximately 2.5 cm using the modified method previously described (Shastri et al., 2000). Finally, the salt leaching step results in increased processing times (Mikos and Temenoff, 2000).

1.8.2 Fibre bonding

Two variations of this method were reported in literature (Thomson et al., 1995; Mooney et al., 1996b). In the first method, PLLA was dissolved in methylene chloride followed by immersion of PGA fibres in the resulting solution. Since PGA does not dissolve in methylene chloride, the PGA fibres were unaffected when they were immersed in the solution. The solvent was then allowed to evaporate and residual amounts were removed by vacuum-drying, leaving behind a composite of non-bonded PGA fibres in a PLLA matrix. Next, the composite was heated to a temperature above the melting point of both polymers; since PGA and PLLA are immiscible in the molten state they did not mix but the PGA fibres bonded to one another at their cross-points during heating while the PLLA melted and filled the voids in the composite. The PLLA helped to maintain the integrity of PGA fibre mesh to prevent it from collapsing during heating. The composite was then quenched to prevent further melting of the PGA fibres during cooling and this was followed by further heat treatment. The composite was then immersed in methylene chloride to selectively leach off the PLLA, leaving behind bonded PGA fibres. Finally, the PGA fibre scaffold was vacuum-dried to remove any residual solvent (Thomson et al., 1995; Mikos and Temenoff, 2000; Mikos et al., 1993). Gomes et al. (2003) reported the fabrication of scaffolds from a starch/polycaprolactone (30:70) blend by a fibre bonding process. The authors further reported that the scaffold had a fibre diameter of ≈181 μm with highly interconnected pores

and a porosity of approximately 75%. Furthermore, the scaffold was reported to show good proliferation and mineralisation after several days when marrow stromal cells from the femoras and tibias of Wistar rats were seeded on it. The good cell-scaffold interaction was attributed to the interconnected nature of the pores (Gomes et al., 2003).

In a second method reported by Mooney et al. (1996), a scaffold consisting of a core of PGA mesh and coating of PLLA or PGA was produced by spraying a non-bonded PGA fibre mesh with a solution of PLLA or PLGA dissolved in chloroform. The PGA fibres were unaffected by the PLLA or PLGA solution because PGA is only weakly soluble in chloroform. The spraying caused the PGA fibres to become bonded at their cross-points while a layer of PLLA or PLGA was built up on the surface of the PGA fibres. After spraying, the solvent was evaporated, leaving behind a scaffold made of a core of PGA bonded fibres and a coating of PLLA or PLGA. It should be noted that when this scaffold is implanted in a host, it is the PLLA or PLGA coating that the cells attach to while the PGA fibres would provide mechanical strength for the scaffold. The thickness of the coating can be controlled by varying the spraying time (Mooney et al., 1996b).

The disadvantages of this method of scaffold preparation include the fact that it cannot be used to produce complex 3-D shapes (Thomson et al., 1995) and the use of solvents that could be toxic to cells if not completely removed from the scaffolds prior to use.

1.8.3 Membrane lamination

This method is an improvement on the solvent casting/particulate leaching method in an attempt to produce 3-D scaffolds. In this method, membranes which are produced by solvent casting and particulate leaching are cut out to match the exact shape of the intended application of the scaffold. These membranes are then bonded together by

coating the adjacent surfaces with chloroform. It can be visualized as a 'sandwich' structure of different layers of membranes. The desired 3-D geometry can be constructed layer by layer; however, this must be done in such a way that the boundaries between any two layers must be indistinguishable from the bulk. It is particularly useful for processing scaffolds to be used in regeneration of hard tissues such as cartilage and bone (Thomson et al., 1995; Maquet and Jerome, 1997).

One limitation of this method include is that, like solvent casting, it also makes use of toxic solvents.

1.8.4 Melt moulding

In this technique, a polymer powder is mixed with porogen particles and poured into a mould followed by heating the mould to a temperature above the glass transition temperature (T_g) of the polymer (for amorphous polymers) or melting temperature (for semi-crystalline polymers). The porogen particles are leached off from the composite with deionized water after the composite has been removed from the mould. This leaves a porous polymer scaffold with a shape that is identical to that of the mould. The porosity can be controlled by varying the ratio of porogen to the polymer powder while the pore size can be controlled independent of the porosity by altering the size of the porogen particles (Thomson et al., 1995; Maquet and Jerome, 1997).

Advantages of this method include the fact that it can be used to produce 3-D scaffolds and it can be used to process any scaffold of any geometry by altering the geometry of the mould. Additionally, because the process makes use of only water as a solvent, bioactive molecules can be added during cell culture although the excessively high operating

temperatures can inactivate the molecules (Murphy and Mikos, 2007). It is also limited by the complexity of the design of the mould (Puppi et al., 2010).

1.8.5 Gas foaming

In order to eliminate the use of organic solvents, scaffolds can be produced by a gas foaming process. In this process, solid polymer discs made by compression moulding are exposed to high pressure carbon dioxide (CO_2) (usually about 5.5 MPa) after which the pressure is rapidly reduced to atmospheric pressure. Porosities of up to 93% and pore sizes of 100 µm can be obtained, the pores however, are largely unconnected (Mooney et al., 1996a).

Kim et al. (2006b), in a modification of this method reported the production of highly porous PLGA/nano-hydroxyapatite composite scaffolds by combining the gas foaming technique with particulate leaching. Discs were made by compression moulding from a mixture of PLGA particles, HA and NaCl (utilized as the porogen). The discs were then exposed to high pressure CO_2 gas to saturate the polymer with the gas. Decreasing the gas pressure afterwards created a thermodynamic instability which resulted in the nucleation and growth of CO_2 pores within the polymer scaffolds. The NaCl particles were subsequently removed from the scaffolds by leaching with distilled water. The authors reported that these scaffolds showed interconnected porous structures and when implanted into the subcutaneous space of athymic mice for 8 weeks, extensive bone formation was observed on the scaffolds (Kim et al., 2006b).

1.8.6 Phase separation techniques

Although the methods previously described are capable of producing scaffolds with high porosity and interconnected pores, none of them is capable of fabricating nano-fibrous scaffolds (Smith and Ma, 2004; Barnes et al., 2007). As it has recently been shown that cells

can attach and organize better on nanoscale materials than microscale materials; there is an increased motivation for the fabrication of nano-fibrous scaffolds (Liao et al., 2008).

The phase separation technique uses thermodynamic means to separate a homogenous multi-component polymer solution system into a polymer rich phase and a polymer-poor/solvent rich phase (Barnes et al., 2007). The phase separation process occurs in five steps, namely:

1. Dissolution of a polymer;
2. Phase separation to produce a gel;
3. Solvent extraction from gel by addition of water;
4. Freezing the gel (usually to a temperature below the glass transition temperature of the polymer) and;
5. Freeze-drying in vacuum (Smith and Ma, 2004; Barnes et al., 2007).

The scaffolds produced by this method have been reported to exhibit porosities as high as 98%, and fibres with diameters in the range 50-500 nm (Smith and Ma, 2004; Barnes et al., 2007). This range of diameters closely matches that of natural collagen in ECM. Porogens such as inorganic salt, sugar, and paraffin spheres can be added to the polymer solution during the phase separation process to increase the porosity of the scaffold (Smith and Ma, 2004; Barnes et al., 2007).

Although this method is simple and versatile as it gives great control over the properties of the scaffolds, and does not require large specialized equipment, it is limited because it can only be used with a few polymers and can also only be used on a laboratory scale (Smith and Ma, 2004; Barnes et al., 2007; Ramakrishna et al., 2005). There are two common phase separation methods described in the literature.

1.8.6.1 Solid-liquid phase separation

In this method, water is added to a polymer solution to form an emulsion. This mixture is then cast in a mould and quenched to very low temperatures, causing crystallisation of the solvent from the mixture. This is followed by freeze-drying at low temperatures to remove the solvent crystals and water, causing the spaces hitherto occupied by them to become pores (Ma, 2004; Maquet and Jerome, 1997; Mikos and Temenoff, 2000; Murphy and Mikos, 2007). The porosity and pore sizes can be controlled by altering the ratio of the polymer solution to water, and the viscosity of the emulsion (Mikos and Temenoff, 2000). Ma et al. (2001) reported the fabrication of PLLA/nano-hydroxyapatite scaffolds by thermally induced phase separation and obtained scaffolds with porosities of 89.2%. Osteoblasts seeded on these scaffolds were reported to proliferate and show bone-specific markers during 6 weeks of *in vitro* cultivation (Ma et al., 2001).

1.8.6.2 Liquid-liquid phase separation

In this method, the polymer is dissolved in a low melting point solvent (e.g. naphthalene) followed usually by the addition of a non-solvent such as water. The non-solvent induces phase separation. The solution is then cooled below the melting point of the solvent followed by vacuum drying for several days to ensure complete sublimation of the solvent (Ma, 2004; Maquet and Jerome, 1997; Mikos and Temenoff, 2000).

1.8.7 Self assembly

Self assembly is a process in which individual components spontaneously organize themselves into a pattern or ordered structure with pre-programmed non-covalent bonds (Ma, 2004; Barnes et al., 2007). The major driving forces for this process are the intermolecular forces created between the individual components involved in the self

assembly by bonds such as hydrogen bonds, hydrophobic interactions, van der Waals interactions etc (Zhang, 2003; Ramakrishna et al., 2005). Peptide-based scaffolds have shown promise in the *in vitro* culture of osteoblasts, chondrocytes, and hepatocytes. Scaffold assembly and size can be controlled by pH, peptide concentration, and divalent ion induction (Murphy and Mikos, 2007; Smith and Ma, 2004).

While self assembly is a process that occurs in nature and its occurrence is common (Zhang, 2003), it can only be used for polymers with certain configurations (di-block copolymers, tri-block copolymers, tri-blocks from peptide-amphiphiles, and dendrimers) (Barnes et al., 2007). Another disadvantage of this processing method is that it is complex and gives very low quantity of fibres so that it cannot really be used for mass production of tissue engineering scaffolds (Barnes et al., 2007).

1.9 Electrospinning

1.9.1 Introduction

Electrospinning is a process which works on the electrohydrodynamic principle that electric fields concentrated at a tip are capable of ionizing surrounding fluids. Electrohydrodynamic phenomena such as “St. Elmo’s fire,” have been recorded since at least the times of Julius Caesar (Heidorn, 1998). However, it was William Gilbert who first recorded the behaviour of liquid droplets in electric fields during the 17^{th} century and published his observations in his work, *De Magnete;* in which he described the use of charged amber to deform the shape of water droplets without physical contact. Further development in this field did not arise until 1882 when Lord Rayleigh published a theoretical model that described the electrical forces needed to cause droplets to eject liquid. In the 1960s, Sir Geoffrey Taylor undertook a

rigorous theoretical study on charged liquid droplets. He observed that droplets within an electric field could deform into a new equilibrium shape that resembled a cone (Taylor cone) which emitted fluid from their tip. He discovered that the ejected fluid could exhibit two distinct behaviours, either forming discrete droplets that travel directly to the counter-electrode plate or forming long strands of liquid that whip around before reaching the electrode (Laudenslager and Sigmund, 2011; Ero-Phillips, 2011).

Although Anton Formhals patented the process in 1934, it was discarded by many industries and researchers for the purpose of making fibres in favour of other methods until the mid-1990s when Reneker and co-workers demonstrated the applicability of electrospinning for nanotechnology research (Hutmacher and Dalton, 2011). In fact, it was Reneker and co-workers who coined the term “electrospinning” from “electrostatic spinning” (Huang et al., 2003; Ero-Phillips, 2011). Since then, research in this area has grown exponentially due to the versatility of the process.

Over the years, hardly anything has changed about the process (Barnes et al., 2007) and most of the processes used today even with their variations are based on the process described by Baumgarten in 1971 (Huang et al., 2003). Originally, it was mostly used for manufacturing fabrics (Ma, 2004; Barnes et al., 2007), but over the last decade, it has recently generated much interest amongst researchers partly due to the growing interest in nanotechnology and the simplicity with which the process can be used to produce nanofibres (Barnes et al., 2007; Huang et al., 2003; Zong et al., 2002; Ramakrishna et al., 2005; Ramakrishna et al., 2006).

1.9.2 Principles of electrospinning and the electrospinning process

The main requirements of the electrospinning process are (Boland et al., 2001; Huang et al., 2003; Lannutti et al., 2007):

1. A polymer source (the polymer could be in solution or in molten form although it is usually in solution);
2. A high voltage source; and
3. A grounded target/collector.

Before the application of voltage to the polymer solution, the solution at the tip of the capillary tube is held in place by surface tension, however with the application of voltage, the polymer solution becomes charged and on increasing the applied voltage, the shape of the droplet at the tip of the capillary tube begins to deform from that caused by the surface tension alone as a result of the repulsion of charges within the droplet. As the electric field created by the applied voltage exerts a force that approaches that which is equal to that of the surface tension, the meniscus begins to have convex sides with a rounded tip. At a certain critical voltage, the shape of the meniscus becomes conical having a semi-vertical angle of 49.3^{o}, this is called the Taylor cone. When the voltage exceeds this critical voltage, an electrically charged polymer jet is ejected from the capillary tube. This electrically charged polymer jet is then accelerated towards the grounded target due to the electric field (Barnes et al., 2007; Ramdhanie et al., 2006; Sill and von Recum, 2008; Boland et al., 2001; Huang et al., 2003; Lannutti et al., 2007; Zong et al., 2002; Ramakrishna et al., 2005; Reneker and Chun, 1996a). As the polymer jet travels towards the target, the solvent is evaporated leaving polymer fibres; a non-axisymmetric (whipping) instability causes bending and stretching of the polymer jet which yields the production of fibres with sub-

micron diameters (Shin et al., 2001). These fibres remain unbroken during their travel to the target due to polymer chain entanglements (Shenoy et al., 2005). In melt electrospinning, the polymer jet solidifies as it travels through the air to the target.

A typical electrospinning set-up is shown in Figure 6. However, many variations have been developed to fabricate fibres with complex and controlled morphology; these include multi-layer electrospinning (Liang et al., 2007), coaxial electrospinning (Yu et al., 2004; Sun et al., 2003; Saraf et al., 2009), blowing-assisted electrospinning (Liang et al., 2007), and conjugate electrospinning (Xinsong et al., 2008).

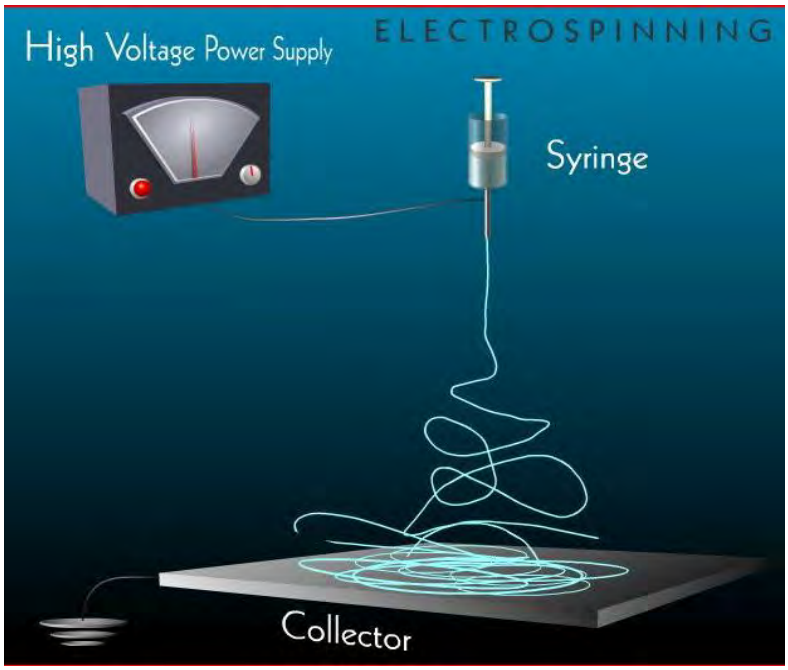

Figure 6: Typical electrospinning set-up (Hill, 2005)

There are three sets of parameters that determine the properties of electrospun fibres, these are (Huang et al., 2003; Ramakrishna et al., 2005):

a) Polymer solution parameters – These are molecular weight and viscosity, surface tension, solution conductivity and dielectric effect of solvent. Each parameter has different ways in which it affects the properties of electrospun fibres. For instance, high molecular weight polymers would likely form viscous solutions and these are

likely to produce fibres with large diameters and un-beaded fibres. These parameters can all be varied in order to obtain optimum results (Huang et al., 2003; Ramakrishna et al., 2005).

b) Processing conditions – These are voltage, feed-rate, temperature, effect of collector, needle diameter, and distance between needle tip and collector. As with the polymer solution parameters, these all have ways in which they influence the properties of the fibres produced and they can all be varied to obtain optimum results. For instance, using very high voltages for electrospinning would create high electric fields; this would cause the polymer jet to travel faster to the target and could lead to formation of fine fibres. This also may affect the degree of crystallinity of the fibres. It should be noted however, that these parameters can be varied at the same time with the polymer solution parameters (Huang et al., 2003; Ramakrishna et al., 2005).

c) Ambient parameters – These can be termed as environmental factors and they include pressure, temperature, humidity and the electrospinning atmosphere (Ramakrishna et al., 2005).

The fact that the electrospinning process is a versatile method, coupled with the advantage of relatively high production rates has made it find applications in many different areas such as energy, defence and security, environmental engineering and biotechnology and healthcare (Barnes et al., 2007; Huang et al., 2003; Ramakrishna et al., 2005; Ramakrishna et al., 2006).

The literature shows that the electrospinning process has been thoroughly reviewed by a number of researchers (Teo and Ramakrishna, 2006; Sill and von Recum, 2008; Ramakrishna

et al., 2010; Laudenslager and Sigmund, 2011; Barnes et al., 2007; Hutmacher and Dalton, 2011; Huang et al., 2003; Ramakrishna et al., 2005; Ramakrishna et al., 2006).

1.9.3 Effect of electrospinning on polymer properties

The interest in electrospinning has grown exponentially over the last two decades as mentioned above due to the relative simplicity with which nanofibres can be produced by this process. Electrospinning is capable of producing fibres with large surface area-to-volume ratios (Kongkhlang et al., 2008). An advantage of the process over conventional fibre forming methods is that only a small amount of polymer, typically as low as 50 mg, is required for electrospinning, in comparison to tens of kilograms of polymer required in conventional spinning methods (Stephens et al., 2004). However, in spite of the amount of research that has been carried out on electrospinning and electrospun fibres, studies on the effect of electrospinning on polymer properties have been limited. While most studies have focussed on the effect of electrospinning parameters on electrospun fibre diameter (Tong and Wang, 2011; Boland et al., 2001; Sukigara et al., 2003; Tan et al., 2005) and the development of controlled morphology (He et al., 2009; Katta et al., 2004; Kidoaki et al., 2005; Saraf et al., 2009; Sun et al., 2003) very few have focussed on the effect of electrospinning on polymer properties, such as molecular orientation of polymer chains (Kongkhlang et al., 2008), polymer crystallisation chain conformation (Stephens et al., 2004) and polymer degradation (Kim and Lee, 2000; Stephens et al., 2004).

Although electrospun fibres have potential applications in many different areas, their use as tissue engineering scaffold materials is probably the most popular application of electrospun fibres (Zhang et al., 2007c). However, an important question that needs to be addressed before electrospinning can be viewed as an acceptable method of fabricating

tissue engineering scaffolds is – 'Will polymer degradation occur during electrospinning?' Furthermore, because these electrospun fibres are intended for use in biomedical applications, it is imperative that an understanding of their properties, such as crystalliinity and degradation kinetics, which will impact their functionationality when in service, be properly developed.

In their study on melt electrospinning of poly(ethylene terephthalate) (PET) and poly(ethylene naphthalate) (PEN) and their blends, Kim and Lee (2000) reported that melt electrospinning of PET and PEN resulted in a decrease in molecular weight of the polymers after electrospinning (Kim and Lee, 2000). This led to an increase in the degree of crystallinity, and a decrease in glass transition temperature and crystallisation temperature. The decrease in polymer molecular weight post-electrospinning was attributed to thermal degradation (Kim and Lee, 2000).

Similarly, Zhou et al. (2006) reported the degradation of PLA during melt electrospinning. The authors observed a decrease in molecular weight from 186,000 to ≈40,000 in the first hour of fibre collection (Zhou et al., 2006). The degradation observed on the fibres was attributed to both thermal degradation and mechanical scission. Thermal degradation was considered to occur within the melt reservoir and the electrospinning nozzle, while mechanical scission was considered to occur as the polymer melt was forced through the thin nozzle during electrospinning. For comparison, the authors investigated degradation during solution electrospinning of PLA, but reported that no significant degradation was observed on the PLA fibres during solution electrospinning (Zhou et al., 2006).

In another work, Stephens et al. (2004) also reported that polymer degradation was not significant during solution electrospinning of Nylon-6 and Nylon-12 fibres (Stephens et al., 2004). Furthermore, they reported that the crystalline structure of the Nylon-12 fibres

remained unchanged; however, the crystalline structure of Nylon-6 was changed from an α-form to a γ-form after electrospinning. The change in the crystalline structure of the Nylon-6 fibres was attributed to the high stress to which the fibres were subjected during the electrospinning process (Stephens et al., 2004). Consequently, it is clear that although melt electrospinning is likely to cause some amount of polymer degradation, solution electrospinning on the contrary causes little or no polymer degradation.

As mentioned in the Section 1.1, a material proposed for use as a tissue engineering scaffold must be biodegradable and have a controllable degradation rate. The rate of degradation has been reported to vary directly proportionally to crystallinity (Middleton and Tipton, 2000). It is therefore crucial to have an understanding of the effect of electrospinning on polymer crystallinity. If as observed by Stephens et al. (2004), electrospinning is capable of changing the crystalline structure of a material, it would be interesting to determine what effect, if any, electrospinning has on polymer crystallinity.

Regarding the effect of electrospinning on polymer crystallinity, it has been generally reported that electrospun fibres possess lower crystallinity than films cast from solutions or melts and the as-received polymer. Bognitzki et al. (2001a) reported that electrospun PLLA fibres had a lower degree of crystallinity than fibres from melt and dilute solutions and attributed this to the rapid deposition rate of the fibres, which allowed very little time for crystallisation to occur (Bognitzki et al., 2001). Zong et al. (2002) reported a lower degree of crystallinity in electrospun PLLA fibres as compared to as-received PLLA resin and attributed this to the rapid solidification of the stretched polymer chains during the electrospinning process (Zong et al., 2002). However, because the work of both groups focussed on electrospinning PLLA within a fixed set of parameters, it is probable that their results may be limited to the electrospinning parameters which were used.

Other researchers have compared the crystallinity of various electrospun fibres to those of the un-processed materials from which they were electrospun. Ramdhanie et al. (2006) electrospun blends of PLA and PGA to produce both aligned and random fibres (Ramdhanie et al., 2006). They reported generally lower values of crystallinity (measured by DSC) for the PLA fibres than for the as-received PLA pellets, while some of the PGA electrospun fibres showed an increase in crystallinity. Deitzel et al. (2001a, 2001b) studied the wide angle X-ray diffraction (WAXD) peaks of electrospun polyethylene oxide (PEO) fibres and as-received PEO powder (Deitzel et al., 2001b; Deitzel et al., 2001a). The (120) and (112) reflections of the electrospun fibres were weak and broad in comparison to the sharp peaks obtained for the powder, indicating that the crystalline microstructure of the electrospun fibres was not well developed. In their work on protein polymer with fibronectin functionality (SLPF), Buchko et al. (1999) observed lower crystallinity for electrospun films than in the pristine powder using wide-angle X-ray scattering (WAXS) and attributed this to the rapid solidification of the electrospun fibres (Buchko et al., 1999). Similarly, Ayutsede et al. (2005) obtained crystallinities of 48% and 39% for pristine *Bombyx mori* silk and electrospun fibres, respectively using WAXD (Ayutsede et al., 2005).

Conversely, Zhao et al. (2004) suggested, that the degree of crystallinity of electrospun ethyl-cyanoethyl cellulose fibres was greatly influenced by the crystallisation time as the jet travelled from the capillary tip to the collector and molecular orientation was brought about by the electrostatic field (Zhao et al., 2004). Their results showed that the degree of crystallinity of the electrospun fibres increased with increasing voltage up to a maximum after which the degree of crystallinity began to decline. Their results suggested that by optimizing the electrospinning parameters, it may be possible to increase the degree of crystallinity of the electrospun fibres.

More recently, Kongkhlang et al. (2008) reported the electrospinning of random and aligned fibres of polyoxymethylene (POM), during which the morphology of polyoxymethylene (POM) was changed from a folded chain crystal structure (FCC) to an extended chain crystal structure – ECC, for both random and aligned nanofibres during electrospinning. In the ECC crystal structure, fully extended molecules align parallel to the needle axis whereas the FCC structure is characterised by folded molecular chains at the lamellar surface with the stems aligning normal to the surface (Kobayashi and Sakashita, 1992). The ECC structure of POM has been reported to develop during drawing of POM samples (Kobayashi and Sakashita, 1992). Kongkhlang et al. (2008) also observed molecular orientation on both the random and aligned electrospun fibres and reported that the molecular orientation was parallel to the fibre axis for both types of electrospun fibres (Kongkhlang et al., 2008). Hot-stretched fibres and aligned fibres have been reported to possess a high level of molecular orientation (Hou et al., 2010; Inai et al., 2005; Fennessey and Farris, 2004) and hence increased crystallinity compared to random electrospun fibres (Hou et al., 2010; Kongkhlang et al., 2008); their high crystallinity has been attributed to the increased molecular orientation produced by the drawing process that occurs during hot-stretching or collection of electrospun fibres by a rotating collector [the molecular orientation has also been reported to increase with increasing the speed of rotating collector (Fennessey and Farris, 2004)]. However, Kongkhlang et al. (2008) observed the formation of the ECC structure, and molecular orientation even on the random electrospun fibres, and concluded that it was possible to produce POM nanofibres with a well developed ECC morphology and molecular orientation without the application of any tensile force [which occurs during collection of electrospun fibres by a rotating collector (Yee et al., 2008)]. The existence of molecular orientation in the electrospun scaffolds was attributed to the substantial stretching forces

imposed on the polymer solution by the electric field during the electrospinning process (Kongkhlang et al., 2008).

Furthermore, it has been commonly reported by researchers that during electrospinning, polymer chains within the electric field experience high elongation strains and shear stresses which cause the macromolecular chains to align along the fibre axis, leading to a high degree of molecular orientation in the fibres (Arinstein et al., 2007; Baji et al., 2010; Wong et al., 2008; Kongkhlang et al., 2008; Stephens et al., 2004). The recent work of Wong et al. (2008) on aligned electrospun fibres of PCL of diameters ranging between 250 nm and 900 nm indicated that molecular orientation is directly proportional to crystallinity (Wong et al., 2008; Baji et al., 2010). It is therefore reasonable to suggest that if electrospinning causes molecular orientation of polymer chains, then it may be possible to influence the degree of molecular orientation of polymer chains and hence the degree of crystallinity by carefully controlling the electrospinning parameters.

The crystalline properties of a material are important when considering the material for medical applications because the crystalline properties of a polymer have a direct bearing upon the degradation behaviour *in vivo* (Kister et al., 2000; Dong et al., 2009; Middleton and Tipton, 2000; Hollinger and Battistone, 1986). A high or low degradation rate may be desirable, depending on the application of the material. It would therefore be beneficial if the degree of crystallinity of electrospun fibres can be tailored by controlling the electrospinning process/parameters. Although poly(lactic acid) is one of the most researched biodegradable polymers (Gomes and Reis, 2004; Rasal et al., 2010), there is no comprehensive systematic study in the literature about the effect of varying different electrospinning parameters on its degree of crystallinity. The previous work on the study of crystallinity of electrospun PLLA in the literature (Bognitzki et al., 2001; Zong et al., 2002;

Inai et al., 2005) have all been carried out within a fixed set of parameters which limits their results to the parameters used. A study of the possibility of controlling the degree of crystallinity of electrospun PLLA fibres is therefore required to provide much needed understanding in this area.

1.9.4 Electrospinning PLLA, gelatin and their blends in bone-tissue engineering

One reason for the growing interest in electrospinning amongst tissue engineering researchers is the fact that it can be used to produce nanofibres; and nanofibrous scaffolds have structural similarities to the extra-cellular matrices of tissues and organs (Barnes et al., 2007; Ramakrishna et al., 2006). Electrospun scaffolds possess high surface area to volume ratios which means they are conducive for tissue in-growth (Yoshimoto et al., 2003; Liao et al., 2008; Lannutti et al., 2007). In fact, it can be argued that the majority of electrospinning research is geared towards tissue engineering (Zhang et al., 2007c).

PLLA, because of its hydrophobicity, is rarely used as a standalone component for bone-tissue engineering; rather, it is usually blended with either organic or inorganic materials. As a result, blends of PLLA with inorganic materials (e.g. HA) and organic materials (natural and synthetic polymers) have been electrospun.

Chuenjitkuntaworn et al. (2010) reported the electrospinning of PLLA with and without HA; after culturing the scaffolds with MC3T3-E1 cells for 14 days, they reported that the PLLA-HA scaffolds showed greater amounts of osteocalcin mRNA than they did on the PLLA scaffolds and concluded that the presence of HA in the PLLA-HA scaffolds enhanced their osteoconductivity (Chuenjitkuntaworn et al., 2010).

Li et al. (2009) reported the electrospinning of PLLA and PLLA/keratin non-woven scaffolds; after 7 days of culturing with MC3T3 cells, they reported significantly higher cell viability and

differentiation on PLLA/keratin scaffold than on the PLLA scaffold. They concluded that keratin may have improved the interaction between the polymer and the osteoblast cells (Li et al., 2009a). Similarly, Schofer et al. (2009) reported blending PLLA with Collagen I with the aim of improving the ability of PLLA to promote growth and osteogenic differentiation of stem cells *in vitro*. They reported that the PLLA/Collagen I nanofibres were more hydrophilic compared to the PLLA nanofibres; when cultured with human mesenchymal stem cells over a period of 22 days, the PLLA/Collagen I nanofibres were observed to show improved growth as well as osteoblast differentiation compared to the PLLA nanofibres (Schofer et al., 2009).

According to the electrospinning literature, it is only within the last decade that gelatin was successfully electrospun into nanofibres (Huang et al., 2004). This may have been due to the fact that there are very few high polarity organic solvents available to dissolve gelatin (Huang et al., 2004). However, since the work of Huang and co-workers, numerous other research groups have electrospun gelatin (Sisson et al., 2010; Li et al., 2005a; Zhang et al., 2006; Songchotikunpan et al., 2008), synthetic polymer/gelatin and gelatin/inorganic material blends (Gupta et al., 2009; Su et al., 2010; Gu et al., 2009; Andric et al., 2010; Kim et al., 2008a; Francis et al., 2010; Barnes et al., 2007; Linh et al., 2010; Meng et al., 2010; Meng et al., 2011; Lee et al., 2008) with potentials for use in drug delivery and tissue engineering.

Although gelatin has been electrospun alone as a bone-tissue engineering scaffold, because of its poor mechanical properties, it is more commonly blended with organic or inorganic materials for electrospinning.

Sisson et al. (2010) reported the electrospinning of gelatin fibres with different diameters and observed good growth, migration and differentiation of MG63 cells on all the scaffolds.

Their results also revealed that osteoblasts exhibited different behaviours dictated by the fibre diameter of the scaffold upon which they were cultured (Sisson et al., 2010).

Zhang et al. (2005) reported the fabrication of gelatin and gelatin/PCL fibres by electrospinning. The gelatin/PCL fibres were observed to be more hydrophilic, with improved mechanical properties compared to pure gelatin or PCL alone. After 7 days of culturing the gelatin/PCL with bone-marrow stromal cells, the cells were reported to not only show favourable attachment and growth on the surface of the scaffolds, but they were also observed to be able to migrate inside the scaffold up to a depth of 114 μm (Zhang et al., 2005). In a similar work by the same research group, Venugopal et al. (2008) reported the fabrication of composite scaffolds of PCL/HA/gelatin. These scaffolds were observed not only to exhibit high flexibility but compared to pure PCL scaffolds, they showed significantly higher cell proliferation, alkaline phosphatase activity and mineralisation when cultured with human fetal osteoblasts for 6 days (Venugopal et al., 2008d).

Kim et al. (2008) reported the electrospinning of nanofibrous matrices of PLLA and PLLA/gelatin; the authors further reported, that the addition of gelatin to PLLA improved its wettability and significantly increased cellular growth of MC3T3-E1 cells after 7 days of culture (Kim et al., 2008a).

Andric et al. (2010) reported the fabrication of scaffolds which consisted of concentric layers of PLLA or PLLA/gelatin nanofibres wrapped around a PGA microfibre core with the aim of mimicking the organization of an osteon. The scaffolds were reported to be successfully mineralized when incubated in simulated body fluid (SBF) for two hours, with scaffolds of gelatin/PLLA (10:90) showing significantly higher amounts of calcium phosphate. The scaffolds were also observed to support cellular attachment and proliferation of MC3T3 cells over a period of 28 days (Andric et al., 2010).

1.10 Methods of Fabricating Biodegradable Electrospun Polymer/Hydroxyapatite Biocomposites

The possibility of combining the osteoconductivity of hydroxyapatite and the tailorable biodegradability of polyesters has led researchers to develop polymer/ceramic composite scaffolds for bone-tissue engineering either by direct mixing or by a biomimetic approach (Wei and Ma, 2004; Thomson et al., 1998; Zhang and Ma, 1999a; Zhang and Ma, 1999b).

Electrospinning has been widely researched as a biomimetic approach to fabricate polymer/hydroxyapatite composite scaffolds for bone-tissue engineering because electrospun scaffolds possess certain characteristics such as high surface area to volume ratio, high porosity and well interconnected open pore network, which make them similar to native bone extra-cellular matrix (ECM) (Liao et al., 2008).

During the fabrication of polymer/HA composites, fine HA particles tend to combine together to form strongly bonded aggregates which may further lead to larger structures (agglomerates). To form high quality and high performance polymer-HA composites, the particle aggregates or agglomerates must be broken down into primary particles which are sufficiently dispersed in the polymer matrix (Supova, 2009). This is important because the optimal performance of a polymer matrix composite material is achieved when the smaller particles are uniformly distributed throughout the polymer matrix and interact strongly with the organic matrix (Venugopal et al., 2010). However, homogeneous dispersion of HA particles in electrospun scaffolds is a big challenge. Some of the methods which have been utilized in order to overcome the above challenge are described below.

1.10.1 Mixing (Blending)

In this method, the polymer is dissolved in a solvent whereas HA particles are added to the solution and then stirred to bring about homogeneity. Venugopal et al. (2008a) reported the production of scaffolds of PCL/HA (1:1) with nanofibre diameters in the range of 352-625 nm and pore sizes of 4-20 μm by electrospinning. Additionally, the surfaces of the scaffolds were modified by oxygen plasma treatment to improve wettability and therefore cell adhesion. It was observed that the PCL/HA composite scaffolds had lower mechanical properties compared to the PCL scaffold, however, human fetal osteoblast (hFob) cells were found to proliferate and mineralize better on the composite scaffolds than the PCL scaffold, with HA acting as a chelating agent for the mineralisation of osteoblasts to form bone-like apatite (Venugopal et al., 2008a). In another work by the same group, Prabhakaran et al. (2009) reported the production of an electrospun PLLA-HA composite scaffold at a weight ratio of 80:20, using 1,1,1,3,3,3-hexafluoro-2-propanol (HFP) as a solvent. The authors also reported a good dispersion of HA within the polymer matrix as well as possible molecular interaction between HA and PLLA in the composite, although the mechanical strength was found to have decreased (Prabhakaran et al., 2009). When cultured with human fetal osteoblast cells (hFob), the PLLA-HA composite scaffolds were found to have higher levels of proliferation, differentiation, and mineralisation than PLLA scaffolds. Sui et al. (2007) reported the use of a two-solvent system to obtain a PLLA-HA dispersion prior to electrospinning PLLA-HA scaffolds. They reported, that the introduction of HA nanoparticles increased the specific surface area, mechanical properties and slowed down the degradation rate of the PLLA-HA scaffold. The slower degradation rate of the PLLA-HA scaffold was attributed by the authors to the presence of alkaline HA particles that could possibly help to neutralise the acidic environment arising from the release of the

degradation products of PLLA. Additionally, when cultured with osteoblast cells (MG-63), the composite scaffolds showed higher levels of cell proliferation and adhesion than the PLLA scaffolds.

Although mixing is a very straightforward method, the major drawback of this method is that hydrophilic ceramics have very little affinity with the organic solvent and the hydrophobic polymer (Kim et al., 2006a). This usually results in agglomeration of the HA particles causing an uneven distribution of the HA particles in the polymer matrix. The agglomerated particles could serve as the origin of failure (Kim et al., 2006a) and this almost always leads to a reduction of mechanical properties, for instance as has been reported by Venugopal et al. (2008a) and Prabhakaran et al. (2009).

Essentially, during mixing, there is a lack of adhesion between the two mechanically mismatched materials and as such, the interfacial strength between the HA and the polymer is very low resulting in early failure (Francis et al., 2010; Supova, 2009; Gupta et al., 2009) of the material. This may be another reason for the reduction in mechanical strength reported by Venugopal et al. (2008a) and Prabhakaran et al. (2009).

To overcome this limitation, Kim et al. (2006a) reported the introduction of a surfactant, 12-hydroxy-stearic acid (HSA) into a poly(D,L-lactic acid)/HA (PDLLA/HA) solution to create a homogeneous dispersion of HA particles in the solution prior to electrospinning. It was then reported that the surfactant was effective in dispersing the HA powder and the composite scaffolds showed significantly better osteoblastic cellular response than the PDLLA scaffold. However, there was no report on the mechanical properties of the scaffolds and it cannot be ascertained if the action of the surfactant helped to improve or maintain the mechanical properties of the composite scaffold.

Furthermore, the mixing approach may lead to masking of the osteoinductive property of HA as the particles are embedded inside the polymer fibre (Gupta et al., 2009).

1.10.2 Simultaneous electrospinning and electrospraying

Electrospraying is a technique of liquid atomization by electrical forces. Due to these forces, the meniscus of a liquid flowing out of a capillary nozzle elongates, forming a fine jet, which is then atomized into fine droplets (Jaworek et al., 2009). Electrospraying has recently been combined with electrospinning to fabricate biocomposite scaffolds with properties superior to those of scaffolds fabricated by mixing. The laboratory set-up for this simultaneous electrospinning-electrospraying is shown in Figure 7. Gupta et al. (2009) reported the use of simultaneous electrospinning-electrospraying to produce biocomposite nanofibrous scaffolds of poly(L-lactic acid)-*co*-poly(ε-caprolactone)/Gelatin/HA (PLACL/Gel/HA). Nanofibrous composites electrospun from blended PLACL/Gel/HA were used as a comparison. The electrospun-electrosprayed PLACL/Gel/HA scaffolds showed higher tensile strength and tensile strain than the blended PLACL/Gel/HA scaffolds. After 15 days of culturing both scaffolds with hFob cells, a significant increase in cell proliferation was observed on the electrospun-electrosprayed scaffolds; also, the electrospun-electrosprayed scaffolds were reported to show 50% higher mineralisation after 30 days of hFob cell culture. The improved mechanical properties of the electrospun-electrosprayed PLACL/Gel/HA scaffolds over the blended PLACL/Gel/HA was attributed to the fact that electrospraying created a superficial dispersion of HA nanoparticles which did not affect the intrinsic property of the polymer as physical mixing would have done. The complete exposure of HA nanoparticles in the electrospun-electrosprayed PLACL/Gel/HA scaffold improved their osteoblast response and expression of mineralisation.

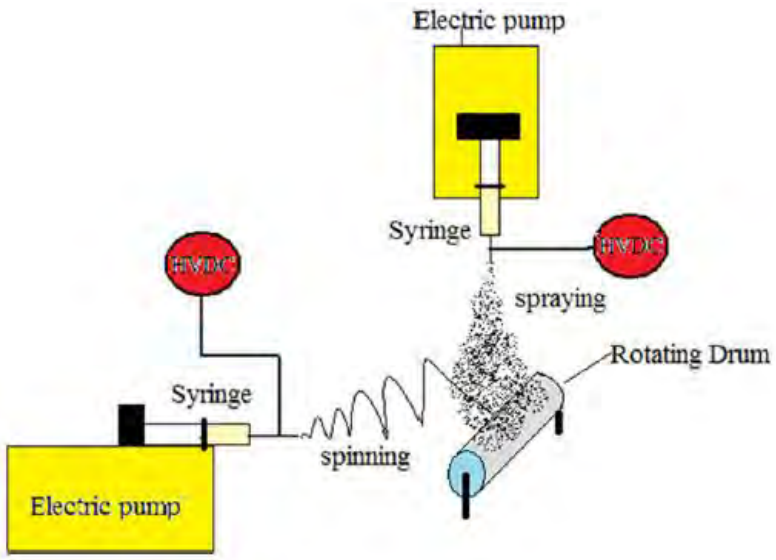

Figure 7: Laboratory set-up for simultaneous electrospinning-electrospraying (Francis et al., 2010)

Francis et al. (2010) reported the properties of nanofibrous scaffolds of Gelatin/HA (Gel/HA) fabricated by simultaneous electrospinning-electrospraying in comparison to scaffolds produced by electrospinning blends of various ratios of Gel/HA. The scaffolds were all cross-linked by glutaraldehyde to improve their mechanical properties. The pore size and porosity of the electrospun-electrosprayed Gel/HA scaffolds were comparatively greater than those of the blended scaffolds. In this case, the Gel/HA (2:1) blended nanofibrous scaffold showed a higher tensile stress (3.24 ± 0.17 MPa) than the electrospun-electrosprayed Gel/HA scaffold (2.7 ± 0.14 MPa). On the contrary, the electrospun-electrosprayed Gel/HA scaffold had a higher tensile strain at break of 41.5% as compared to 35% for the blended Gel/HA (2:1) scaffold. After 15 days of hFob cell culture, cell proliferation and mineralisation were reported to be significantly higher on the electrospun-electrosprayed scaffolds than on the blended scaffolds.

The advantage of this method over the mixing/blending method is that it creates a superficial dispersion of HA compared to the physical mixing of mechanically mismatched materials (Francis et al., 2010; Gupta et al., 2009). This inevitably results in the electrospun-electrosprayed scaffolds having better mechanical properties than the blended scaffolds. By electrospraying the HA nanoparticles, an optimum cell-material interaction can be achieved unlike in the case of blended scaffolds where the HA nanoparticles are distributed inside the nanofibres (Gupta et al., 2009; Francis et al., 2010). Furthermore, electrospraying of the HA nanoparticles onto the surface of the electrospun fibres helps to obtain a rougher surface morphology, which may improve cell attachment and proliferation (Gupta et al., 2009).

1.10.3 *In situ* synthesis followed by electrospinning

There are two stages involved in this method - firstly, the nanocomposite particles are usually made by a precipitation reaction, followed by electrospinning of the precipitated nanocomposite. Precursors such as $Ca(NO_3)_2.4H_2O$ or $Ca(OH)_2$ and $(NH_3)_2.HPO4$ or H_3PO_4 are usually mixed with the polymer (the Ca/P ratio is always kept at 1.67) and the solution is synthesised to obtain nanocomposite particles. The nanocomposite particles are then mixed with an organic solvent to form an electrospinnable mixture from which nanofibrous scaffolds are subsequently fabricated (Kim et al., 2005; Zhang et al., 2008).

Figure 8 shows the method reported by Kim et al. (2005) to produce nanofibrous scaffolds of Gel/HA with various levels of HA concentration. At high concentrations of HA (> 40%), formation of beads and non-continuous fibres was reported, suggesting that there was a maximum amount of HA that could be incorporated into the gelatin matrix to get uniform and continuous fibres. Kim et al. (2005) attributed the bead formation to the precipitation of HA crystals that were inhomogenously dispersed and formed agglomerates within the

polymer matrix. The internal structure of the nanocomposite fibre as revealed by transmission electron microscopy (TEM) showed the existence of precipitated nanocrystals of HA within the nanocomposite fibre. Compared to the tensile strength of the pure gelatin scaffold (4.6 MPa), the Gel/HA (80:20) was reported to show a higher tensile strength of 5.2 MPa but a lower strain at failure, suggesting that the HA improved the mechanical strength of the gelatin. The authors attributed this to the HA minerals integrating well with the gelatin by adopting efficient nanocomposite structure of inorganic-organic systems, thus making them stiffer and less plastic in deformation. After 3 days of MG-63 cell culture, the nanocomposite scaffolds were reported to show higher levels of alkaline phosphatase activity than the pure gelatin scaffolds (Kim et al., 2005).

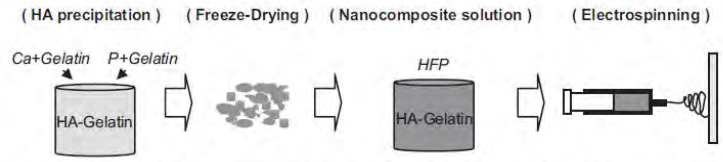

Figure 8: Electrospinning Gelatin/HA nanocomposite scaffolds using a two step process involving *in situ* synthesis followed by electrospinning (Kim et al., 2005)

Electrospinning of nanofibrous scaffolds of Chitosan (CTS)/HA through a similar two-stage method which involved the use of ultrahigh molecular weight poly(ethylene oxide) (UHMWPEO) as a fibre forming additive (in order to improve the electrospinnability of CTS which has been largely reported to be difficult to electrospin) was reported by Zhang et al. (Zhang et al., 2008). TEM and selected area electron diffraction (SAED) (Figure 9) analysis showed that the co-precipitated HA particles within the CTS matrix were unaffected by the acetic acid-dominant solvent system. On the contrary, when HA was mixed with CTS-acetic acid solution, the haze effect and characteristic diffraction rings associated with HA in Figure

9 were absent, indicating loss of the crystalline nature of HA. Zhang et al. (2008) suggested that individual HA particles interacted intensively with the CTS and were wrapped by the CTS macromolecular chains, preventing them from being directly attacked by the surrounding H^+ ions. Although both sets of scaffolds showed an initial low cell response when cultured with hFob (the authors attributed this to the presence of UHMWPEO in the scaffolds), after 15 days, the nanocomposite CTS/HA scaffolds showed a significantly higher level of cell proliferation and mineralisation in comparison to the CTS scaffolds. After 10 and 15 days of cell culture, the composite CTS/HA scaffolds were reported to show more mineral deposits than the plain CTS scaffolds, suggesting that the former favour bone formation due to the excellent osteoconductivity of HA (Zhang et al., 2008).

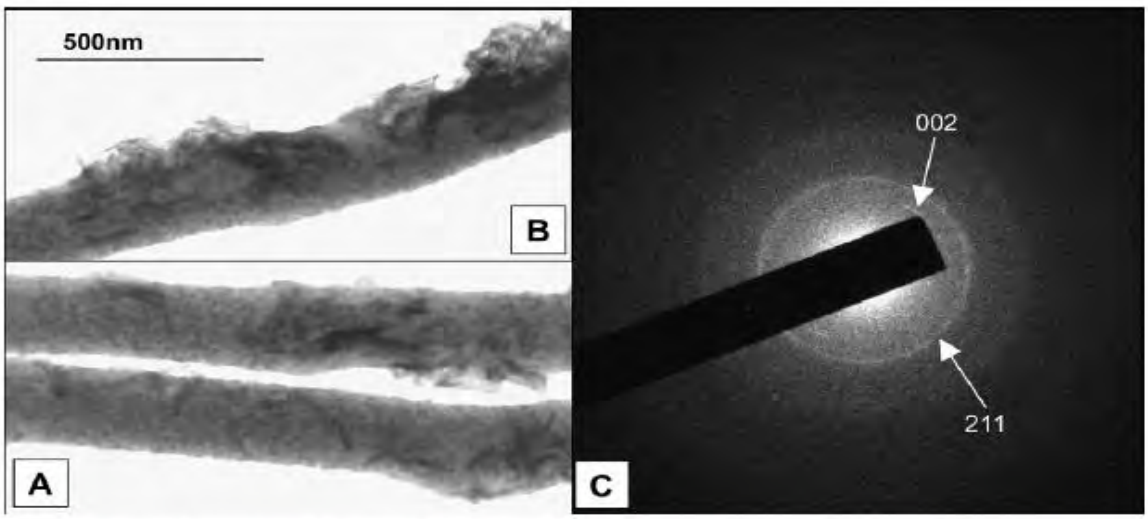

Figure 9: TEM image of as-spun CTS/HA (A,B) and SAED diffraction pattern of incorporated HA nanoparticles (C) (Zhang et al., 2008)

One major advantage of this method is the ability to fabricate nanocomposite polymer/HA scaffolds in which the HA particles are homogeneously dispersed (Kim et al., 2005). Also, it is possible to electrospin nanocomposite polymer/HA scaffolds using polymers that may be difficult to electrospin e.g. chitosan (Zhang et al., 2008). Additionally, since the HA particles

are wrapped by the macromolecular polymer chains, this could prevent demineralisation of the HA particles when the solvent system is H^+ rich (Zhang et al., 2008). However, as observed by both Kim et al. (2005) and Zhang et al. (2008), the fibre diameter of the nanocomposite fibres is usually higher than that of the plain polymer scaffold due to the inclusion of HA nanocrystals within the polymer fibre.

1.10.4 Electrospinning polymer nanofibres containing entrapped calcium or phosphorus precursors followed by *in-situ* growth of calcium phosphate on and/or within the polymer nanofibres

Polymer nanofibres can be electrospun with appropriate precursors entrapped within the fibres after which HA can be grown within and on the surface of the fibres by a precipitation reaction. Cui et al. (2007) reported the production of nanocomposite fibres of PDLLA/HA using this method. Briefly, PDLLA fibres were impregnated with calcium nitrate by electrospinning them from a solution containing calcium nitrate. The electrospun mats were then incubated in diammonium hydrogen phosphate solution - DAP. The incubation temperature and time, and also pH of the incubation solution were varied to check for their effect on the formation of the composite. The fibre diameter of the calcium nitrate-impregnated fibres as revealed by SEM (Figure 10) was 1.08 µm and the diameter further increased upon *in situ* formation of HA in and around the fibres. Cui et al. (2007) reported that the degree of developed crystals in the composite scaffolds increased with increasing incubation time; however, it seemed to peak on the 7th day after which it remained fairly constant. Furthermore, HA content and crystallinity also increased with increasing incubation temperature (Cui et al., 2007).

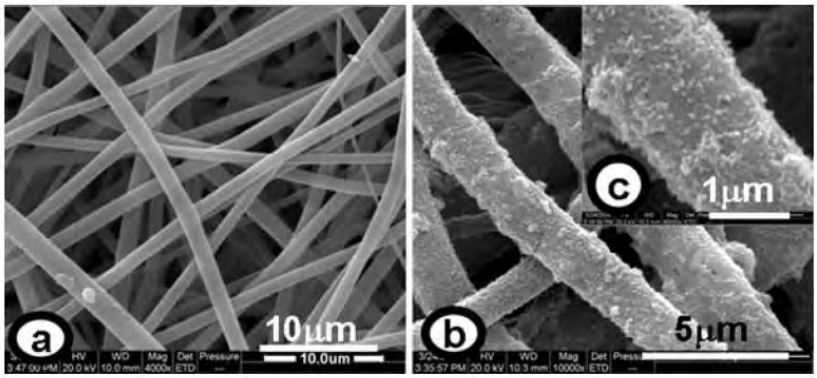

Figure 10: SEM micrographs of electrospun PDLLA fibre mat (a) with entrapment of calcium nitrate, (b) after incubation in DAP solution of pH 9.0 at 25°C for 7 days, and (c) higher magnification of (b) (Cui et al., 2007)

Much as this method is able to create homogenous dispersion of HA in and around electrospun polymer fibres, it has the disadvantage of degrading the polymer during the process. It is already established that biodegradable polymers degrade by hydrolysis (Hollinger and Battistone, 1986; Gomes and Reis, 2004; St. Pierre and Chiellini, 1986; Zong et al., 2003), and Cui and co-workers reported that there was some level of polymer degradation at all combinations of incubation time and temperature that yielded considerable amounts of HA (Figure 11).

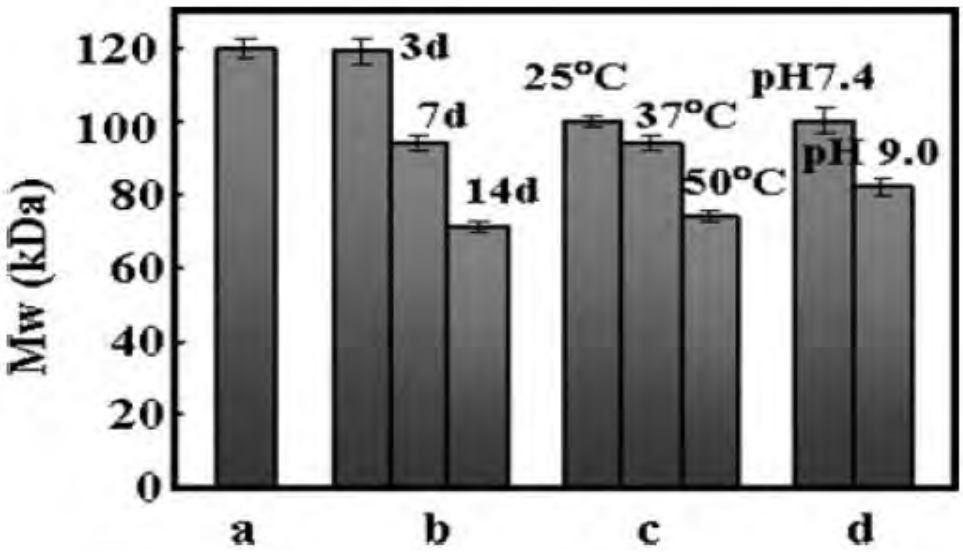

Figure 11: The molecular weight of (a) matrix polymer of electrospun fibre mats with calcium nitrate entrapment before incubation, (b) HA/PDLLA composites after incubation at 37°C in pH 7.4 DAP solution for different time periods, (c) composites after incubatation for 7 days in pH 7.4 DAP solution at different temperatures, and (d) composites after incubation at 25°C for 7 days in DAP solutions of different pH values (*n* = 3) (Cui et al., 2007)

1.10.5 Electrospinning followed by mineralisation

Electrospun polymer/HA composites can be obtained by subjecting electrospun polymer scaffolds to a mineralisation treatment (during which hydroxyapatite grows on the surface of the polymer scaffold) either by incubating them in simulated body fluid (SBF) (Chen et al., 2006; Mavis et al., 2009; Yang et al., 2008; Andric et al., 2010; Andric et al., 2011) or by subjecting them to calcium and phosphorous solution dipping treatments (Ngiam et al., 2009; Wei et al., 2011).

Composites of PLLA-HA were prepared by Chen et al. (2006) using a combination of electrospinning with a mineralisation treatment in SBF. After electrospinning, the scaffolds were incubated in SBF at 37°C for varying periods of time. The mineral phase started to form

on the surface of the fibres after 4 days of incubation. Chen et al. (2006) reported that fibre diameter and deposited mineral phase increased with increasing incubation time. It was further reported that certain conditions such as the presence of chelating agents (e.g. citric acid) and water-soluble polyanionic proteins (e.g. poly(L-aspartic acid)), and surface functional groups of PLLA have an effect on the size, shape and aggregation behaviour of the deposited mineral phase. Chelating agents and polyanionic proteins reduce the mineral growth rate and the mineral particle size. The presence of a high amount of carboxylic acid groups on the surface of the PLLA enhanced the deposition of HA on the scaffold surface, however, because these carboxylic acid groups are released from the PLLA during hydrolysis (and thus degradation of the polymer), only short term hydrolysis is advantageous for increasing HA deposition.

More recently, Andric et al. (2010) reported the electrospinning of PLLA and PLLA/Gelatin scaffolds which were subsequently mineralized in SBF in vacuum at room temperature for 2 hours. XRD characterisation of the resulting scaffolds revealed hydroxyapatite and brushite peaks, confirming the presence of hydroxyapatite on the scaffolds. The mineral content on the scaffolds increased with the addition of gelatin (their results also suggested that the mineral content varied proportionally to the gelatin content). Additionally, the mineralized scaffolds supported cellular attachment, proliferation and showed higher mineralisation than the non-mineralized scaffolds when seeded with MC3T3 cells (Andric et al., 2010).

Ngiam et al. (2009) reported the fabrication of PLGA/Collagen (PLGA/Col) scaffolds through electrospinning followed by a series of calcium and phosphate treatments. Nano-HA (n-HA) was preferentially deposited on the PLGA/Col, and the mineralized scaffolds had better early osteoblast attachment. It was found that mineralisation improved early cell capture on the fibres within a short period of time (within minutes). n-HA had a greater influence on

the functionality of cells at an early time point of culture than in intermediate cell stages (Ngiam et al., 2009).

Using the same method reported by Ngiam et al. (2009), n-HA was deposited by Wei et al. (2011) on regenerated silk fibroin nanofibrous scaffolds. It was reported that there was a good distribution of n-HA on the nanofibrous substrates and an improved alkaline phosphatase expression for mineralized silk/n-HA scaffolds in spite of the fact that at some time points during cell culture, there was a reduction in cell number. Consequently, Wei et al. (2011) concluded that the presence of nHA in the silk/n-HA nanofibres had a greater improvement on differentiation stages than on the early stages of cultivation, such as adhesion and proliferation.

With this method, it is possible to produce a polymer/HA composite with homogeneous dispersion of HA in the polymer matrix. However, as with the previous method, the disadvantage of this method lies in the fact that polymer degradation may occur during incubation, although the method used by Ngiam et al. (2009) and Wei et al. (2011) seems to overcome this limitation since the mineralisation treatment is carried out without soaking the nanofibrous scaffolds for an extended period of time.

1.11 Degradation Behaviour of Electrospun Polymer/HA Scaffolds

Recent research on electrospun polymer/hydroxyapatite composite scaffolds has been more focussed on the investigation of cell-nanofibre interactions and other characteristics such as mechanical properties and homogeneity of HA particle dispersion in the polymer (Chuenjitkuntaworn et al., 2010; Kim et al., 2006a; Prabhakaran et al., 2009; Thomas et al., 2006) and only few (Sui et al., 2007; Xu et al., 2007; Jose et al., 2010; Ito et al., 2005) have

reported any studies on the degradation properties of these composite scaffolds. HA has been shown to improve cell-scaffold interaction (Peng et al., 2011; Chuenjitkuntaworn et al., 2010) and mechanical properties (Sui et al., 2007) of electrospun polymer/HA scaffolds, however, if these materials are intended for clinical purposes, then it is essential to not only have an understanding of their cell-scaffold interaction behaviour, but an understanding of their degradation behaviour *in vitro* is also crucial as this may give an indication of their *in vivo* degradation characteristics.

Sui and co-workers (2007) reported the electrospinning of PLLA and PLLA-HA nanofibre scaffolds and conducted *in vitro* degradation studies on the scaffolds in PBS (pH 7.4) at 37^{o}C (Sui et al., 2007). For the PLLA nanofibre scaffold (average fibre diameter of 368 nm), a 10% loss in mass and a decrease in molecular weight (M_w) from 268 kDa to 201 kDa after 8 weeks were reported. Additionally, a reduction in pH from 7.40 to 7.08 and water uptake of approximately 12% was reported. On the contrary, the PLLA-HA nanofibre scaffold (average fibre diameter of 313 nm) was reported to have lost only approximately 6% of its original mass while the molecular weight had reduced from 268 kDa to 241 kDa. Furthermore, the pH was observed to decrease slightly during the first 4 weeks, and then increase up to the initial pH. According to Sui et al. (2007), the presence of HA particles in the PLLA-HA electrospun scaffold imparted hydrolytic stability to the scaffold, which was attributed to the presence of alkaline HA particles that could possibly help to neutralise the acidic environment caused by the release of the polymer degradation products (Sui et al., 2007).

In another work on the degradation of electrospun PLLA-HA composite, Xu et al. (2007) reported the electrospinning of composite fibres composed of poly(L-lactide)-grafted hydroxyapatite (PLA-g-HAP) nanoparticles within a polylactide matrix (PLA-g-HAP/PLA) (Xu et al., 2007). The authors reported an improvement in wettability as the PLA-g-HAP content

was increased. They further reported that the amount and distribution of PLA-g-HAP nanoparticles affected the degradation rate of the composite fibres, where the degradation rate was determined by calculating the reduction in mass of the electrospun scaffolds. The mass loss observed on the scaffolds was attributed to the hydrolytic degradation of the PLA and the falling-off of the PLA-g-HAP nanoparticles from the fibres. At low PLA-g-HAP content, the degradation rate was reported to be delayed due to the presence of HA particles, which due to their alkaline nature neutralised the acidic products of PLA degradation. However, the degradation rate of the scaffolds increased with an increase in the PLA-g-HAP content. The increased degradation rate with increase in the PLA-g-HAP content was attributed to the enhanced wettability of the composite fibres and the escape of the nanoparticles from the fibre surfaces during incubation. Furthermore, they reported higher pH values for degradation media of PLA-g-HAP/PLA fibres than those of PLA fibres indicating the neutralizing effect of HA particles. Similar to Sui et al. (2007), Xu et al. attributed the difference in pH values to the presence of HA particles which are alkaline in nature (Xu et al., 2007).

More recently, Jose et al. (2010) reported the electrospinning of scaffolds of PLGA (85:15) and PLGA/collagen/HA with varying PLGA/Collagen:HA ratios, on which degradation studies were conducted in a 1.0% trypsin in PBS solution (pH 7.4) at 37^{o}C over a 4-week period (Jose et al., 2010). The authors characterised the degradation behaviour of the scaffolds by calculating the reduction in mass of the scaffolds. For the multicomponent scaffolds, a high initial mass loss, followed by gradual decline for the rest of the degradation period, was observed. The PLGA scaffold, on the contrary, exhibited an initial low mass loss during the 1st day, followed by a tremendous decline in mass over the remainder of the degradation period. The high initial mass loss of the multicomponent scaffolds was ascribed to a

combination of high surface area of nanofibres and the increased hydrophilicity of the scaffolds (due to the presence of nano-HA and collagen). However, it was further noted that the presence of high molecular weight chains of PLGA, cross-linked gelatin and nano-HA (which exhibits an acid-neutralising characteristic) resulted in stable mass retention after the large initial mass loss (Jose et al., 2010).

The method of simply mixing HA particles with polymer solutions prior to electrospinning in order to fabricate electrospun polymer/HA scaffolds has been reported to cause a decrease in fibre diameter. Chuenjitkuntaworn et al. (2010) reported a reduction in fibre diameter from 3.3 ± 1.1 µm to 2.3 ± 0.7 µm when the concentration of HA particles mixed with PLLA prior to electrospinning was increased from 0 wt% to 0.25 wt% (Chuenjitkuntaworn et al., 2010). Chuenjitkuntaworn et al. (2010) attributed the decrease in fibre diameter to an increase in flow restriction of the polymer solution due to the presence of the HA particles. This reason is plausible, considering the relatively large diameter (≈234 nm) (Chuenjitkuntaworn et al., 2010) reported for the HA particles used in their work. Similarly, Jose et al. (2010) reported a reduction in fibre diameter from 269 nm to 179 nm when the concentration of HA particles mixed with PLGA/Collagen was increased from 0 wt% to 1 wt%. The reduction in fibre diameter was attributed to the presence of phosphate and calcium ions of HA in polymer solution which resulted in increased solution conductivity, increased stretching of the electrospinning jet and a consequent decrease in fibre diameter (Jose et al., 2010). As in the work of Chuenjitkuntaworn et al. (2010), it is also possible that the large diameters of the HA particles in this work (100-150 nm) (Jose et al., 2010) caused a restriction in the flow of the polymer solution during electrospinning. Xu et al. (2007) reported a similar reduction in fibre diameter from 1.10 µm to 600 nm when the concentration of PLA-g-HAP particles was increased from 0 wt% to 30 wt%. They also

reported that increasing the PLA-g-HAP concentration resulted in an increase in electrical conductivity and a decrease in viscosity of the polymer solutions. The increase in electrical conductivity was attributed to the polarity of the HAP particles, while the decrease in viscosity was attributed to the molecular aggregation of PLA chains around the PLA-g-HAP particles (Xu et al., 2007). In this case, it was difficult to determine if the PLA-g-HAP particles caused a restriction of polymer solution flow, because although the HAP particle diameter was reported to be in the range of 20-40 nm (Xu et al., 2007), no dimensions were reported for the PLA-g-HAP particles.

The reduction in fibre diameter of electrospun polymers upon inclusion of HA particles may be due to a combination of all of the above reasons given by Jose et al. (2010), Chuenjitkuntaworn et al. (2010) and Xu et al. (2007). The work of Takahashi et al. (1978) established clearly that the OH^- ion is the charge carrier in hydroxyapatite (Bouhaouss et al., 2001; Takahashi et al., 1978), and therefore the increase in solution conductivity may be due to the OH^- ions.

Contrary to the above reports, Sui et al. (2007) reported only a small decrease of the fibre diameter in the composite scaffolds (Mei et al., 2007; Sui et al., 2007). The reason for this may be due to the fact that Sui et al. (2007) did not directly mix HA particles with the polymer solution, but instead they used a two solvent system, where HA particles were dispersed first in 1,4-dioxane prior to the addition of PLLA dissolved in dichloromethane to the suspension. In addition, the diameter of the HA particles reported in their work (15 nm) (Sui et al., 2007) was very small in comparison to the works of Chuenjitkuntaworn et al. (2010) and Jose et al. (2010), so that the possibility of the HA particles restricting the flow of the polymer solution during electrospinning was much lower.

The reduction in fibre diameter upon the mixing of HA particles with polymer solutions prior to electrospinning could result in a change in their degradation characteristics. Degradation has been shown to vary with fibre diameter. For instance, Bolgen et al. (2005) reported the *in vitro* degradation of PCL electrospun nanofibres of different diameters for a period of 6 months. The authors reported, that overall, thinner fibres exhibited higher degradation rates in mechanical strength when compared to thicker ones (Bolgen et al., 2005). On the contrary, Dong et al. (2009), in their review, suggested that the degradation rate of electrospun PLGA (both 75:25 and 50:50) nanofibres decreased with reduction in fibre diameter (Dong et al., 2009). Furthermore, in their work on the *in vitro* degradation of PLLA nanofibre foams produced by liquid-liquid phase separation, Chen and Ma (2006) reported faster degradation rates for PLLA nanofibre foams when compared to solid-walled PLLA foams and attributed the faster degradation rate of the PLLA nanofibre foams to the higher surface area of the nanofibre foams in comparison to the solid-walled foams (Chen and Ma, 2006). Unlike the degradation of millimetre and micron-sized polymers, in which an increase in size has been reported to result in faster degradation rates due to autocatalysis (Grizzi et al., 1995), it has been reported recently, that the probability of the occurrence of autocatalysis during degradation of polymer nanofibres is low because the soluble hydrolytic products can be easily diffused into the degradation medium (Dong et al., 2009; Dong et al., 2010; Kim et al., 2003; Dahlin et al., 2011; Chen and Ma, 2006). Consequently, since fibres with smaller diameters will possess a higher surface area-to-volume ratio, it may be possible that the thinner fibres formed as a result of the mixing of HA particles with polymer solutions prior to electrospinning may exhibit higher degradation rates in comparison to larger fibres.

However, there have been no studies covering what effect the reduction of fibre diameter upon the inclusion of HA particles in electrospun polymer scaffolds will have on the degradation characteristics of the electrospun scaffold. A study of the *in vitro* degradation properties of electrospun polymer/HA scaffolds will therefore help to provide some indication into how successful such scaffolds with small average fibre diameters will perform when utilized *in vivo.*

1.12 Aims and Objectives

Electrospinning as a research area has developed exponentially over the last two decades. However, although a lot of progress has been made regarding the formation of fibres with uniform and controlled morphology, there is still a lack of understanding of certain aspects of the process:

1. Control over the crystallinity of electrospun fibres; and
2. Degradation behaviour of electrospun scaffolds, especially of electrospun polymer/HA scaffolds.

This may be due to one or more of the following reasons. Firstly, although the process is relatively simple to set up, the dynamic nature of the process, the effect of which can be seen in the drastic changes which can occur in fibre properties by a small variation in one of the electrospinning parameters, has probably made it difficult to understand in full details certain aspects of the process. Additionally, the fact that the process is influenced by environmental factors such as temperature and humidity may introduce some inadvertent variation in the properties of fibres produced using the same electrospinning parameters albeit on different days.

Since electrospun fibres are considered as potential materials for use in areas such as energy, defence and security, environmental engineering and biotechnology and healthcare, it is therefore important that an understanding of the properties of these fibres be properly investigated. It is also important that investigations be conducted into how the electrospinning process can be used to control/alter the properties of fibres so produced; in particular, the crystalline properties of electrospun fibres. This is because the crystalline properties of a material are very important as they have a direct influence on other properties such as the mechanical strength and degradation rate of the material. If the electrospinning process can be used to control the degree of crystallinity of electrospun fibres, it means that it will be possible to produce fibres of controllable/tailorable crystallinities. The impact of this will be far reaching and would not be confined to the fabrication of tissue engineering scaffolds, as it will be possible to electrospin fibres with superior mechanical properties for use as filler materials in composites by simply controlling their crystallinity.

Research on electrospinning for tissue engineering purposes has established that the addition of materials such as hydroxyapatite to biodegradable polymers is capable of improving scaffold properties such as tensile strength and biocompatibility, however, an area where there is currently limited understanding of the properties of these electrospun polymer/HA fibres is their degradation properties. Studies have shown that addition of hydroxyapatite particles does not only improve the mechanical properties of electrospun polymer/hydroxyapatite scaffolds, but hydroxyapatite also maintains the pH at non-toxic levels by neutralising the acidic degradation products of polyesters (Zhang et al., 2007b). Studies have also shown that mixing HA particles with polymer solutions prior to electrospinning reduces the diameters of the electrospun fibres. Furthermore, it has been

shown that the fibre diameter can influence the degradation behaviour/characteristics of an electrospun scaffold. However, there have been no reports in the literature concerning what effect the reduction in fibre diameter upon inclusion of HA particles in electrospun polymer scaffolds will have on the degradation characteristics of the scaffolds.

Furthermore, bone-tissue engineering researchers have sought to electrospin materials with characteristics similar to those of bone. Usually, a synthetic polymer has been blended with/without a natural polymer, and then hydroxyapatite is incorporated into the polymer system using one of the methods described in Section 1.10. However, the research for the ideal scaffold for bone-tissue engineering is still ongoing, and is probably still in its early stages.

Based on the previous paragraphs, this work aims to achieve the following:

I. To investigate the possibility of tailoring the crystallinity of electrospun scaffolds by carefully controlling the electrospinning parameters (henceforth also referred to as crystallinity studies);
II. Based on the understanding and experience developed in achieving Objective I, electrospin PLLA and PLLA-HA scaffolds and study their degradation behaviour; and
III. To fabricate and characterise bi- and multicomponent scaffolds of PLLA for bone-tissue engineering.

2.0 Materials and Methods

2.1 Materials

PLLA (M_w ≈ 220,000) was supplied by Goodfellow Chemicals, Cambridge, UK. Dichloromethane (DCM) (puriss. p.a., ACS reagent, ≥99.9%) and Gelatin (from porcine skin) type A, ≈300g Bloom were purchased from Sigma Aldrich, UK. In addition, hydroxyapatite nanopowder (particle size < 200 nm), 2,2,2-Trifluoroethanol (TFE) (puriss., ≥99.0%), methanol (puriss. p.a. Reagent ACS) and phosphate buffer saline (PBS) tablets were purchased from Sigma Aldrich, UK. N,N-Dimethylformamide (DMF) (>99% assay) was purchased from Fisher Chemicals, while glass coverslips (15 mm diameter) were purchased from VWR International Ltd., Lutterworth, UK.

Adult human osteoblasts (HOBs) were purchased from Health Protection Agency (HPA) (formerly known as European Collection of Animal Cell Cultures). Fetal calf serum, Dulbecco's modified eagle medium (DMEM) and Dulbecco's phosphate buffered saline (PBS) for cell culture were purchased from PAA laboratories. Cetylpyridinium chloride, Alizarin red powder, Hexamethyldisilazan (HMDS) (Fluka, for GC derivatization, ≥99.0%), Tris (BioXtra, pH 10.5–12.0, ≥99.9%), Sodium chloride (NaCl) (Bioreagent, ≥99.5%), Ethylenediaminetetraacetic acid (EDTA) (Aldrich, ≥99.995% assay), Hydrochloric acid, Hoechst 33258, Triton X-100, Goat serum, Bovine serum albumin and *p*-nitrophenylphosphate tablets (SigmaFast) were purchased from Sigma Aldrich, UK. FTIC-conjugated phalloidin, 4',6-diamidino-2-phenylindole (DAPI) Prolong Gold Antifade Reagent and AlamarBlue® were purchased from Molecular Probes.

2.2 Methods

2.2.1 Solution preparation

Two different types of PLLA solutions were prepared:

a) PLLA in DCM/DMF – PLLA granules were dissolved in a 75:25 mixture of Dichloromethane/N,N-Dimethylformamide. The dissolution was carried out at room temperature with gentle stirring. For crystallinity studies, four solutions of PLLA in DCM/DMF with different concentrations were made, specifically, 2, 5, 8, and 10 wt%.

   In order to prepare the PLLA-HA solution, PLLA granules and HA were mixed in the ratio 95:5 in a 75:25 mixture of DCM/DMF to give a 5 wt% solution (with respect to the solvent). The mixture was sonicated for 1 hour prior to electrospinning.

   At a later stage of the project, four solutions of PLLA in DCM/DMF with different concentrations were made, specifically, 5, 6, 7 and 8 wt%.

b) PLLA in TFE – PLLA granules were dissolved in TFE at various concentrations. The dissolution was carried out at room temperature with gentle stirring. Solutions of 8, 9, 10, 11, 12, 13, 14, and 15 wt% were prepared.

   In order to prepare the PLLAGel solution, PLLA and gelatin were blended at various weight ratios in TFE to yield solutions of 2, 3, 4, 5, 8, 9 and 15 wt% with respect to the solvent. Specifically, for the 2, 3, 4 and 5 wt% solutions, PLLA and gelatin were blended in a 1:1 ratio; for the 8 wt% solution, PLLA and gelatin were blended in the following ratios – 75:25 and 80:20; for the 9 wt% solution,

PLLA and gelatin were blended in a 75:25 ratio whilst for the 15 wt% solution, they were blended in the following ratios – 90:10 and 80:20.

The HA solution was prepared by mixing HA nanopowder with methanol to give a 4 wt% solution of HA in methanol in accordance with the method reported by Gupta et al. (Gupta et al., 2009).

For cell culture, immunocytochemistry (ICC) block buffer was made up in Dulbecco's PBS with 1% goat serum, 1 mg/ml bovine serum albumin, and 0.1% Triton X-100. Additionally, Tris-Sodium Chloride-EDTA buffer solution - TNE was made by adding 0.121 g Tris (10 mM), 11.688 g NaCl (2 M) and 0.0292 g of EDTA (1 mM) to 100 ml of deionized water. The final pH of the solution was adjusted to 7.4 with concentrated HCl. Hoechst stock solution was made by dissolving 1 mg of Hoechst 33258 per 1 ml of deionized water. The Hoechst stain working solution was made by diluting Hoechst stock solution with TNE to a final concentration of 20 µg/ml.

2.2.2 Kinematic viscosity

The kinematic viscosities of the different PLLA-DCM/DMF solutions described above were obtained using an Ostwald U-tube viscometer (Cannon Instrument, USA) enclosed in a water bath at 25^{o}C. The viscosities were calculated using the following formula supplied by the manufacturer

$$\nu = t\ x\ k \qquad (1)$$

Where

ν = kinematic viscosity (cSt), t = efflux time (s), and k = viscometer constant (0.03 cSt/s).

2.2.3 Electrospinning

Two different electrospinning machines were used during the course of the project. The first electrospinning machine was a Model ES1a electrospinning machine manufactured by Electrospinz Ltd, New Zealand. This electrospinning machine is shown in Figure 12. This machine was only used to electrospin fibres used for crystallinity studies and degradation studies on PLLA-HA. A static aluminium foil target was used to collect the non-woven electrospun fibres. In order to prepare the samples used for the crystallinity studies, a systematic variation of three electrospinning parameters, namely: polymer solution concentration, applied voltage and needle tip to collector distance (NTCD) was conducted. During each electrospinning experiment, two of these parameters were held constant while the third one was varied. The electrospinning was carried out at room temperature. The electrospun fibres were stored in a dessicator for 1 week to allow for complete evaporation of the residual solvent. The 2 and 10 wt% solutions could not be electrospun due to their low and high viscosities, respectively. Additionally, a low yield of fibres from the 5 and 8 wt% solution concentrations was also observed using 10 kV applied voltage, showing that 10 kV was too low for successful electrospinning of the solutions. In preparing the samples used to study the degradation characteristics of electrospun PLLA and PLLA-HA, fibres were electrospun from the 5 wt% solutions of PLLA and PLLA-HA solutions at room temperature, electrospinning voltage of 25 kV and needle-tip-to-collector distance of 12.5 cm for both sets of electrospun scaffolds. The needle tips (Axygen, T-200-4) used to electrospin the fibres for crystallinity studies had an orifice diameter of 0.8 mm, while the needle tips (Diamond D200, Gilson) used to electrospin fibres for degradation studies of PLLA and PLLA-HA had an orifice diameter of 0.9 mm. The electrospun scaffolds were stored in a vacuum desiccator for 1 week to remove any residual solvent.

At a later stage of the research project, another electrospinning machine was set up. This design was based on the more commonly used programmable syringe pump-horizontal collector design and is shown in Figure 13. Although this machine was briefly used to electrospin 5, 6, 7 and 8 wt% PLLA in DCM/DMF solutions, it was otherwise strictly used to produce the nanofibrous scaffolds of PLLA, PLLAGel and PLLAGel-HA from TFE and methanol solutions.

The electrospinning set-up consisted of an adjustable DC power supply (Model 73030P, Genvolt, UK) capable of generating DC voltage in the range 0-30 kV, a programmable syringe pump (Aladdin 300, World Precision Instruments, USA) on which a 10 ml syringe (BD, New Jersey) was attached to a blunted 25G 1-inch stainless steel needle (BD, New Jersey), and a stainless steel plate covered with aluminium foil as collector.

For the electrospinning of PLLA, the electrospinning parameters used were (Table 1):

a) Applied voltage of 13 kV;
b) Collector distance of 17.5 cm; and
c) Flow rate of 0.5 ml/h.

For the electrospinning of PLLAGel, the electrospinning parameters used were (Table 1):

a) Applied voltage of 12 kV;
b) Collector distance of 18 cm; and
c) Flow rate of 0.75 ml/h.

For the cell culture and the degradation study specimens, glass coverslips of 15 mm diameter were placed on to the aluminium-foil-covered-collector to collect nanofibrous scaffolds.

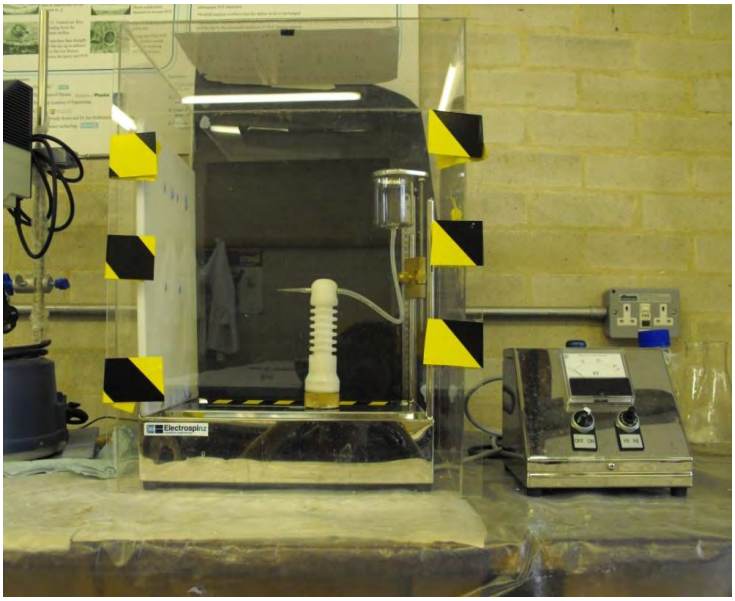

Figure 12: ES1a Electrospinning machine

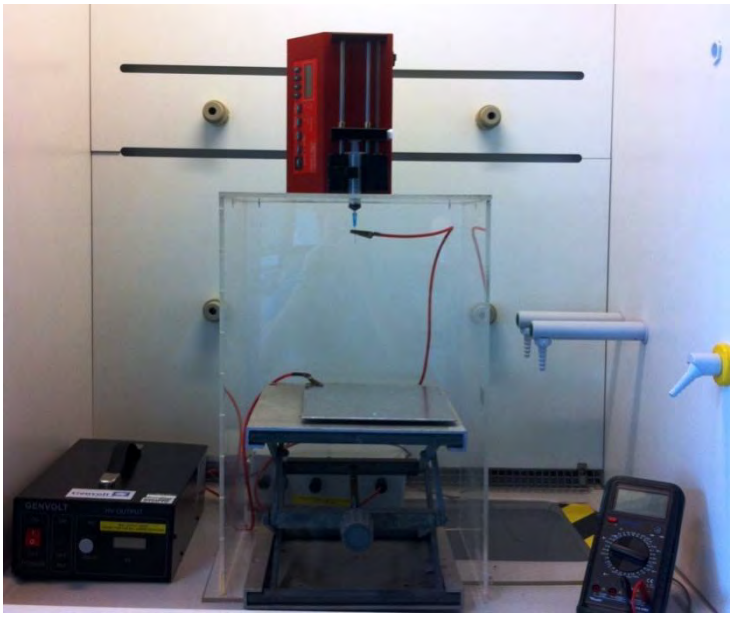

Figure 13: 2nd electrospinning machine

Table 1: **Electrospinning parameters**

Sample	Composition	Flow rate (ml/h)	NTCD (cm)	Voltage (kV)
PLLA	15 % (w/v) in TFE	0.5	17.5	13
PLLAGel (90:10)	15% (w/v) in TFE	0.75	18	12

2.2.4 Electrospraying

The HA-methanol mixture was sonicated for 1 hour prior to electrospraying. This mixture was fed into a syringe and then electrosprayed onto a freshly electrospun PLLAGel nanofibrous scaffold (Francis et al., 2010; Gupta et al., 2009). The HA:PLLAGel ratio used was 5:95. The optimum conditions for electrospraying HA were determined to be at an applied voltage of 9 kV, collector distance of 12 cm and flow rate of 2 ml/h.

All the prepared scaffolds were stored in a dessicator for 7 days to allow for complete evaporation of the residual solvent before further processing.

2.2.5 Characterisation

2.2.5.1 Porosity

The apparent density and porosity of the nanofibrous scaffolds were calculated using the following equations (Gupta et al., 2009; He et al., 2005; Ma et al., 2005):

$$\text{Scaffold apparent density } (\text{g/cm}^3) = \frac{\text{Scaffold mass (g)}}{\text{Scaffold thickness (cm)X Scaffold area (cm}^2\text{)}} \quad (2)$$

$$\text{Scaffold porosity } (\%) = \left(1 - \frac{\text{Scaffold apparent density } \left(\frac{\text{g}}{\text{cm}^3}\right)}{\text{Bulk density of PLLA } \left(\frac{\text{g}}{\text{cm}^3}\right)}\right) \text{X } 100\% \quad (3)$$

The thicknesses of the nanofibrous scaffolds were measured by a digital micrometer (Mitutoyo IP65, Japan) with an accuracy of ± 0.001 mm. The bulk density of PLLA was taken

as 1.25 g/cm³ (given by manufacturer) while the bulk density of gelatin was taken as 1.27 g/cm³ (Whelan, 1994). The bulk density of the blended scaffolds was calculated using the following equation (Whelan, 1994):

$$\rho_{PLLAGel} = (W_{PLLA} X\ \rho_{PLLA}) + (W_{Gelatin} X\ \rho_{Gelatin}) \quad (4)$$

Where

$\rho_{PLLAGel}$ = Bulk density of PLLAGel, W_{PLLA} = Weight fraction of PLLA in polymer blend, ρ_{PLLA}= Bulk density of PLLA, $W_{Gelatin}$= Weight fraction of gelatin in polymer blend, and $\rho_{Gelatin}$ = Bulk density of gelatin.

10 thicknesses, measured from different areas on the scaffold were recorded per scaffold type. These thickness measurements were used to calculate the scaffold apparent density using equation (2), values of which were used to calculate the scaffold porosity according to equation (3). The scaffold porosity results were calculated as the average ± standard deviation.

2.2.5.2 Scanning electron microscopy

In scanning electron microscopy, a fine beam of electrons is scanned across the surface of a specimen to which a light conducting film has been applied. Secondary electrons emitted when the beam hits the specimen are collected to provide a signal used to modulate the intensity of the electron beam in a television tube to form an image that corresponds to the small raster and information, pixel by pixel, emanating from the specimen surface, scanning in synchronism with the microscope beam (Billmeyer, 1984).

An Environmental Scanning Electron Microscope (ESEM) was used in this case in order to obtain high resolution images. The morphology of the nanofibrous scaffolds was obtained using a Philips XL-30 FEG ESEM at an accelerating voltage of 10 kV. Four different specimens

were cut from each sample and then mounted on an aluminium stub using a carbon adhesive film. Prior to viewing in the microscope, the specimens were sputter coated with platinum using an Emscope SC500 (Emscope laboratories, Kent, UK) Sputter Coater. Coating was carried out at a current of 25 mA for 3 minutes. The diameters of 320 different random fibres were measured from four different ESEM images using Image J software (National Institutes of Health, USA). The average fibre diameters were calculated as the average of these 320 measurements. For the samples used in the degradation study, the initial and final average fibre diameters of the degraded samples were calculated from ESEM images of electrospun scaffolds taken pre-degradation and post-degradation, respectively.

Using at least 8 different images of each type of electrospun nanofibrous scaffold, inter-fibre distances, F_d, were calculated using the empirical model (Chuenjitkuntaworn et al., 2010; Sanders et al., 2005):

$$F_d = 0.5/\sqrt{N/A} \quad (5)$$

Where

N = Number of fibres, and A = Viewing area.

2.2.5.3 Fourier transform infrared spectroscopy

Fourier transform infrared spectroscopy (FTIR) works on the principle that emission or absorption spectra arise when molecules undergo transitions between quantum states corresponding to two different internal energies. Most polymers absorb electromagnetic radiation in the infrared region (i.e. 1-50 μm). Frequencies within this range are associated with molecular vibration and vibration-rotation spectra. The infrared spectra of polymers is relatively simple, first, because the vibrations of groups of atoms take place at a frequency which is often independent of the length of the polymer chain and, second, from the strict

selection rules that prevent many of the vibrations from causing absorptions. It is possible to use FTIR spectroscopy for structural characterisation as well as identification (Billmeyer, 1984; Young, 1981).

Since FTIR is capable of identifying chemical groups (Billmeyer, 1984), it was used to confirm the presence of gelatin in the nanofibrous scaffolds electrospun from the polymer blend.

FTIR spectra of the scaffolds were obtained with a Nicolet FTIR spectrometer (Magna-IR 860) using a golden gate single reflection diamond Attenuated Total Reflectance attachment. 100 scans were recorded for each spectrum at a resolution of 4 cm^{-1} in the range 650–4000 cm^{-1}.

2.2.5.4 Energy dispersive X-ray spectroscopy

Energy dispersive X-ray spectroscopy (EDS) is a chemical microanalysis technique used in conjunction with SEM. The EDS technique detects x-rays emitted from the sample during bombardment by an electron beam to characterise the elemental composition of the analysed volume. During elemental mapping, characteristic x-ray intensity is measured relative to lateral position on the sample. Variations in x-ray intensity at any characteristic energy value indicate the relative concentration for the applicable element across the surface. One or more maps are recorded simultaneously using image brightness intensity as a function of the local relative concentration of the element(s) present (Hanke, 2010).

The presence and distribution of HA in the electrospun PLLA-HA and PLLAGel-HA nanofibrous scaffolds was characterised qualitatively using Energy Dispersive Spectroscopy (EDS; Oxford INCA) mapping in a Philips XL-30 FEG ESEM. Specimens were cut from the edges and the middle of the electrospun scaffolds. These specimens were coated with

carbon prior to EDS to avoid the overlap of the peaks of gold and phosphorous (Hong et al., 2008; Chuenjitkuntaworn et al., 2010; Sui et al., 2007).

2.2.5.5 Differential scanning calorimetry

Differential scanning calorimetry is a technique which combines the ease of measurement of heating and cooling curves with the quantitative features of calorimetry. Typically, a small portion of a sample is placed in an aluminium pan and heated and/or cooled in a controlled manner. A reference material simultaneously undergoes the same programmed time/temperature routine. Temperature is measured continuously, and a differential technique is used to assess the heat flow into the sample and to equalize incidental heat gains and losses between the reference and the sample (Hanke, 2010; Wunderlich, 2005).

A PerkinElmer DSC 7 was used to obtain the thermal characteristics of the electrospun nanofibrous scaffolds. In order to avoid oxidative degradation, the samples and reference pans were purged with nitrogen gas (Loo et al., 2006) at a rate of 20.0 mL/minute. The temperature and power were calibrated using an indium standard. Approximately 5 mg of sample were taken through a temperature scan of 25^{o}C to 200^{o}C at a heating rate of 10^{o}C/min (1st heating cycle), held at 200^{o}C for 2 minutes, followed by cooling to 25^{o}C at a heating rate of 10^{o}C/min. After this scan, the samples were reheated from 25^{o}C to 200^{o}C at 10^{o}C/min (2nd heating cycle).

For the PLLA scaffold, the value for the degree of crystallinity was calculated using the equation below (Mezghani and Spruiell, 1998; Fambri et al., 1997; Sichina, 2000):

$$X_c\ (\%) = \frac{\Delta H_f^m - \Delta H_c^m}{\Delta H_f^{100\%}} \times 100\% \qquad (6)$$

Where

X_c = Degree of crystallinity (%), ΔH_f^m = Heat of fusion (J.g^{-1}), ΔH_c^m = Heat of cold crystallisation (J.g^{-1}), and $\Delta H_f^{100\%} =$ Heat of fusion for 100% crystalline material (93.6 J.g^{-1}) (Fambri et al., 1997).

For the blend-based scaffolds, the values for degree of crystallinity of the PLLA phase were calculated using a modified form of equation (6) (Chen et al., 2005):

$$X_c^{PLLA}\,(\%) = \frac{\Delta H_f^m - \Delta H_c^m}{W_{PLLA}\,\mathrm{X}\,\Delta H_f^{100\%}} \times 100\% \qquad (7)$$

Where

W_{PLLA} = Weight fraction of PLLA in the blend, and X_c^{PLLA} = Degree of crystallinity of the PLLA phase.

2.2.5.6 Tensile testing

A tensile test is a method for determining behaviour of materials under axial loading. The tests are conducted by fixturing the specimen into the test apparatus and then applying a force to the specimen by separating machine crossheads (Hanke, 2010).

The tensile properties of the electrospun nanofibrous scaffolds were characterised using a MicroTester (INSTRON 5848; Norwood, MA, USA) with a 100 N load cell moving at a crosshead speed of 5 mm/min. The specimens were cut out using a dumb-bell shaped die according to ASTM Standard D638 to ensure uniformity and to isolate the failure point away from the grips. The specimens had a width of 3.9 mm, a gauge length of 14.6 mm and thicknesses that ranged from 28 to 50 µm. Cardboard strips were attached to both ends of the specimens to improve gripping in the tensile testing machine. A sample of the specimens prior to testing is shown in Figure 14. At least seven specimens were tested per sample type, as recommended by ASTM Standard D638. Since the fibres in the scaffolds

were not bonded to one another, and exhibited a microstructure which closely resembled the fibres in paper, the tensile properties were calculated in accordance with the methods recommended for paper in ASTM Standard D828. The tensile strength was calculated by dividing the load by the initial width of the specimen, while the engineering strain (hereafter referred to simply as strain) was calculated by dividing the elongation (this was the crosshead displacement of the tensile testing machine) by the initial guage length. The percent elongation at break was calculated by multiplying the strain by 100%. Finally, the tensile stiffness was calculated as the slope of the elastic region of the stress-strain curve.

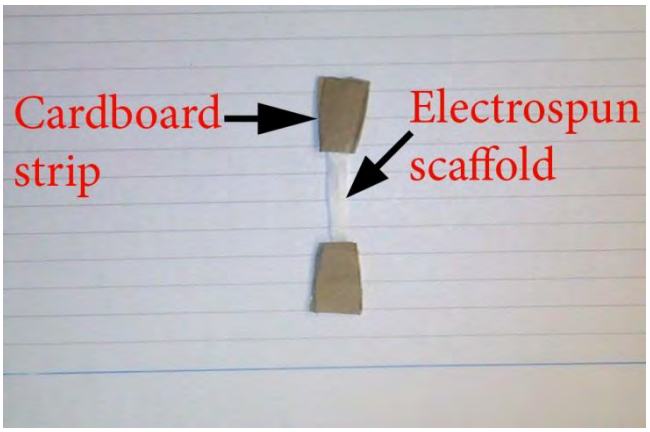

Figure 14: Typical tensile test specimen, showing cardboard strips used for improving grip in machine

2.2.5.7 Interferometry

Interferometric measurements of samples were performed using a MicroXAM2 interferometer (Omniscan, UK), operating using a white light source. Samples were imaged using a 50X objective lens, acquiring images in a grid array, which were subsequently stitched together. Scanning Probe Image Processor software (Image Metrology, Denmark) was employed for the analysis of acquired images, yielding S_a (roughness average) and S_q (root mean square) values for surface roughness. A minimum of 3 samples was tested per scaffold type and results were calculated as the average ± standard deviation.

2.2.5.8 Degradation studies

2.2.5.8.1 Degradation

The degradation solutions were made by dissolving Phosphate Buffer Saline (PBS) tablets in distilled water. Scaffolds of a known initial weight (M_i) were placed into glass vials containing 5 ml of PBS which were then incubated at 37^{o}C. Five samples were taken out at the end of each degradation period, rinsed with distilled water to remove any salt deposits, followed by drying in a desiccator until constant sample weights were observed. After drying, the samples were weighed to obtain their final weight (M_f). Subsequently, the weight loss percentage (W_l) was calculated using equation 8.

$$W_l(\%) = \left(\frac{M_i - M_f}{M_i}\right) X\ 100\% \qquad (8)$$

Where

W_l = Weight loss percentage, M_i = Initial weight, and M_f = Final weight.

2.2.5.8.2 pH monitoring

The pH of the degradation solutions was measured at weekly intervals using a Checker HI 1270 Handheld pH meter. The pH meter was calibrated using standard pH buffers (HANNA instruments) before each use.

2.2.5.8.3 FTIR

FTIR spectra of the scaffolds were obtained with a Nicolet FTIR spectrometer (Magna-IR 860) using a golden gate single reflection diamond Attenuated Total Reflectance attachment. 64 scans were recorded for each spectrum at a resolution of 4 cm^{-1} in the range 650–4000 cm^{-1}. The area of the carbonyl (C=O) peak was calculated using the software supplied with the FTIR equipment (OMNIC - Thermo Scientific); in order to avoid any

variations, a constant baseline was used for calculating the area of all specimens within each scaffold type. Finally, the C=O peak area was plotted as a function of degradation time.

2.2.5.8.4 Molecular weight

The molecular weights of the samples were measured by Gel Permeation Chromatography (GPC) at Smithers Rapra, Shawbury, UK. Chloroform was used as the eluent; the flow rate was 1.0 mL/min; and PLgel guard columns were used. Polydispersity was calculated as a ratio of the weight-average molecular weight (M_w) to the number-average molecular weight (M_n).

2.2.5.9 Biocompatibility studies

2.2.5.9.1 Adult human osteoblasts (HOB) cell culture

HOBs were cultured in DMEM supplemented with 10% fetal calf serum and grown in a humidified incubator at 37^{o}C with 5% CO_2. The cells used were at a passage number from 2 - 5, and were harvested at 80% confluence. All quantitative results were obtained from three independent experiments. The data generated was calculated as the mean of the triplicate experiments and presented as mean ± standard deviation.

2.2.5.9.2 Cell attachment and morphology (SEM, Confocal microscopy – phalloidin staining for f-actin)

The morphology and attachment of cells seeded onto the electrospun nanofibrous scaffolds were investigated by SEM. The electrospun scaffolds were sterilized under UV light for 30 minutes after which they were placed into 12-well cell culture plates. The electrospun scaffolds were then seeded with cells at a density of 1 x 10^5 cells/well. Plain glass coverslips

were used as control. The electrospun scaffold samples seeded with HOBs (constructs) for both SEM and fluorescence microscopy, were incubated for 1.5, 4 and 24 hours.

At the end of each time period, the constructs were gently rinsed twice with PBS and then fixed with glutaraldehyde in Dulbecco's PBS for at least 30 minutes at 4^{o}C. Thereafter, they were rinsed twice with PBS and then dehydrated using a series of graded alcohol solutions (50%, 70%, 90% and 100%), taking special care to prevent the cells from drying out. Finally, the constructs were placed in HMDS and left in a fume cupboard until the HMDS completely evaporated. The dried constructs were sputter coated with gold and observed under SEM (Zeiss EVO 60 EP SEM) at an accelerating voltage of 5 kV.

Cell attachment was investigated using fluorescence microscopy by staining the f-actin cytoskeleton using FTIC-conjugated phalloidin and nuclear staining with DAPI-Prolong. Cells were fixed with 3% paraformaldehyde (PFA) for 15 minutes at room temperature before being permeabilised and blocked using ICC block buffer at room temperature for 30 minutes. For each sample, 5 µl of a 6 µM stock solution of FTIC-phalloidin was added to 200 µl ICC buffer and incubated at room temperature for 30 minutes. The constructs were analysed using a confocal microscope (Zeiss LSM 510 Meta) at 63x magnification.

2.2.5.9.3 Cell proliferation and viability

Prior to being seeded with cells, the electrospun scaffolds were sterilized under UV light for 30 minutes after which they were placed into 12-well cell-culture plates. Finally, cells were seeded on to the scaffolds at a density of 2 x 10^3 cells/well. Plain glass coverslips were used as control. The culture media was changed twice each week (every 3-4 days) and replaced with fresh complete culture media, i.e. DMEM + 10% fetal bovine serum + 150 mg/l of ascorbic acid. Samples were incubated for 1, 3, 7, 14 and 21 days for both assays.

2.2.5.9.3.1 Hoechst based DNA assay

At the end of each incubation period, the cell culture medium was removed and the constructs were rinsed twice with Dulbecco's PBS, followed by addition of 500 µl of deionized water. The samples were then frozen at -80^{o}C for 30 minutes before being thawed at room temperature; this procedure was repeated three times. Next, an amount of 50 µl of each sample was aliquoted into flat bottom 96-well plates followed by addition of 50 µl of TNE buffer per well. This was carried out in triplicate for each sample. Subsequently, 100 µl of Hoechst stain solution was added to each well and finally, the fluorescence was measured in a Fluostar Optima fluorescence plate reader (BMG Labtech, UK), at excitation and emission wavelengths of 355 nm and 460 nm respectively.

2.2.5.9.3.2 AlamarBlue® assay

At the end of each incubation period, the media was removed from the constructs and the constructs were rinsed thrice with warm Dulbecco's PBS. 1 ml of fresh culture medium was added to each well, followed by addition of 100 µl of alamarBlue®solution to each well. The samples were incubated at 37^{o}C after which 200 µl of each solution was transferred in triplicate into a 96-well plate. The fluorescence was measured in a Fluostar Optima fluorescence plate reader (BMG Labtech, UK), at excitation and emission wavelengths of 530 nm and 590 nm respectively.

2.2.5.9.4 Alkaline phosphatase activity

Alkaline phosphatase activity is used to measure ALP activity by a kinetic rate method using 2-amino-2methyl-1-propanol buffer. In this reaction, ALP catalyzes the hydrolysis of colourless organic phosphate ester substrate, *p*-nitrophenylphosphate, to a yellow product,

p-nitrophenol, and phosphate. This reaction occurs at a pH of 10.3 (Venugopal et al., 2008d).

The substrates were prepared as directed by the manufacturer and then placed in a water bath at 37^{o}C. Next, an amount of 20 µl of each sample was aliquoted into flat bottom 96-well plates followed by addition of 200 µl of the enzyme-substrate solution to the sample. This was carried out in triplicate for each sample. The change in absorption of the solution at 405 nm was measured over a 30 minute period in a Multiskan Ascent (Labsystems, UK).

2.2.5.9.5 Mineralisation (Alizarin red-S staining and quantification)

Alizarin red-S is a dye that binds selectively to calcium salts and is widely used for calcium mineral histochemistry (Guo et al., 2007).

Prior to being seeded with cells, the electrospun scaffolds were sterilized under UV light for 30 minutes after which they were placed into 12-well cell culture plates. Finally, cells were seeded on to the scaffolds at a density of 2 x 10^{3} cells/well. Plain glass coverslips were used as control. The culture media was changed twice each week (every 3-4 days) and replaced with fresh complete culture media.

ARS staining was used to detect and quantify mineralisation after 7, 14 and 21 days of cell culture. Alizarin red solution was prepared by adding 2% alizarin red powder to deionized water (heated to 45^{o}C), followed by continuous stirring while cooling to room temperature. Finally, the pH of the solution was adjusted to 4.2 with NaOH and then filtered through a 0.22 µm pore-size syringe filter (Fisher Scientific, UK).

At the end of each cell culture period, the constructs were fixed in cold 70% ethanol for 2 minutes and then rinsed twice with PBS. These constructs were stained with 1 ml of alizarin red solution for approximately 5 minutes and then rinsed with PBS severally until they were

clear. The stains were desorbed with some agitation using 1 ml of 10% cetylpyridinium chloride (CPC) for 30 minutes at room temperature. This was carried out in triplicate for each sample. 200 µl of this dye solution was transferred to a 96-well cell culture plate and the absorbance at 562 nm was measured in a Multiskan Ascent (Labsystems UK).

2.2.6 Statistical analysis

Statistical significance of difference was calculated using One-way ANOVA and Kruskal-Wallis ANOVA at a significance level of $p \leq 0.05$ with the aid of Origin 8.0 (OriginLab, USA). Prior to conducting the One-way ANOVA analysis, the data were tested for normality using the Shapiro-Wilk method and for homogeneity of variance using the Levene's test (absolute deviations) method; further tests on means comparison were carried out using the Tukey test.

3.0 Results and Discussion

The results presented in this chapter are divided into three broad sections, each relating to the three objectives of the project. In Section 3.1, the possibility of tailoring the crystallinity of PLLA electrospun fibres is discussed. In Section 3.2, the degradation behaviour of PLLA and PLLA-HA electrospun scaffolds is discussed, while Section 3.3 discusses the characterisation of bi- and multicomponent scaffolds of PLLA. As was mentioned in Chapter 2, and as shall be explained into more detail subsequently, two different electrospinning machines were used during these experiments, i.e. the ES1a machine (Figure 12) was used to electrospin the scaffolds discussed in Sections 3.1 and 3.2 while the 2nd electrospinning machine shown in Figure 13 was used to produce scaffolds discussed in Section 3.3.

3.1 Tailoring the Crystallinity of Electrospun PLLA Fibres by Controlling the Electrospinning Parameters

3.1.1 Effect of polymer solution parameters and processing conditions on electrospinning process

Several attempts were made to electrospin fibres from the 2 wt% PLLA solution (kinematic viscosity of 2.22 cSt), however a mixture of electrospraying and electrospinning was observed (Figure 15A). The low polymer solution concentration resulted in a low polymer chain entanglement density (Shenoy et al., 2005), which caused the chains to break up at the tip of the capillary due to the high surface tension (Deitzel et al., 2001a). Fibres, as well as some beads were obtained when the polymer solution concentration was increased to 5 wt% (Figure 15B), however, when the polymer solution concentration was increased to 8 wt%, bead-free fibres were obtained (Figure 15C). The 10 wt% polymer solution was too

viscous with a kinematic viscosity of 142.57 cSt (Figure 16) and it was difficult to electrospin even at very high applied voltages.

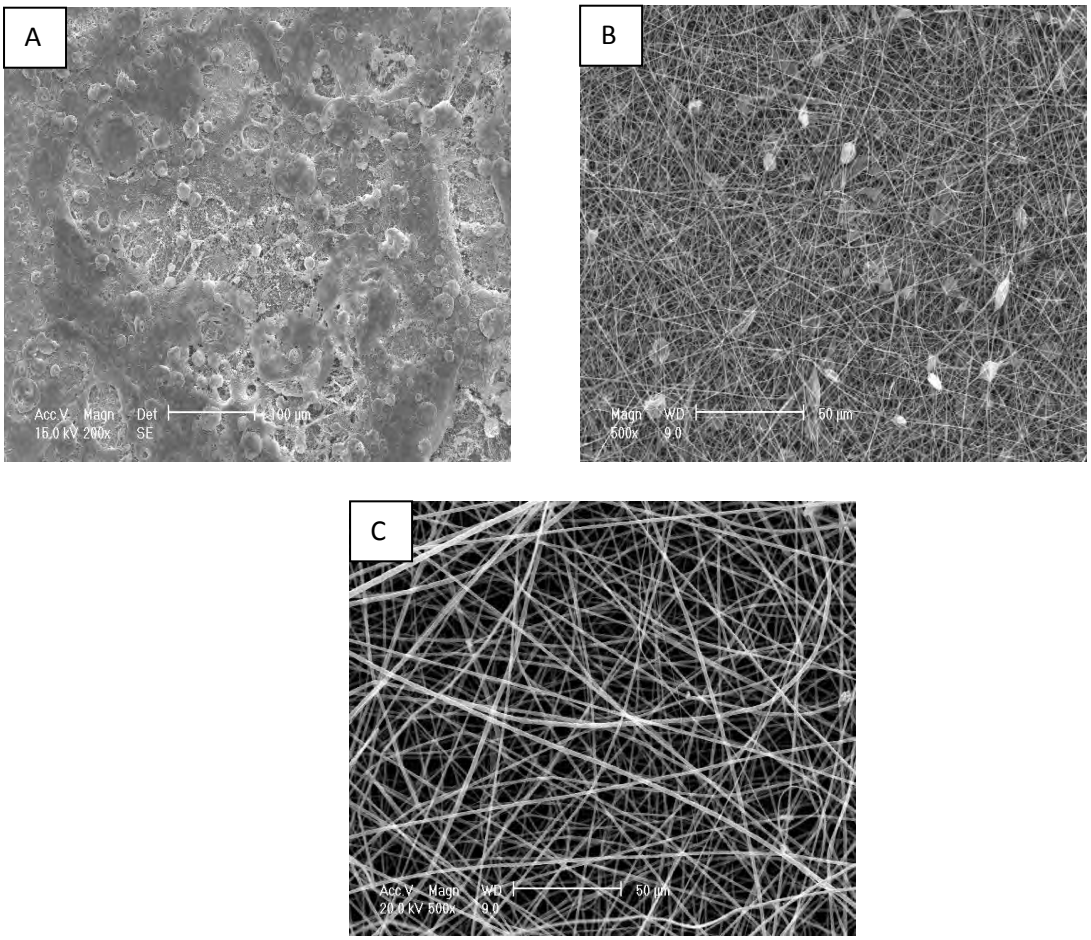

Figure 15: SEM micrographs of electrospun polymer fibres obtained when electrospinning from (A) 2 wt%, (B) 5 wt%, and (C) 8 wt% polymer solutions at 20 kV and NCTD of 12.5 cm, respectively

Polymer solution concentration, which has a direct bearing upon the number of polymer chain entanglements within the solution, is one of the major factors which determine if fibres can be formed during electrospinning. During electrospinning, there are three important forces responsible for the formation of a jet, i.e., Coloumbic force, viscoelastic force (a result of entanglement of polymer chains) and surface tension. At low polymer solution concentrations, the viscoelastic force is smaller in comparison to the Coloumbic

force due to the limited number of polymer chain entanglements. This causes over-stretching and breaking up of the jet, leading to the formation of beads due to surface tension. Conversely, at high polymer solution concentrations, the viscoelastic force is higher in comparison to the Coloumbic force, which results in elongation of the jet and prevents the jet from breaking up into beads (Mit-Uppatham et al., 2004).

Consequently, below certain critical polymer solution concentration, either droplets (formed due to the effect of surface tension) (as seen in Figure 15A) or fibres with beads (as seen in Figure 15B) are formed due to the breaking up of the polymer chains during the electrospinning process (Ramakrishna et al., 2005; Shenoy et al., 2005; Sill and von Recum, 2008). Conversely, above certain critical polymer solution concentration, electrospinning will not be possible as either the solution will dry up at the needle/capillary tip (Zong et al., 2002) or it will not be pumped through the needle/capillary (Ramakrishna et al., 2005), as was observed when electrospinning from the 10 wt% solution concentration. Therefore, there is an optimum range of polymer solution concentrations within which uniform fibres can be electrospun when all other parameters are held constant (Sill and von Recum, 2008), and in this study, this range of polymer solution concentration was found to between > 2 wt% and < 10 wt%.

When electrospinning was carried out at 10 kV, the amount of fibres produced was very small. The voltage applied during electrospinning induces charges into the polymer solution/melt and it is when the electrostatic forces created by these charges overcome the surface tension of the droplet at the needle tip that electrospinning occurs. Hence, if the applied voltage is too low, the electrostatic forces may be too low to initiate electrospinning. Similar to polymer solution concentration, the applied voltage has been shown to have a window within which electrospinning can successful (Tong and Wang,

2011), and in this study, 10 kV was considered as the minimum voltage at which electrospinning will occur.

Figure 16 shows the variation of viscosity with polymer solution concentration. The viscosity of the polymer solution increased with increasing polymer solution concentration as a result of increased number of polymer chain entanglements (Shenoy et al., 2005).

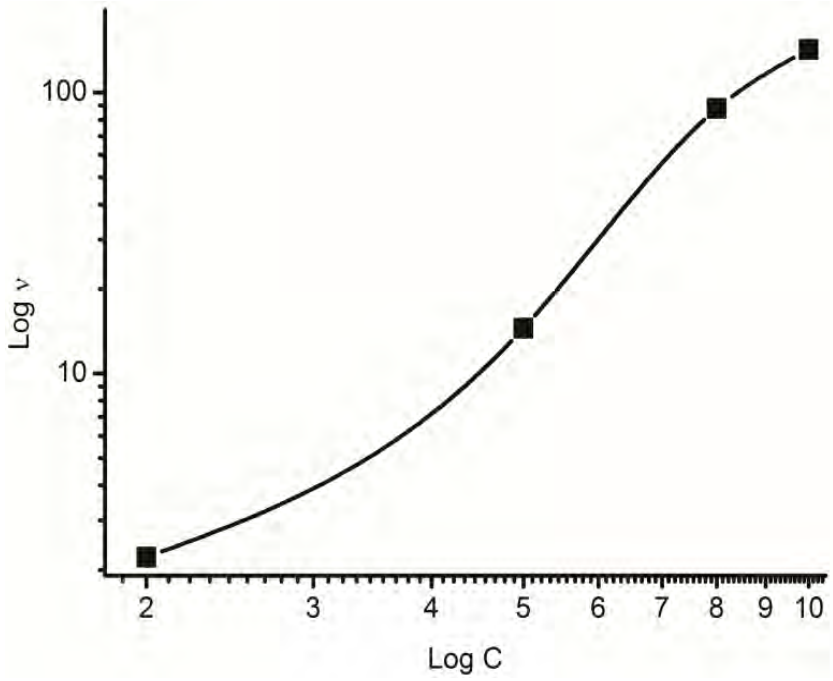

Figure 16: Kinematic viscosity of polymer solutions

3.1.2 Effect of electrospinning on glass transition temperature (T_g)

The glass transition temperature, T_g, of the electrospun fibres under any of the experimental parameters and for all the polymer solutions was lower than that of the as-received granules (67^{o}C) and ranged from 52^{o}C to 63^{o}C (Table 2). Varying the voltage or the NTCD had no effect on the T_g of the electrospun fibres. The T_g increased by approximately 8–11^{o}C when the polymer concentration was increased from 5 to 8 wt%; this was due to increased polymer chain interaction, but the T_g remained lower compared to the as-

Table 2: **Variation of T_g and X_c with electrospinning parameters (Values of X_c were calculated during 1st heating cycle)**

PLLA electrospinning solution	Electrospinning parameters		T_g (^oC)		X_c (%)	PLLA electrospinning solution	Electrospinning parameters		T_g (^oC)		X_c (%)
	NTCD (cm)	Voltage (kV)	1st heating cycle	2nd heating cycle			NTCD (cm)	Voltage (kV)	1st heating cycle	2nd heating cycle	
Granule	n/a	n/a	67	n/a	37.4	n/a	n/a	n/a	-	-	-
5%	7.5	15	52	56	45.3	8%	7.5	15	61	61	37.3
		20	54	54	45.1			20	64	61	43.8
		25	52	54	44.8			25	63	61	46.3
	10	15	53	54	43.9		10	15	60	61	30.5
		20	52	55	42.2			20	60	61	36.7
		25	53	54	37.9			25	62	60	43.9
	12.5	15	55	54	45.5		12.5	15	60	61	33.4
		20	53	55	43.7			20	58	61	36.9
		25	54	55	42.4			25	64	61	46.6
	15	15	52	55	46.6		15	15	60	61	31.2
		20	55	54	28.4			20	60	61	34.7
		25	56	54	26.2			25	63	61	45.8

n/a – not applicable

received polymer. Carrizales et al. (2008) have suggested that the decrease in the glass transition temperature of electrospun fibres could be due to the presence of absorbed water in the electrospun fibres (Carrizales et al., 2008). Carrizales et al. (2008) reported a decrease of 20^{o}C for T_g of electrospun Poly(methyl methacrylate) (PMMA) nanofibres compared to the T_g of the as-received PMMA powder during the 1st heating cycle of a DSC study (Carrizales et al., 2008). However, during the 2nd heating cycle of the electrospun nanofibres, it was reported that the T_g of the electrospun nanofibres was equal to that of the as-received PMMA powder. This observation was attributed to the presence of absorbed water present in the electrospun PMMA nanofibres. Although this was not expected to be the case in this project because the electrospun fibre scaffolds were properly dried before conducting DSC analysis on them, a 2nd DSC heating cycle was conducted on the electrospun PLLA fibres in order to investigate the possibility of entrapped solvent or humidity present in these samples (Table 2). The glass transition temperature of the electrospun fibres was generally slightly increased in the 2nd heating cycle compared to the 1st heating cycle, but it remained always lower compared to the glass transition temperatures of the as-received granules, indicating clearly that the decrease in T_g observed during the 1st heating cycle was not due to the presence of residual solvent or absorbed water. Similar results of lower T_g have previously been reported for electrospun fibres (Cui et al., 2006; Zong et al., 2002; Zong et al., 2003). The decrease in T_g in electrospun PLLA fibres was attributed by Zong et al. (2002) to the very large surface area to volume ratio of the fibres (Zong et al., 2002), while Cui et al. (2006) ascribed a similar observation in electrospun Poly(D,L-lactic acid) (PDLLA) fibres to the inner stress and higher degree of molecular alignment and orientation of polymer chains caused by the electrospinning process (Cui et al., 2006).

3.1.3 Effect of polymer solution concentration on the degree of crystallinity

Figure 17 presents DSC scans of polymer fibres electrospun from 5 and 8 wt% PLLA solutions at 15 kV and 10 cm NTCD. Just above the T_g, a hysteresis endothermic peak was observed (Figure 17), characteristic of enthalpic relaxation that occurs after the rapid structure formation of the fibres during electrospinning as has also been reported by Bognitzki et al. (Bognitzki et al., 2001). An exothermic peak observed around 75^{o}C was associated with "cold crystallisation" as has been reported also in the literature (Inai et al., 2005; Zong et al., 2002). Cold crystallisation is a low-temperature crystallisation that arises due to enhanced primary nucleation when heating from the glassy state (Wunderlich, 2005). Due to the fast formation rate of fibres during electrospinning, polymer crystallisation may be incomplete during electrospinning. It is therefore expected that while some of the crystals may be properly formed during the process, there may be other small crystals formed due to incomplete crystallisation. During heating in the DSC, as heat energy is supplied to the pre-existing crystals within the polymer, these small crystals grow by ordering/re-arrangement of the polymer chains through a cold crystallisation process. The cold crystallisation is exothermic, and it gives a heat of transition, i.e. heat of cold crystallisation (ΔH_c). These crystals that grow during nucleation and those that were already in the polymer before cold crystallisation will all melt at the melting temperature, giving a heat of transition, i.e. heat of fusion (ΔH_f).

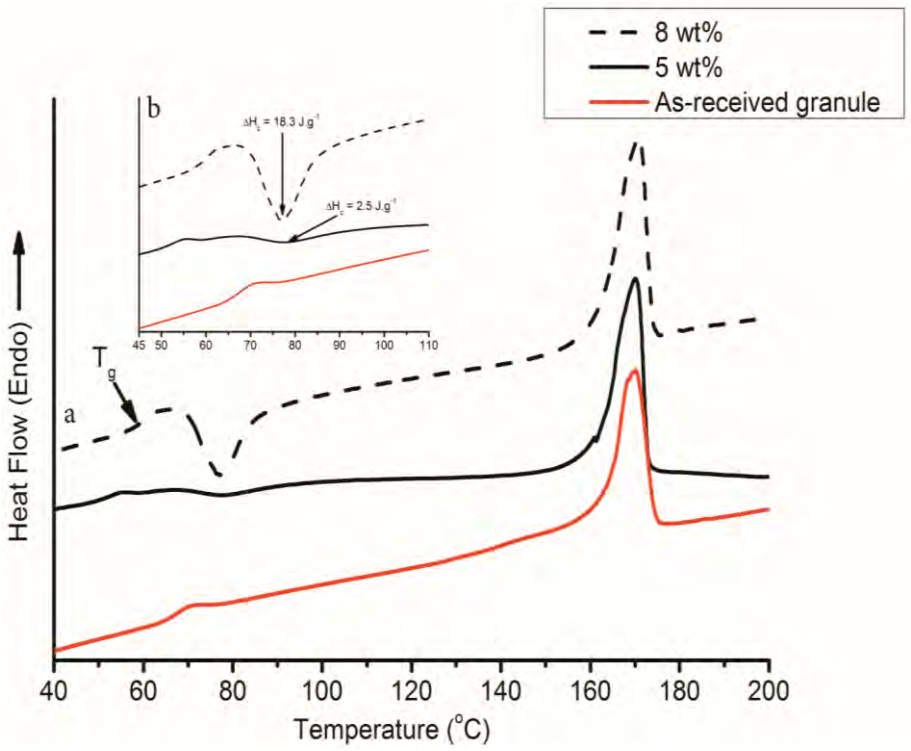

Figure 17: (A) DSC scans of fibres electrospun from 5 and 8 wt% solutions at 15 kV and 10 cm NTCD and (B) Cold crystallisation region of scans shown in A

It should be noted that because all the crystals, i.e. those developed during cold crystallisation, and those that were already pre-existing in the polymer before cold crystallisation give rise to the ΔH_f. Therefore, in order to determine the crystallinity of the polymer prior to cold crystallisation, the ΔH_c has to be subtracted from the ΔH_f, hence the formula in Equation 6.

The degree to which a polymer shows cold crystallisation will be dependent on how amorphous/crystalline it is. A completely amorphous polymer will show a very large cold crystallisation peak that will be equal to its melting peak, showing that all the crystals that melted were only developed during cold crystallisation. However, a semi-crystalline material will show a cold crystallisation peak smaller in size than the melting peak, indicating that there were some other crystals present in the sample before cold crystallisation. However,

the fact that a material shows cold crystallisation does not necessarily indicate that it is less crystalline than another polymer that does not show cold crystallisation, because ΔH_f, the other factor that determines the degree of crystallinity may still be higher than the ΔH_c.

For instance, in this study, the cold crystallisation enthalpy (ΔH_c), increased from 2.5 $J.g^{-1}$ to 18.3 $J.g^{-1}$ when the polymer solution concentration was increased from 5 to 8 wt% and voltage and NTCD were held constant at 15 kV and 10 cm, respectively (Figure 17). At low polymer solution concentrations, the polymer chains are more mobile due to relatively small number of chain entanglements resulting in higher molecular orientation during electrospinning compared to fibres electrospun from higher solution concentrations.

Also, the solidification process is expected to be slower for a low polymer solution concentration resulting in higher electric-field assisted molecular orientation during electrospinning (Inai et al., 2005). Therefore, it is clear that low polymer concentration solutions will yield fibres with higher molecular orientation and therefore lower degree of cold crystallisation, hence higher degree of crystallinity during electrospinning. Conversely, higher polymer concentration solutions will yield fibres with reduced molecular orientation due to higher viscosity, and therefore generally higher degree of cold crystallisation and lower crystallinity as the solidification process must be faster compared to the low polymer concentration solutions. As a result, the degree of crystallinity was generally found to decrease with increasing polymer solution concentration except in the case of fibres electrospun from the 8 wt% polymer solution concentration at a voltage of 25 kV (Table 2). The reason for this is discussed in Section 3.1.4.

3.1.4 Effect of electrospinning voltage on the degree of crystallinity

In Figure 18, the degree of crystallinity of the fibres electrospun from the 5 wt% PLLA solution generally decreased with increasing voltage from 15 kV to 25 kV albeit in some cases, the reduction was only minimal. For instance, when the voltage was increased from 15 kV to 25 kV at a constant NTCD of 10 cm, the cold crystallisation enthalpy, ΔH_c, increased from 2.5 $J.g^{-1}$ to 6.7 $J.g^{-1}$ (Figure 19). Consequently, the degree of crystallinity, X_c, calculated using Equation 6, decreased with increasing the voltage from 15 to 25 kV (Figure 18). On the contrary, the degree of crystallinity for the fibres electrospun from the 8 wt% solution concentration increased as the voltage was increased from 15 kV to 25 kV (Figure 20). Zhao et al. (2004) reported that during the electrospinning process, as the jet travels from the needle tip to the collector, both molecular orientation induced by the electric field, and crystallisation of the polymer occur (Zhao et al., 2004). It has also been reported, that as the voltage is increased, the number of charges in the polymer solution increases and the effect of this is that there will be more stretching of the jet (Tong and Wang, 2011). Furthermore, increasing the voltage while keeping the all the other parameters constant will lead to an increase in the electric field strength and an increase in the alignment of the polymer chains (molecular orientation) during electrospinning and consequently an increase in the degree of crystallinity of the electrospun fibres as reported by Zhao et al. (Zhao et al., 2004). But as Ramakrishna et al. (2005) explain, above a certain voltage, the crystallinity of the nanofibres does not increase but on the contrary it is reduced (Ramakrishna et al., 2005). It was suggested, that the degree of crystallinity is influenced by the flight time of the jet, which at high voltages is short enough to leave insufficient time for the polymer to crystallise. Increasing the voltage beyond a certain maximum will therefore lead to a reduction in the

flight time due to the higher acceleration of the jet, and will result in decreased crystallinity (Zhao et al., 2004; Ramakrishna et al., 2005).

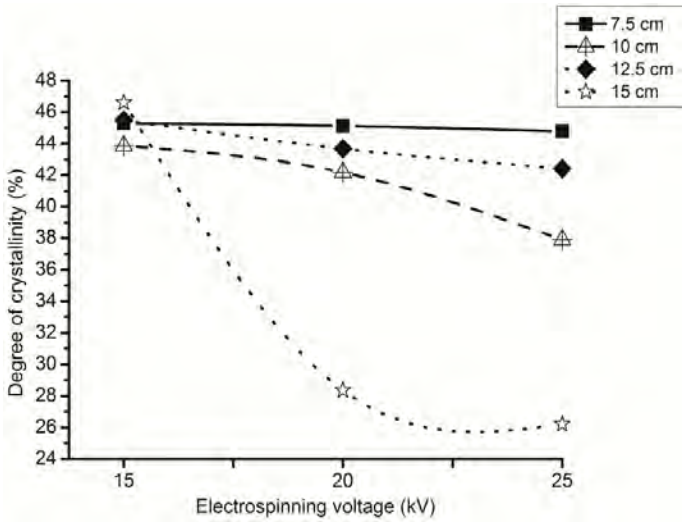

Figure 18: Effect of voltage on the degree of crystallinity of fibres electrospun from 5 wt% solution concentration at different NTCDs

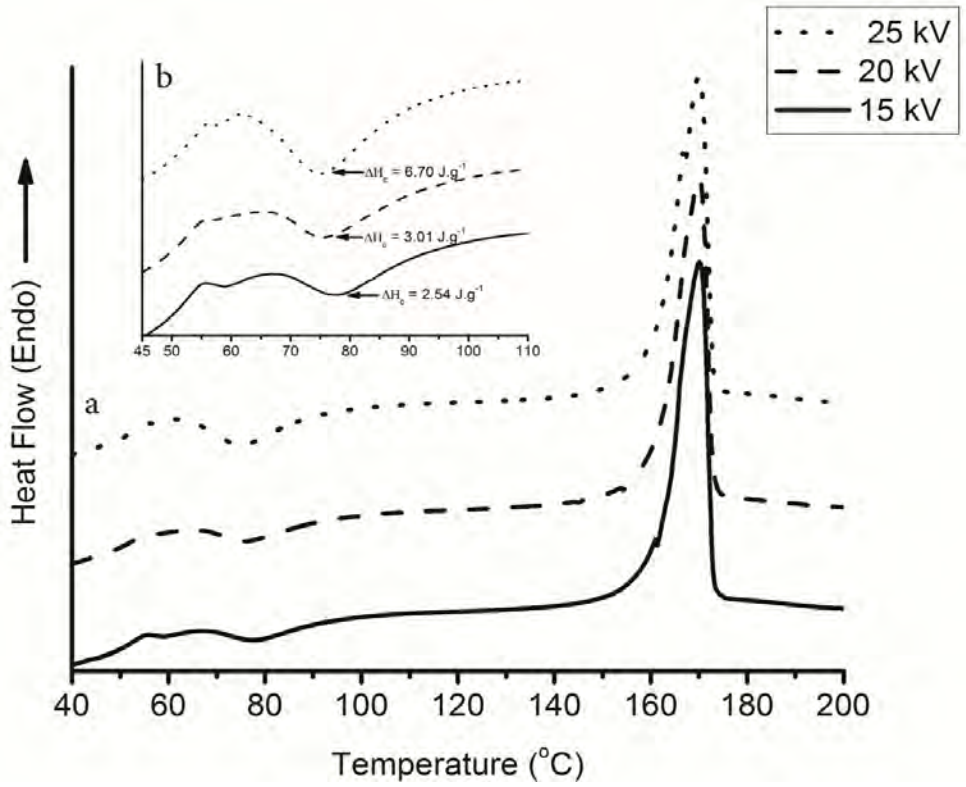

Figure 19: **(A) DSC scans of fibres electrospun from 5 wt% solution at a constant NTCD of 10cm and varying voltages, and (B) Cold crystallisation region of scans shown in A**

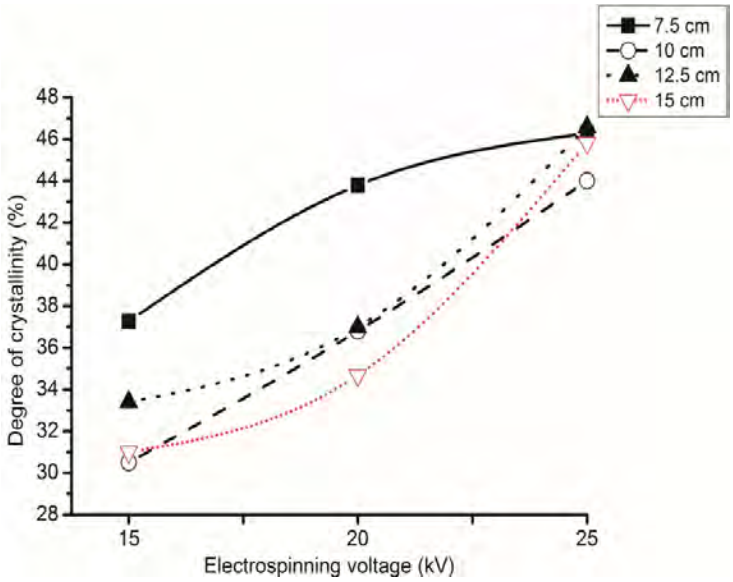

Figure 20: **Effect of voltage on the degree of crystallinity of fibres electrospun from 8 wt% solution concentration at different NTCDs**

Considering the above, it is suggested that for each polymer solution, there is an optimum electrospinning voltage, above and below which the degree of crystallinity will decrease and increase, respectively. Generally, it is expected the degree of crystallinity will increase from an initial crystallinity, X_c^1 (this is the degree of crystallinity of the first electrospinnable fibres) with increasing voltage up to a maximum after which it will decline with further increases in voltage, as is shown in Figure 21. It should be noted however, that this is only a general trend, as in reality, the curve may or may not be parabolic and/or asymmetric, and it is also possible that the shape of the curve will vary from one polymer solution to another (as seen in Figures 18 and 20). However, it is believed that, independent of the rate of change of crystallinity and the symmetry of the curve, the degree of crystallinity will increase with voltage up to an optimum electrospinning voltage (V_o), above which the degree of crystallinity will begin to decrease. The degree of crystallinity is reduced due to the effect of the acceleration imposed on the spun fibres by the electric field. From Figure 18 and Table 2, it can be observed that in the case of 5 wt% PLLA solution,

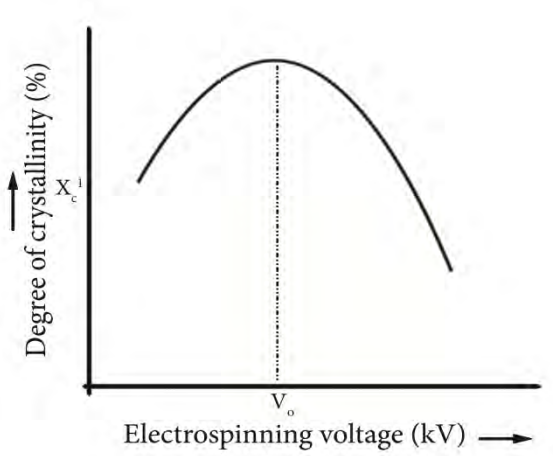

Figure 21: **Graphical representation of the general trend in variation of degree of crystallinity with voltage (where X_c^1 is the degree of crystallinity of the first electrospinnable fibres, and V_o is the optimum electrospinning voltage)**

the degree of crystallinity changes in a very similar way. It is suggested, that 15 kV seems to be at or close to the optimum voltage and therefore the degree of crystallinity will be expected to reach a maximum. As the maximum degree of crystallinity (X_c) was obtained at 15 kV, after which X_c began to decrease, it is highly probable that if a voltage lower than 15 kV was used to electrospin the polymer solution, the degree of crystallinity would increase with voltage up to a maximum at *circa* 15 kV after which reduction of the flight time of the jet occurs with a consequent decrease in the degree of crystallinity. It was attempted to electrospin the polymer solutions at lower voltages than 15 kV (i.e. 10 kV) but this was not possible as has been explained previously in Chapter 2 and Section 3.1.1. Consequently, it is believed that the range of voltages used in this study may have been on the right-hand side of the curve shown in Figure 21. Within this range, it is likely that increases in voltage will lead to increased acceleration of the jet to the extent that it reduces its flight time; the result of this was that there was insufficient time for crystallisation and hence lower degree of crystallinity was observed beyond 15 kV.

For the 8 wt% solution, the degree of crystallinity always reached a maximum at 25 kV when the voltage was increased from 15 kV to 25 kV (Figure 20). This suggests that the optimum voltage at which maximum degree of crystallinity can be obtained is at or close to 25 kV. It is therefore believed that the range of voltages used in this study fall on the left-hand side of the curve shown in Figure 21. Following the curve shown in Figure 21, it is very likely that further increases in voltage beyond 25 kV will lead to a reduction in the degree of crystallinity. It was interesting to note, however, that the optimum voltage at which the maximum degree of crystallinity can be obtained for the fibres electrospun from the 5 wt% solution concentration was lower than that for the fibres electrospun from the 8 wt% solution concentration, i.e. 15 kV and 25 kV for the 5 and 8 wt% solutions, respectively. As has been explained in Section 3.1.3, the polymer chains are more mobile in polymer solutions of low concentration; it is therefore believed, that this will make them more susceptible to influences of voltage at low voltage values. As the polymer solution concentration is increased however, there are more polymer chain entanglements, hence higher solution viscosity, resulting in the polymer chains exhibiting a higher resistance to stretching (Jarusuwannapoom et al., 2005) during electrospinning. As a result, the probability of the electric field inducing molecular orientation in the electrospun fibres at low voltages will be small, except at higher voltages (specifically, in this study, this voltage was approximately ≥ 25 kV).

A comparison of the degree of crystallinity of fibres electrospun from the 8 wt% solution at 25 kV with the degree of crystallinity of fibres electrospun from the 5 wt% solution at the same voltage shows that the degree of crystallinity was slightly higher for the former. As explained above, at voltages above the optimum voltage at which the maximum degree of crystallinity can be obtained, the degree of crystallinity of the fibres will decrease. As the

optimum voltage for fibres electrospun from the 5 wt% solution was at or close to 15 kV, any further increase in voltage will lead to a reduction in the flight time of the jet and consequently a decrease in the degree of crystallinity. However, for the 8 wt% solution, because the optimum voltage was at *circa* 25 kV, the maximum degree of crystallinity was observed at this voltage.

3.1.5 Effect of NTCD on the degree of crystallinity

As molecular orientation can be induced by the electric field as the jet travels from the needle tip to the collector, if the flight time of the jet is increased by increasing the NTCD (Zhao et al., 2004), it would be theoretically reasonable to suggest that the molecular orientation of the electrospun fibres could increase, with a consequent increase in the degree of crystallinity. The recent work of Tong and Wong (2011) however, show that increasing the NTCD may not necessarily increase the flight time of the jet due to the complicated three-dimensional spiralling trajectory of the jet (Tong and Wang, 2011). In this study, for fibres electrospun from the 5 wt% solution, no constant trend was observed in the variation of the degree of crystallinity (X_c) with changing NTCD, suggesting that the NTCD influences the degree of crystallinity of the electrospun fibres but not in a predictable and consistent way (Figure 18). Although the reason for this is not particularly clear, it is suggested that it could be due to the inconsistency of trajectory of the polymer jet as Tong and Wang suggested (Tong and Wang, 2011). However, it was interesting to note, that for the 5 wt% solutions, at 15 kV which was the optimum electrospinning voltage for this solution, the degree of crystallinity remained fairly constant in the whole range of NTCD used in this study, suggesting that the degree of crystallinity is not affected by variations in NTCD when electrospinning at or close to the optimum voltage. Similar observations as

above were also made for fibres electrospun from the 8 wt% solution concentration (Figure 20).

3.2 Degradation Behaviour of PLLA and PLLA-HA Electrospun Scaffolds

Following the observations and results of the experiments reported in Section 3.1, two types of electrospun scaffolds were fabricated, specifically, PLLA and PLLA-HA. As the scaffolds were being investigated for use in bone-tissue engineering, experimental conditions which would produce scaffolds with a modest amount of crystallinity were chosen. Furthermore, because of the large amount of samples that was required for the various characterisation experiments during the degradation study, experimental conditions which would give a high-throughput were considered. During the crystallisation study experiments, it was observed that higher voltages yielded a higher throughput of electrospun fibres. Similar results were reported by Mouthuy (2008) during electrospinning of PVA and PLLA fibres; this was attributed to an increase in the electrospinning rate as a result of higher volume of solution being drawn from the needle tip to the collector (Mouthuy, 2008). Consequently, the electrospinning parameters for the experiments reported in this section were chosen as voltage of 25 kV and NTCD of 12.5 cm. However, at this stage of the project, the needle tips (orifice diameter of 0.8 mm) which had been supplied by Electrospinz along with the machine were exhausted, so a different set of needle tips (orifice diameter of 0.9 mm) were utilized in electrospinning the scaffolds characterised in this section. Various properties of the electrospun scaffolds, which were measured both prior to degradation and after degradation were used to characterise their degradation behaviour and are reported in the following sections.

A low HA content (5 wt%) was utilized in fabricating the PLLA-HA scaffolds in order to keep the dispersion of the HA in the PLLA matrix homogenous, as high HA content has been reported to cause agglomeration of HA particles in electrospun polymer/HA scaffolds, when fabricated by mixing HA particles with the polymer prior to electrospinning (Kim et al., 2005; Prabhakaran et al., 2009).

3.2.1 Morphology

The average fibre diameters of both sets of scaffolds (pre-degradation and post-degradation) are shown in Table 3. It was interesting to observe that the average fibre diameter of the PLLA-HA was ≈59% less than that of the PLLA. This reduction in fibre diameter size has been previously attributed to the combination of reduced polymer solution concentration/viscosity and the restriction of flow of the PLLA solution by the HA particles as the solution was being drawn from the needle tip during electrospinning (Chuenjitkuntaworn et al., 2010; Xu et al., 2007). The polymer solution concentration plays an important role in determining the properties of electrospun fibres, and previous reports in the literature show that fibre diameter is directly proportional to polymer solution concentration (Mit-Uppatham et al., 2004; Sill and von Recum, 2008; Boland et al., 2001). An agglomeration of HA particles (≈200 nm in diameter) at the tip of the needle (900 nm in diameter) would have reduced the effective orifice diameter of the needle. Needle tips with small orifice diameters have been reported to produce fibres with smaller diameters in comparison to fibres produced from needle tips with larger orifice diameters (Tong and Wang, 2011; Ramakrishna et al., 2005). The effect of needle tip orifice diameter was attributed to the dependence of the Taylor cone size (which determines the size of the

initial electrospinning jet) on needle tip orifice diameter (Tong and Wang, 2011). Essentially, a large Taylor cone will initiate a large electrospinning jet and vice versa.

The reduction in the fibre diameter of PLLA electrospun fibres upon inclusion of HA particles in this study was therefore considered to be due to a combination of the above reasons and an increase in electrical conductivity of the polymer solution. The OH^- ion in the HA was considered to be the reason for an increase in electrical conductivity as it has been shown to be the charge carrier in hydroxyapatite (Bouhaouss et al., 2001; Takahashi et al., 1978).

The presence of HA in the PLLA-HA scaffold was qualitatively confirmed by EDS mapping for the presence of calcium and phosphorous (Figure 22).

Table 3: Average fibre diameter, pre- and post-degradation

Sample	Initial fibre diameter (Pre-degradation) (nm)	Diameter of dry fibres (Post-degradation) (nm)
PLLA	781 ± 380	921 ± 318
PLLA-HA	316 ± 146	481 ± 184

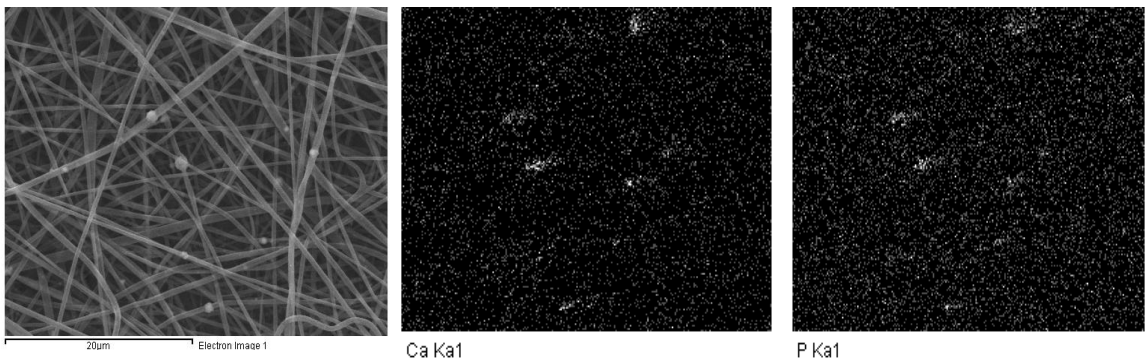

Figure 22: **EDS maps of PLLA-HA scaffold**

After 4 weeks of degradation, both sets of electrospun scaffolds exhibited a puffy/swollen morphology (Figure 23). In addition, at the end of the 4 week degradation period, the fibre diameters had increased by 140 nm and 165 nm for the PLLA and PLLA-HA scaffolds, respectively, which amounted to an increase of ≈18% and ≈52% compared to the initial fibre diameters for the PLLA and PLLA-HA scaffolds, respectively (Table 3). Similar results of a swollen morphology during degradation of electrospun poly(D,L-lactide) (PDLLA) and PLLA fibres have been reported in the literature (Cui et al., 2006; Cui et al., 2008; Ishii et al., 2009). Cui et al. (2006) attributed the swelling characteristic to the chain relaxation of the polymer after incubation at elevated temperature (Cui et al., 2006). Based on the results of Section 3.1 and previous reports in the literature, it is evident that under certain conditions, electrospinning can retard the crystallisation of PLLA due to the rapid solidification of stretched chains at high elongational rates which leaves insufficient time for the stretched chains to organize into suitable crystal registration before they are solidified (Zong et al., 2002). This is because the crystallisation of PLLA is a quite slow process (Martinez et al., 2007), whereas, the deposition of fibres during electrospinning is a very rapid process, on the order of several metres per second (Bognitzki et al., 2001) which will leave very little room for crystallisation of PLLA during electrospinning. However, Zong et al. (2002) noted that the polymer chains in electrospun nanofibres possess a high degree of orientation and are in a metastable state (Zong et al., 2002). Consequently, it may be possible for these highly-oriented, stretched chains to undergo some relaxation during incubation at elevated temperatures, i.e., degradation study conditions. The thermally induced relaxation of stretched chains in electrospun fibres has been reported to cause large dimensional changes (Zong et al., 2003).

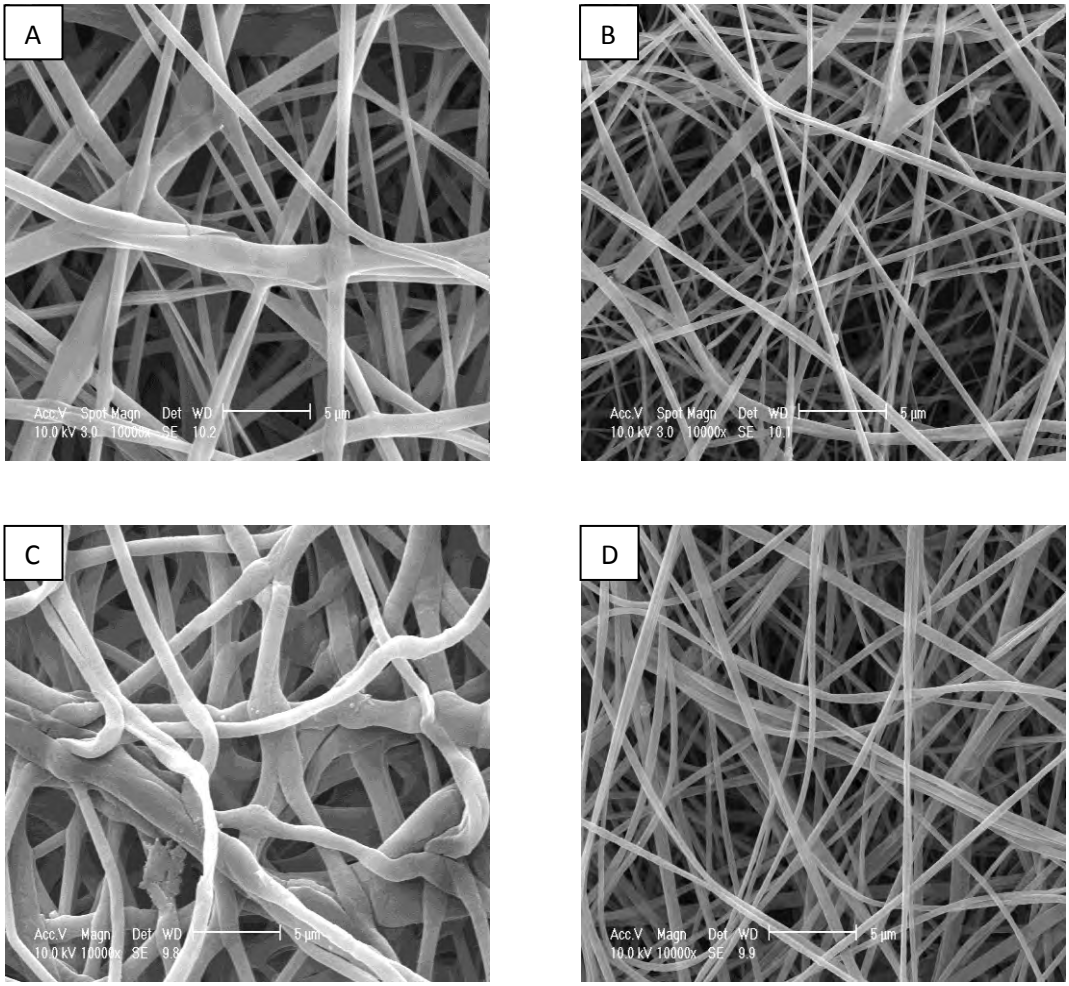

Figure 23: **PLLA (A, C) and PLLA-HA (B, D) electrospun scaffolds after 0 and 4 weeks of degradation, respectively**

Nanofibres of polyesters such as PLLA, PCL, PGA and their co-polymers have been reported to rupture during degradation (Dong et al., 2009; Sui et al., 2007; Zeng et al., 2004; Dong et al., 2010). Due to the rigidity of polymer chains in the crystalline regions of these polyesters, it is considered that when weak points develop along the electrospun fibres as a result of hydrolysis, the fibres rupture (Dong et al., 2009). However, ruptured fibres were not observed on the scaffolds utilized in this study (Figure 23A-D). Similar results of unruptured electrospun PLA fibres were reported by You et al. (2005) after 45 days of degradation, however, Sui et al. (2007) reported the formation of ruptured fibres after 56 days of

degradation (Sui et al., 2007; You et al., 2005). It is therefore possible, that electrospun PLLA fibres will start to rupture at longer degradation time period than the one reported in this research.

3.2.2 Molecular weight (M_w)

The variations in molecular weight studied by GPC are shown in Figure 24. The two sets of electrospun scaffolds showed extensive decrease in M_w with time, however, the rate of decrease of the PLLA-HA scaffolds (slope of 19,625/week) was higher in comparison to those of the PLLA scaffolds (slope of 10,250/week). This showed that the PLLA-HA scaffolds degraded at approximately two times the rate at which the PLLA scaffolds degraded. This was contrary to the results reported by Sui et al. (2007), who reported that PLLA scaffolds showed a larger decrease in M_w in comparison to PLLA-HA scaffolds. According to Sui et al., it was the HA particles that slowed down the degradation rate of the PLLA-HA scaffolds due to their alkaline nature (Sui et al., 2007). However, the authors did not provide details of the concentration of HA in their PLLA-HA scaffolds. It is therefore probable that the HA content of their PLLA-HA scaffolds was much higher than the HA content of the PLLA-HA scaffolds in this study (5%), and may have resulted in the difference between the results of this work and those of Sui et al. (2007).

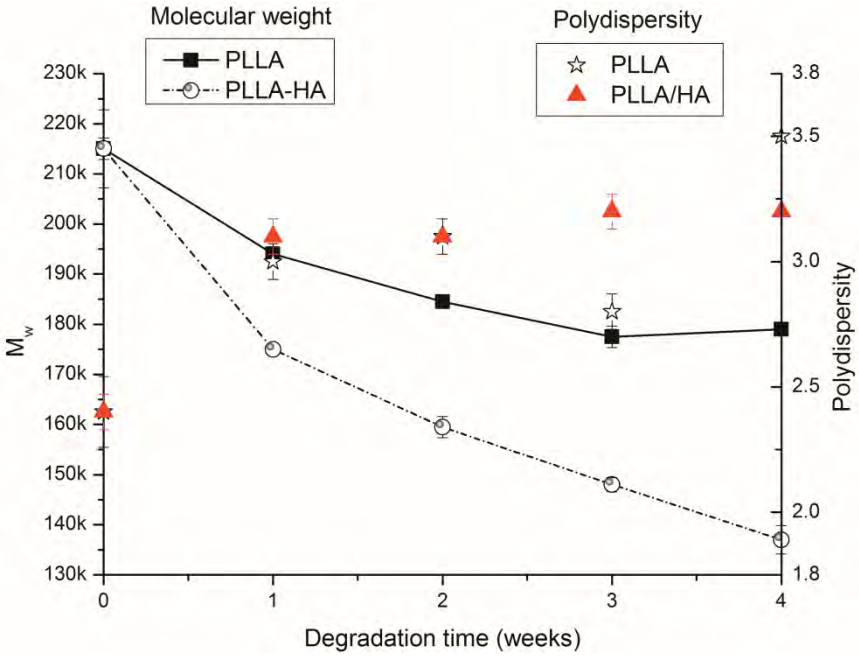

Figure 24: **Variation of molecular weight and polydispersity with degradation time (Error bars indicate standard deviation)**

Based on previous reports in the literature, about the absence of autocatalysis during nanofibre degradation as previously discussed in Section 1.11, it was considered that there was no autocatalysis during the degradation of the PLLA and PLLA-HA electrospun scaffolds studied in this project.

The smaller average fibre diameter of the PLLA-HA scaffolds implied that they had higher surface area-to-volume ratios (SVR) than the PLLA scaffolds, resulting in a higher contact area with the degradation medium and thus, were more prone to hydrolytic attack of their ester bonds. Furthermore, because of their higher SVRs, the PLLA-HA scaffolds would have absorbed water at a faster rate than the PLLA scaffolds hence, their higher degradation rate.

The change in polydispersity with degradation time is shown in Figure 24 where a general increase of polydispersity with passing degradation time was observed. This indicates that as a result of the degradation process, the polymer became a disperse mixture of fragments of varying molecular weights which is characteristic of a random degradation process

(Billmeyer, 1984). It has been reported previously, that the initial stages of degradation of semicrystalline polyesters are characterised by random chain scission as a result of hydrolysis (Li, 1999; Pitt et al., 1981) which is in good agreement with the polydispersity data presented in Figure 24.

3.2.3 pH variation

The change in pH over the degradation period is shown in Figure 25. Both scaffolds showed similar pH profiles, and remained within the neutral pH region throughout the 4-week degradation period. There was no significant difference in the pH profiles of both scaffolds, although the PLLA-HA scaffolds exhibited a lower pH in comparison to the PLLA scaffolds during the first week of degradation, after which their pH values were approximately equal. On the contrary, Sui et al. (2007) reported that there was a continuous decrease in the pH of PLLA scaffolds during 8 weeks of degradation, while there was only a slight decrease in the pH of the PLLA-HA scaffolds during the first 4 weeks after which it increased up to the initial pH within the next 4 weeks. The authors attributed the increase in pH to the release of OH^- from degradation of HA particles in the PLLA-HA scaffold (Sui et al., 2007). However, the thermodynamical solubility of HA has been reported to be very low, limiting the possibility of physicochemical degradation, or dissolution of HA *in vitro* (Barrère et al., 2008). It is therefore suggested, that it was the exposure of alkaline HA particles to the degradation medium that caused the pH of the degradation medium to increase. During electrospinning of polymer/HA scaffolds, due to the tendency of HA particles to agglomerate, some of the HA particles would not have been fully embedded within the polymer fibres, as a result, some of them would have protruded from the surfaces of the fibre surfaces. The possibility

of this occurring will increase, as the concentration of HA particles is increased, as has been reported by other researchers (Prabhakaran et al., 2009; Xu et al., 2007).

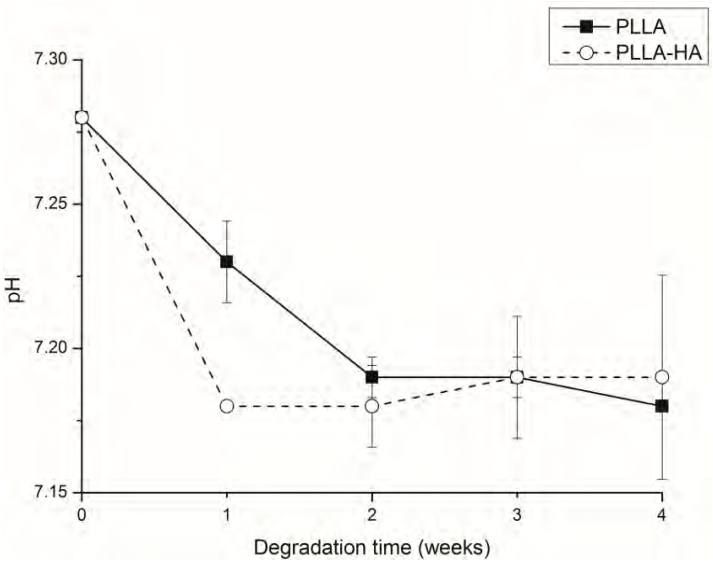

Figure 25: **Change in pH of degraded electrospun scaffolds with degradation time (Error bars indicate standard deviation)**

It was interesting to note, that all the reports in the literature about the neutralising effect of HA particles during degradation of polymer/HA scaffolds have been reported when a relatively high concentration of HA particles (typically ≥10%), was used (Wang et al., 2010; Xu et al., 2007; Zhang et al., 2007a). In this work, it was therefore considered that the reason the neutralising effect of HA was not observed was that the concentration of HA particles in the PLLA-HA scaffold was low.

3.2.4 FTIR analysis

FTIR spectra of the PLLA and PLLA-HA scaffolds are shown in Figure 26. One of the main bonds affected by the degradation process has been shown to be the v(C=O) stretching mode of the carbonyl groups, therefore, the FTIR spectra evaluation was focussed within the range of 1700-1800 cm^{-1} (Kister et al., 1995; Tan et al., 2009). FTIR analysis of the

carbonyl group will be an effective method of qualitatively determining and comparing the amount of degradation in the electrospun scaffolds.

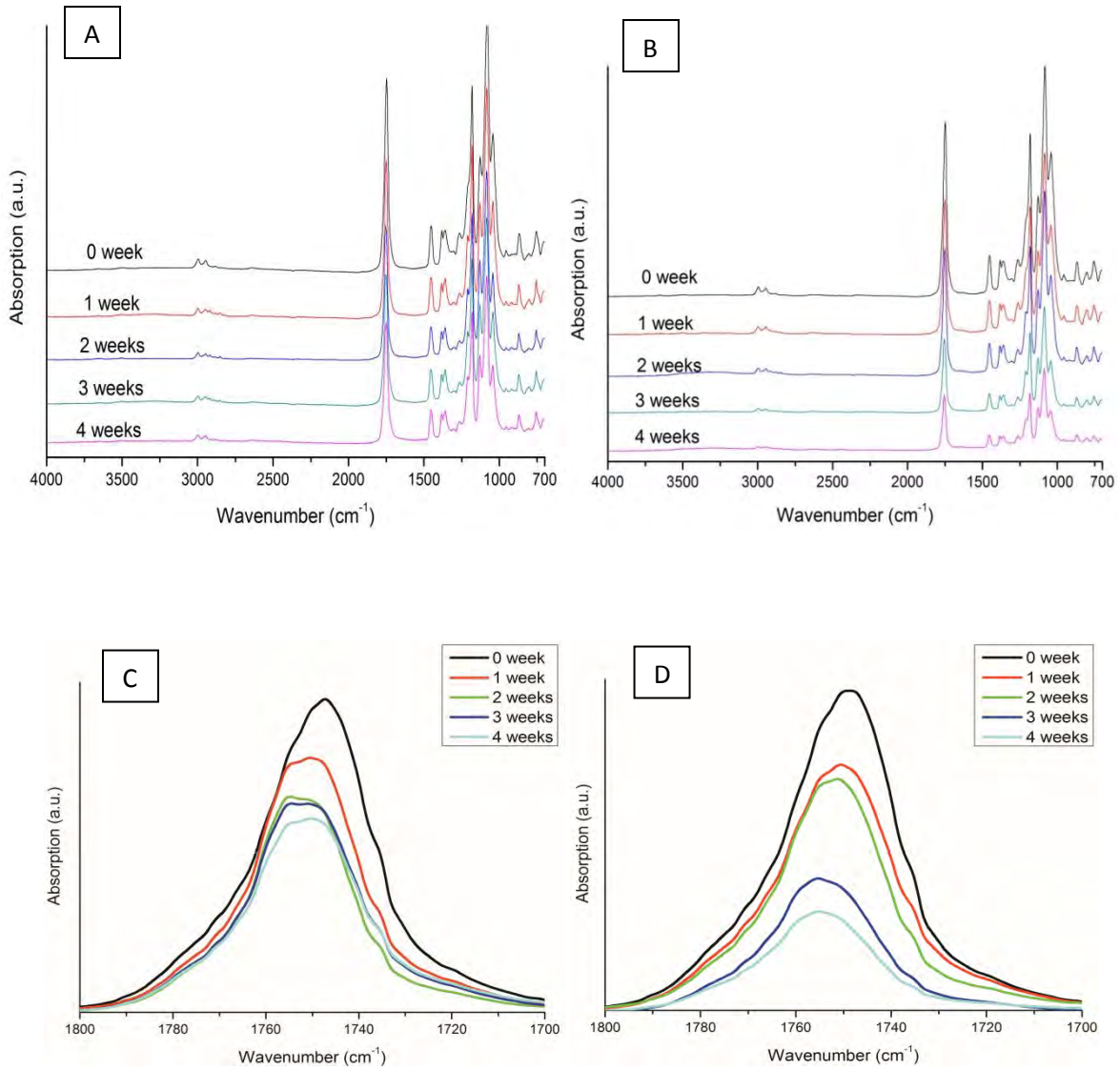

Figure 26: (**A) FTIR spectra of PLLA scaffolds (after 0, 1, 2, 3, and 4 weeks of degradation), (B) FTIR spectra of PLLA-HA scaffolds (after 0, 1, 2, 3 and 4 weeks of degradation), (C) FTIR spectra of C=O region of PLLA scaffolds (after 0, 1, 2, 3, and 4 weeks of degradation) and (D) FTIR spectra of C=O region of PLLA-HA scaffolds (after 0, 1, 2, 3, and 4 weeks of degradation)**

Polymer degradation and erosion occurs in three stages; during the first stage, there is random chain scission coupled with significant decrease in molecular weight but no

appreciable weight loss or formation of soluble monomer products. In the second stage, there is a further decrease in molecular weight, which is later accompanied by rapid mass loss and formation of soluble oligomeric and monomeric products. In the final stage, soluble monomer products are formed from soluble oligomeric fragments, which signifies complete solubility of the polymer (Raghuvanshi et al., 1993). A decrease in the number of C=O groups should be observed during the degradation process as reported by Tan et al. (Tan et al., 2009). A decrease in the number of C=O groups was also observed here for both types of electrospun scaffolds as seen in Figure 26C and 26D where the intensity of the relevant peak decreased significantly with degradation time, supporting that degradation occurred.

Figure 27 shows an area analysis of the C=O peak. The initial amount of C=O groups in the PLLA scaffold was higher than those in the PLLA-HA scaffolds due to the higher PLLA content of the former. The rate of decrease in C=O groups for each scaffold (calculated as the slope of the graph in Figure 27) was calculated in order to account for this difference, so that whatever difference that was observed in the slopes reflected only the difference in their individual degradation rates. The area analysis of the C=O peak revealed that the area of the carbonyl peak varied inversely with degradation time for both sets of electrospun scaffolds (Figure 27). However, the rate of C=O group loss for the PLLA-HA electrospun scaffold (3.34/week) was higher than that of the PLLA electrospun scaffold (1.90/week), indicating a faster degradation rate in comparison to the PLLA electrospun scaffold. The ratio PLLA-HA C=O group loss:PLLA C=O group loss was ≈1.9. This value was similar to the ratio PLLA-HA M_w decrease:PLLA M_w decrease, which was calculated as ≈1.8 from the GPC results presented in Section 3.2.2. This indicates that the FTIR results support the results of the GPC.

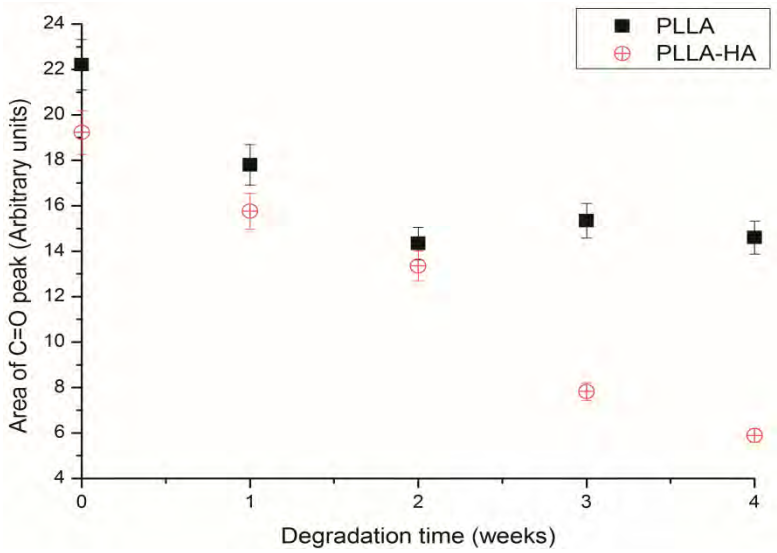

Figure 27: **Changes to the C=O peak area as a function of degradation time measured by FTIR (Error bars indicate standard deviation)**

3.2.5 Thermal analysis

In Figure 28, the DSC scans of the various fibre scaffolds are shown, while Table 4 presents some of their thermal properties. There was a large difference between the degree of crystallinity exhibited by these PLLA electrospun scaffolds (33%) and those exhibited by the electrospun scaffolds used in the crystallinity studies (42%) (Table 2 and Table 4). As the needle tips used when electrospinning fibres for crystallinity studies had a smaller orifice diameter (0.8 mm) than the needle tips used when electrospinning fibres for degradation studies (0.9 mm), it was considered that there was a possibility that the average fibre diameters of fibres produced by both electrospinning experiments would be different. As explained in Section 3.2.1, orifice diameter of the needle tip influeces fibre diameter. The average fibre diameter of the scaffolds (electrospun from the 5 wt% PLLA solution at 25 kV and 12.5 cm NTCD, that is, the same conditions under which the scaffolds used for this degradation study were electrospun) used for crystallinity studies was calculated and determined to be 465 ± 148 nm.

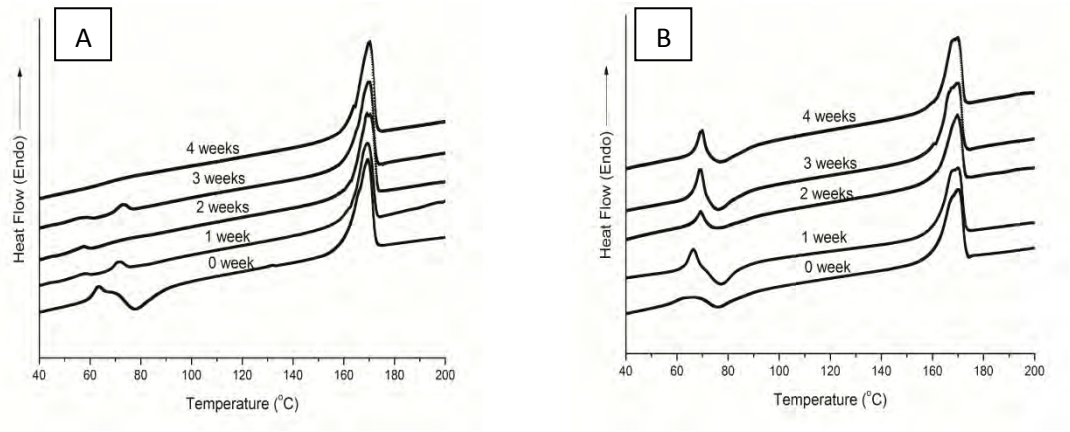

Figure 28: **DSC scans of (A) PLLA scaffolds (after 0, 1, 2, 3, and 4 weeks of degradation) and (B) PLLA-HA scaffolds (after 0, 1, 2, 3 and 4 weeks of degradation)**

According to Wong et al. (2008), fibre diameter influences the degree of crystallinity (Wong et al., 2008). In their work on electrospun PCL fibres of various diameters ranging from 250 nm to 900 nm, they reported an increase in the degree of crystallinity and molecular orientation of fibres, as the fibre diameter was reduced (Wong et al., 2008). The work of Prilutsky et al. (2008) on electrospun PAN/MWCNT showed that electrospun fibres exhibit core-shell morphology (Prilutsky et al., 2008). The authors reported that the relative orientation coefficient of the shell region was higher in comparison to that of the core region (Prilutsky et al., 2008). Specifically, the shell regions consist of oriented layer planes while the core regions consist of random coil chains (Baji et al., 2010). Therefore, as the fibre diameter is reduced, at some critical fibre diameter, the size of the shell region becomes similar to that of the overall fibre diameter. At this point, the oriented layer planes on either side of the fibre wall become linked and influence the overall properties of the fibres (Baji et al., 2010). As a result, thinner fibres will exhibit higher crystallinity in comparison to larger fibres.

Table 4: Variation of T_g, ΔH_m and X_c with degradation time during the 1st DSC heating cycle

Sample	Degradation time (weeks)	T_g (^oC)	ΔH_m (Heat of fusion) ($J.g^{-1}$)	X_c (Degree of crystallinity) (%)	Sample	Degradation time (weeks)	T_g (^oC)	ΔH_m (Heat of fusion) ($J.g^{-1}$)	X_c (Degree of crystallinity) (%)
PLLA	0	62	44.1	33.4	PLLA-HA	0	60.7	43.3	36.9
	1	56	35.8	38.2		1	nd	39.9	44.8
	2	56	38.6	41.2		2	nd	34.4	38.7
	3	54	39.2	41.9		3	nd	40.4	45.5
	4	nd	42.1	45.0		4	nd	37.4	42.0

nd – not detected

The 67% increase in fibre diameter when the orifice diameter of the needle tip was changed from 0.8 mm to 0.9 mm probably resulted in the difference in the degree of crystallinity exhibited by the scaffolds used in this section and those used in Section 3.1. Similarly, the slightly higher crystallinity of the PLLA-HA scaffold in comparison to that of the PLLA may have been due to the smaller fibre diameter of the former. In contrast, although the fibre diameter of the PLLA-HA scaffold (316 ± 147 nm) was lower in comparison to the fibre diameter of the scaffolds used in Section 3.1 (465 ± 148 nm), the degree of crystallinity of the PLLA-HA scaffold (36%) was lower than that of the scaffold used in Section 3.1 (42%). HA has been reported to reduce the crystallinity of PLLA due to the low crystallinity of HA particles (Sui et al., 2007), and this was the reason for the relatively lower crystallinity of the PLLA-HA scaffold. The initial degree of crystallinity of the polymer has been reported to have an influence on the degradation rate of the polymer (Kister et al., 2000; Li and McCarthy, 1999b; Vert et al., 1994; Dahlin et al., 2011); specifically, a polymer with a high crystallinity will exhibit a slow degradation rate and vice versa. In this study, because the PLLA and PLLA-HA scaffolds exhibited comparable initial crystallinities, the effect of initial crystallinity was not considered to be a major influence on the difference on the degradation rates of both scaffolds.

A number of the electrospun scaffolds exhibited an endothermic peak at ≈70^{o}C (Figure 28). Polyester degradation is characterised by random chain scission through hydrolysis (Zong et al., 2003; Gomes and Reis, 2004; Middleton and Tipton, 2000), resulting in the formation of oligomers. It is probable that it was these oligomers which melted at ≈70^{o}C. It was interesting to note that these endothermic peaks observed in the case of PLLA-HA scaffolds were much larger than those observed for the PLLA scaffolds (Figure 28). Similarly, Chen and Ma reported such low melting peaks during degradation of PLLA nanofibres prepared by

liquid-liquid phase separation. The low melting peaks were attributed to low molar mass crystallites which were formed during the degradation process (Chen and Ma, 2006). The increase of polydispersity with time (Figure 24) indicates that as degradation advanced, random chain scission in the polymer resulted in the formation of fragments of shorter and varying chain lengths; some of which may have melted at ≈70^{o}C.

An increase in crystallinity was observed for both the PLLA and PLLA-HA electrospun scaffolds during the degradation study (Table 4). It has been established that polymer degradation is initiated in the amorphous regions since it is less organized and more accessible to water molecules by diffusion (Middleton and Tipton, 2000; Zong et al., 2003). Therefore, as the polymer chain scission continues during degradation, the mobility of the amorphous chains is increased dramatically, facilitating and leading to crystallisation of the degraded amorphous regions - referred to as cleavage-induced crystallisation (Dong et al., 2009; Zong et al., 2003; Zong et al., 1999). The increase in crystallinity observed for the scaffolds in this study was therefore due to cleavage-induced crystallisation.

Additionally, a decrease in T_g from 61^{o}C to 54^{o}C for the PLLA electrospun scaffolds was observed within the first 3 weeks of degradation, while the T_g of the PLLA-HA electrospun scaffolds could not be detected after the 1st week of degradation (Table 4). Similar decrease in the T_g of polyesters during degradation have been reported in the literature (Lostocco and Huang, 1998; Dong et al., 2010; Li and McCarthy, 1999a). The decrease in T_g occurred as a result of the decrease in M_w. Since at the initial stages of degradation, random chain scission occurs as a result of hydrolysis, the polymer chains are severed into chains of smaller lengths which will inevitably exhibit lower glass-transition temperatures (Li, 1999).

3.3 Preparation and Characterisation of Bi- and Multicomponent Tissue Engineering Scaffolds of PLLA

3.3.1 Optimisation of electrospinning parameters

It had been expected that the results and understanding gained during the experiments reported in Sections 3.1 and 3.2 would be used to fabricate bi- and multicomponent scaffolds of PLLA, however, the use of the ES1a electrospinning machine was discontinued after these two sets of experiments due to the following reasons:

a) Restrictive nature of the machine – The design of the machine made it impossible to vary the needle-tip-to-collector distance beyond a certain maximum (15 cm);
b) Fibre diameter – It was difficult to regularly produce nanofibres, i.e. <500 nm due to the size of the needle tips/capillary tips that could be used on the machine;
c) Flow rate – The design of the machine made it largely difficult to exercise great control over the flow rate of the electrospinning solution. According to the manufacturers of the ES1a, the machine works on a constant pressure system and not on a constant flow rate system;
d) Cell culture – The design of the machine made it difficult to attach glass slides for the purpose of collecting fibres to be used for biocompatibility studies.

Consequently, it was decided that the electrospinning apparatus shown in Figure 13 should be used (described in detail in Section 2.2.3). Optimisation experiments were conducted to determine the electrospinning parameters which would yield uniform, bead-free nanofibres. As explained in Chapter 1, cells have been found to grow better on nanoscale materials than on macroscale materials, hence the aim of creating nanofibres.

Based on previous experience with the ES1a electrospinning machine, an attempt was made to use the 2nd electrospinning machine to electrospin 5 wt% PLLA in DCM/DMF. However, the fibres electrospun from this solution concentration using the 2nd electrospinning set up exhibited a large number of beads (Figure 29A). The electrospinning parameters tested were: voltages ranging between 15 kV and 20 kV; NTCDs ranging between 12 to 17.5 cm; and flow rates varying between 0.3 ml/h and 1 ml/h. The voltage and NTCD were chosen based on the experimental conditions used during the crystallinity study experiments. However, because the ES1a operates on a constant pressure system rather than a constant flow rate system, it was difficult to calculate the flow-rate during the crystallinity study experiments. As a result, various flow-rates were used during the optimisation experiments on the 2nd electrospinning machine in order to determine an optimum flow-rate. SEM images of fibres electrospun from the ES1a and the 2nd electrospinning machine with similar electrospinning parameters showed the absence of beads on the fibres electrospun from the ES1a (Figure 29B) while beads were observed on the fibres electrospun from the 2nd machine (Figure 29A). The reason for this may have been due to any, or combination of these two reasons:

a) A more stable Taylor cone in the ES1a – As mentioned previously, the ES1a machine works on a constant pressure system and not on a constant flow rate system. The Taylor cone is generated as a result of the combination of the surface tension, the charge repulsion at the surface and internal pressure of the droplet (Electrospinz, 2008). The internal pressure of a constant flow rate system is variable while that of a constant pressure system is constant. This is likely to result in a more stable Taylor cone, hence the lower probability of bead formation in the ES1a.

b) The vertical set-up of the 2nd machine would have meant all beads/droplets coming from the needle tip will be deposited on the collector, whereas for the ES1a, the beads/droplets may fall on the chassis of the machine and not reach the collector due to the effect of gravity. Visual examination of the ES1a after electrospinning revealed the presence of tiny white spots, which were droplets of the PLLA solution.

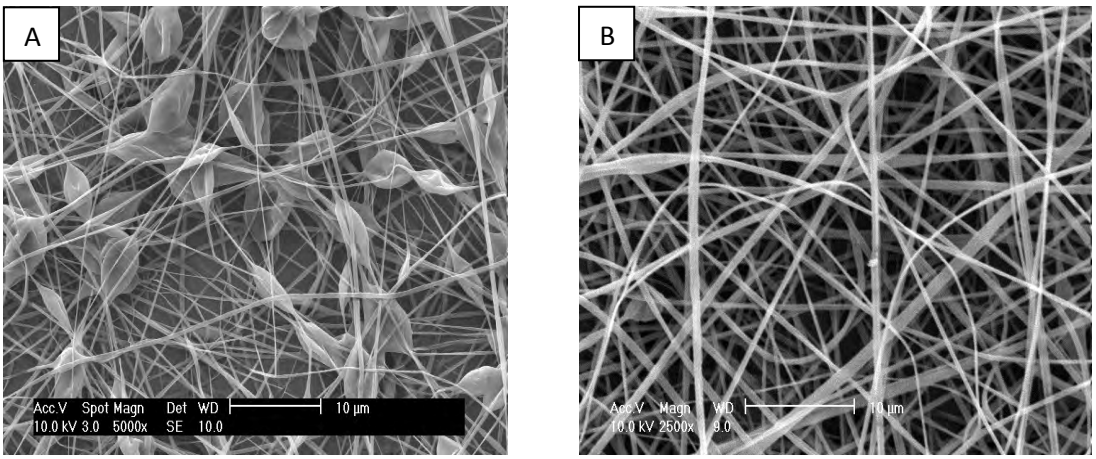

Figure 29: ESEM images of fibres electrospun from 5 wt% PLLA in DCM/DMF solution at 15 kV and NTCD of 15 cm using (A) 2nd electrospinning machine and (B) ES1a electrospinning machine

Following this, the polymer solution concentration was increased stepwise by 1 wt% until 8 wt% when bead-free fibres were obtained (Figure 30A and Figure 30B). Electrospinning parameters similar to those described in the preceeding paragraph were utilized to electrospin these solutions. The reasons for bead formation during electrospinning have been previously explained in Section 3.1.1.

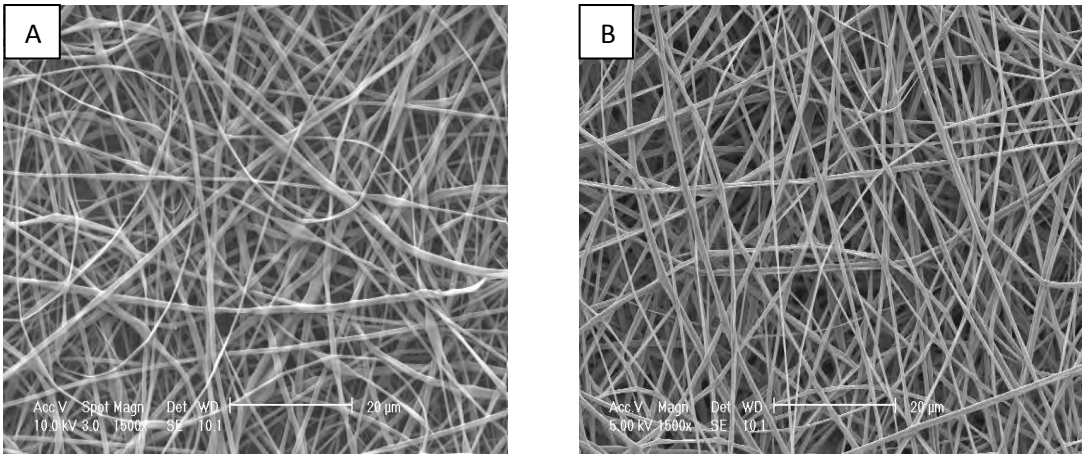

Figure 30: **ESEM images of PLLA fibres electrospun at an applied voltage of 14 kV, NTCD of 12 cm and flow rate of 0.3 ml/h from (A) 7 wt% and (B) 8 wt% PLLA in DCM/DMF solutions**

Since gelatin is a biopolymer with strong polarity, there are very few organic solvents of high polarity available to dissolve it (Huang et al., 2004). However, researchers have reported the use of fluorinated alcohols such as TFE to dissolve gelatin prior to electrospinning (Kim et al., 2008a; Meng et al., 2010; Huang et al., 2004). Based on this, it was considered that DCM/DMF would not be a suitable solvent; hence, TFE was chosen as the solvent for gelatin in this project. It was therefore decided, that since the PLLAGel would be dissolved in TFE, for the purpose of comparison, the PLLA should also be dissolved in TFE. As a result, the use of DCM/DMF as a solvent was discontinued and TFE was used as the only solvent after this point.

Consequently, a series of polymer solution concentrations of PLLA in TFE were tested until bead-free fibres were obtained. Based on the previous work with dichloromethane/N,N-dimethylformamide, the polymer solution concentration was tested from 8 wt% until 15 wt% when, cylindrical, bead-free fibres were obtained (Figure 31 A – H). The electrospinning parameters utilized at this point were similar to those used in the previously described optimisation experiments, although lower voltages of 13 kV and 14 kV were also used.

These parameters were chosen based on the previously described optimisation experiments. As the polymer solution concentration was increased from 8 wt% to 15 wt%, the bead concentration gradually decreased until they were totally absent on the fibres from the 15 wt% polymer solution. Additionally, the shape of the beads changed progressively from spherical to spindle-like until bead-free fibres were obtained (Figures 31A - 31H).

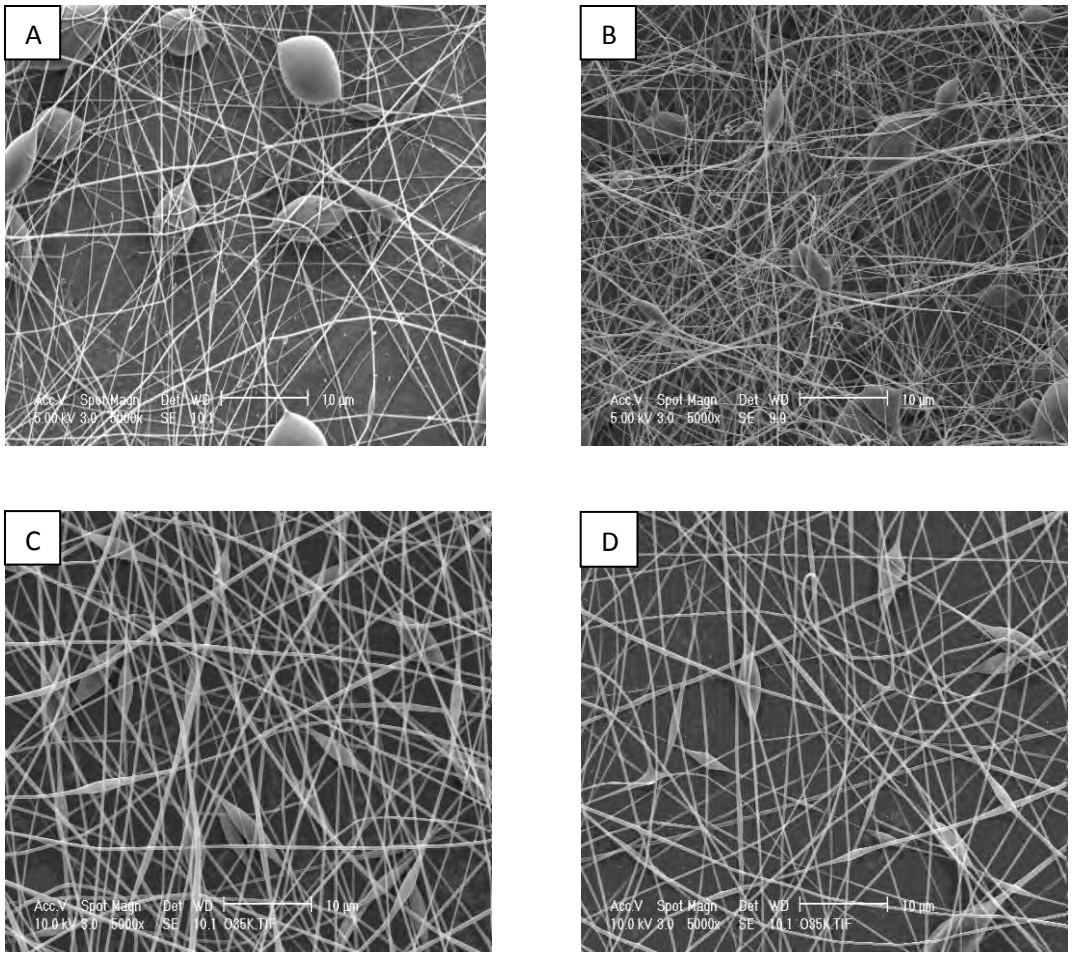

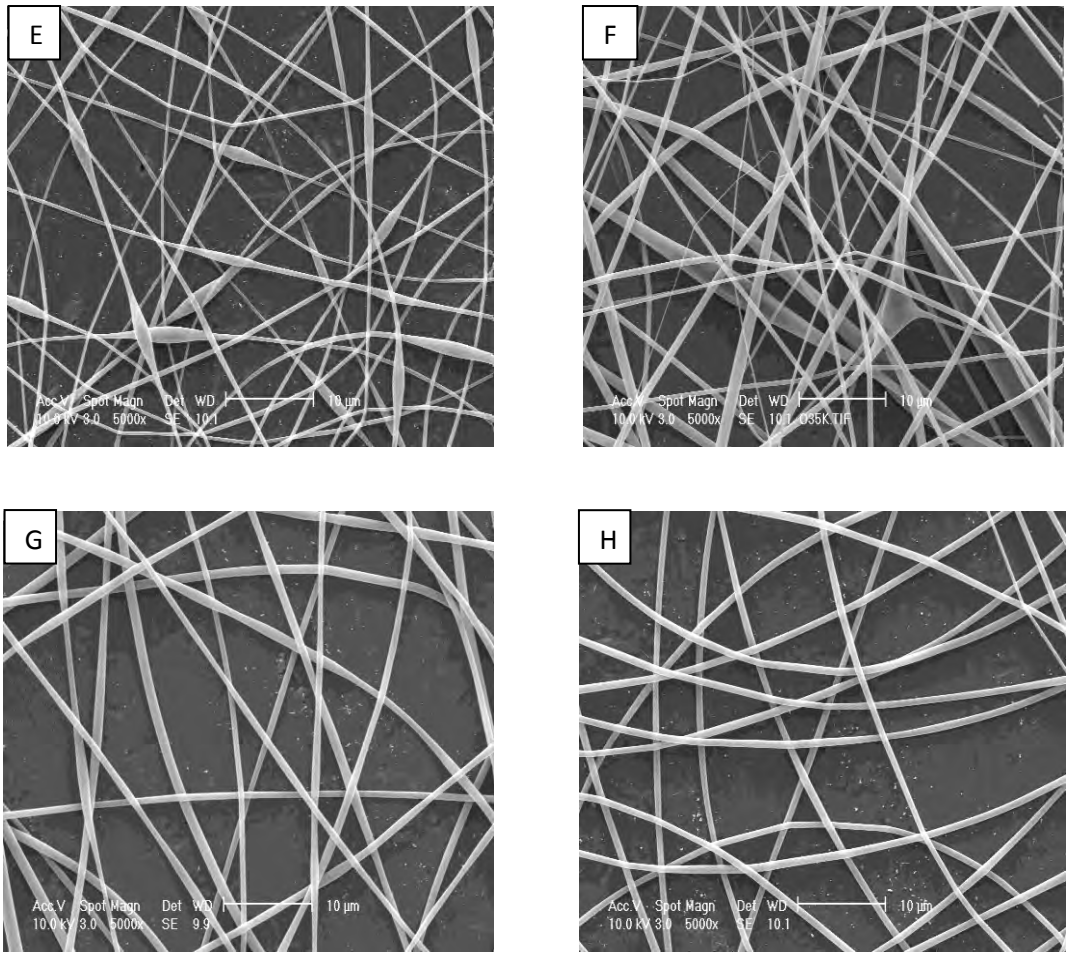

Figure 31: **ESEM images of fibres electrospun from (A) 8 wt%, (B) 9 wt%, (C) 10 wt%, (D) 11 wt%, (E) 12 wt%, (F) 13 wt%, (G) 14 wt%, and (H) 15 wt% polymer solution concentrations**

Upon determination of the minimum polymer solution concentration at which bead-free PLLA fibres could be obtained, other electrospinning parameters, specifically the voltage and flow rate were varied to obtain the optimum conditions for electrospinning. Although all combinations of electrospinning parameters produced bead-free fibres, a combination which produced the most uniform fibres was determined, details of which have been previously reported in Chapter 2.

During optimisation experiments on the 2nd electrospinning machine, it was observed that the fibres obtained from electrospinning PLLA in DCM/DMF were mostly flat, with fibre fusions (Figure 32A), whilst those obtained when electrospinning from the PLLA in TFE

solutions were cylindrical/tubular and independent fibres (Figure 33A). At the initial stages of electrospinning, as the solvent evaporates, a thin skin may form over the surface of the polymer jet, resulting in a structure consisting of a thin solid skin over a liquid core. When the solvent eventually evaporates from the core, the fibre collapses due to atmospheric pressure (Baji et al., 2010; Zhang et al., 2007a), resulting in flat fibres as seen in Figure 31A. Furthermore, if the solvent does not completely evaporate during the fibre forming process, fibre-fibre fusions may occur (Baji et al., 2010) at fibre junctions. These effects can be eliminated by using a highly volatile solvent (Baji et al., 2010). Another possible reason for the production of flat fibres could be that, due to incomplete evaporation of the solvent during the flight time of the jet, the fibres were still wet at the point of deposition on the collector; these fibres would have flattened upon impact with the collector. A similar observation was made by Koski et al. (2004) when electrospinning PVA of different molecular weights. The authors attributed the production of flat fibres to the slow rate of solvent evaporation due to increase in solution viscosity as the molecular weight of PVA was increased (Koski et al., 2004). Additionally, the fibres obtained by electrospinning PLLA from the DCM/DMF solution exhibited large diameters, mostly in the 700–800 nm range (Figure 32B) whereas those obtained by electrospinning PLLA from TFE solution exhibited smaller diameters, mostly in the 400–500 nm range (Figure 33B). The fibres electrospun using DCM/DMF as a solvent exhibited higher diameters compared to those electrospun from the TFE solvent because of the higher conducitivity of TFE (0.57 mS/m) (Marsano et al., 2010) compared to that of DCM/DMF (0.273 mS/m) (Theron et al., 2004). Uyar and Besenbacher (2008) demonstrated the effect of solvent conductivity on the solution conductivity of different solutions of polystyrene (PS) using DMF of varying electrical conductivities as solvents (Uyar and Besenbacher, 2008). It was reported, that the DMF with the highest

electrical conductivity produced the PS solutions with the highest electrical conductivities irrespective of solution concentration. Furthermore, it was reported, that when PS solutions of equal concentrations were electrospun under similar electrospinning conditions, the polymer solutions which yielded bead-free fibres with the lowest average diameters were those with the highest solution conductivities (Uyar and Besenbacher, 2008). In this research project, it was observed that polymer solutions of high electrical conductivity (based on TFE) resulted in thinner electrospun polymer fibres compared to lower electrical conductivity solutions (based on DCM/DMF). It was also noteworthy, that although both fibre scaffolds were electrospun from the lowest polymer solutions at which bead-free fibres could be electrospun using comparable electrospinning parameters, the fibre morphologies were distinct from each other. The difference in the morphology of both sets of electrospun fibres was likely due to a combination of the difference in conductivity of the solvents used and the difference in the viscosity of the solutions used for electrospinning.

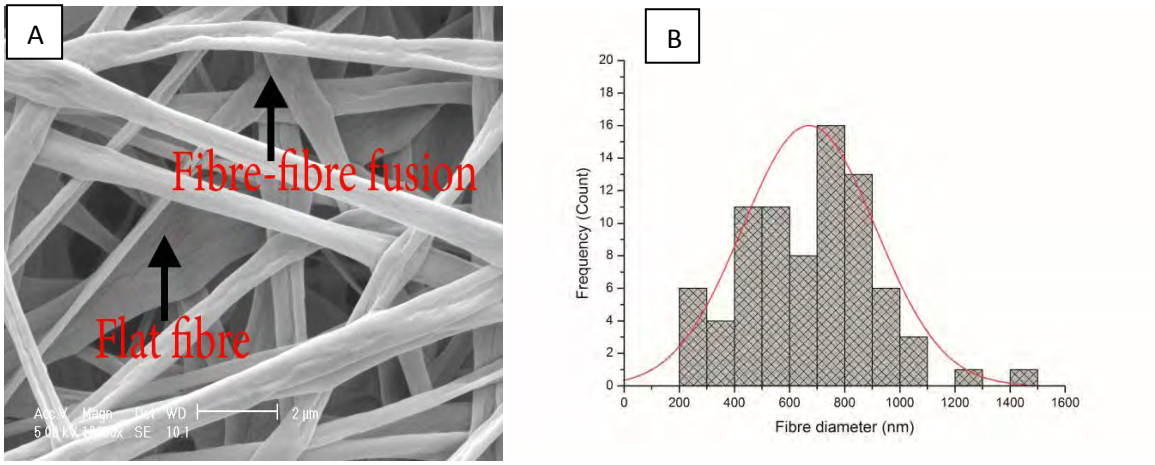

Figure 32: (A) ESEM image and (B) Fibre diameter distribution of PLLA fibres electrospun from 8 wt% PLLA in DCM/DMF solution at an applied voltage of 14 kV, flow rate of 0.3 ml/h and NTCD of 17.5 cm

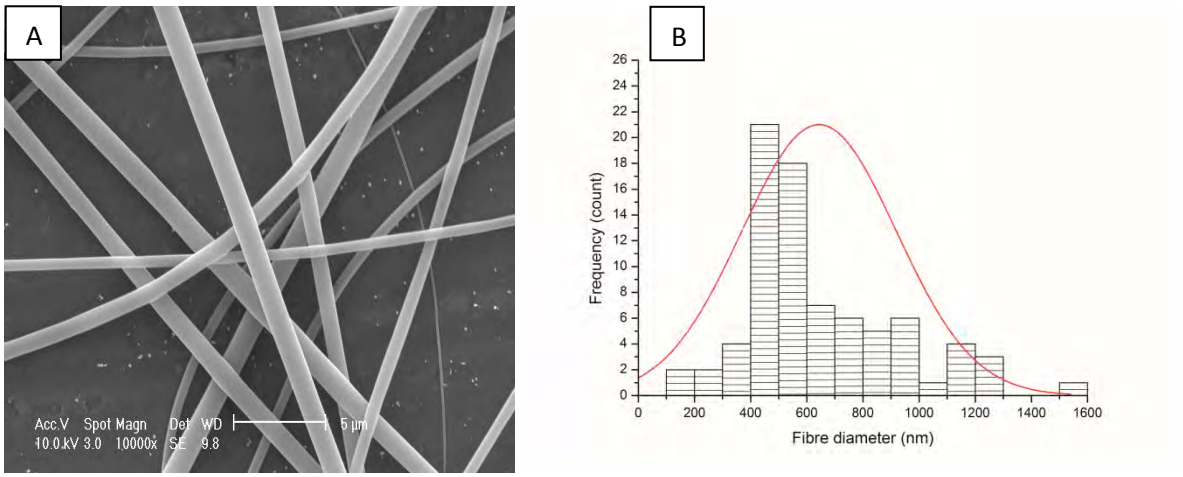

Figure 33: **(A) ESEM image and (B) Fibre diameter distribution of PLLA fibres electrospun from 15 wt% PLLA in TFE solution at an applied voltage of 14 kV, flow rate of 0.3 ml/h and NTCD of 17.5 cm**

During the optimisation experiments, it was also observed, that increasing the flow rate can also result in the formation of beads. For instance, during the optimisation experiments for 8 wt% PLLA in DCM/DMF solutions, although it had been established that beadless fibres could be electrospun from the 8 wt% solution, it was however observed that beaded fibres could be produced at high flow rates. For instance, when a flow rate of 0.3 ml/h was used to electrospin the fibres, there were no beads observed on the fibre scaffolds (Figure 34A). However, when the flow rate was increased to 0.5 ml/h, beads were formed on the surface of the fibre scaffold (Figure 34B). The bead density was observed to increase when the flow rate was further increased to 1.0 ml/h (Figure 34C). At a high flow rate, there is a greater volume of solution at the needle tip, meaning that the solution is being supplied to the needle tip at a faster rate than it is being drawn away. This may result in inability of the fibres to dry completely before reaching the collector, and the consequent formation of beads (Sill and von Recum, 2008).

Subsequent to determining the optimum polymer solution concentration at which bead-free fibres of PLLA can be electrospun from TFE solutions, optimisation experiments were

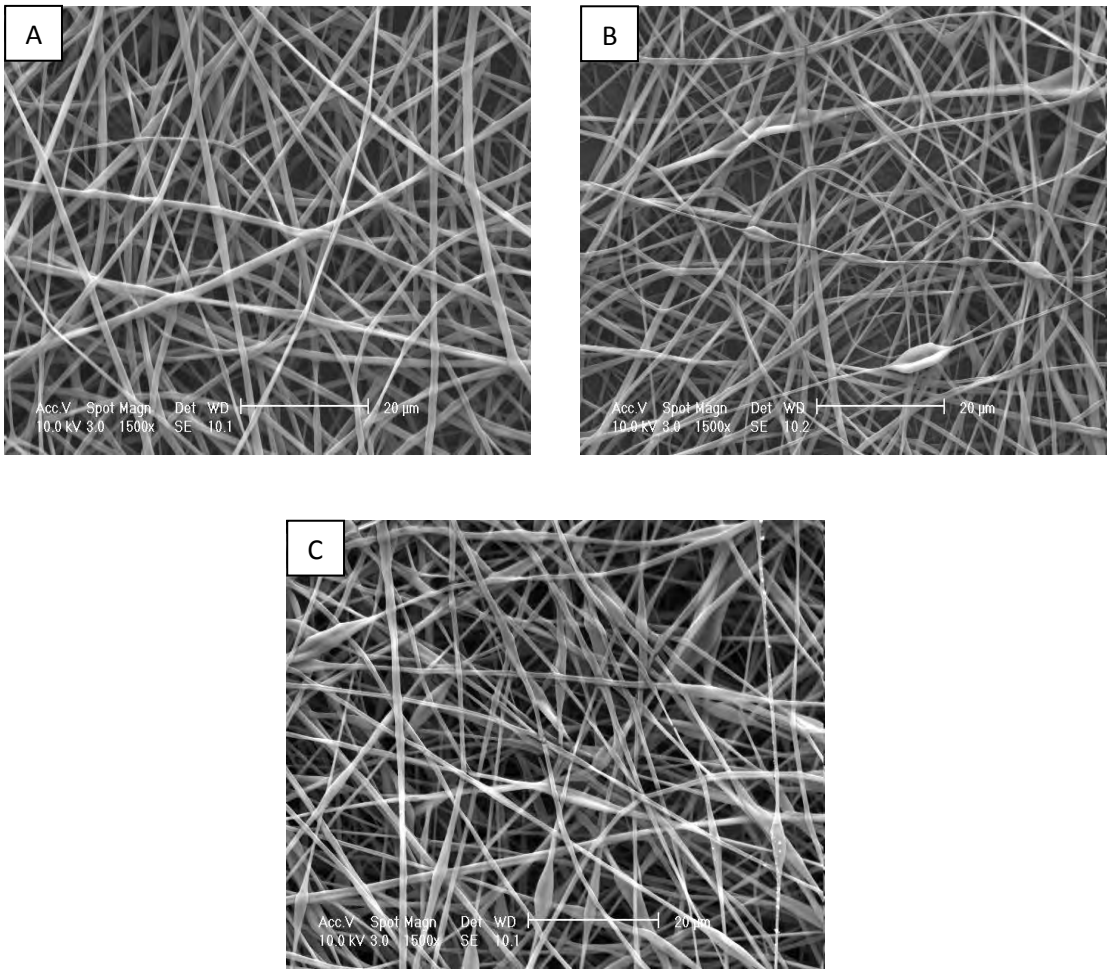

Figure 34: ESEM images of fibres electrospun from 8 wt% PLLA in DCM/DMF solution at an applied voltage of 14 kV, NTCD of 12 cm and flow rate of (A) 0.3 ml/h, (B) 0.5 ml/h, and (C) 1.0 ml/h

conducted to determine the optimum polymer solution at which bead-free fibres of PLLAGel could be electrospun from TFE solutions.

The 2 wt% PLLAGel (1:1) solution produced large globules of polymer without formation of any fibres (Figure 35A) while the 3 wt% PLLAGel (1:1) solution yielded a small amount of fibres, although it also exhibited a large amount of polymer globules (Figure 35B). The

amount of fibres electrospun from the solutions gradually increased while the amount of polymer globules decreased until at 5 wt% PLLAGel (1:1) solution when fibres with large diameters (1.26 ± 0.57 µm) were obtained without the presence of any globules (Figure 35D). In a bid to produce bead-free fibres with smaller diameters, the polymer solution concentration was increased to 8 wt%, although the PLLA:Gelatin ratio was changed to 75:25 and 80:20. Although thinner fibres (≈239 ± 60 nm for the former and 138 ± 62 nm for the latter) were obtained from these polymer solution concentrations, a few beads were observed on these fibres (Figure 35 E and F, respectively). Similarly, the diameters of fibres obtained by electrospinning the 9 wt% PLLAGel (75:25) solution were in the nanometre range – 458 ± 181 nm, but large beads were still observed on the scaffolds (Figure 35G). Following this, and for the purpose of easy comparison with the PLLA nanofibre scaffolds, the PLLAGel solution was increased to 15 wt% while PLLA and gelatin were blended at a ratio of 90:10 and 80:20. Bead-free nanofibres (≈499 ± 194 nm) were obtained from the former (Figure 35H) while the latter solution was very difficult to electrospin and a wide distribution of fibres ranging from the micrometer range to the nanometre range (1.72 ± 1.34 µm) were obtained (Figure 35I).

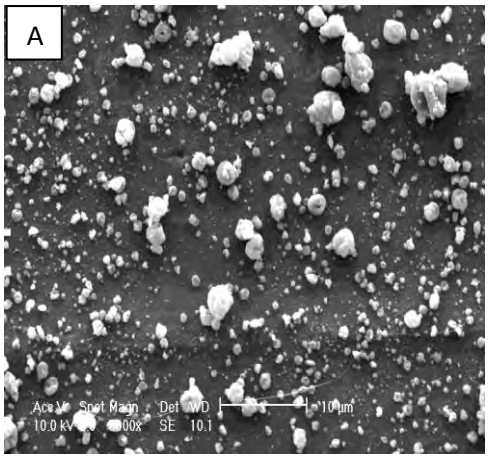

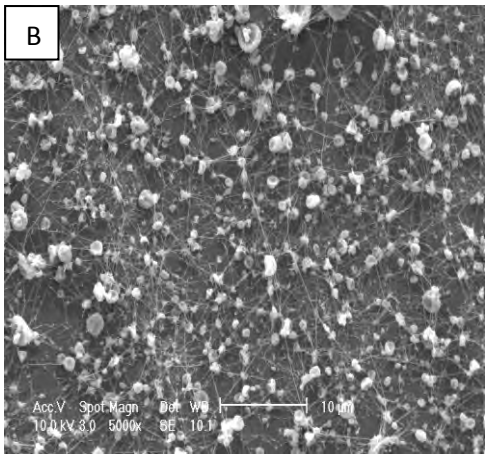

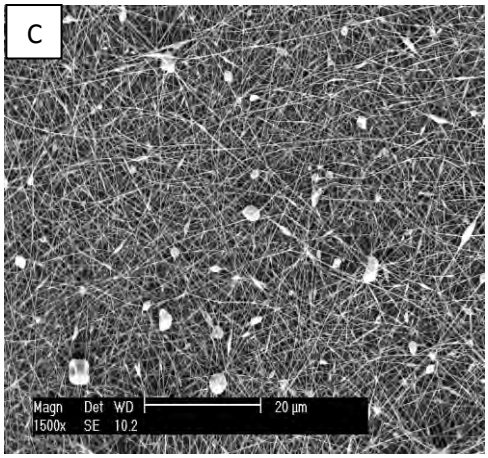
C
Magn Det WD
1500x SE 10.2
20 µm

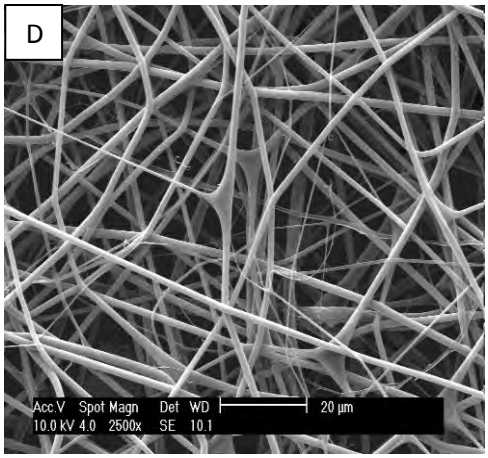
D
Acc.V Spot Magn Det WD
10.0 kV 4.0 2500x SE 10.1
20 µm

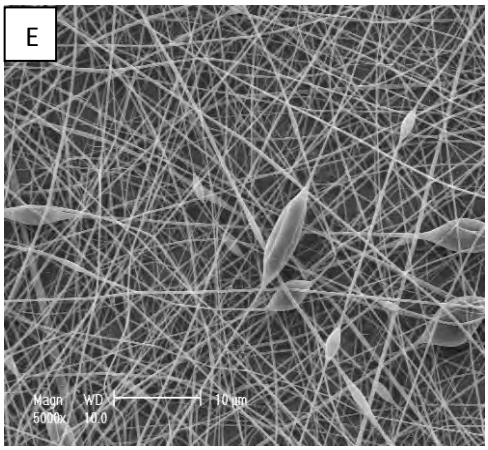
E
Magn WD
5000x 10.0
10 µm

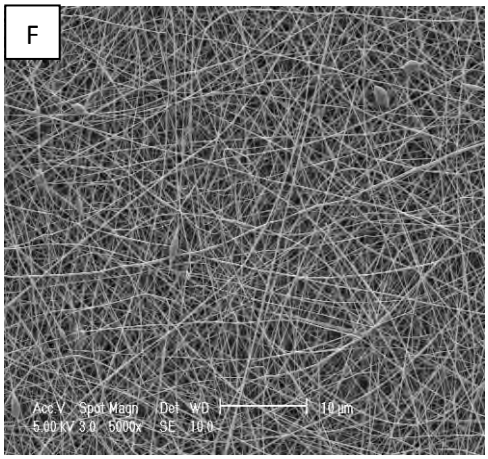
F
Acc.V Spot Magn Det WD
5.00 kV 3.0 5000x SE 10.0
10 µm

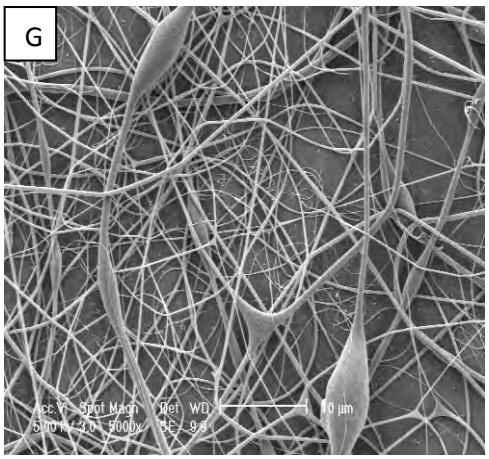
G
10 µm

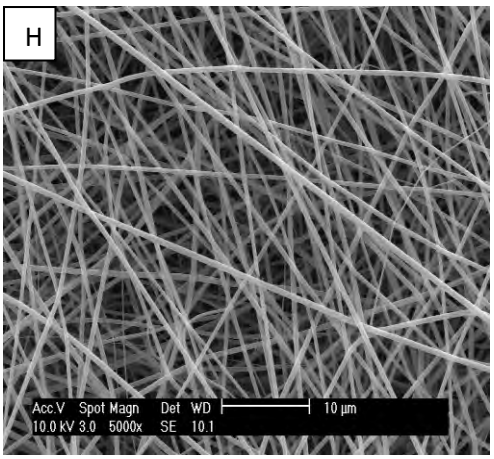
H
Acc.V Spot Magn Det WD
10.0 kV 3.0 5000x SE 10.1
10 µm

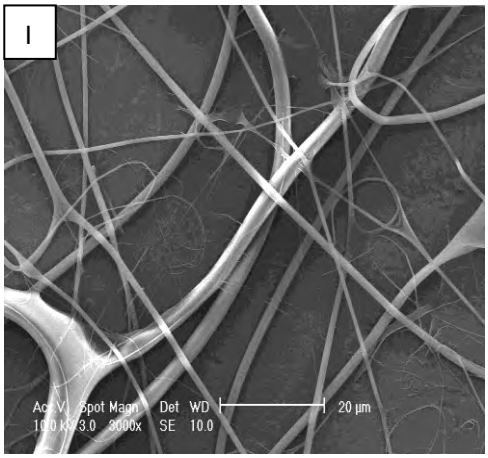

Figure 35: **ESEM images of PLLAGel fibres electrospun from (A) 2 wt%, (B) 3 wt%, (C) 4 wt%, (D) 5 wt%, (E) 8 wt% (75:25), (F) 8 wt% (80:20), (G) 9 wt% (75:25), (H) 15 wt% (90:10), and (I) 15 wt% PLLAGel (80:20) polymer solution concentrations**

Based on this, the 15 wt% PLLAGel (90:10) solution was chosen as the optimum polymer solution concentration for the project. Following this, other electrospinning parameters, specifically, the voltage and flow rate were varied to determine the combination of electrospinning parameters which would yield the most uniform fibres. Although all combinations of electrospinning parameters produced bead-free fibres, a combination which produced the most uniform fibres was determined, details of which have been previously reported in Chapter 2.

Of all the methods of fabricating biodegradable electrospun polymer/hydroxyapatite composites reported in the literature as discussed in Section 1.10, electrospraying was preferred as the method of producing the PLLAGel-HA scaffolds in this study because of the following reasons:

I. In order to avoid the problem of agglomeration which has been associated with the mixing method (Supova, 2009), attempts were made to obtain a homogenous dispersion of HA in PLLA-DCM/DMF solution by using a surfactant, HSA, as reported

by Kim et al. (2006a). However, when thermal analysis of the scaffolds so produced were carried out by DSC, during the 1st heating cycle, an endotherm was observed at around 80°C, and the melting temperature was lower in comparison to the scaffolds electrospun without HSA (Figure 36A). During the cooling cycle, two exotherms (around 95°C and 63°C) were observed on scaffolds containing HSA (Figure 36B), suggesting enhanced crystallisation of PLLA. After erasing the thermal history of both sets of samples, during the 2nd heating cycle, the endotherm observed during the 1st heating cycle was still present, cold crystallisation seemed to be suppressed (occurring at a lower temperature), and the melting point was lower in comparison to the scaffolds electrospun without HSA (Figure 36C). The endotherms observed during the 1st and 2nd heating cycles were ascribed to the HSA, because a strong endotherm was observed when HSA alone was tested (Figure 36D). Similarly, the exotherms observed during the cooling cycle were due to the HSA, because a strong exotherm was observed during cooling of HSA alone (Figure 36E). In order to avoid any negative effect that the presence of HSA may have on biocompability or thermal characteristics of the scaffolds, the method was discontinued altogether;

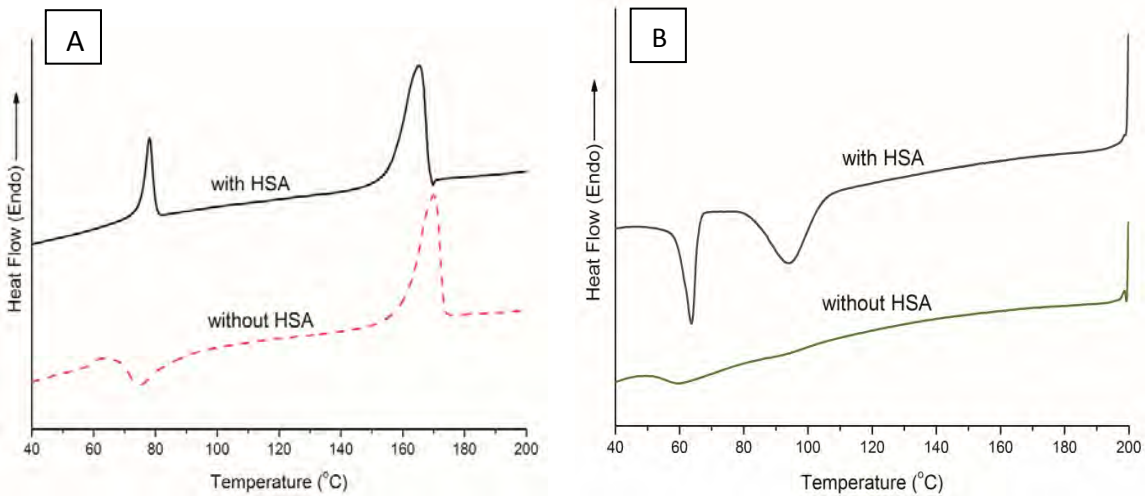

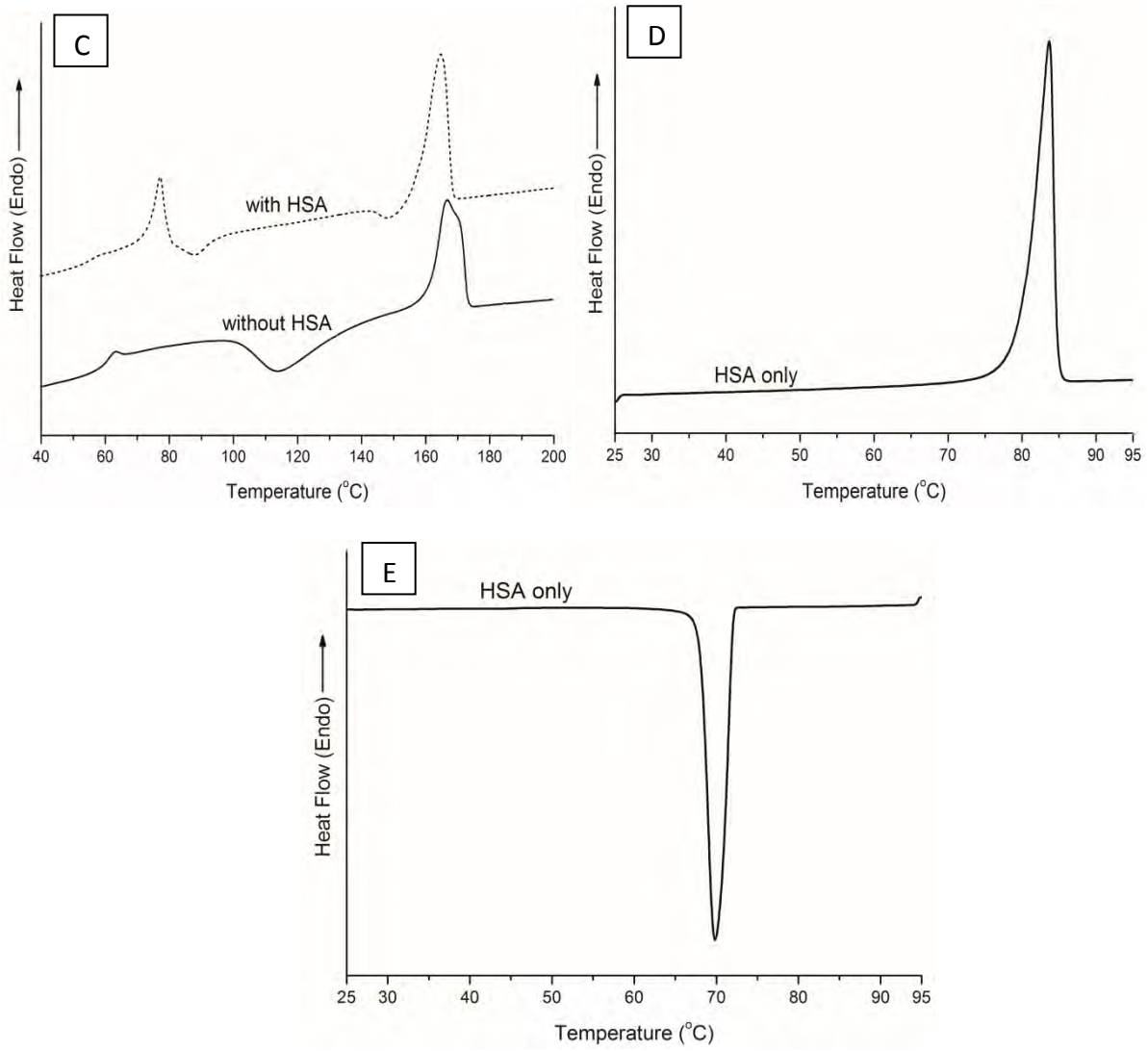

Figure 36: DSC scans of (A) 1st heating cycle of PLLA-HA (90:10) compared with PLLA-HA (90:10) + 0.5 wt% HSA, (B) Cooling cycle of PLLA-HA (90:10) compared with PLLA-HA (90:10) + 0.5 wt% HSA, (C) 2nd heating cycle of PLLA-HA (90:10) compared with PLLA-HA (90:10) + 0.5 wt% HSA, (D) 1st heating cycle of HSA alone, and (E) Cooling cycle of HSA alone

II. From the study on the degradation behaviour of PLLA and PLLA-HA electrospun scaffolds reported in Section 3.2 and the literature, it was considered that it was the exposure of HA particles that caused the neutralisation of the degradation medium during degradation of polymer/HA scaffolds, it was therefore considered that their

complete exposure on the surface of the electrospun nanofibres may lead to an improvement in the degradation properties of the electrospun polymer/HA scaffolds;

III. It had been reported by previous researchers that the exposure of HA particles on the surface of scaffolds improved osteoblast adhesion (Francis et al., 2010; Gupta et al., 2009); and

IV. The simplicity of the method in comparison to the *in-situ* synthesis and mineralisation methods.

Furthermore, the same concentration of HA (5 wt%) used in fabricating the PLLA-HA scaffolds studied in Section 3.2 was used during these experiments to avoid the agglomeration of HA particles on the surface of the scaffold, and also for the purpose of easy comparison of the degradation properties of both sets of scaffolds. Additionally, it was considered that since the HA particles would be completely exposed on the surface of the polymer scaffold, their reported neutralising effect may be more prominent, since it was not observed in the PLLA-HA scaffolds studied in Section 3.2.

Following this, experiments were conducted to determine the optimum conditions for electrospraying HA. The optimum conditions were determined as the conditions under which the best distribution of HA particles and least agglomeration was obtained as revealed by ESEM. The parameters tested were voltages ranging from 9 kV to 12 kV, and flow rates ranging from 1.5 ml/h to 2 ml/h were tested. ESEM micrographs of the specimens obtained during the optimization experiments are shown in Figure 37.

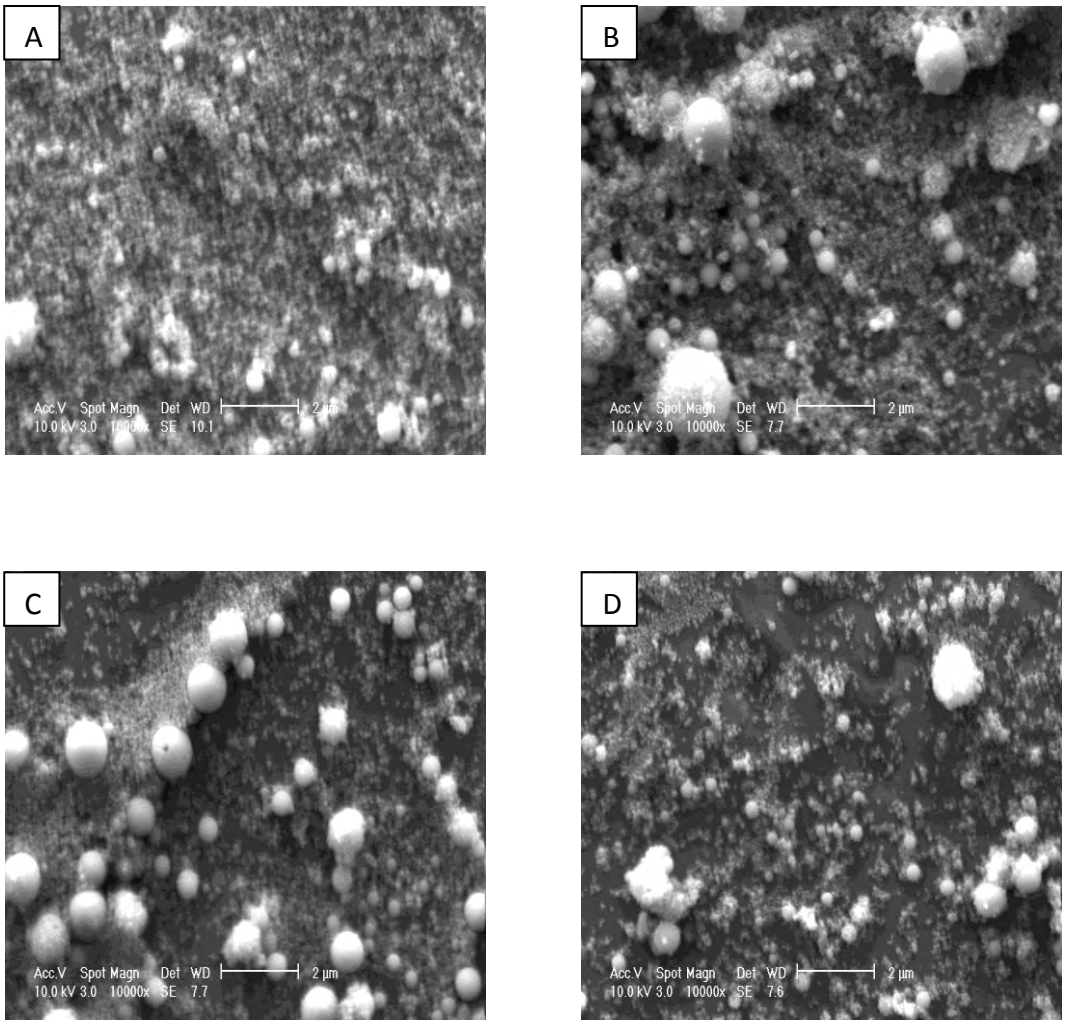

Figure 37: ESEM micrographs of HA particles electrosprayed at (A) 9 kV and 2 ml/h (B) 12 kV and 2 ml/h (C) 9 kV and 1.5 ml/h, and (D) 12 kV and 1.5 ml/h

3.3.2 Characterisation of bi- and multicomponent electrospun scaffolds of PLLA

3.3.2.1 ESEM

ESEM micrographs of the electrospun scaffolds revealed porous, beadless and nanofibrous structures (Figures 38A, C and E). The electrospun scaffolds exhibited porosities ranging

between 68 and 77%, with fibre diameters ranging between 392 and 760 nm (Table 5).

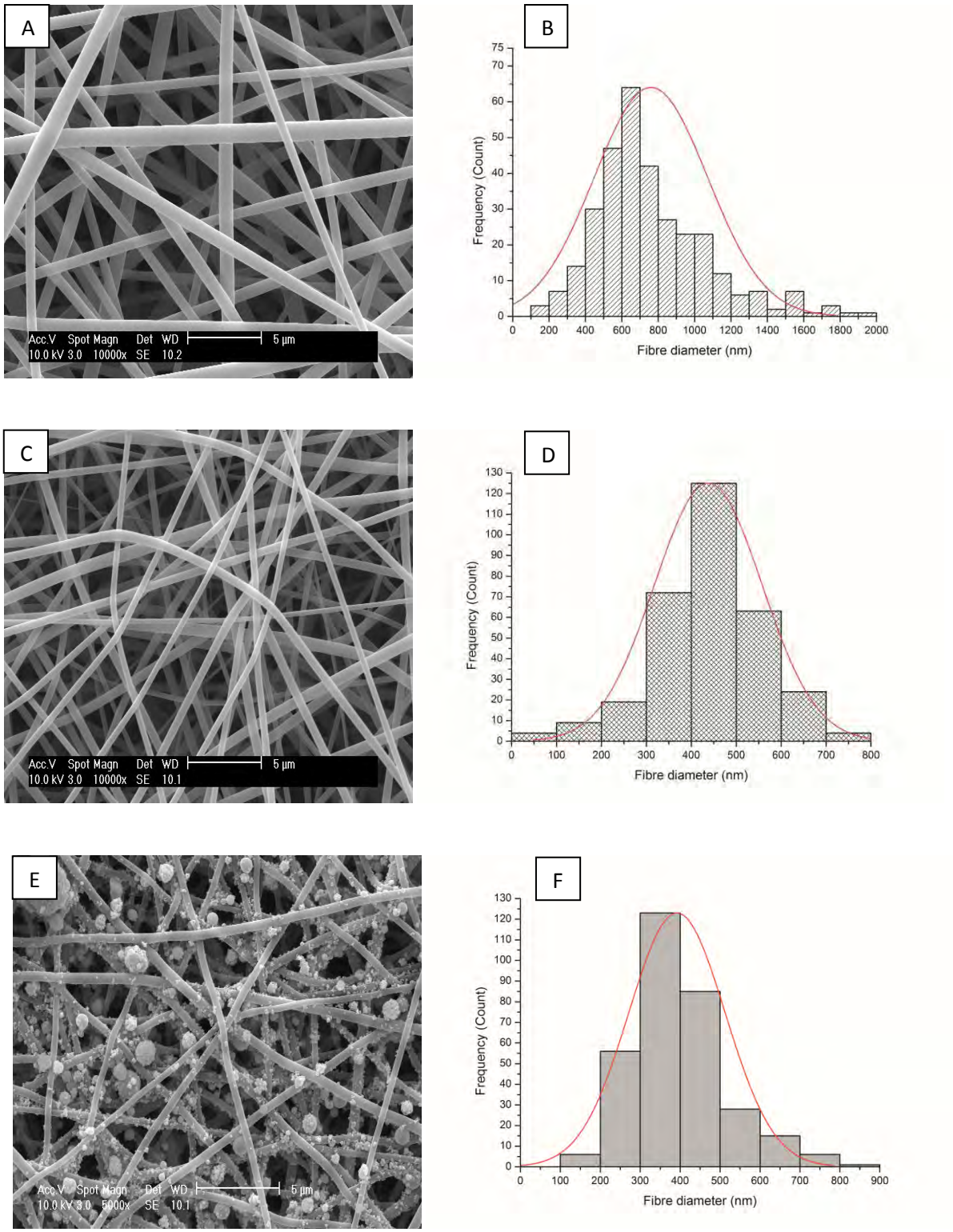

Figure 38: **ESEM micrographs and fibre diameter distributions of PLLA (A and B), PLLAGel (C and D), and PLLAGel-HA (E and F) electrospun scaffolds**

Table 5: **Characteristics of electrospun nanofibrous scaffolds**

Sample	Porosity (%)	Inter-fibre distance (μm)	Average fibre diameter (nm)
PLLA	69 ± 17	1.57 ± 0.15	760 ± 312
PLLAGel	77 ± 10	1.29 ± 0.04	438 ± 120
PLLAGel-HA	68 ± 13	1.23 ± 0.12	392 ± 121

The addition of gelatin (10%) to the PLLA resulted in approximately 50% significant ($p < 0.05$) decrease in fibre diameter (Table 5).

Polymer solution conductivity is another polymer solution parameter that influences the properties of electrospun fibres, although to a lower degree than polymer solution concentration (Sill and von Recum, 2008). During electrospinning, the polymer jet is stretched by the repulsion of electric charges at its surface (Ramakrishna et al., 2005). Therefore, the presence of a high amount of charges i.e. high solution conductivity will result in greater stretching of the polymer jet and hence smaller diameters of the electrospun fibres. Solution conductivity has been reported to influence fibre diameter within 1–2 orders of magnitude (Sill and von Recum, 2008). Gelatin is a polyelectrolyte polymer with many ionisable groups (Huang et al., 2004), therefore it is likely to increase the conductivity of the electrospinning solution when blended with PLLA in TFE. The fibre diameter of the PLLAGel scaffolds were almost half that of the PLLA scaffolds because gelatin molecules have a high dielectric constant, which gave rise to an electrospinning jet with high amount of excess charges and resulted in increased stretching of the jet and ultimately thinner fibres (Su et al., 2010); this may be analogous to increase of draw rate in

conventional fibre spinning (Mo et al., 2004). Meng et al. (2010) reported a similar decrease in fibre diameter of electrospun PLGA/gelatin scaffolds when gelatin and PLGA were blended at various ratios. The authors attributed this to the combined effect of lower viscosity of the blended solution and the amino acids of the gelatin (which increased the charge density of the electrospinning jet), causing an increment in the stretching force and self-repulsion of the electrospinning jet (Meng et al., 2010). Similar observations of fibre diameter reduction have also been made by other authors who worked with either gelatin or collagen (Kwon and Matsuda, 2005; Su et al., 2010; Lee et al., 2008).

Additionally, increased charges cause greater bending instability of the electrospinning jet which will aid the formation of fibres with smaller diameters since the jet path is increased (Ramakrishna et al., 2005).

The fibre diameter distributions of all the electrospun scaffolds were symmetric and unimodal although that of the PLLA scaffold was more widespread (Figures 38B, 38D and 38F). The widespread of the fibre diameter distribution of the PLLA scaffold may be due to the formation of secondary jets during electrospinning, otherwise known as splaying of the jet (Ramakrishna et al., 2005; Reneker et al., 2000; Reneker and Chun, 1996b); the splaying of the jet is itself a result of radial charge repulsion within the primary electrospinning jet (Shin et al., 2001). This also explains the higher standard deviation obtained for this scaffold when compared to the blend-based scaffolds. Similar wide-spread fibre diameter distribution has been reported by other researchers and this has generally been attributed to splaying of the electrospinning jet (Deitzel et al., 2001a; Demir et al., 2002).

The addition of gelatin to PLLA resulted in an 8% increase in porosity but an approximate 17% decrease in inter-fibre distance (pore size). The smaller fibre diameters of the blend-based scaffolds probably resulted in denser packing of the nanofibres causing a decrease in

inter-fibre distance. Lee et al. (2008) reported an increase in the porosity of electrospun fibre sheets when gelatin was blended with PLCL at certain ratios and attributed this to the dense packing of the soft and elastic PLCL fibres (Lee et al., 2008).

3.3.2.2 FTIR

Fourier Transform Infrared spectra of the electrospun scaffolds (Figure 39A) revealed that the blends of PLLA and gelatin had a mixture of the characteristic bands of both pure PLLA [≈1085 cm^{-1} (C-O stretching), ≈1182 cm^{-1} (C-O stretching mode of ester group), ≈1380 cm^{-1} (δCH_3 symmetric bending), ≈1452 cm^{-1} (δCH_3 asymmetric bending), ≈1750 cm^{-1} (C=O vibration)] and gelatin amides [≈1534 cm^{-1} (amide II peak for N-H bend coupled with C-N stretch), ≈1655 cm^{-1} (amide I band for C=O stretch) and ≈3310 cm^{-1} (amide A)] (Table 6) (Birshtein and Tul'chinskii, 1982; Kister et al., 1995).

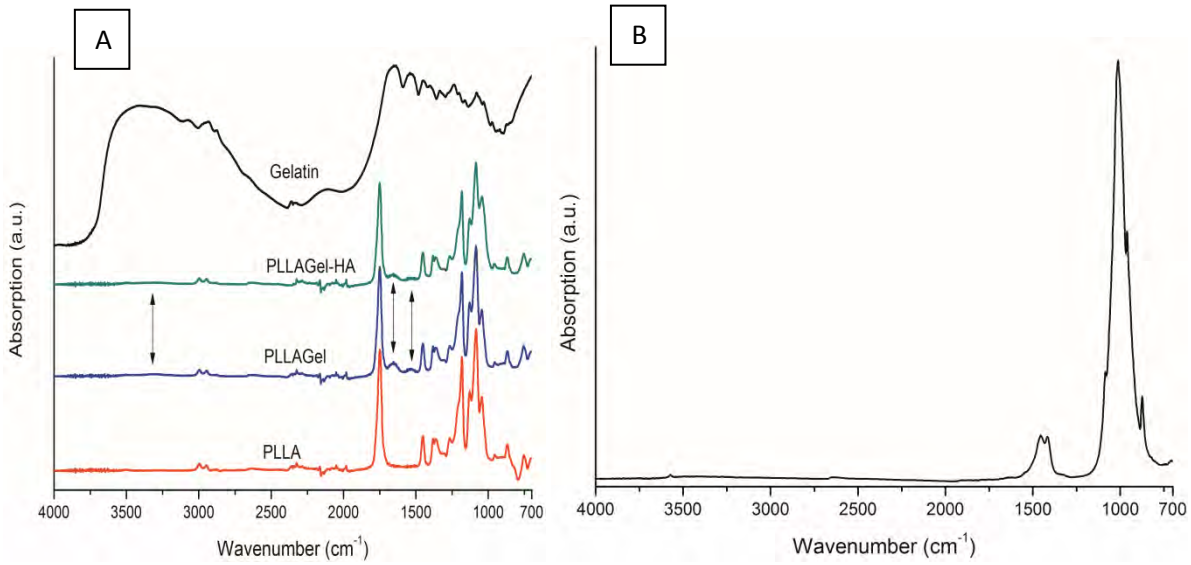

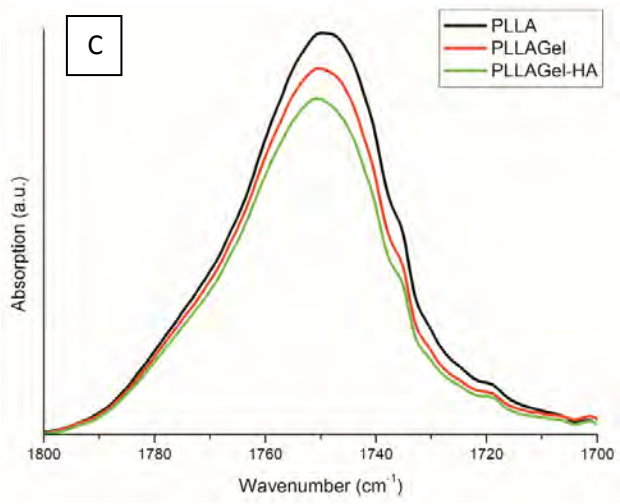

Figure 39: **(A) FTIR spectra for PLLA, PLLAGel and PLLAGel-HA scaffolds (Amide peaks in the gelatin-based scaffolds are indicated by arrows), (B) FTIR spectrum for HA, and (C) FTIR spectra of C=O peaks for PLLA, PLLAGel and PLLAGel-HA**

The phosphate (PO_4^{3-}) stretching peak of HA at 1012 cm^{-1} (Figure 39B) was not observed in the PLLAGel-HA scaffold because it overlapped with the 1040 cm^{-1} PLLA peak corresponding to the *v*C-CH_3 stretching mode (Kister et al., 1995). Jose et al. (2010) reported similar results of overlapping of the PO_4^{3-} stretching peak of HA with the 1047 cm^{-1} PLGA peak during FTIR studies of aligned nanofibrous electrospun scaffolds of PLGA-collagen-nanoHA (Jose et al., 2010). The carbonate group of HA at 874 cm^{-1} (Figure 39B) was not observed because it also overlapped with the 875 cm^{-1} PLLA peak corresponding to the *v*C-COO stretching unit (Kister et al., 1995).

Table 6: FTIR peaks observed on PLLA, PLLAGel and PLLAGel-HA nanofibrous scaffolds

Wavenumber (cm^{-1})	**Peak assignment** (Birshtein and Tul'chinskii, 1982; Kister et al., 1995)
3310	amide A (gelatin)
1750	C=O vibration (PLLA)
1655	amide I band for C=O stretch (gelatin)
1534	amide II peak for N-H bend coupled with C-N stretch (gelatin)
1452	δCH_3 asymmetric bending (PLLA)
1380	δCH_3 symmetric bending (PLLA)
1182	C-O stretching mode of ester group (PLLA)
1085	C-O stretching (PLLA)
1040	*v*C-CH_3 (PLLA)
875	*v*C-COO stretching unit (PLLA)

There were no new peaks observed in the FTIR spectra of the blend-based scaffolds (Figure 39A), and the nanofibres of PLLAGel-based scaffolds were just blends of PLLA and gelatin. Similar results have been reported in the literature (Su et al., 2010; Kim et al., 2008a; Huang et al., 2004; Gupta et al., 2009). However, a decrease in the intensity of the C=O peak was observed in the FTIR spectra of the blend-based scaffolds (Figure 39C). In addition, the gelatin amide II band (associated with the N-H bend coupled with C-N stretch) of the as-

received gelatin powder was observed to have shifted to a lower wavenumber from 1540 cm^{-1} to 1534 cm^{-1} when compared to the as-received gelatin.

These suggest the existence of intermolecular bonding between PLLA and gelatin in the blend-based scaffolds. Chen et al. (2005) reported a similar decrease in the intensity of the carbonyl band of PLLA upon blending with chitosan. The authors attributed the decrease in the intensity of the PLLA carbonyl band to intermolecular hydrogen bonds which resulted mainly from interactions between the PLLA carbonyls and the chitosan amino groups in the amorphous phase (Chen et al., 2005). However, in this project, it was also considered that the reduction in intensity of the C=O peak could also be due to the lower concentration of PLLA in the blend-based scaffolds. The presence of intermolecular bonding between PLLA and gelatin will therefore be confirmed by DSC.

3.3.2.3 Thermal analysis

The thermal transitions of the electrospun scaffolds were investigated by DSC. Representative DSC scans of the three sets of scaffolds during the 1^{st} heating cycle are shown in Figure 40. It should be noted, that the values for the PLLAGel-HA scaffolds would have been affected by the lower weight of polymer present in the samples, as some portion of the sample weight measured would have corresponded to the weight of the HA particles on the surface of the scaffold. This may be the reason for the lower values of ΔH_m (and consequently X_c^{PLLA}) recorded for this particular scaffold.

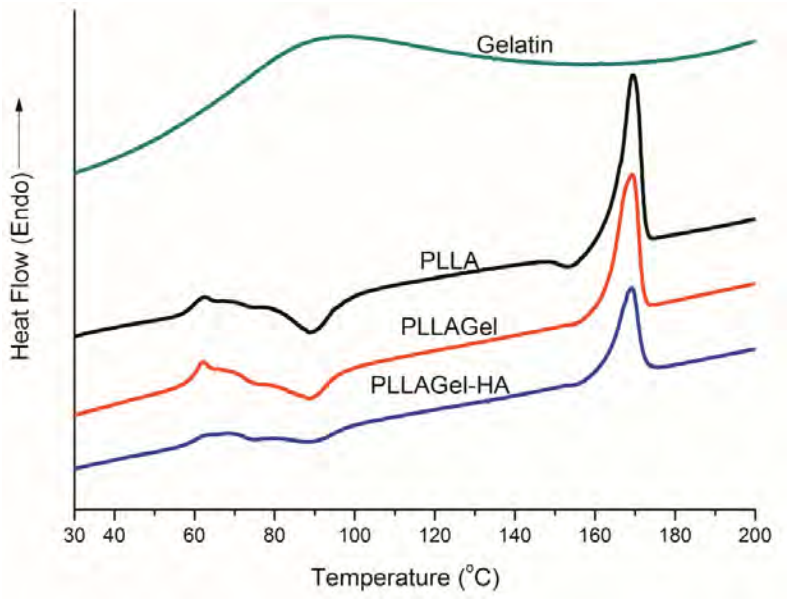

Figure 40: **DSC scans of 1st heating cycle for PLLA, PLLAGel, PLLAGel-HA electrospun scaffolds and gelatin**

During the 1st heating cycle, the glass-transition temperature, T_g, was observed at approximately 60°C for all sets of scaffolds (Table 7). Just above the T_g, there was an endothermic peak characteristic of enthalpic relaxation (Figure 40) as was reported for electrospun PLLA fibres in Section 3.1 and also by Bognitzki et al. (Bognitzki et al., 2001). Similar results were also reported for electrospun PLGA fibres by Jose et al. (Jose et al., 2010).

Furthermore, an exothermic peak associated with cold-crystallisation was observed at about 88°C for all the electrospun scaffolds. A second but smaller exothermic peak was observed around 153°C. This peak is characteristic of highly nucleated samples that crystallize at very low temperatures (Deplaine et al., 2010).

For the pure gelatin powder, an endothermic peak due to denaturation was obtained at approximately 96°C. Although gelatin is a denatured collagen (Bigi et al., 1998), it is capable of undergoing a renaturation process when it is in solid form (Bigi et al., 2001), hence the

term denaturation temperature for the endothermic peak observed during the 1st heating cycle (Zhang et al., 2006).

Table 7: DSC data

Composition	Cycle	T_g (^oC)	T_m (^oC)	ΔH_m ($J.g^{-1}$)	X_c^{PLLA} (%)
PLLA	1st	59.9	169.5	44.4	21.9
	2nd	61.4	170.3	37.4	22.7
PLLAGel	1st	60.3	169.3	37.1	21.3
	2nd	61.2	168.4	32.5	11.7
PLLAGel-HA	1st	60.3	169.2	23.5	16.1
	2nd	61.1	168.9	20.7	9.3

ΔH_m – heat of fusion; X_c^{PLLA} – degree of crystallinity of PLLA phase

The presence of a single T_g without any denaturation peaks for the blend-based nanofibrous scaffolds during the 1st heating cycle suggests that the PLLA and gelatin formed a miscible blend. Heterogeneous blends will exhibit distinctly different thermal transitions corresponding to the individual components of the blend, as opposed to the single, composition dependent thermal transitions exhibited by a homogeneous blend (Olabisi et al., 1979; Manson and Sperling, 1976; Lee et al., 2008). Lee et al. (2008) reported the study of the glass transition temperatures, morphology, mechanical and biological properties of fibres of poly(L-lactide-*co*-ε-caprolactone) (PLCL) and gelatin electrospun at various blend ratios. The authors reported the presence of two endothermic transitions, one corresponding to the glass transition of PLCL and the other corresponding to the denaturation of gelatin, on the DSC thermograms of fibres electropun from all blend ratios of PLCL/gelatin, except the PLCL/gelatin (90:10) blend ratio, which exhibited a single

endothermic transition corresponding to the T_g of the PLCL phase. Lee et al. (2008) attributed the occurrence of a single T_g without a denaturation peak of gelatin to a good dispersion of the gelatin within the PLCL phase and limited miscibility of PLCL and gelatin at that blend ratio (Lee et al., 2008). On the contrary, Linh et al. (2010) reported two endothermic peaks, one corresponding to the glass transition of PVA and the other corresponding to the denaturation of gelatin, when conducting DSC studies on PVA/gelatin fibres electrospun from PVA/gelatin blends of different ratios (Linh et al., 2010). The results of Linh et al. (2010) suggested that PVA and gelatin were immiscible at all the blend ratios tested, and corresponded with the work of Guisti et al. (1998), who showed by SEM analysis that various blends of PVA and gelatin exhibited a biphasic morphology (Giusti et al., 1998). The absence of a denaturation peak in the blend-based nanofibrous scaffolds of this current study indicated that the electrospun nanofibres were a miscible blend of PLLA and gelatin. The results obtained in this study are in agreement with those reported by Kim et al. (2008a) who investigated electrospun blends of PLLA and gelatin of various compositions. The authors reported, that internal morphological characterisation by transmission electron microscopy (TEM) of electrospun PLLA/gelatin (1:1) fibres revealed a homogenous blend of PLLA and gelatin (Kim et al., 2008a).

Hydrogen bonds are considered to be the most probable molecular forces of attraction in miscible polymer systems than any of the other types of interactions responsible for miscibility (Olabisi et al., 1979). It was therefore considered in this project, that during polymer blending, hydrogen bonds were formed between the PLLA carbonyl groups and the amide groups of the gelatin (Figure 41) which led to the miscibility of PLLA and gelatin. These results confirm the results obtained by FTIR.

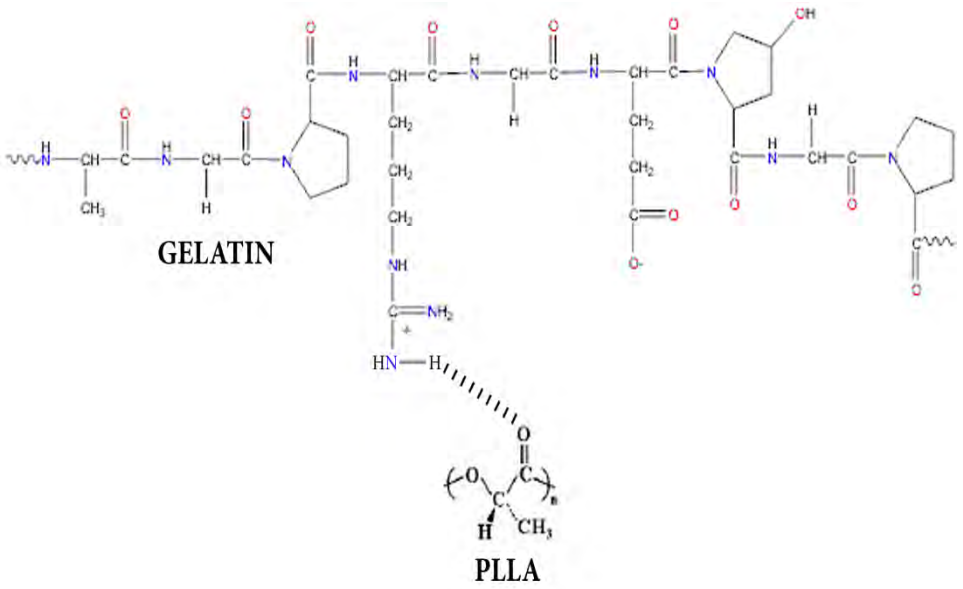

Figure 41: **Formation of intermolecular hydrogen bonds between gelatin and PLLA components in the blend-based electrospun scaffolds**

The miscibility of polymer blends can be determined by analyzing their thermal properties, especially the melting temperature, T_m (Ramdhanie et al., 2006; You et al., 2006). In a miscible polymer blend, there is always a depression of the melting point temperature (Silvestre and Cimmino, 2003; Olabisi et al., 1979), and if one of the blend components is crystalline, its crystallisation is hindered by the miscible component in the blend (Ramdhanie et al., 2006). Thus, the T_m and X_c would significantly decrease with increasing addition of the blended component (Ramdhanie et al., 2006). The DSC data for the 1st heating cycle (Figure 40 and Table 7) shows that the T_m of the blend-based scaffolds was not significantly lower than that of the PLLA scaffold. It is probable that the decreases in T_m and X_c^{PLLA} were small due to the relatively low gelatin content (10%) in the blend nanofibrous scaffolds. It is possible that if the gelatin content had been increased, an appreciable decrease in T_m would have been observed. For instance, Chen et al. (2005) reported a decrease of only 1^{o}C in T_m when the chitosan content of a PLLA/chitosan blend was

increased from 0 wt% to 25 wt%; however, when the chitosan content was increased to 50 wt%, there was an 11^{o}C decrease in T_m (Chen et al., 2005).

Contrary to expectations, the degree of crystallinity of the PLLA phase, X_c^{PLLA}, observed for the PLLA scaffold was not significantly different from that of the PLLAGel scaffold (Table 7). It may be that the reason the X_c^{PLLA} of the PLLAGel scaffold was not much lower than that of the PLLA scaffold was due to the smaller fibre diameter of the PLLAGel scaffold. As explained previously in Section 3.2.5, the degree of crystallinity has been shown to vary inversely proportional to fibre diameter. It is therefore probable that there were two opposing phenomena occurring during the electrospinning of the PLLAGel scaffold. One phenomenon in which the formation of thinner fibres led to an increase in molecular orientation and an increase in crystallinity; another phenomenon in which the hydrogen bonds between PLLA and gelatin led to an impediment to the rearrangement of PLLA chains during crystallisation. However, due to the value of X_c^{PLLA} for the PLLAGel scaffold being in very close proximity to that of the PLLA scaffold, it is more likely that the first phenomenon was more dominant during electrospinning.

During the cooling cycle, two small exothermic peaks were observed at approximately 60^{o}C and 95^{o}C (Figure 42). This has been attributed to the partial crystallisation of the PLLA (Deplaine et al., 2010).

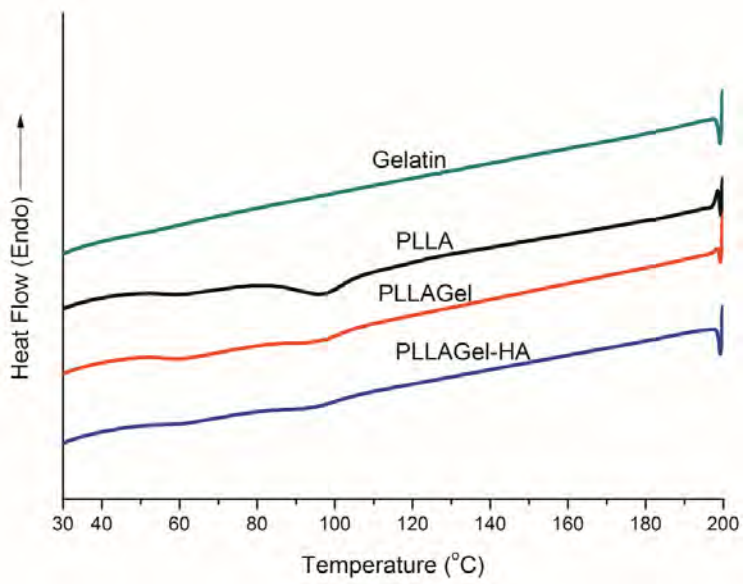

Figure 42: **DSC scans of cooling cycle for PLLA, PLLAGel, PLLAGel-HA electrospun scaffolds and gelatin**

During the 2nd heating cycle, crystallisation and melting followed the same trend as in the 1st heating cycle, although the T_cs were much higher, and the endothermic ageing peak was absent (Figure 43 and Table 7). The occurrence of T_c at a lower temperature during the 1st heating cycle in comparison to 2nd heating cycle was attributed to the alignment of polymer chains in the as-spun fibres which allowed crystallisation to occur at a lower temperature than for an isotropic sample (Bognitzki et al., 2001).

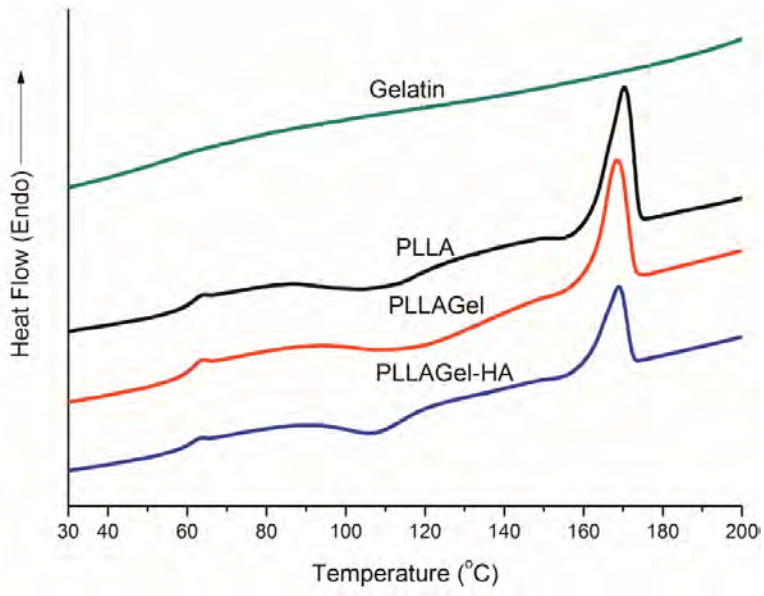

Figure 43: **DSC scan of 2nd heating cycle for PLLA, PLLAGel, PLLAGel-HA electrospun scaffolds and gelatin**

It is worth noting, that after erasing the thermal history of all the samples by cooling them from the melt, during the 2nd heating cycle, the PLLA scaffold exhibited the highest X_c^{PLLA} of all the three scaffold types. The reduction in X_c^{PLLA} in the blend-based scaffolds during the 2nd heating cycle can be attributed to the miscible nature of the PLLA/gelatin blend. The glass transition temperature of gelatin has been reported to be above 200°C (Giusti et al., 1998), therefore, when PLLA was blended with gelatin, PLLA molecular chains were trapped in a glassy environment thus reducing the mobility of PLLA chains and constituting a hindrance to the rearrangement of PLLA chains during crystallisation (Chen et al., 2005). Consequently, there was a considerable amount of imperfect crystal formation. The imperfect crystals thus formed would melt at a lower T_m, hence the decrease in T_m observed in the blend-based scaffolds during the 2nd heating cycle. Chen et al. (2005) reported a decrease in T_m, ΔH_m, and X_c when studying different blend ratios of PLLA/Chitosan prepared by precipitation (Chen et al., 2005); the authors attributed these observations to the

presence of intermolecular hydrogen bonds between the two components which mainly resulted from the interactions between PLLA carbonyl groups and chitosan amino groups.

3.3.2.4 EDS

The presence of HA on the PLLAGel-HA nanofibrous scaffold was confirmed qualitatively by EDS mapping (Figure 44).

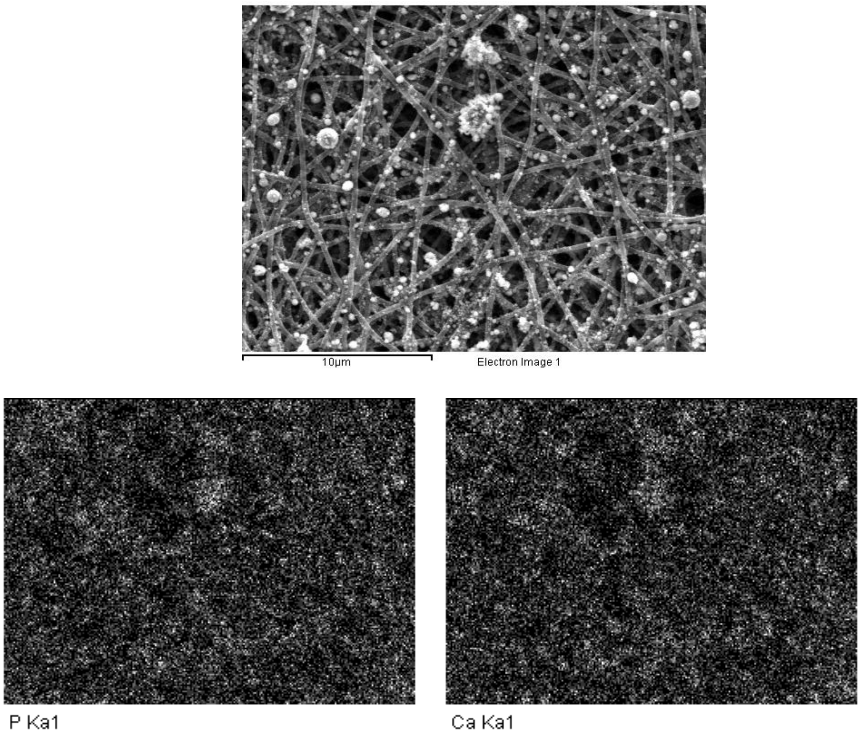

Figure 44: **Representative EDS maps for the PLLAGel-HA electrospun scaffold showing HA distribution**

The EDS maps revealed the presence of calcium and phosphorous (characteristic elements of HA), confirming the presence of HA on the PLLAGel-HA scaffold (Figure 44), and indicating that the electrospraying process created a layer of hydroxyapatite particles on the surface of the PLLAGel-HA.

The EDS maps also showed that HA was homogeneously distributed on the surface of the scaffold by the electrospraying process, indicating that electrospraying is an effective method for fabricating electrospun polymer/HA scaffolds.

3.3.2.5 Interferometry

Representative surface topographies of the scaffolds as revealed by interferometry are shown in Figure 45. The roughness average and root mean square values are shown in Table 8.

The PLLAGel-HA scaffolds showed the highest surface roughness average whilst the PLLA showed the smallest surface roughness average.

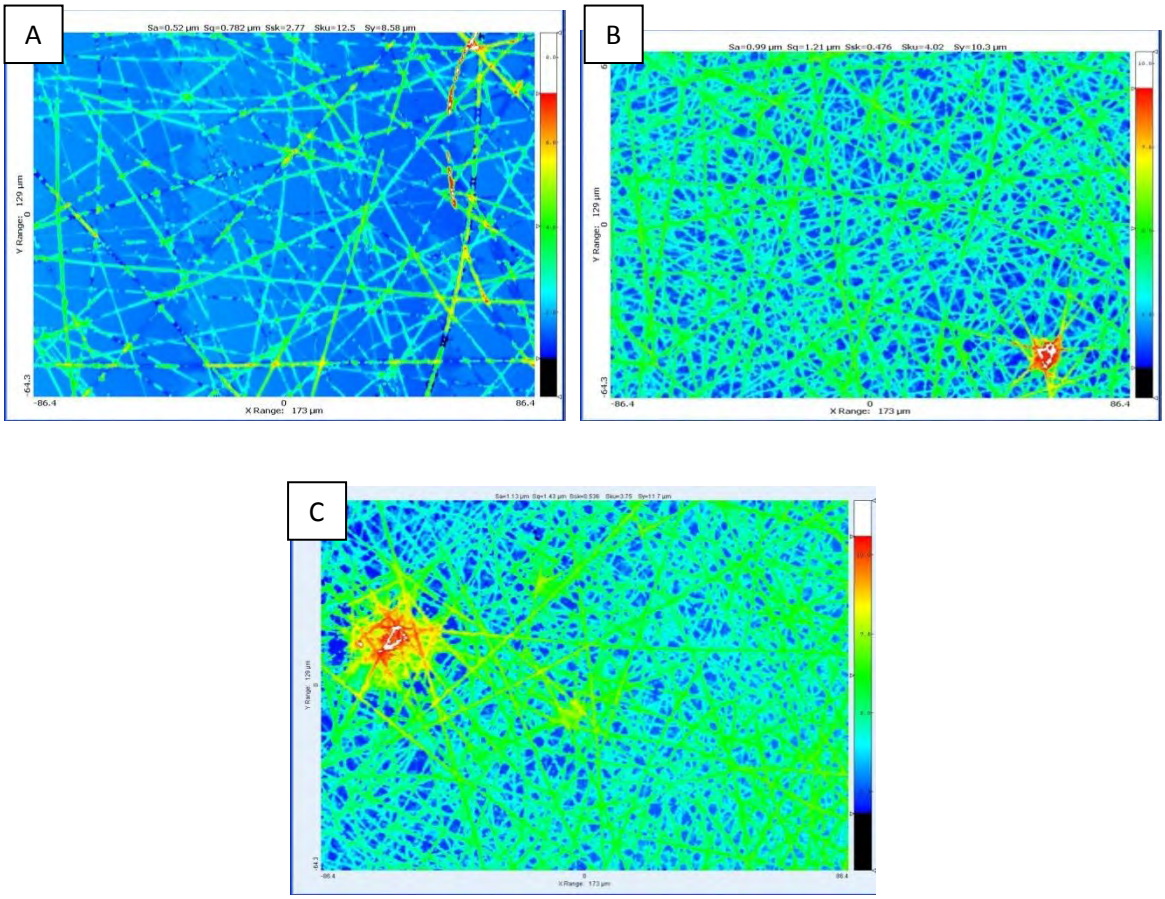

Figure 45: **Representative surface topography of (A) PLLA, (B) PLLAGel, and (C) PLLAGel-HA electrospun scaffolds**

Table 8: **Surface roughness average and roughness root mean square of electrospun scaffolds**

Composition	Roughness average (µm) (Mean ± SD)	Roughness root mean square (µm) (Mean ± SD)
PLLA	0.416 ± 0.099	0.609 ± 0.119
PLLAGel	0.921 ± 0.081	1.080 ± 0.102
PLLAGel-HA	0.983 ± 0.216	1.220 ± 0.320

The surface roughness average of the PLLA scaffolds was lower in comparison to the blend-based scaffolds. This may have been due to the closer/denser packing of the nanofibres in the blend-based scaffolds (as revealed by the calculated inter-fibre distances shown in Table 5) which would have created a surface with relatively more grooves or rougher topography. The relatively high surface roughness average of the PLLAGel-HA was due to the exposure of HA electrosprayed onto the surface of the nanofibres, which imparted a rough surface topography on the scaffolds.

Cells have been reported to respond to topographical stimuli (Martinez et al., 2007). Martinez et al. (2007) reported that chrondrocytes seeded on PLLA of different surface topographies (with different surface roughnesses) showed different morphologies. Specifically, they reported that when chrondrocytes were seeded on PLLA films containing small spherulites (hence, uniform surface topography), they showed the characteristic monolayer pattern distribution and morphology whilst those seeded on PLLA films containing bigger spherulites (hence rough surface topography) showed a more elongated morphology with an isolated disposition (Martinez et al., 2007).

The effect of surface roughness on cell adhesion and morphology were analysed during biocompatibility studies, results of which are reported later in Section 3.3.2.8.

3.3.2.6 Tensile properties

Representative stress-strain curves for the three sets of scaffolds are shown in Figure 46. Table 9 gives details of the average tensile strength, average tensile stiffness and average percent elongation at break.

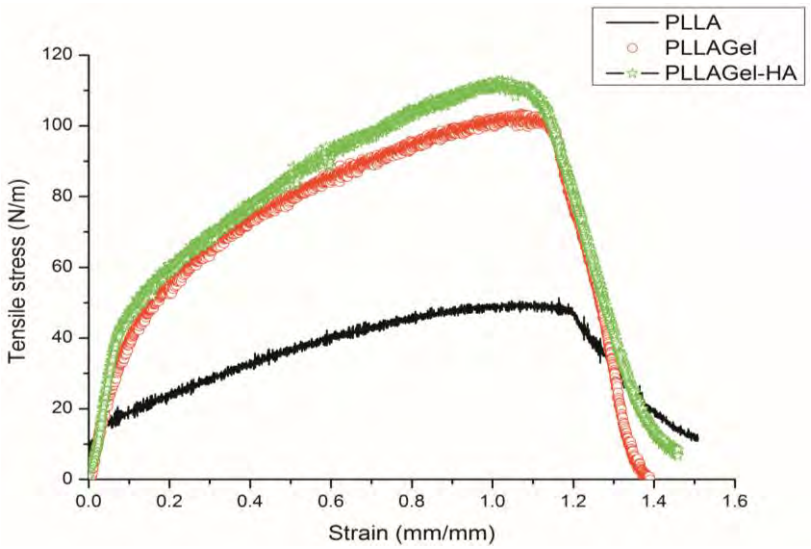

Figure 46: **Representative tensile stress-strain curves of PLLA, PLLAGel and PLLAGel-HA electrospun scaffolds**

Table 9: **Average tensile strength, average tensile stiffness and average percent elongation at break (%) of electrospun scaffolds**

Composition	Average tensile strength (N/m)	Average tensile stiffness (N/m)	Average percent elongation at break (%)
PLLA	45.4 ± 3.7	66.8 ± 21.0	132.9 ± 15.9
PLLAGel	54.2 ± 10.1	84.4 ± 24.9	108.0 ± 13.7
PLLAGel-HA	51.2 ± 10.3	88.5 ± 18.5	126.7 ± 7.2

The blend-based electrospun scaffolds showed a slight increase in tensile strength compared to the PLLA scaffolds (Table 9). Similarly, they generally showed improvements in tensile stiffness although in contrast, the percent elongation at break was slightly reduced (Table 9). As has been shown in Section 3.3.2.3, blending PLLA with gelatin resulted in the formation of hydrogen bonds between PLLA and gelatin molecules; the slight increase in strength was attributed to the presence of these bonds in the blend-based scaffolds.

According to Baji et al. (2010), the tensile properties of individual fibres of an electrospun scaffold influence the tensile properties of the electrospun scaffold. As the diameters of electrospun fibres are reduced, their tensile properties are enhanced. This is due to (i) the gradual ordering of molecular chains; and (ii) densely packed lamellae and fibrillar structures. Lamellae and fibrillar structures are oriented along the fibre axis for thin fibres. The fibrillar structure is highly orientated and provides high resistance to the axial tensile force. Therefore, an increase in fibre diameter results in a decrease in the alignment of the fibrillar and lamellae structure, leading to a decrease in mechanical properties (Baji et al., 2010). Although the tensile properties of individual fibres were not measured in this study, it is suggested that the thinner fibre diameters of the blend-based scaffolds also contributed to their higher tensile strengths.

The tensile properties of the PLLAGel-HA scaffolds were very similar to those of the PLLAGel scaffold. This is in contrast to the previous reports in the literature about the decrease in the mechanical properties of scaffolds electrospun from polymers-HA mixtures as elucidated previously in Section 1.10. This indicates that electrospraying HA particles onto the surface of an electrospun scaffold has no detrimental effects on the mechanical properties of the electrospun scaffold.

3.3.2.7 Degradation studies

3.3.2.7.1 pH monitoring

The pH of the degradation medium of all scaffold types decreased from 7.4 to ≈6.7 during the degradation period (Figure 47).

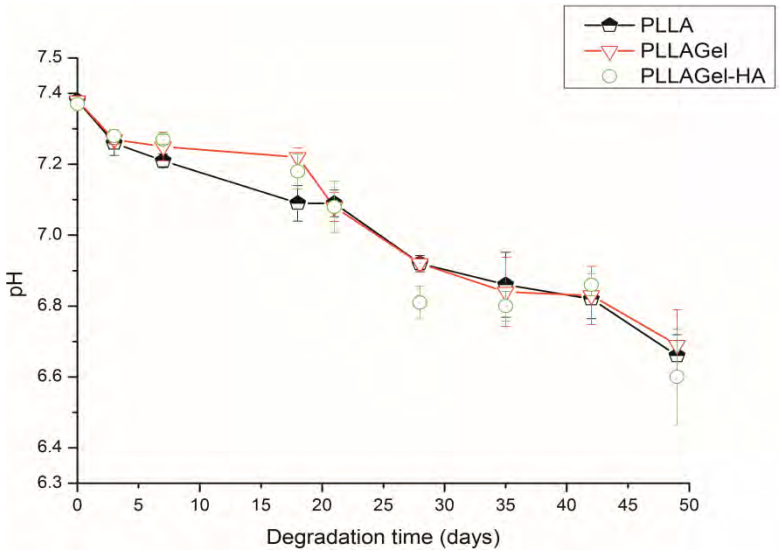

Figure 47: **pH variation with degradation time (Error bars indicate standard deviation)**

As explained in Section 3.2, during polymer degradation, by-products which are constituent monomers of the polymer are released into the degradation medium. The release of these by-products will be consequently observed by a change in pH of the degradation medium. In the case of PLLA, the degradation by-product is lactic acid, and being an acid, its continued release into the degradation medium would be expected to cause a decrease in pH.

The pH of the degradation medium was monitored over the 49-day degradation period to qualitatively observe the release of lactic acid into the degradation medium and hence the degradation of PLLA (Figure 47). The relatively high PLLA content (90%) in the blend-based nanofibrous scaffolds resulted in a similar pH decrease profile to the pure PLLA nanofibrous scaffold.

A comparison of the pH profile of the PLLA scaffolds studied in Section 3.2 (pH of 7.18 after 28 days – Figure 25) to the pH profile of the PLLA scaffolds studied in this section (pH of 6.92 after 28 days – Figure 47) suggests that their degradation rates were different. This was probably due to the difference in their original degree of crystallinity, which for the former was 33.4% and for the latter was 21.9%. Crystallinity is one of the factors that determines the degradation rate of a polymer; a high crystallinity will result in a lower degradation rate and vice versa (Middleton and Tipton, 2000). The difference in crystallinity of both scaffolds is in agreement with the difference observed in their pH profiles during *in vitro* degradation. The commonly reported neutralising effect of HA was not observed in the pH profile of the PLLAGel-HA scaffolds. It had been expected that the exposed HA particles on the surface of the polymer scaffold would neutralise the acidic degradation by-products, however, this was not observed. Similar to the results reported in Section 3.2.3, it is considered that no neutralising effect of HA particles was seen in the pH profile of the PLLAGel-HA scaffolds because of the low concentration of HA (5 wt%).

3.3.2.7.2 Gelatin leaching

Figure 48 shows the FTIR scan for PLLAGel scaffolds (Figure 48A) and PLLAGel-HA scaffolds (Figure 48B) within the range 1480 cm^{-1} to 1700 cm^{-1}, depicting the gelatin amide peaks at ≈1536 cm^{-1} (amide II peak for N-H bend coupled with C-N stretch) and ≈1655 cm^{-1} (amide I band for C=O stretch). The scans are limited to only the non-degraded scaffolds and scaffolds degraded for 21 days because the main purpose was to determine the possibility of gelatin leaching out of the polymer scaffold during cell culture.

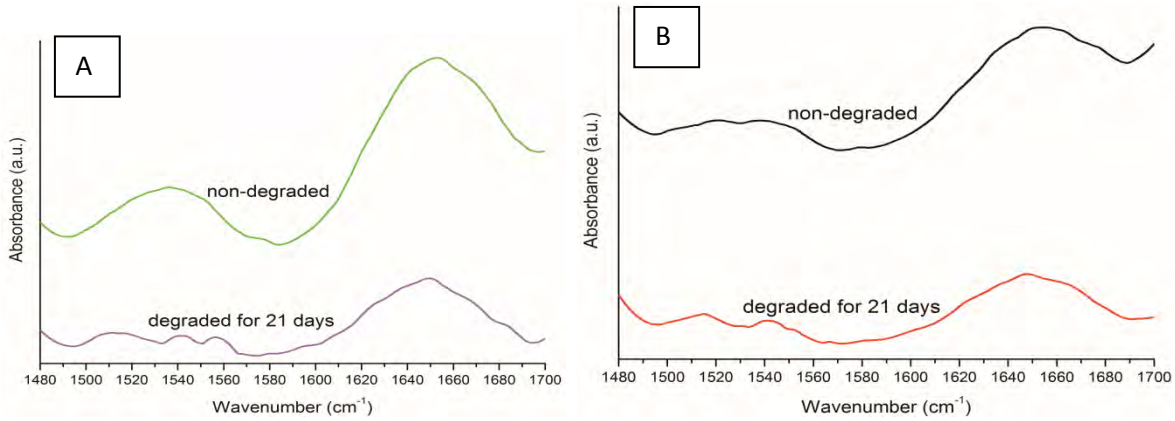

Figure 48: FTIR spectra showing loss of gelatin during degradation for (A) PLLAGel and (B) PLLAGel-HA scaffolds

In Figure 48, the intensity of the amide peaks is observed to have decreased after 21 days of degradation. This indicates that some gelatin leached out of the polymer matrix during degradation. Gelatin is a water-soluble polymer and can easily dissolve in water when it is in an uncrosslinked state (Bigi et al., 2001; Zhang et al., 2006). As a result, some gelatin in the blend-based scaffolds was probably lost during degradation. The implication of this is that some gelatin may have leached out into the cell culture medium during biocompatibility studies as the cell culture was carried out at 37^{o}C, the same temperature at which the degradation study was carried out.

3.3.2.7.3 Weight loss percentage

During polymer degradation, when the M_w has decreased to a critical minimum, a rapid decrease in weight and formation of soluble oligomeric and monomeric products are observed (Raghuvanshi et al., 1993). The weight decrease of the three types of electrospun nanofibrous scaffolds monitored over the 49-day degradation period is shown in Figure 49. The weight loss percentage for the three scaffold types over the 49-day degradation period was almost negligible, and there was no statistically significant difference between the

weight losses observed on the three scaffold types. However, in general terms, the blend-based scaffolds showed the highest weight loss while the PLLA scaffolds showed the lowest weight loss. As gelatin had been observed to have leached from the PLLAGel scaffolds (Figure 48), a significant portion of the weight loss observed on the blend-based scaffolds was attributed to the leaching out of gelatin from the scaffold.

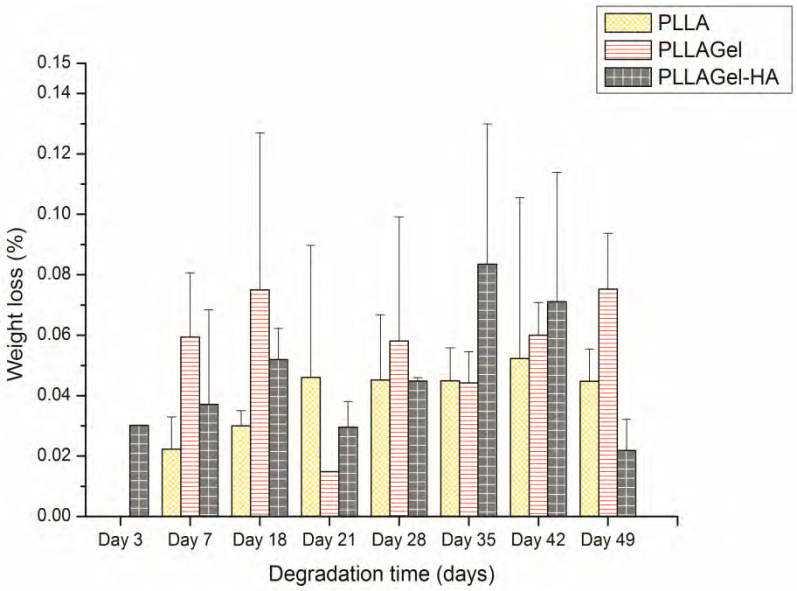

Figure 49: **Percentage weight loss (%) during degradation (Error bars indicate standard deviation)**

PLLA is a hydrophobic and semi-crystalline polyester, hence its slow degradation (Dong et al., 2009). PLLA has been reported to have a half-life (time taken for half of initial material to be lost) of 110 weeks during degradation in phosphate buffer of pH 7.4 at 37^{o}C (Li, 1999), and it can take between 2 and 5 years for complete weight loss (Andric et al., 2010; Gomes and Reis, 2004; Middleton and Tipton, 2000). The high PLLA content of the blend-based nanofibrous scaffolds probably made them less susceptible to degradation hence, the small weight loss observed during the degradation period.

3.3.2.7.4 Morphology

The morphology of the degraded electrospun nanofibrous scaffolds was investigated by ESEM and is shown in Figure 50.

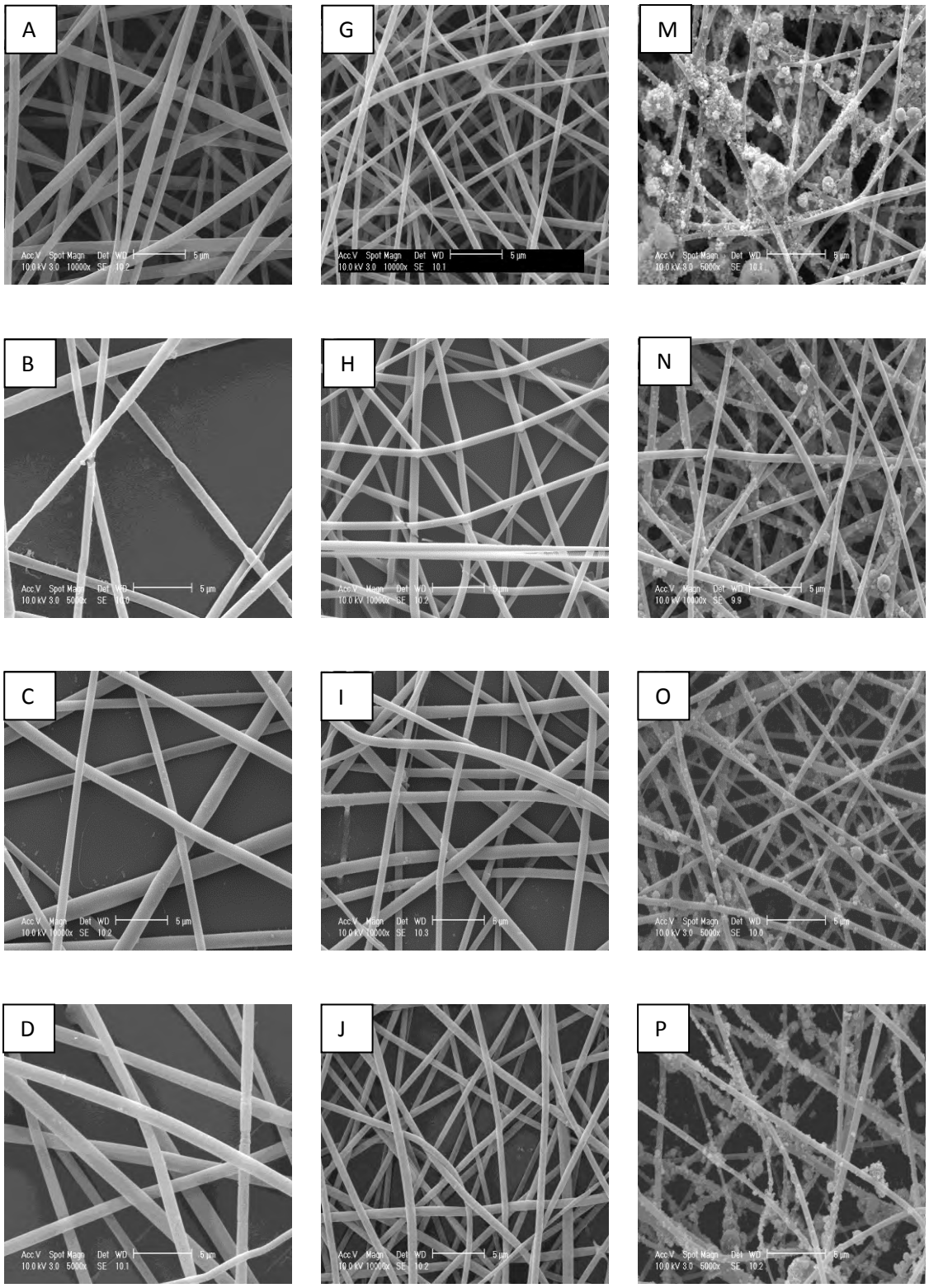

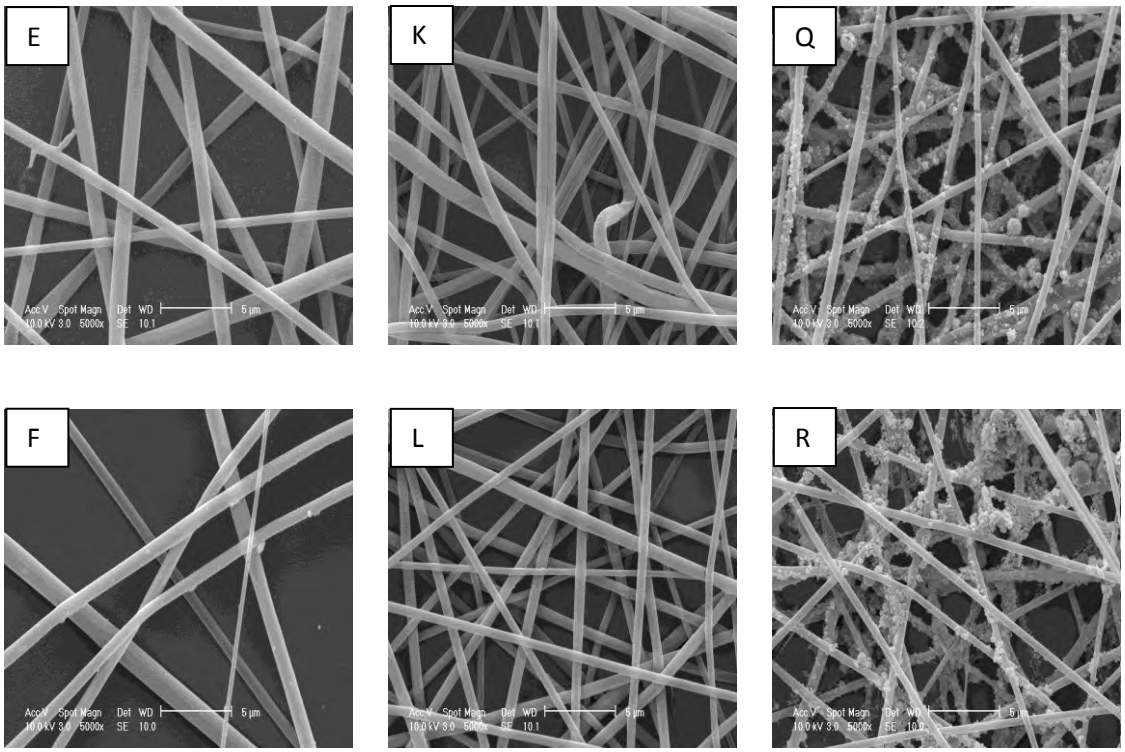

Figure 50: **ESEM images of electrospun nanofibrous scaffolds of PLLA (A-F), PLLAGel (G-L) and PLLAGel-HA (M-R) after 0, 3, 18, 21, 35, and 49 days of degradation, respectively**

As mentioned in Section 3.2.1, nanofibre morphology has been reported to change significantly during degradation (Dong et al., 2009), characterised by broken fibres for PLLA in particular (Sui et al., 2007). The broken fibres were attributed to breakage in weak points along the rigid, immobile polymer chains of the crystalline region (Dong et al., 2009). However, the morphology of the degraded nanofibres in this study did not change significantly during the 49-day degradation period (Figure 50). The lack of significant changes in the morphology of the electrospun nanofibrous scaffolds post-degradation indicates the possibility of occurrence of only a minimum amount of degradation during this time.

It was also noteworthy that the HA particles were still visible on the surface of the PLLAGel-HA scaffold even after degradation for 49 days, showing that the interfacial strength of the

polymer-HA was strong enough to prevent the HA particles from being delaminated from the polymer during degradation. This indicates that electrospraying HA post-electrospinning is a good method for fabricating electrospun polymer-HA composite scaffolds.

3.3.2.7.5 Effect of degradation on average fibre diameter

During degradation of electrospun nanofibres, an increase in fibre diameter is usually observed on electrospun fibres (Dong et al., 2009). As previously explained in Section 3.2.1, these large dimensional changes are due to the thermally induced relaxation of stretched chains in the electrospun fibres (Zong et al., 2003).

As seen in Figure 51, all the three scaffold types exhibited some increase in fibre diameter, albeit, the PLLAGel and PLLAGel-HA scaffolds exhibited higher increases in fibre diameter in comparison to the PLLA scaffolds.

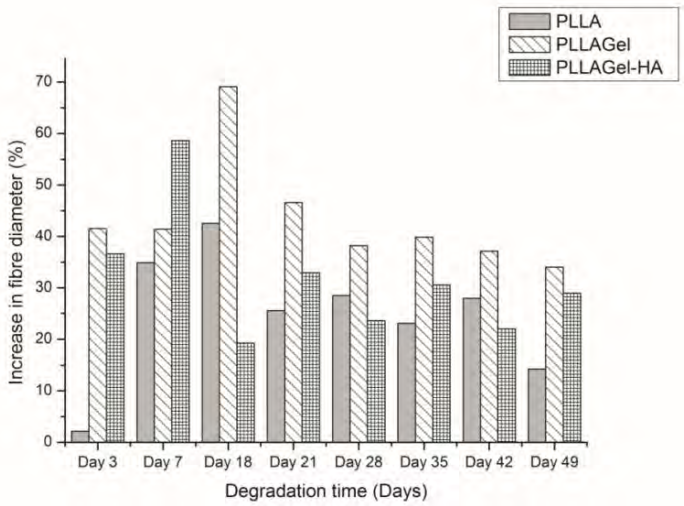

Figure 51: **Percentage increase in fibre diameter (%) during degradation**

PLLA is hydrophobic (Rasal et al., 2010), but gelatin has been reported to improve its hydrophilicity (Gu et al., 2009; Kang et al., 2010; Kim et al., 2008a), therefore the blend-based scaffolds had a greater propensity to absorb water than the pure PLLA scaffold, hence the greater increases in fibre diameter observed in the blend-based scaffolds during

degradation (Figure 51). Similar results of increased swelling ratios of electrospun scaffolds when gelatin was blended with PLGA were reported by Meng et al. (2011). The increased swelling ratios were attributed to the improved hydrophilicity of the PLGA-gelatin nanofibres (Meng et al., 2011).

The blend-based scaffolds would also have higher SVRs relative to the PLLA scaffolds due to their thinner fibres. They would thus have had more contact area with the degradation medium, resulting in higher water penetration relative to the PLLA scaffolds, as seen from the results presented in Section 3.2 and in the literature (Chen and Ma, 2006).

Similar to the comparison between the pH profiles of the PLLA scaffolds studied in Section 3.2, the increase in fibre diameter of the PLLA scaffolds studied in this Section show that they exhibited higher increases in fibre diameter at comparable periods of the degradation study. As with the pH profiles, the reason for this was due to the difference in their crystallinity; water penetration would have been relatively higher in the PLLA scaffolds studied in this Section due to their lower crystallinity.

3.3.2.8 Biocompatibility studies

3.3.2.8.1 Cell attachment and morphology

The morphology and attachment of the HOBs seeded on the electrospun nanofibrous scaffolds was investigated by SEM. The SEM images (Figure 52) revealed that HOBs were successfully seeded on all scaffold types.

After 1.5 hours, very few cells had attached to the PLLA scaffold whilst cells were observed to have spread over the PLLAGel-HA scaffold (Figure 52 A – F). The HOBs generally had a compact morphology with round nuclei and diameter/length of approximately 15-20 µm. However, the cells on the blend-based scaffolds (especially the PLLAGel-HA scaffold) (Figure

52 D and F) showed some signs of extended processes (filapodia), indicating that HOBs attached better to the blend-based scaffolds at this early time point.

After 24 hours, cell spreading was more obvious on the blend-based nanofibrous scaffolds when compared to the cells on the PLLA nanofibrous scaffold (Figure 52 G, I and K). HOBs on the PLLA scaffold seemed more compact, with round nuclei and a diameter/length of approximately 20 µm (Figure 52 H) whilst the cells on the blend-based scaffolds appeared flatter, with diameter/lengths between 20–50 µm (Figure 52 J and L). Furthermore, the cells on the PLLAGel-HA nanofibrous scaffolds seemed to be anchored very strongly onto the scaffold with processes (filapodia) extended far out along the fibres - this is observed by the cells seemingly 'pulling in' the fibres (Figure 52K). This was not observed on any of the other scaffold materials, and indicates that the PLLAGel-HA scaffold facilitated the best cell attachment after 24 hours of cell culture.

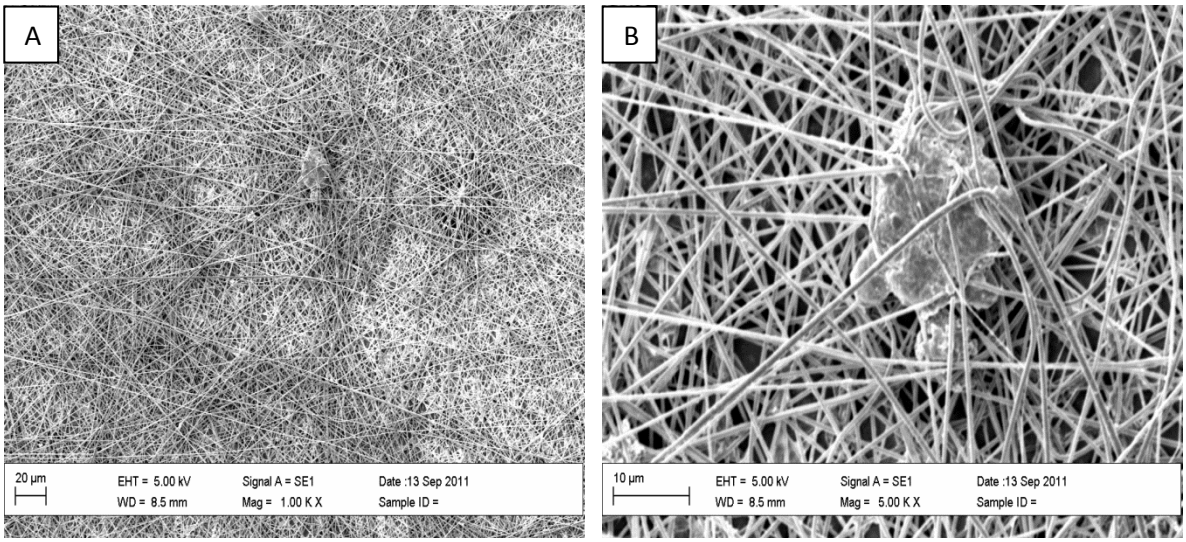

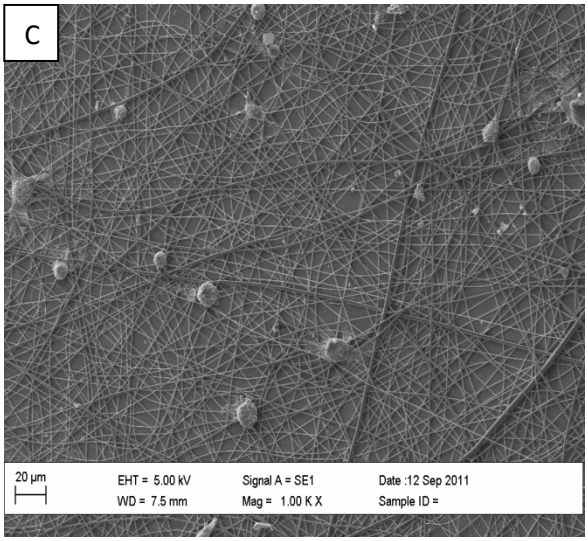
C
20 µm
EHT = 5.00 kV
WD = 7.5 mm
Signal A = SE1
Mag = 1.00 K X
Date :12 Sep 2011
Sample ID =

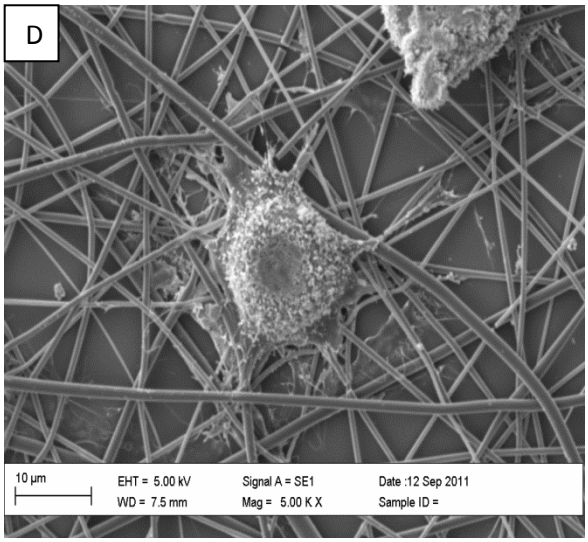
D
10 µm
EHT = 5.00 kV
WD = 7.5 mm
Signal A = SE1
Mag = 5.00 K X
Date :12 Sep 2011
Sample ID =

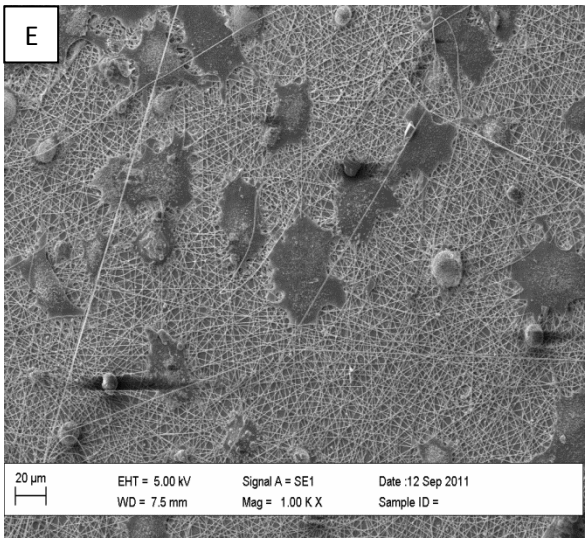
E
20 µm
EHT = 5.00 kV
WD = 7.5 mm
Signal A = SE1
Mag = 1.00 K X
Date :12 Sep 2011
Sample ID =

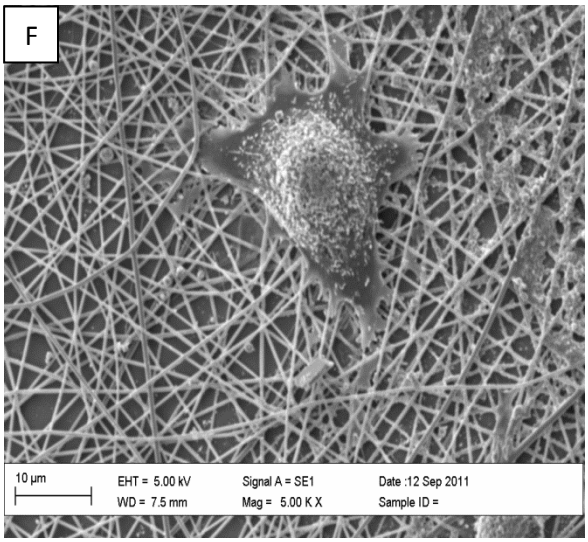
F
10 µm
EHT = 5.00 kV
WD = 7.5 mm
Signal A = SE1
Mag = 5.00 K X
Date :12 Sep 2011
Sample ID =

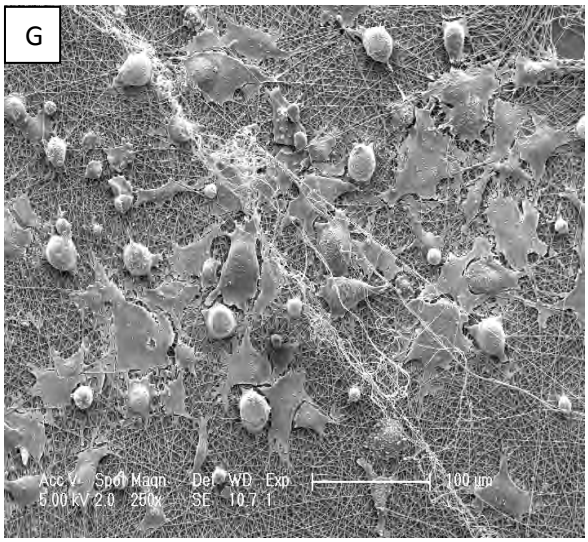
G
Acc.V Spot Magn Det WD Exp
5.00 kV 2.0 250x SE 10.7 1
100 µm

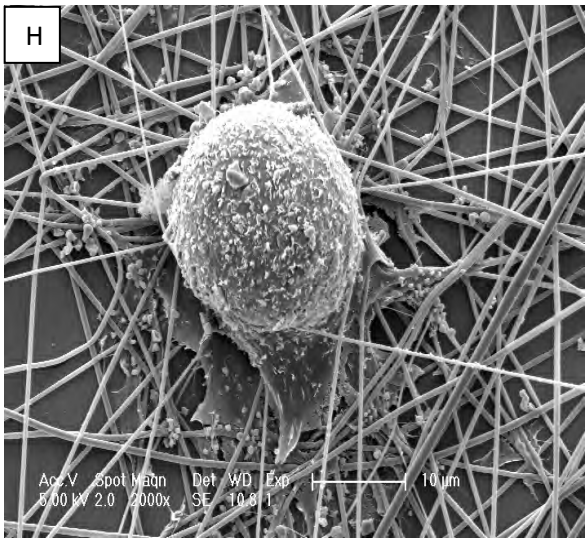
H
Acc.V Spot Magn Det WD Exp
5.00 kV 2.0 2000x SE 10.8 1
10 µm

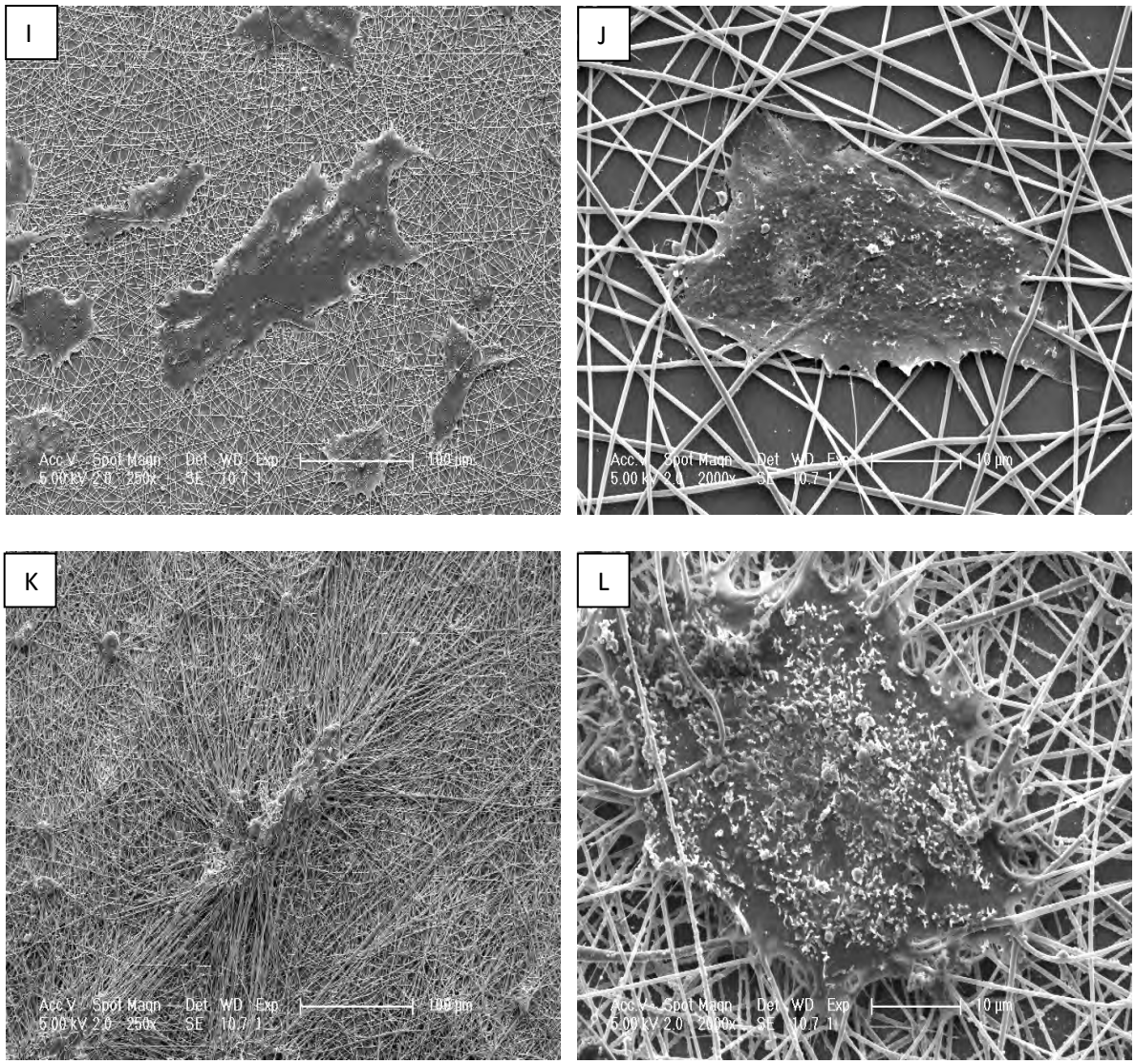

Figure 52: SEM images showing attachment of HOBs cultured on electrospun nanofibrous scaffolds of: (A) PLLA after 1.5 hours, (B) higher magnification of A, (C) PLLAGel after 1.5 hours, (D) higher magnification of C, (E) PLLAGel-HA after 1.5 hours, (F) higher magnification of E, (G) PLLA after 24 hours, (H) higher magnification of G, (I) PLLAGel after 24 hours, (J) higher magnification of I, (K) PLLAGel-HA after 24 hours, and (L) higher magnification of K

Although PLLA has been widely researched as a potential material for tissue engineering scaffolds, its scaffolds have the disadvantages of lacking cell recognition signals and being hydrophobic, which may adversely affect cell attachment, growth and proliferation (Chen

and Su, 2011). Like most other synthetic biodegradable polymers, one of the methods used to overcome this drawback is to blend it natural polymers (Zhang et al., 2007c). Natural polymers such as collagen, gelatin and chitosan have been shown to possess integrin binding sites for cell adhesion (Gupta et al., 2009). Zhang et al. (2005) reported the study of electrospun blends of gelatin and gelatin-PCL, and observed that bone-marrow stromal cells contracted into a round shape on PCL electrospun scaffolds, but spread and stretched on gelatin-PCL scaffolds. Furthermore, they reported cellular infiltration up to a depth of 48 µm and 114 µm for the PCL and gelatin-PCL scaffolds respectively. The authors attributed these observations to the good hydrophilicity and cellular affinity of the gelatin-PCL composite scaffold. In addition, they explained that the consistent release of gelatin molecules from the gelatin-PCL scaffold by dissolution created space for cell migration (Zhang et al., 2005).

Cell attachment and spreading was studied by confocal microscopy on FITC-phalloidin and DAPI-Prolong stained constructs (Figure 53). The confocal micrographs showed that after 1.5 hours (Figure 53), the cells had adhered to all scaffolds, albeit the cells on the blend-based scaffolds showed the presence of more f-actin. Additionally, the f-actin on the PLLA scaffold was concentrated around the nucleus indicating minimal spreading of cells at this

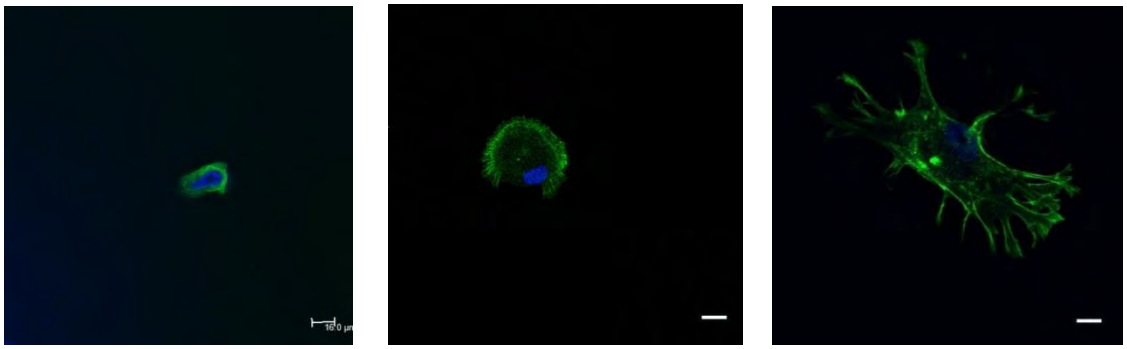

PLLA 1.5 hours PLLAGel 1.5 hours PLLAGel-HA 1.5 hours

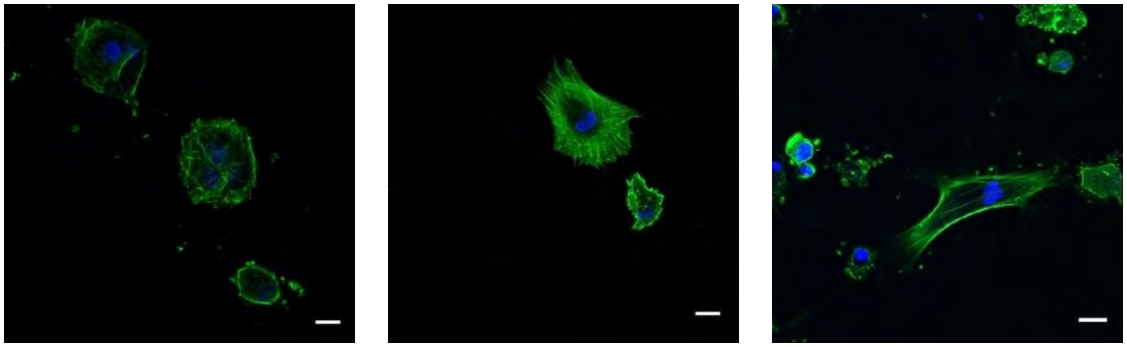

PLLA 4hrs PLLAGel 4hrs PLLAGel-HA 4hrs

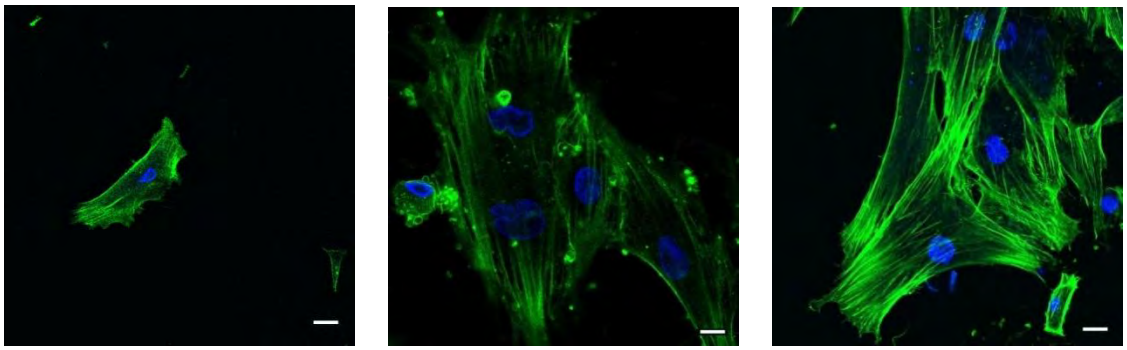

PLLA 24hrs PLLAGel 24hrs PLLAGel-HA 24hrs

Figure 53: **Confocal micrographs of HOBs stained with FITC-phalloidin for the f-actin component of cytoskeleton (green) and DAPI stained nuclei (blue) after 1.5, 4 and 24 hours of cell culture. Scale bar indicates 16 µm (magnification 63x)**

time point (Figure 53). A comparison of the f-actin filaments on the PLLAGel and PLLAGel-HA scaffolds at this early time point showed that cells on both scaffolds had well-defined f-actin staining spreading out from the nucleus indicating cell spreading. However, the f-actin of cells on the PLLAGel-HA scaffolds were better organized than those on the PLLAGel, indicating that the HOBs attached better on PLLAGel-HA scaffolds at this early time point.

After 4 hours, the cells on all the scaffolds had formed more defined cyctoskeleton (Figure 53). However, as observed after 1.5 hours of cell culture, cells on the blend-based scaffolds showed better organized and extended cytoskeleton compared to the PLLA scaffold. Cells on the PLLAGel scaffold showed a polygonal morphology (although cells on the PLLAGel-HA

scaffold had exhibited this morphology after 1.5 hours of cell culture) whilst cells on the PLLAGel-HA scaffold seemed to have been elongated in a bipolar manner.

At the 24 hour time-point, the cells on the PLLA scaffold had just started to exhibit a polygonal morphology and show f-actin filaments spreading away from the nucleus whilst the cells on the blend-based scaffolds showed a high degree of elongation with many groups of f-actin filaments spreading away from the nucleus.

These results indicate that HOBs spread preferentially over the blend-based scaffolds when compared to the PLLA scaffold.

Both the SEM and confocal microscopy images revealed that at all time points (1.5, 4 and 24 hours) HOBs attached and spread better onto the blend-based scaffolds, specifically best on the PLLAGel-HA scaffold.

HOBs spread best on the PLLAGel-HA scaffolds becaused of the presence of HA on the scaffolds. HA adsorbs proteins, such as fibronectin and vitronectin, from serum, which should promote better binding with integrins for osteoconductivity (Kilpadi et al., 2001). Such integrin binding induces the rearrangement of cytoskeletal f-actin fibres, leading to cell anchorage and spreading, and triggers signals that direct subsequent cellular responses, including cell proliferation and differentiation (Francis et al., 2010).

It was difficult to determine if the improved surface roughnesses of the blend-based scaffolds also contributed to the better cell attachment and spreading observed on the blend-based scaffolds within the first 24 hours of cell culture. Reports in the literature about the effect of surface roughness on initial cell adhesion are somewhat conflicting, in some instances, increased surface roughness has been reported to improve cell adhesion (Chung et al., 2003; Linez-Bataillon et al., 2002), whereas in other instances, it has been reported to reduce cell adhesion (Anselme et al., 2000; Thapa et al., 2003; Xu et al., 2004). In this study,

it was difficult to isolate the contribution of surface roughness to initial cell adhesion because other factors such as the presence of gelatin and HA in some of the scaffolds may have contributed to an improvement in the initial cell adhesion.

3.3.2.8.2 Proliferation and viability

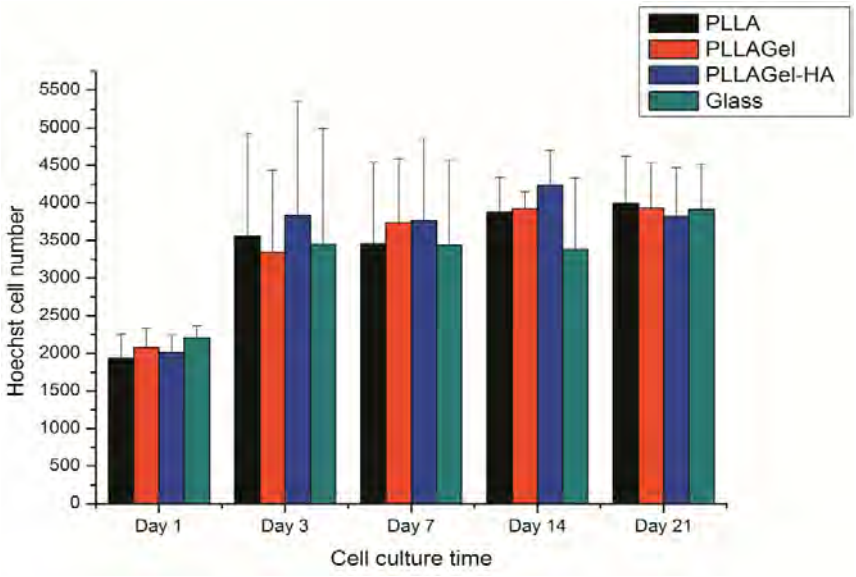

Figure 54: **Hoechst based DNA assay for HOBs proliferation on electrospun nanofibrous scaffolds and glass control after 1, 3, 7, 14 and 21 days of culture (Error bars represent standard deviation)**

Cell proliferation of the HOBs on the different scaffold types was determined by Hoechst based DNA assay (Figure 54). All nanofibrous scaffolds supported cell proliferation over the cell culture period as seen from the general increase in cell number between Day 1 and Day 21 (Figure 54). At all time points of cell culture, there was no statistically significant difference in cell profileration between the three types of electrospun nanofibrous scaffolds.

The cell numbers on Day 1 showed the preference of cell adhesion/attachment at the initial stage (Lee et al., 2008). The cells adhered initially on the electrospun nanofibrous scaffolds

in the order PLLAGel (2.08×10^3) ≈ PLLAGel-HA (2.02×10^3) > PLLA (1.93×10^3). These results support the observations from the SEM images of the scaffolds 24 hours after cell seeding that the HOBs attached better onto the blend-based scaffolds (Figures 52 G - L).

After Day 1, cell numbers on the PLLAGel scaffolds were generally lower than those on the PLLA scaffolds. The PLLAGel-HA electrospun nanofibrous scaffolds showed higher cell proliferation over the PLLA and PLLAGel scaffolds between Day 3 and Day 14, showing that the cells proliferated best on the PLLAGel-HA scaffold until Day 21, when the cell numbers on the three scaffolds types were approximately equal.

HOBs had been expected to exhibit significantly higher proliferation on the blend-based scaffolds compared to the PLLA scaffold due to the presence of gelatin which possesses integrin binding sites for cell adhesion (Francis et al., 2010) and the osteoconductivity of HA, however, whilst HOBs on the blend-based scaffolds generally showed higher proliferation compared to HOBs on the PLLA scaffold, they were not statistically significantly higher. One reason for this may have been due to the dissolution of the water soluble gelatin since it was not cross-linked. This possibility is supported by the leaching of gelatin observed during the degradation studies (Figure 48). Gelatin has been reported to improve cell proliferation, however, it has mostly been in the cross-linked state (Andric et al., 2010). Similar observations were made by Andric et al. (2010) where the MC3T3 cell numbers on PLLA and PLLAGel (90:10) were not significantly different after Day 7 of cell culture (Andric et al., 2010).

In addition, the influence of gelatin during cell culture may not have been significant because only a small amount of gelatin was present in the blend-based scaffolds.

According to Patlolla et al. (2010), most studies have shown that cell proliferation decreases as surface roughness is increased (Patlolla et al., 2010), however, there have also been other

studies where increased surface roughness has been reported to improve cell proliferation (Chung et al., 2003; Volpato et al., 2011). In this research, it is possible that the higher surface roughness of the PLLAGel-HA scaffolds in comparison to the PLLAGel scaffolds enabled the HOBs to proliferate better on the former scaffolds. However, as mentioned in Section 3.3.2.8.1, it was difficult to isolate the effect of surface roughness because the presence of HA on the surface on the PLLAGel-HA scaffolds would have also contributed to improve HOB proliferation on the scaffolds as HA has been reported to improve cell proliferation (Zhang et al., 2008).

The activity per cell was calculated from the alamarBlue® assay results. The results show that the activity per cell on the three scaffolds types were highest on Day 7 after which it declined gradually (Figure 55).

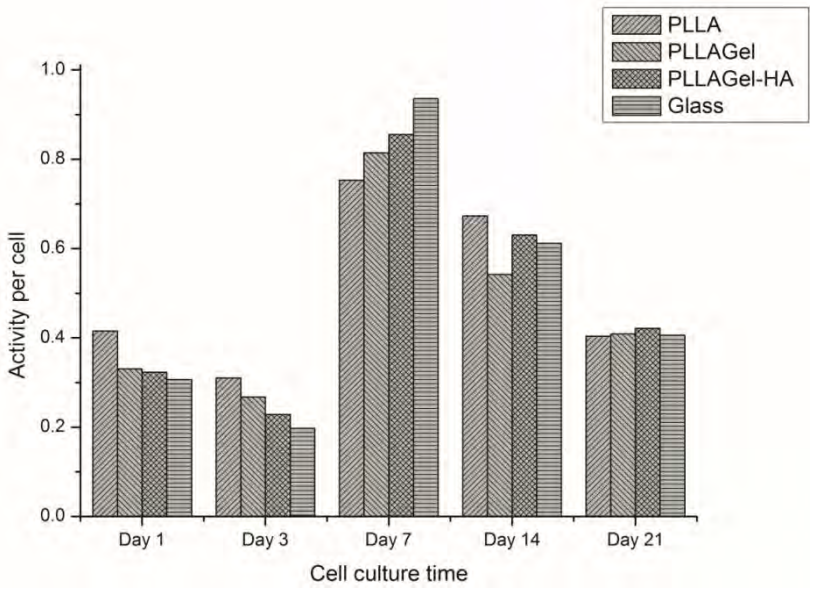

Figure 55: **Activity per cell for HOBs cultured on electrospun nanofibrous scaffolds and glass control after 1, 3, 7, 14 and 21 days of culture**

Cells were seeded at a low cell concentration and so intially, overall metabolic acivity was low. This was likely due to a lack of cell-to-cell mediated growth signals. As the cells

increased in number, intra-cellular signalling pathways were activated, resulting in increased metabolic activity of individual cells. Once the cells had reached limits of growth at day 21, all samples had a similar, decreased metabolic activity (Figure 55). The highest cellular activities on all three scaffolds were observed on Day 7, suggesting the possibility that the cells became confluent very close to this time point. Although the HOBs spread and attached well on the blend-based scaffolds at early time points, the lower inter-fibre distances (pore size) of the blend-based scaffolds may have made it initially difficult for cells to interact with the scaffolds in a 3D manner (i.e. penetrate into the depths of the scaffolds). However, with the leaching of gelatin into the culture medium, this would have created more space for cell migration into the depths of the scaffold, thereby allowing 3D cell growth. It has been reported previously in the literature, that the leaching of gelatin into the cell culture medium enhanced the infiltration of BMSCs into an electrospun gelatin/PCL scaffold (Zhang et al., 2005).

3.3.2.8.3 Alkaline phosphatase activity

Alkaline phosphatase is a membrane bound enzyme and its activity is used as an osteoblastic differentiation marker (Gupta et al., 2009). ALP is important in cell culture studies because it can initiate the mineralisation process and causes calcification at the nucleation sites (Francis et al., 2010). An important characteristic of mature osteoblast phenotypes is their ability to synthesise ALP, an early marker of osteoblast differentiation (Prabhakaran et al., 2009).

The ALP activities for the three types of electrospun nanofibrous scaffolds are shown in Figure 56. Over the 21 days of cell culture, there was no significant difference in the ALP activity of cells on the three different scaffolds.

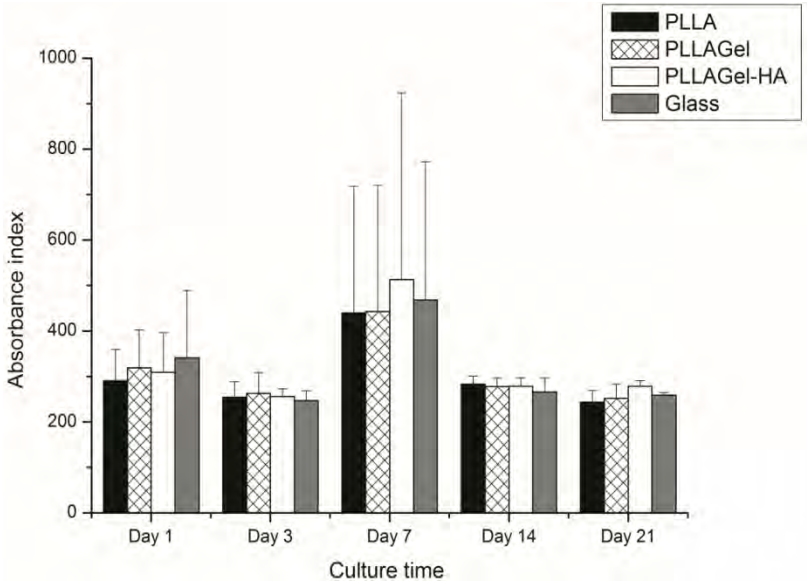

Figure 56: **Alkaline phosphatase activity for HOBs cultured on electrospun nanofibrous scaffolds and glass control after 1, 3, 7, 14 and 21 days of culture (Error bars represent standard deviation)**

ALP activities on the three scaffolds were found to increase with increasing culture time (Figure 56). The maximum ALP activity of each scaffold type was observed at Day 7, with HOBs on the PLLAGel-HA scaffold showing the highest ALP activity. The decrease in ALP activity after Day 7 suggests that the mineralisation of the HOBs was initiated after this time point. Similar results were obtained by Jones et al. (2007) where ALP activity for human osteoblast cells was highest on Day 14 after which a decrease was obtained due to the beginning of mineralisation in the cells (Jones et al., 2007). In general, ALP activity increases in levels up to the progressed mineralisation stage at which stage ALP activity declines (Wozniak and Jel Haj, 2007).

The presence of HA on the PLLAGel-HA scaffold caused a stimulation of bone cell response, hence its high ALP activity.

3.3.2.8.4 Mineralisation

Mineralisation refers to cell-mediated deposition of extra-cellular calcium and phosphorus salts where anionic matrix molecules take up the calcium and phosphate ions and serve as nucleation and growth sites, leading to calcification (Francis et al., 2010).

The results of the quantification of mineralisation of HOBs seeded on the PLLA, PLLAGel and PLLAGel-HA scaffolds measured by ARS staining are shown in Figure 57.

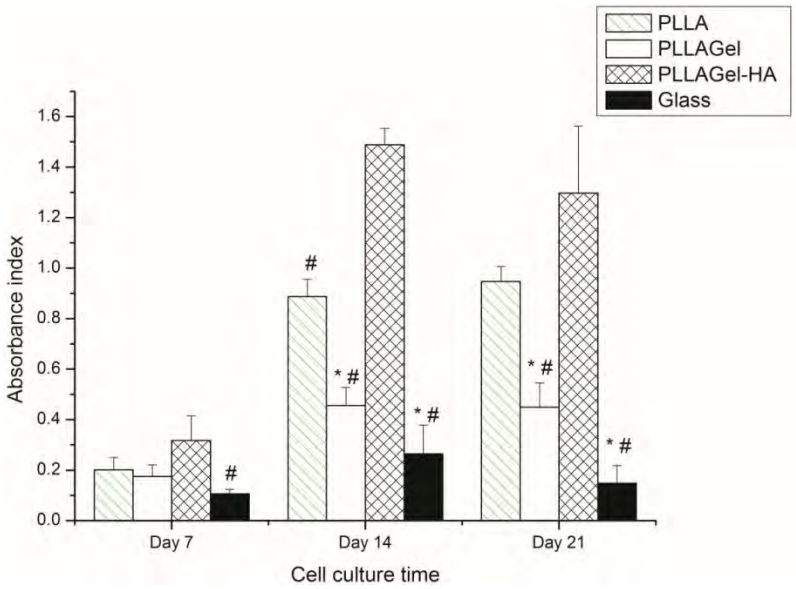

Figure 57: **Quantification of mineralisation of HOBs by Alizarin Red-S staining on glass (control), PLLA, PLLAGel and PLLAGel-HA electrospun nanofibrous scaffolds. [Error bars represent standard deviation, while * and # represent significant differences ($p \leq 0.05$) compared to PLLA and PLLAGel-HA scaffolds respectively]**

The results show that at all time points, the amount of mineralisation was in the order PLLAGel-HA > PLLA > PLLAGel. Specifically, on Day 7, the PLLAGel-HA showed a significantly higher mineralisation compared to the glass control. Likewise, on Day 14, the PLLAGel-HA scaffolds showed significantly higher mineralisation compared to all the other scaffolds whilst PLLA showed significantly higher mineralisation compared to the PLLAGel scaffolds

and the glass control. On Day 21, both the PLLA and PLLAGel-HA scaffolds showed significantly higher mineralisation compared to the PLLAGel and glass control.

HA enhances formation of new bone tissue by increasing osteoblast adhesion, osteointegration, and deposition of calcium-containing minerals on its surface (Nejati et al., 2008). The PLLAGel-HA scaffolds showed the highest mineralisation probably due to the presence of HA which acted as a chelating agent for the mineralisation of HOBs. Similar results of increased mineralisation on electrospun polymer composites due to the presence of HA have been reported previously by other researchers (Francis et al., 2010; Prabhakaran et al., 2009; Venugopal et al., 2007).

4.0 Conclusions

The main objectives of this work were: (i) to investigate the possibility of tailoring the crystallinity of PLLA fibres by carefully controlling the electrospinning parameters; (ii) to investigate the degradation behaviour of PLLA and PLLA-HA electrospun fibres; and (iii) to fabricate bi- and multicomponent scaffolds of PLLA for tissue engineering.

For the crystallinity studies, PLLA polymer fibres were electrospun from two different polymer solution concentrations, i.e. 5 wt% and 8 wt%, at varying voltages and NTCDs using an ES1a electrospinning machine manufactured by Electrospinz Ltd, New Zealand. The thermal characterisation as conducted by DSC revealed that the electrospun fibres exhibited crystallinities ranging from 23 to 46% while that for the as-received granules was approximately 37%. This suggests that by optimizing the solution and processing parameters during the electrospinning process, it may be possible to tailor the degree of crystallinity of PLLA. It was also observed that factors such as polymer solution concentration, electrospinning voltage and NTCD influenced significantly, the degree of crystallinity of the electrospun fibres. Specifically, the degree of crystallinity decreased with increasing the polymer solution concentration. In addition, an optimum electrospinning voltage at which the maximum degree of crystallinity can be obtained was observed. At voltages higher or lower than the optimum electrospinning voltage, the degree of crystallinity will decrease or increase, respectively. It is believed that each polymer solution concentration would exhibit its individual optimum electrospinning voltage. The effect of the NTCD on the degree of crystallinity followed no predictable and consistent pattern. However, it was interesting to observe that the degree of crystallinity remained fairly constant in spite of changes in NTCD when electrospinning at the optimum electrospinning voltage.

In order to study the degradation behaviour of PLLA and PLLA-HA electrospun scaffolds, PLLA and PLLA-HA scaffolds were fabricated by electrospinning. The average fibre diameter of the PLLA scaffold was 781 nm, while that of the PLLA-HA scaffold was 316 nm. Thermal analysis by DSC revealed that both electrospun scaffolds exhibited similar crystallinities. The degradation behaviour of both sets of electrospun scaffolds were investigated by ESEM, GPC, pH measurements and FTIR. Although it has been previously reported in the literature, that the presence of HA in a PLLA-HA electrospun scaffold slowed down the degradation process, the results of this project showed that this stabilizing effect of HA particles is negligible if the fibre diameter of the PLLA-HA electrospun scaffolds is small, and possibly also if the HA content is low. Since both sets of electrospun scaffolds exhibited similar crystallinities, and the main difference between both sets of scaffolds was their fibre diameters, it was highly suggestive that the difference in their degradation behaviour was due to this. The smaller diameters of the PLLA-HA electrospun scaffolds resulted in a high surface area to volume ratio (SVR), which caused them to absorb water at a higher rate than the PLLA electrospun scaffolds, thus resulting in faster degradation.

Finally, three scaffolds based on PLLA were fabricated by electrospinning i.e. PLLA, PLLAGel and PLLAGel-HA. Gelatin was chosen as one of the components of the bi-component scaffold due to its relative low-cost, hydrophilicity and the possibility of its miscibility with PLLA. HA was chosen as a component of the multicomponent scaffold due to its osteoconductivity. The electrospraying technique was preferred over other methods of incorporating HA into the polymer matrix due to its ability to produce a superficial coating of HA on the electrospun polymer; this was expected to improve both cell-scaffold interaction and degradation characteristics. The three electrospun scaffolds were

characterised for their morphology, structure, thermal properties, mechanical properties, degradation properties as well as biocompatibility.

ESEM analysis of the electrospun scaffolds showed that the scaffolds possessed fibre diameters in the order PLLA > PLLAGel ≈ PLLAGel-HA. The approximate 50% difference between the fibre diameters of the PLLA and blend-based scaffolds was ascribed to the presence of gelatin whose molecules have a high dielectric constant which provided excess charges within the electrospinning solution.

The FTIR scans showed no new peaks developed on the blend-based scaffolds, however, the intensity of the carbonyl C=O peak decreased with the addition of gelatin to PLLA, while gelatin amide band shifted to a lower wavenumber. This indicated the possibility of hydrogen bonding between the amide groups of gelatin and the carbonyl group of PLLA.

Thermal analysis of the electrospun scaffolds by DSC revealed that the blend-based scaffolds possessed a single T_g without any denaturation peaks, confirming that gelatin and PLLA were miscible at the concentration from which the blend-based scaffolds were electrospun. This miscibility was ascribed to the presence of hydrogen bonds between gelatin and PLLA.

The blend-based scaffolds showed a slight improvement in tensile strength compared to the PLLA scaffold. This observation was ascribed to the presence of hydrogen bonds between gelatin and PLLA in the blend-based scaffolds. In addition, the thinner fibre diameters of the blend-based scaffolds probably enhanced their properties in comparison to the PLLA scaffold. Nano-HA particles in the PLLAGel-HA scaffolds served as particulate reinforcements for the PLLAGel polymer matrix, increasing their stiffness and consequently, their tensile strength.

A 49-day degradation study was conducted to determine the degradation properties of the three electrospun scaffolds. All scaffolds types exhibited negligible weight loss and no

changes in nanofibre morphology during the degradation. However, the pH reduced from 7.4 to ≈6.7 for the three scaffold types. All the scaffolds retained their integrity throughout the degradation study, suggesting that they are promising tissue engineering scaffolds for applications requiring slow degradation rates such as in bone regeneration. The fact that after 49 days of degradation, HA particles were still observed on the surface of the degraded PLLAGel-HA scaffolds indicates that electrospraying HA post-electrospinning is a good method of fabricating electrospun polymer-HA composite scaffolds.

Biocompatibility studies were conducted on the three electrospun scaffolds by culturing HOBs on them. All scaffolds supported cell attachment and spreading after 24 hours of cell culture, however, the HOBs attached best onto the PLLAGel-HA scaffold. At this time point, SEM revealed that the HOBs were flat, and possessed filapodia extended far out along the fibres of the blend-based scaffolds while the HOBs on the PLLA scaffold were observed to be round and compact. The reason for this was attributed to the presence of gelatin and HA. The gelatin provided integrin which allowed for improved cell attachment whilst the HA improved osteoconductivity. Similarly, HOBs were found to proliferate best on the PLLAGel-HA scaffold. Furthermore, significantly higher mineralisation was observed on the PLLAGel-HA scaffold. This was ascribed to the presence of HA nanoparticles which enhanced formation of new bone tissue by increasing osteoblast adhesion, osteointegration, and deposition of calcium-containing minerals on its surface. The exact effect of surface roughness on HOB response was difficult to analyse because of the vast differences in the composition of the three scaffold types.

Finally, in conclusion it was seen that blending gelatin with PLLA had significant effects on the properties of the electrospun scaffold. The highly charged gelatin molecules aided in obtaining nanofibres with smaller diameters for the blend-based scaffolds. The presence of

hydrogen bonding between gelatin and PLLA in the blend also helped to improve the mechanical properties of PLLA. In addition, gelatin improved HOB attachment on PLLA. Furthermore, electrospraying HA onto the surface of PLLAGel scaffold helped to provide an exposed layer of HA on the surface of the scaffold. The presence of the exposed HA particles helped to improve the biological properties of the resulting scaffold, indicating that the PLLAGel-HA scaffold is a promising material for bone-tissue engineering.

5.0 Future Work

Based on the challenges encountered, observations made, and the results obtained during this research project, the following will be suggested as work to be done on this area in the future:

1) The blend-based scaffolds should be cross-linked to prevent the leaching of gelatin during cell culture and degradation study;
2) An electrospinning machine should be set up to collect aligned fibres; the properties (e.g. mechanical, thermal and degradation) of these aligned fibres should be studied and compared to those of the random non-woven scaffold;
3) The degradation study should be conducted over a longer period of time (≥ 110 weeks), and the effect of degradation on molecular weight should be studied by GPC;
4) It will also be beneficial to conduct degradation studies on other electrospun PLLA-HA scaffolds containing higher HA concentrations to see the effect of continually increasing HA concentration on fibre diameter, and the consequent effect of the fibre diameter on degradation properties. Since the results of this work showed that the stabilizing effect of HA is neglible at low HA concentrations, it will be useful to conduct degradation experiments to determine the minimum HA concentration at which the stabilizing effect becomes significant;
5) The *in vivo* characteristics of the PLLA, PLLAGel and PLLAGel-HA scaffolds should be investigated using animal models;
6) Although there have been various studies on crystallinity of electrospun fibres, a few pertinent questions that have not been answered by any of the studies are:
    a) "During electrospinning, when does crystallisation start and when does it end?"

b) “Does it start just as the solution is ejected from the needle tip and end once the fibres are deposited on the collector? Or does it continue after the fibres have been deposited on the collector?”

In this project, it has been assumed that all/majority of the crystallisation that occurs during electrospinning occurs during the time when the fibres are in the electric field between the needle tip and the collector. However, it is possible that some portion of the crystallinity of the fibres obtained by DSC may have developed after the fibres had been deposited on the collector. It will therefore be benefical to conduct experiments to determine the beginning and the end of crystallisation during electrospinning as this will be crucial to understanding the amount of crystallinity induced specifically by electrospinning. The complexity of such an experiment is appreciated, and it may only be possible to do this by modelling, e.g. by using finite element analysis.

7) It has been explained in the literature that an electrospun fibre consists of a skin and a core region, both of which differ in properties from each other (Baji et al., 2010). The work of Aristein et al. (2007) and Curgul et al. (2007) have given some insight into some of the molecular properties of the skin and core regions of electrospun fibres (Arinstein et al., 2007; Curgul et al., 2007), however, it would be beneficial to conduct studies that can give an understanding of the effect of varying different electrospinning parameters (e.g. voltage and polymer solution concentration) on the molecular structures of these two distinct regions. Again, the difficulty of conducting such experiments practically is envisaged, and such studies may only be feasible by simulation.

8) More studies should be carried out on tailoring the crystallinity of PLLA electrospun fibres using voltages (e.g. 12 kV, 13 kV, 26 kV etc) and polymer solution concentrations (e.g. 6 wt%, 7 wt% etc) over a wider range than was tested in this study.

9) Systematic study on tailoring the crystallinity of polymer fibres as conducted for PLLA in this research should be conducted for other polymer systems;

10) During this research, an attempt was made to compare the values of the weight-average molecular weight obtained by GPC with the viscosity-average molecular weight computed by viscosimetry. However, it was not possible to obtain the Mark-Houwink constants for PLLA solution in DCM/DMF, both from the literature and from the National Physical Laboratory, UK. Determination of these values fell beyond the scope of this research project, but considering the volume of research being conducted on fabricating PLLA scaffolds from DCM/DMF solutions, it was rather surprising that the Mark-Houwink constants had not been calculated previously in the literature. It will therefore make an interesting study to conduct a series of experiments which will determine the values of these constants for the PLLA-DCM/DMF system;

11) Further confirmation of miscibility between PLLA and gelatin in the electrospun scaffolds should be obtained by a suitable method such as transmission electron microscopy (TEM);

12) Since Alizarin red-S binds selectively to calcium salts, the quantification of mineralisation which was studied by ARS staining may have been exaggerated in the case of the PLLAGel-HA scaffold due to the HA that was already on the surface of the scaffold prior to cell culture. In the future, it would be preferable to quantify mineralisation by a more suitable method such as Raman microscopy. The intensities of the symmetric stretching vibration (v_1) of the PO_4^{3-} group of HA can be measured prior to cell culture and after cell culture can be subtracted from each other to give an idea of the amount of HA that was formed during mineralisation. ESEM micrographs may also be used to qualitatively compare the level of mineralisation between the different scaffold types.

References

ANDRIC, T., SAMPSON, A. C. & FREEMAN, J. W. (2010) Fabrication and characterization of electrospun osteon mimicking scaffolds for bone tissue engineering. *Materials Science & Engineering C-Materials for Biological Applications,* 31**,** 2-8.

ANDRIC, T., WRIGHT, L. D. & FREEMAN, J. W. (2011) Rapid Mineralization of Electrospun Scaffolds for Bone Tissue Engineering. *Journal of Biomaterials Science-Polymer Edition,* 22**,** 1535-1550.

ANSELME, K., LINEZ, P., BIGERELLE, M., LE MAGUER, D., LE MAGUER, A., HARDOUIN, P., HILDEBRAND, H. F., IOST, A. & LEROY, J. M. (2000) The relative influence of the topography and chemistry of TiAl6V4 surfaces on osteoblastic cell behaviour. *Biomaterials,* 21**,** 1567-1577.

ARINSTEIN, A., BURMAN, M., GENDELMAN, O. & ZUSSMAN, E. (2007) Effect of supramolecular structure on polymer nanofibre elasticity. *Nature Nanotechnology,* 2**,** 59-62.

AYUTSEDE, J., GANDHI, M., SUKIGARA, S., MICKLUS, M., CHEN, H.-E. & KO, F. (2005) Regeneration of Bombyx mori silk by electrospinning. Part 3: Characterization of electrospun nonwoven mat. *Polymer,* 46**,** 1625-1634.

BAJI, A., MAI, Y. W., WONG, S. C., ABTAHI, M. & CHEN, P. (2010) Electrospinning of polymer nanofibers: Effects on oriented morphology, structures and tensile properties. *Composites Science and Technology,* 70**,** 703-718.

BARNES, C. P., SELL, S. A., BOLAND, E. D., SIMPSON, D. G. & BOWLIN, G. L. (2007) Nanofiber technology: Designing the next generation of tissue engineering scaffolds. *Advanced Drug Delivery Reviews,* 59**,** 1413-1433.

BARRÈRE, F., NI, M., HABIBOVIC, P., DUCHEYNE, P. & GROOT, K. D. (2008) Degradation of bioceramics. IN VAN BLITTERSWIJK, C., THOMSEN, P., LINDAHL, A., HUBBELL, J., WILLIAMS, D. F., CANCEDDA, R., DE BRUIJN, J. D. & SOHIER, J. (Eds.) *Tissue Engineering.* Amsterdam, Elsevier Inc.

BERGSMA, J. E., DEBRUIJN, W. C., ROZEMA, F. R., BOS, R. R. M. & BOERING, G. (1995) Late Degradation Tissue-Response to Poly(L-Lactide) Bone Plates and Screws. *Biomaterials,* 16**,** 25-31.

BIGI, A., BOANINI, E. & RUBINI, K. (2004) Hydroxyapatite gels and nanocrystals prepared through a sol-gel process. *Journal of Solid State Chemistry,* 177**,** 3092-3098.

BIGI, A., BRACCI, B., COJAZZI, G., PANZAVOLTA, S. & ROVERI, N. (1998) Drawn gelatin films with improved mechanical properties. *Biomaterials,* 19**,** 2335-2340.

BIGI, A., COJAZZI, G., PANZAVOLTA, S., RUBINI, K. & ROVERI, N. (2001) Mechanical and thermal properties of gelatin films at different degrees of glutaraldehyde crosslinking. *Biomaterials,* 22**,** 763-768.

BILLMEYER, F. W. (1984) *Textbook of Polymer Science,* Singapore, John Wiley & Sons, Inc.

BIRSHTEIN, V. & TUL'CHINSKII, V. (1982) A study of gelatin by IR spectroscopy. *Chemistry of Natural Compounds,* 18**,** 697-700.

BLACKWOOD, K. A., MCKEAN, R., CANTON, I., FREEMAN, C. O., FRANKLIN, K. L., COLE, D., BROOK, I., FARTHING, P., RIMMER, S., HAYCOCK, J. W., RYAN, A. J. & MACNEIL, S. (2008) Development of biodegradable electrospun scaffolds for dermal replacement. *Biomaterials,* 29**,** 3091-3104.

BOCCACCINI, A. R., BLAKER, J. J., MAQUET, V., CHUNG, W., JEROME, R. & NAZHAT, S. N. (2006) Poly(D,L-lactide) (PDLLA) foams with TiO2 nanoparticles and PDLLA/TiO2-

Bioglass (R) foam composites for tissue engineering scaffolds. *Journal of Materials Science,* 41**,** 3999-4008.

BOGAERT, J. C. & COSZACH, P. (2000) Poly(lactic acids): A potential solution to plastic waste dilemma. *Macromolecular Symposia,* 153**,** 287-303.

BOGNITZKI, M., CZADO, W., FRESE, T., SCHAPER, A., HELLWIG, M., STEINHART, M., GREINER, A. & WENDORFF, J. H. (2001) Nanostructured fibers via electrospinning. *Advanced Materials,* 13**,** 70-72.

BOLAND, E. D., WNEK, G. E., SIMPSON, D. G., PAWLOWSKI, K. J. & BOWLIN, G. L. (2001) Tailoring tissue engineering scaffolds using electrostatic processing techniques: A study of poly(glycolic acid) electrospinning. *Journal of Macromolecular Science-Pure and Applied Chemistry,* 38**,** 1231-1243.

BOLGEN, N., MENCELOGLU, Y. Z., ACATAY, K., VARGEL, I. & PISKIN, E. (2005) In vitro and in vivo degradation of non-woven materials made of poly(epsilon-caprolactone) nanofibers prepared by electrospinning under different conditions. *Journal of Biomaterials Science-Polymer Edition,* 16**,** 1537-1555.

BOUHAOUSS, A., LAGHZIZIL, A., BENSAOUD, A., FERHAT, M., LORENT, G. & LIVAGE, J. (2001) Mechanism of ionic conduction in oxy and hydroxyapatite structures. *International Journal of Inorganic Materials,* 3**,** 743-747.

BUCHKO, C. J., CHEN, L. C., SHEN, Y. & MARTIN, D. C. (1999) Processing and microstructural characterization of porous biocompatible protein polymer thin films. *Polymer,* 40**,** 7397-7407.

BURG, K. J. L., PORTER, S. & KELLAM, J. F. (2000) Biomaterial developments for bone tissue engineering. *Biomaterials,* 21**,** 2347-2359.

BUTTERY, L. D. K. & BISHOP, A. E. (2005) Introduction to Tissue Engineering. IN HENCH, L. L. & JONES, J. R. (Eds.) *Biomaterials, artificial organs and tissue engineering.* Cambridge, Woodhead Publishing Limited.

CALLISTER, W. D. J. (2003) *Materials Science & Engineering An Introduction,* New York, John Wiley & Sons, Inc.

CAO, H. & KUBOYAMA, N. (2010) A biodegradable porous composite scaffold of PGA/beta-TCP for bone tissue engineering. *Bone,* 46**,** 386-395.

CARRIZALES, C., PELFREY, S., RINCON, R., EUBANKS, T. M., KUANG, A. X., MCCLURE, M. J., BOWLIN, G. L. & MACOSSAY, J. (2008) Thermal and mechanical properties of electrospun PMMA, PVC, Nylon 6, and Nylon 6,6. *Polymers for Advanced Technologies,* 19**,** 124-130.

CHANDRA, R. & RUSTGI, R. (1998) Biodegradable polymers. *Progress in Polymer Science,* 23**,** 1273-1335.

CHEN, C., DONG, L. & CHEUNG, M. K. (2005) Preparation and characterization of biodegradable poly(L-lactide)/chitosan blends. *European Polymer Journal,* 41**,** 958-966.

CHEN, J. L., CHU, B. & HSIAO, B. S. (2006) Mineralization of hydroxyapatite in electrospun nanofibrous poly(L-lactic acid) scaffolds. *Journal of Biomedical Materials Research Part A,* 79A**,** 307-317.

CHEN, J. P. & SU, C. H. (2011) Surface modification of electrospun PLLA nanofibers by plasma treatment and cationized gelatin immobilization for cartilage tissue engineering. *Acta Biomaterialia,* 7**,** 234-243.

CHEN, V. J. & MA, P. X. (2006) The effect of surface area on the degradation rate of nano-fibrous poly(L-lactic acid) foams. *Biomaterials,* 27**,** 3708-3715.

CHUENJITKUNTAWORN, B., SUPAPHOL, P., PAVASANT, P. & DAMRONGSRI, D. (2010) Electrospun poly(L-lactic acid)/hydroxyapatite composite fibrous scaffolds for bone tissue engineering. *Polymer International,* 59**,** 227-235.

CHUNG, T.-W., LIU, D.-Z., WANG, S.-Y. & WANG, S.-S. (2003) Enhancement of the growth of human endothelial cells by surface roughness at nanometer scale. *Biomaterials,* 24**,** 4655-4661.

COOMBES, A. G. A. & MEIKLE, M. C. (1994) Resorbable synthetic polymers as replacements for bone graft. *Clinical Materials,* 17**,** 35-67.

COREY, J. M., GERTZ, C. C., WANG, B. S., BIRRELL, L. K., JOHNSON, S. L., MARTIN, D. C. & FELDMAN, E. L. (2008) The design of electrospun PLLA nanofiber scaffolds compatible with serum-free growth of primary motor and sensory neurons. *Acta Biomaterialia,* 4**,** 863-875.

CUI, W., LI, X., ZHOU, S. & WENG, J. (2008) Degradation patterns and surface wettability of electrospun fibrous mats. *Polymer Degradation and Stability,* 93**,** 731-738.

CUI, W. G., LI, X. H., ZHU, X. L., YU, G., ZHOU, S. B. & WENG, J. (2006) Investigation of drug release and matrix degradation of electrospun poly(DL-lactide) fibers with paracetanol inoculation. *Biomacromolecules,* 7**,** 1623-1629.

CUI, W. U., LI, X. H., ZHOU, S. B. & WENG, J. (2007) In situ growth of hydroxyapatite within electrospun poly(DL-lactide) fibers. *Journal of Biomedical Materials Research Part A,* 82A**,** 831-841.

CURGUL, S., VAN VLIET, K. J. & RUTLEDGE, G. C. (2007) Molecular dynamics simulation of size-dependent structural and thermal properties of polymer nanofibers. *Macromolecules,* 40**,** 8483-8489.

DAHLIN, R. L., KASPER, F. K. & MIKOS, A. G. (2011) Polymeric Nanofibers in Tissue Engineering. *Tissue Engineering Part B-Reviews,* 17**,** 349-364.

DAS, S., HOLLISTER, S. J., FLANAGAN, C., ADEWUNMI, A., BARK, K., CHEN, C., RAMASWAMY, K., ROSE, D. & WIDJAJA, E. (2003) Freeform fabrication of Nylon-6 tissue engineering scaffolds. *Rapid Prototyping Journal,* 9**,** 43-49.

DE JONG, W. H., BERGSMA, J. E., ROBINSON, J. E. & BOS, R. R. M. (2005) Tissue response to partially in vitro predegraded poly-L-lactide implants. *Biomaterials,* 26**,** 1781-1791.

DEITZEL, J. M., KLEINMEYER, J., HARRIS, D. & BECK TAN, N. C. (2001a) The effect of processing variables on the morphology of electrospun nanofibers and textiles. *Polymer,* 42**,** 261-272.

DEITZEL, J. M., KLEINMEYER, J. D., HIRVONEN, J. K. & BECK TAN, N. C. (2001b) Controlled deposition of electrospun poly(ethylene oxide) fibers. *Polymer,* 42**,** 8163-8170.

DEMIR, M. M., YILGOR, I., YILGOR, E. & ERMAN, B. (2002) Electrospinning of polyurethane fibers. *Polymer,* 43**,** 3303-3309.

DEPLAINE, H., RIBELLES, J. L. G. & FERRER, G. G. (2010) Effect of the content of hydroxyapatite nanoparticles on the properties and bioactivity of poly(L-lactide) - Hybrid membranes. *Composites Science and Technology,* 70**,** 1805-1812.

DONG, Y. X., LIAO, S., NGIAM, M., CHAN, C. K. & RAMAKRISHNA, S. (2009) Degradation Behaviors of Electrospun Resorbable Polyester Nanofibers. *Tissue Engineering Part B-Reviews,* 15**,** 333-351.

DONG, Y. X., YONG, T., LIAO, S., CHAN, C. K., STEVENS, M. M. & RAMAKRISHNA, S. (2010) Distinctive Degradation Behaviors of Electrospun Polyglycolide, Poly(DL-Lactide-co-Glycolide), and Poly(L-Lactide-co-epsilon-Caprolactone) Nanofibers Cultured With/Without Porcine Smooth Muscle Cells. *Tissue Engineering Part A,* 16**,** 283-298.

DRUMRIGHT, R. E., GRUBER, P. R. & HENTON, D. E. (2000) Polylactic acid technology. *Advanced Materials,* 12**,** 1841-1846.

DRURY, J. L. & MOONEY, D. J. (2003) Hydrogels for tissue engineering: scaffold design variables and applications. *Biomaterials,* 24**,** 4337-4351.

ELECTROSPINZ (2008) Frequently Asked Questions. http://www.electrospinz.co.nz/faq.php. Accessed 12 January, 2012.

ERO-PHILLIPS, B. (2011) Electrospin to Win. http://www.eruditiononline.co.uk/experimentation/article.php?id=1128.

FAMBRI, L., PEGORETTI, A., FENNER, R., INCARDONA, S. D. & MIGLIARESI, C. (1997) Biodegradable fibres of poly(L-lactic acid) produced by melt spinning. *Polymer,* 38**,** 79-85.

FAN, L. H., DU, Y. M., HUANG, R. H., WANG, Q., WANG, X. H. & ZHANG, L. N. (2005) Preparation and characterization of alginate/gelatin blend fibers. *Journal of Applied Polymer Science,* 96**,** 1625-1629.

FANG, B., WAN, Y.-Z., TANG, T.-T., GAO, C. & DAI, K.-R. (2009) Proliferation and Osteoblastic Differentiation of Human Bone Marrow Stromal Cells on Hydroxyapatite/Bacterial Cellulose Nanocomposite Scaffolds. *Tissue Engineering Part A,* 15**,** 1091-1098.

FENNESSEY, S. F. & FARRIS, R. J. (2004) Fabrication of aligned and molecularly oriented electrospun polyacrylonitrile nanofibers and the mechanical behavior of their twisted yams. *Polymer,* 45**,** 4217-4225.

FRANCIS, L., VENUGOPAL, J., PRABHAKARAN, M. P., THAVASI, V., MARSANO, E. & RAMAKRISHNA, S. (2010) Simultaneous electrospin-electrosprayed biocomposite nanofibrous scaffolds for bone tissue regeneration. *Acta Biomater,* 6**,** 4100-9.

FREED, L. E., MARQUIS, J. C., NOHRIA, A., EMMANUAL, J., MIKOS, A. G. & LANGER, R. (1993) Neocartilage Formation Invitro and Invivo Using Cells Cultured on Synthetic Biodegradable Polymers. *Journal of Biomedical Materials Research,* 27**,** 11-23.

FUKUSHIMA, K., SOGO, K., MIURA, S. & KIMURA, Y. (2004) Production of D-Lactic Acid by Bacterial Fermentation of Rice Starch. *Macromolecular Bioscience,* 4**,** 1021-1027.

FURTH, M. E. & ATALA, A. (2007) Future Perspectives. IN LANZA, R., LANGER, R. & VACANTI, J. (Eds.) *Principles of Tissue Engineering.* 3rd ed. Burlington, Elsevier Academic Press.

GILDING, D. K. & REED, A. M. (1979) Biodegradable Polymers for Use in Surgery Em Dash Polyglycolic/Poly(Actic Acid) Homo- and Copolymers Em Dash 1. *Polymer,* 20**,** 1459-1464.

GIUSTI, P., BARBANI, N., LAZZERI, L., POLACCO, G., CRISTALLINI, C. & CASCONE, M. G. (1998) Gelatin-poly(vinyl alcohol) blends as bioartificial polymeric materials. IN PRASAD, P. N., MARK, J. E., KANDIL, S. H. & KAFAFI, Z. H. (Eds.) *Science and Technology of Polymers and Advanced Materials - Emerging Technologies and Business Opportunities.* New York, Plenum Press Div Plenum Publishing Corp.

GOMES, M. E. & REIS, R. L. (2004) Biodegradable polymers and composites in biomedical applications: from catgut to tissue engineering - Part 1 - Available systems and their properties. *International Materials Reviews,* 49**,** 261-273.

GOMES, M. E., SIKAVITSAS, V. I., BEHRAVESH, E., REIS, R. L. & MIKOS, A. G. (2003) Effect of flow perfusion on the osteogenic differentiation of bone marrow stromal cells cultured on starch-based three-dimensional scaffolds. *Journal of Biomedical Materials Research Part A,* 67A**,** 87-95.

GOPFERICH, A. (1996) Mechanisms of polymer degradation and erosion. *Biomaterials,* 17**,** 103-114.

GRIZZI, I., GARREAU, H., LI, S. & VERT, M. (1995) Hydrolytic Degradation of Devices Based on Poly(Dl-Lactic Acid) Size-Dependence. *Biomaterials,* 16**,** 305-311.

GU, S. Y., WANG, Z. M., REN, J. & ZHANG, C. Y. (2009) Electrospinning of gelatin and gelatin/poly(L-lactide) blend and its characteristics for wound dressing. *Materials Science & Engineering C-Materials for Biological Applications,* 29**,** 1822-1828.

GUO, X. Y., GOUGH, J. E., XIAO, P., LIU, J. & SHEN, Z. J. (2007) Fabrication of nanostructured hydroxyapatite and analysis of human osteoblastic cellular response. *Journal of Biomedical Materials Research Part A,* 82A**,** 1022-1032.

GUPTA, B., REVAGADE, N. & HILBORN, J. (2007) Poly(lactic acid) fiber: An overview. *Progress in Polymer Science,* 32**,** 455-482.

GUPTA, D., VENUGOPAL, J., MITRA, S., DEV, V. R. G. & RAMAKRISHNA, S. (2009) Nanostructured biocomposite substrates by electrospinning and electrospraying for the mineralization of osteoblasts. *Biomaterials,* 30**,** 2085-2094.

HAKKARAINEN, M. (2002) Aliphatic polyesters: Abiotic and biotic degradation and degradation products. *Degradable Aliphatic Polyesters.* Berlin, Springer-Verlag Berlin.

HALLAB, N. J., JACOBS, J. J. & KATZ, J. L. (2004) Orthopedic Applications. IN RATNER, B. D., HOFFMAN, A. S., SCHOEN, F. J. & LEMONS, J. E. (Eds.) *Biomaterials Science: An Introduction to Materials in Medicine.* 2nd ed. San Diego, Elsevier Academic Press.

HANKE, L. D. (2010) Handbook of Analytical Methods for Materials. http://mee-inc.com/hamm72d.pdf. Accessed 18 July, 2011.

HARTGERINK, J. D., BENIASH, E. & STUPP, S. I. (2001) Self-assembly and mineralization of peptide-amphiphile nanofibers. *Science,* 294**,** 1684-1688.

HE, W., MA, Z. W., TEO, W. E., DONG, Y. X., ROBLESS, P. A., LIM, T. C. & RAMAKRISHNA, S. (2009) Tubular nanofiber scaffolds for tissue engineered small-diameter vascular grafts. *Journal of Biomedical Materials Research Part A,* 90A**,** 205-216.

HE, W., MA, Z. W., YONG, T., TEO, W. E. & RAMAKRISHNA, S. (2005) Fabrication of collagen-coated biodegradable polymer nanofiber mesh and its potential for endothelial cells growth. *Biomaterials,* 26**,** 7606-7615.

HEIDORN, K. C. (1998) The Fire Of St. Elmo. http://www.islandnet.com/~see/weather/elements/stelmo.htm. Accessed 21st August, 2011.

HENCH, L. L. (2005) The skeletal system. IN HENCH, L. L. & JONES, J. R. (Eds.) *Biomaterials, artificial organs and tissue engineering.* Cambridge, Woodhead Publishing Limited.

HENCH, L. L. & WILSON, J. (1984) Surface-Active Biomaterials. *Science,* 226**,** 630-636.

HILL, S. E. (2005) Electrospinning. http://nano.mtu.edu/Electrospinning_start.html. Accessed 10 July, 2011.

HIRAYAMA, S. & UEDA, R. (2004) Production of optically pure D-Lactic acid by Nannochlorum sp 26A4. *Applied Biochemistry and Biotechnology,* 119**,** 71-77.

HOLLINGER, J. O. & BATTISTONE, G. C. (1986) Biodegradable Bone Repair Materials - Synthetic-Polymers and Ceramics. *Clinical Orthopaedics and Related Research***,** 290-305.

HONG, L., PEPTAN, I., CLARK, P. & MAO, J. J. (2005) Ex vivo adipose tissue engineering by human marrow stromal cell seeded gelatin sponge. *Annals of Biomedical Engineering,* 33**,** 511-517.

HONG, Z. K., REIS, R. L. & MANO, J. F. (2008) Preparation and in vitro characterization of scaffolds of poly(L-lactic acid) containing bioactive glass ceramic nanoparticles. *Acta Biomaterialia,* 4**,** 1297-1306.

HOSSEINKHANI, H., HOSSEINKHANI, M. & KOBAYASHI, H. (2006) Proliferation and differentiation of mesenchymal stem cells using self-assembled peptide amphiphile nanofibers. *Biomedical Materials,* 1**,** 8-15.

HOU, X. X., YANG, X. P., ZHANG, L. Q., WACLAWIK, E. & WU, S. Z. (2010) Stretching-induced crystallinity and orientation to improve the mechanical properties of electrospun PAN nanocomposites. *Materials & Design,* 31**,** 1726-1730.

HUANG, Z.-M., ZHANG, Y. Z., KOTAKI, M. & RAMAKRISHNA, S. (2003) A review on polymer nanofibers by electrospinning and their applications in nanocomposites. *Composites Science and Technology,* 63**,** 2223-2253.

HUANG, Z.-M., ZHANG, Y. Z., RAMAKRISHNA, S. & LIM, C. T. (2004) Electrospinning and mechanical characterization of gelatin nanofibers. *Polymer,* 45**,** 5361-5368.

HUTMACHER, D. W. (2000) Scaffolds in tissue engineering bone and cartilage. *Biomaterials,* 21**,** 2529-2543.

HUTMACHER, D. W. & DALTON, P. D. (2011) Melt Electrospinning. *Chemistry-an Asian Journal,* 6**,** 44-56.

INAI, R., KOTAKI, M. & RAMAKRISHNA, S. (2005) Structure and properties of electrospun PLLA single nanofibres. *Nanotechnology,* 16**,** 208-13.

IOKU, K., YAMAUCHI, S., FUJIMORI, H., GOTO, S. & YOSHIMURA, M. (2002) Hydrothermal preparation of fibrous apatite and apatite sheet. *Solid State Ionics,* 151**,** 147-150.

ISHAUG-RILEY, S. L., CRANE-KRUGER, G. M., YASZEMSKI, M. J. & MIKOS, A. G. (1998) Three-dimensional culture of rat calvarial osteoblasts in porous biodegradable polymers. *Biomaterials,* 19**,** 1405-1412.

ISHAUG-RILEY, S. L., CRANE, G. M., GURLEK, A., MILLER, M. J., YASKO, A. W., YASZEMSKI, M. J. & MIKOS, A. G. (1997) Ectopic bone formation by marrow stromal osteoblast transplantation using poly(DL-lactic-co-glycolic acid) foams implanted into the rat mesentery. *Journal of Biomedical Materials Research,* 36**,** 1-8.

ISHII, D., YING, T. H., MAHARA, A., MURAKAMI, S., YAMAOKA, T., LEE, W.-K. & IWATA, T. (2009) In Vivo Tissue Response and Degradation Behavior of PLLA and Stereocomplexed PLA Nanofibers. *Biomacromolecules,* 10**,** 237-242.

ITO, Y., HASUDA, H., KAMITAKAHARA, M., OHTSUKI, C., TANIHARA, M., KANG, I. K. & KWON, O. H. (2005) A composite of hydroxyapatite with electrospun biodegradable nanofibers as a tissue engineering material. *Journal of Bioscience and Bioengineering,* 100**,** 43-49.

JAGUR-GRODZINSKI, J. (2006) Polymers for tissue engineering, medical devices, and regenerative medicine. Concise general review of recent studies. *Polymers for Advanced Technologies,* 17**,** 395-418.

JARUSUWANNAPOOM, T., HONGROJJANAWIWAT, W., JITJAICHAM, S., WANNATONG, L., NITHITANAKUL, M., PATTAMAPROM, C., KOOMBHONGSE, P., RANGKUPAN, R. & SUPAPHOL, P. (2005) Effect of solvents on electro-spinnability of polystyrene solutions and morphological appearance of resulting electrospun polystyrene fibers. *European Polymer Journal,* 41**,** 409-421.

JAWOREK, A., KRUPA, A., LACKOWSKI, M., SOBCZYK, A. T., CZECH, T., RAMAKRISHNA, S., SUNDARRAJAN, S. & PLISZKA, D. (2009) Nanocomposite fabric formation by

electrospinning and electrospraying technologies. *Journal of Electrostatics,* 67**,** 435-438.

JIAO, Y. P., LIU, Z. H. & ZHOU, C. R. (2007) Fabrication and characterization of PLLA-chitosan hybrid scaffolds with improved cell compatibility. *Journal of Biomedical Materials Research Part A,* 80A**,** 820-825.

JONES, J. R. (2005) Scaffolds for tissue engineering. IN HENCH, L. L. & JONES, J. R. (Eds.) *Biomaterials, artificial organs and tissue engineering.* Cambridge, Woodhead Publishing Limited.

JONES, J. R., TSIGKOU, O., COATES, E. E., STEVENS, M. M., POLAK, J. M. & HENCH, L. L. (2007) Extracellular matrix formation and mineralization on a phosphate-free porous bioactive glass scaffold using primary human osteoblast (HOB) cells. *Biomaterials,* 28**,** 1653-1663.

JOSE, M. V., THOMAS, V., XU, Y. Y., BELLIS, S., NYAIRO, E. & DEAN, D. (2010) Aligned Bioactive Multi-Component Nanofibrous Nanocomposite Scaffolds for Bone Tissue Engineering. *Macromolecular Bioscience,* 10**,** 433-444.

KANG, J. C., WANG, M. & YUAN, X. Y. (2010) Bicomponent Fibrous Scaffolds of Controlled Composition for Tissue Engineering Applications. *Imece2009: Proceedings of the Asme International Mechanical Engineering Congress and Exposition, Vol 2.* New York, Amer Soc Mechanical Engineers.

KATTA, P., ALESSANDRO, M., RAMSIER, R. D. & CHASE, G. G. (2004) Continuous electrospinning of aligned polymer nanofibers onto a wire drum collector. *Nano Letters,* 4**,** 2215-2218.

KHORASANI, M. T., MIRZADEH, H. & IRANI, S. (2009) Comparison of Fibroblast and Nerve Cells Response on Plasma Treated Poly (L-lactide) Surface. *Journal of Applied Polymer Science,* 112**,** 3429-3435.

KIDOAKI, S., KWON, I. K. & MATSUDA, T. (2005) Mesoscopic spatial designs of nano- and microfiber meshes for tissue-engineering matrix and scaffold based on newly devised multilayering and mixing electrospinning techniques. *Biomaterials,* 26**,** 37-46.

KILPADI, K. L., CHANG, P. L. & BELLIS, S. L. (2001) Hydroxylapatite binds more serum proteins, purified integrins, and osteoblast precursor cells than titanium or steel. *Journal of Biomedical Materials Research,* 57**,** 258-267.

KIM, H.-W., YU, H.-S. & LEE, H.-H. (2008a) Nanofibrous matrices of poly(lactic acid) and gelatin polymeric blends for the improvement of cellular responses. *Journal of Biomedical Materials Research Part A,* 87A**,** 25-32.

KIM, H. W., LEE, H. H. & KNOWLES, J. C. (2006a) Electrospinning biomedical nanocomposite fibers of hydroxyapatite/poly(lactic acid) for bone regeneration. *Journal of Biomedical Materials Research Part A,* 79A**,** 643-649.

KIM, H. W., SONG, J. H. & KIM, H. E. (2005) Nanofiber generation of gelatin-hydroxyapatite biomimetics for guided tissue regeneration. *Advanced Functional Materials,* 15**,** 1988-1994.

KIM, I. Y., SEO, S. J., MOON, H. S., YOO, M. K., PARK, I. Y., KIM, B. C. & CHO, C. S. (2008b) Chitosan and its derivatives for tissue engineering applications. *Biotechnology Advances,* 26**,** 1-21.

KIM, J. S. & LEE, D. S. (2000) Thermal properties of electrospun polyesters. *Polymer Journal,* 32**,** 616-618.

KIM, K., YU, M., ZONG, X. H., CHIU, J., FANG, D. F., SEO, Y. S., HSIAO, B. S., CHU, B. & HADJIARGYROU, M. (2003) Control of degradation rate and hydrophilicity in electrospun non-woven poly(D,L-lactide) nanofiber scaffolds for biomedical applications. *Biomaterials,* 24**,** 4977-4985.

KIM, S. S., PARK, M. S., JEON, O., CHOI, C. Y. & KIM, B. S. (2006b) Poly(lactide-co-glycolide)/hydroxyapatite composite scaffolds for bone tissue engineering. *Biomaterials,* 27**,** 1399-1409.

KISTER, G., CASSANAS, G., BERGOUNHON, M., HOARAU, D. & VERT, M. (2000) Structural characterization and hydrolytic degradation of solid copolymers of D,L-lactide-co-epsilon-caprolactone by Raman spectroscopy. *Polymer,* 41**,** 925-932.

KISTER, G., CASSANAS, G., VERT, M., PAUVERT, B. & TEROL, A. (1995) Vibrational Analysis of Poly(L-Lactic Acid). *Journal of Raman Spectroscopy,* 26**,** 307-311.

KOBAYASHI, M. & SAKASHITA, M. (1992) MORPHOLOGY DEPENDENT ANOMALOUS FREQUENCY-SHIFTS OF INFRARED-ABSORPTION BANDS OF POLYMER CRYSTALS - INTERPRETATION IN TERMS OF TRANSITION DIPOLE DIPOLE COUPLING THEORY. *Journal of Chemical Physics,* 96**,** 748-760.

KONGKHLANG, T., TASHIRO, K., KOTAKI, M. & CHIRACHANCHAI, S. (2008) Electrospinning as a New Technique To Control the Crystal Morphology and Molecular Orientation of Polyoxymethylene Nanofibers. *Journal of the American Chemical Society,* 130**,** 15460-15466.

KOSKI, A., YIM, K. & SHIVKUMAR, S. (2004) Effect of molecular weight on fibrous PVA produced by electrospinning. *Materials Letters,* 58**,** 493-497.

KOUMOULIDIS, G. C., VAIMAKIS, T. C., SDOUKOS, A. T., BOUKOS, N. K. & TRAPALIS, C. C. (2001) Preparation of hydroxyapatite lathlike particles using high-speed dispersing equipment. *Journal of the American Ceramic Society,* 84**,** 1203-1208.

KURIAKOSE, T. A., KALKURA, S. N., PALANICHAMY, M., ARIVUOLI, D., DIERKS, K., BOCELLI, G. & BETZEL, C. (2004) Synthesis of stoichiometric nano crystalline hydroxyapatite by ethanol-based sol-gel technique at low temperature. *Journal of Crystal Growth,* 263**,** 517-523.

KWON, I. K. & MATSUDA, T. (2005) Co-electrospun nanofiber fabrics of poly(L-lactide-co-epsilon-caprolactone) with type I collagen or heparin. *Biomacromolecules,* 6**,** 2096-2105.

LAKES, R. S. (2009) *Viscoelastic Materials,* Cambridge, Cambridge University Press.

LAKES, R. S. (2010) Biomechanics II: Bone viscoelasticity, bone creep, bone relaxation. http://silver.neep.wisc.edu/~lakes/Biom2.html. Accessed 15 August, 2011.

LAL, B., VIOLA, J., HICKS, D. & GRAD, O. (2003) The Emergence of Tissue Engineering as a Research Field. http://www.nsf.gov/pubs/2004/nsf0450/start.htm.

LANGER, R. & VACANTI, J. P. (1993) Tissue Engineering. *Science,* 260**,** 920-926.

LANNUTTI, J., RENEKER, D., MA, T., TOMASKO, D. & FARSON, D. F. (2007) Electrospinning for tissue engineering scaffolds. *Materials Science & Engineering C-Biomimetic and Supramolecular Systems,* 27**,** 504-509.

LAUDENSLAGER, M. J. & SIGMUND, W. M. (2011) Developments in electrohydrodynamic forming: Fabricating nanomaterials from charged liquids via electrospinning and electrospraying. *American Ceramic Society Bulletin,* 90**,** 22-27.

LAURENCIN, C. T., AMBROSIO, A. M. A., BORDEN, M. D. & COOPER, J. A. (1999) Tissue engineering: Orthopedic applications. *Annual Review of Biomedical Engineering,* 1**,** 19-46.

LEE, C. W. (2007) Production of D-lactic acid by bacterial fermentation of rice. *Fibers and Polymers,* 8**,** 571-578.

LEE, J., TAE, G., KIM, Y. H., PARK, I. S. & KIM, S. H. (2008) The effect of gelatin incorporation into electrospun poly(L-lactide-co-epsilon-caprolactone) fibers on mechanical properties and cytocompatibility. *Biomaterials,* 29**,** 1872-1879.

LEE, K. Y. & MOONEY, D. J. (2001) Hydrogels for tissue engineering. *Chemical Reviews,* 101**,** 1869-1879.

LEONG, K. F., CHEAH, C. M. & CHUA, C. K. (2003) Solid freeform fabrication of three-dimensional scaffolds for engineering replacement tissues and organs. *Biomaterials,* 24**,** 2363-2378.

LI, J. S., LI, Y., LI, L., MAK, A. F. T., KO, F. & QIN, L. (2009a) Preparation and biodegradation of electrospun PLLA/keratin nonwoven fibrous membrane. *Polymer Degradation and Stability,* 94**,** 1800-1807.

LI, M., MONDRINOS, M. J., GANDHI, M. R., KO, F. K., WEISS, A. S. & LELKES, P. I. (2005a) Electrospun protein fibers as matrices for tissue engineering. *Biomaterials,* 26**,** 5999-6008.

LI, M. Y., GUO, Y., WEI, Y., MACDIARMID, A. G. & LELKES, P. I. (2006) Electrospinning polyaniline-contained gelatin nanofibers for tissue engineering applications. *Biomaterials,* 27**,** 2705-2715.

LI, S. M. (1999) Hydrolytic degradation characteristics of aliphatic polyesters derived from lactic and glycolic acids. *Journal of Biomedical Materials Research,* 48**,** 342-353.

LI, S. M., GARREAU, H. & VERT, M. (1990) Structure Property Relationships in the Case of the Degradation of Massive Aliphatic Poly-(Alpha-Hydroxy Acids) in Aqueous-Media .1. Poly(Dl-Lactic Acid). *Journal of Materials Science-Materials in Medicine,* 1**,** 123-130.

LI, S. M. & MCCARTHY, S. (1999a) Further investigations on the hydrolytic degradation of poly(DL-lactide). *Biomaterials,* 20**,** 35-44.

LI, S. M. & MCCARTHY, S. (1999b) Influence of crystallinity and stereochemistry on the enzymatic degradation of poly(lactide)s. *Macromolecules,* 32**,** 4454-4456.

LI, X. M., LIU, X. H., DONG, W., FENG, Q. L., CUI, F. Z., UO, M., AKASAKA, T. & WATARI, F. (2009b) In Vitro Evaluation of Porous Poly(L-Lactic Acid) Scaffold Reinforced by Chitin Fibers. *Journal Of Biomedical Materials Research Part B-Applied Biomaterials,* 90B**,** 503-509.

LI, Z. S., RAMAY, H. R., HAUCH, K. D., XIAO, D. M. & ZHANG, M. Q. (2005b) Chitosan-alginate hybrid scaffolds for bone tissue engineering. *Biomaterials,* 26**,** 3919-3928.

LIANG, D., HSIAO, B. S. & CHU, B. (2007) Functional electrospun nanofibrous scaffolds for biomedical applications. *Advanced Drug Delivery Reviews,* 59**,** 1392-1412.

LIAO, S., MURUGAN, R., CHAN, C. K. & RAMAKRISHNA, S. (2008) Processing nanoengineered scaffolds through electrospinning and mineralization, suitable for biomimetic bone tissue engineering. *Journal of the Mechanical Behavior of Biomedical Materials,* 1**,** 252-260.

LIM, L. T., AURAS, R. & RUBINO, M. (2008) Processing technologies for poly(lactic acid). *Progress in Polymer Science,* 33**,** 820-852.

LIN, K., CHANG, J., CHENG, R. & RUAN, M. (2007) Hydrothermal microemulsion synthesis of stoichiometric single crystal hydroxyapatite nanorods with mono-dispersion and narrow-size distribution. *Materials Letters,* 61**,** 1683-1687.

LINEZ-BATAILLON, P., MONCHAU, F., BIGERELLE, M. & HILDEBRAND, H. F. (2002) In vitro MC3T3 osteoblast adhesion with respect to surface roughness of Ti6A14V substrates. *Biomolecular Engineering,* 19**,** 133-141.

LINH, N. T. B., MIN, Y. K., SONG, H. Y. & LEE, B. T. (2010) Fabrication of polyvinyl alcohol/gelatin nanofiber composites and evaluation of their material properties. *Journal Of Biomedical Materials Research Part B-Applied Biomaterials,* 95B**,** 184-191.

LIU, X. & MA, P. X. (2004) Polymeric scaffolds for bone tissue engineering. *Annals of Biomedical Engineering,* 32**,** 477-486.

LIU, X., SMITH, L. A., HU, J. & MA, P. X. (2009) Biomimetic nanofibrous gelatin/apatite composite scaffolds for bone tissue engineering. *Biomaterials,* 30**,** 2252-2258.

LIU, X. H., SMITH, L., WEI, G. B., WON, Y. J. & MA, P. X. (2005) Surface Engineering of Nano-Fibrous Poly(L-Lactic Acid) Scaffolds via Self-Assembly Technique for Bone Tissue Engineering. *Journal of Biomedical Nanotechnology,* 1**,** 54-60.

LOO, S. C. J., TAN, H. T., OOI, C. P. & BOEY, Y. C. F. (2006) Hydrolytic degradation of electron beam irradiated high molecular weight and non-irradiated moderate molecular weight PLLA. *Acta Biomaterialia,* 2**,** 287-296.

LOSTOCCO, M. R. & HUANG, S. J. (1998) The hydrolysis of poly(lactic acid) poly(hexamethylene succinate) blends. *Polymer Degradation and Stability,* 61**,** 225-230.

LU, Z. D., LU, M. B., HE, F. & YU, L. J. (2009) An economical approach for D-lactic acid production utilizing unpolished rice from aging paddy as major nutrient source. *Bioresource Technology,* 100**,** 2026-2031.

LUNT, J. (1998) Large-scale production, properties and commercial applications of polylactic acid polymers. *Polymer Degradation and Stability,* 59**,** 145-152.

LUO, Y., ENGELMAYR, G., AUGUSTE, D. T., DA SILVA FERREIRA, L., KARP, J. M., SAIGAL, R. & LANGER, R. (2007) Three-Dimensional Scaffolds. IN LANZA, R., LANGER, R. & VACANTI, J. (Eds.) *Principles of Tissue Engineering.* 3rd ed. Burlington, Elsevier Academic Press.

MA, P. X. (2004) Scaffolds for tissue fabrication. *Materials Today,* 7**,** 30-40.

MA, P. X., ZHANG, R. Y., XIAO, G. Z. & FRANCESCHI, R. (2001) Engineering new bone tissue in vitro on highly porous poly(alpha-hydroxyl acids)/hydroxyapatite composite scaffolds. *Journal of Biomedical Materials Research,* 54**,** 284-293.

MA, Z. W., KOTAKI, M., YONG, T., HE, W. & RAMAKRISHNA, S. (2005) Surface engineering of electrospun polyethylene terephthalate (PET) nanofibers towards development of a new material for blood vessel engineering. *Biomaterials,* 26**,** 2527-2536.

MAINILVARLET, P., RAHM, R. & GOGOLEWSKI, S. (1997) Long-term in vivo degradation and bone reaction to various polylactides .1. One-year results. *Biomaterials,* 18**,** 257-266.

MALAFAYA, P. B., SILVA, G. A. & REIS, R. L. (2007) Natural-origin polymers as carriers and scaffolds for biomolecules and cell delivery in tissue engineering applications. *Advanced Drug Delivery Reviews,* 59**,** 207-233.

MANSON, J. A. & SPERLING, L. H. (1976) *Polymer Blends and Composites,* New York, Plenum Press.

MAQUET, V., BOCCACCINI, A. R., PRAVATA, L., NOTINGHER, I. & JEROME, R. (2003) Preparation, characterization, and in vitro degradation of bioresorbable and bioactive composites based on Bioglass (R)-filled polylactide foams. *Journal of Biomedical Materials Research Part A,* 66A**,** 335-346.

MAQUET, V., BOCCACCINI, A. R., PRAVATA, L., NOTINGHER, I. & JEROME, R. (2004) Porous poly(alpha-hydroxyacid)/Bioglass (R) composite scaffolds for bone tissue

engineering. I: preparation and in vitro characterisation. *Biomaterials,* 25**,** 4185-4194.

MAQUET, V. & JEROME, R. (1997) Design of macroporous biodegradable polymer scaffolds for cell transplantation. IN LIU, D.-M. & DIXIT, V. (Eds.) *Porous Materials for Tissue Engineering.* Zurich, Transtec Publications Ltd.

MARSANO, E., FRANCIS, L. & GIUNCO, F. (2010) Polyamide 6 Nanofibrous Nonwovens via Electrospinning. *Journal of Applied Polymer Science,* 117**,** 1754-1765.

MARTINA, M. & HUTMACHER, D. W. (2007) Biodegradable polymers applied in tissue engineering research: a review. *Polymer International,* 56**,** 145-157.

MARTINEZ, E. C., IVIRICO, J. L. E., CRIADO, I. M., RIBELLES, J. L. G., PRADAS, M. M. & SANCHEZ, M. S. (2007) Effect of poly(L-lactide) surface topography on the morphology of in vitro cultured human articular chondrocytes. *Journal of Materials Science-Materials in Medicine,* 18**,** 1627-1632.

MAVIS, B., DEMIRTAS, T. T., GUMUSDERELIOGLU, M., GUNDUZ, G. & COLAK, U. (2009) Synthesis, characterization and osteoblastic activity of polycaprolactone nanofibers coated with biomimetic calcium phosphate. *Acta Biomaterialia,* 5**,** 3098-3111.

MEI, F., ZHONG, J. S., YANG, X. P., OUYANG, X. Y., ZHANG, S., HU, X. Y., MA, Q., LU, J. G., RYU, S. & DENG, X. L. (2007) Improved biological characteristics of poly(L-lactic acid) electrospun membrane by incorporation of multiwalled carbon nanotubes/hydroxyapatite nanoparticles. *Biomacromolecules,* 8**,** 3729-3735.

MENG, Z. X., WANG, Y. S., MA, C., ZHENG, W., LI, L. & ZHENG, Y. F. (2010) Electrospinning of PLGA/gelatin randomly-oriented and aligned nanofibers as potential scaffold in tissue engineering. *Materials Science & Engineering C-Materials for Biological Applications,* 30**,** 1204-1210.

MENG, Z. X., XU, X. X., ZHENG, W., ZHOU, H. M., LI, L., ZHENG, Y. F. & LOU, X. (2011) Preparation and characterization of electrospun PLGA/gelatin nanofibers as a potential drug delivery system. *Colloids and Surfaces B-Biointerfaces,* 84**,** 97-102.

MEZGHANI, K. & SPRUIELL, J. E. (1998) High speed melt spinning of poly(L-lactic acid) filaments. *Journal of Polymer Science Part B-Polymer Physics,* 36**,** 1005-1012.

MIDDLETON, J. C. & TIPTON, A. J. (2000) Synthetic biodegradable polymers as orthopedic devices. *Biomaterials,* 21**,** 2335-2346.

MIKOS, A. G., BAO, Y., CIMA, L. G., INGBER, D. E., VACANTI, J. P. & LANGER, R. (1993) Preparation of Poly(Glycolic Acid) Bonded Fiber Structures for Cell Attachment and Transplantation. *Journal of Biomedical Materials Research,* 27**,** 183-189.

MIKOS, A. G. & TEMENOFF, J. S. (2000) Formation of highly porous biodegradable scaffolds for tissue engineering. *Electronic Journal of Biotechnology.*

MIT-UPPATHAM, C., NITHITANAKUL, M. & SUPAPHOL, P. (2004) Effects of solution concentration, emitting electrode polarity, solvent type, and salt addition on electrospun polyamide-6 fibers: A preliminary report. *Macromolecular Symposia,* 216**,** 293-299.

MO, X. M., XU, C. Y., KOTAKI, M. & RAMAKRISHNA, S. (2004) Electrospun P(LLA-CL) nanofiber: a biomimetic extracellular matrix for smooth muscle cell and endothelial cell proliferation. *Biomaterials,* 25**,** 1883-1890.

MOONEY, D. J., BALDWIN, D. F., SUH, N. P., VACANTI, L. P. & LANGER, R. (1996a) Novel approach to fabricate porous sponges of poly(D,L-lactic-co-glycolic acid) without the use of organic solvents. *Biomaterials,* 17**,** 1417-1422.

MOONEY, D. T., MAZZONI, C. L., BREUER, C., MCNAMARA, K., HERN, D., VACANTI, J. P. & LANGER, R. (1996b) Stabilized polyglycolic acid fibre based tubes for tissue engineering. *Biomaterials,* 17**,** 115-124.

MOUTHUY, P.-A. (2008) Electrospinning of polymer solutions: Effect of charge density on the process and the morphology of spun fibres. *Metallurgy & Materials.* Birmingham, University of Birmingham.

MURPHY, M. B. & MIKOS, A. G. (2007) Polymer Scaffold Fabrication. IN LANZA, R., LANGER, R. & VACANTI, J. (Eds.) *Principles of Tissue Engineering.* 3rd ed. Burlington, Elsevier Academic Press.

MURPHY, W. L., DENNIS, R. G., KILENY, J. L. & MOONEY, D. J. (2002) Salt fusion: An approach to improve pore interconnectivity within tissue engineering scaffolds. *Tissue Engineering,* 8**,** 43-52.

MURUGAN, R. & RAMAKRISHNA, S. (2005) Aqueous mediated synthesis of bioresorbable nanocrystalline hydroxyapatite. *Journal of Crystal Growth,* 274**,** 209-213.

NAM, Y. S., YOON, J. J. & PARK, T. G. (2000) A novel fabrication method of macroporous biodegradable polymer scaffolds using gas foaming salt as a porogen additive. *Journal of Biomedical Materials Research,* 53**,** 1-7.

NEJATI, E., MIRZADEH, H. & ZANDI, M. (2008) Synthesis and characterization of nano-hydroxyapatite rods/poly(L-lactide acid) composite scaffolds for bone tissue engineering. *Composites Part a-Applied Science and Manufacturing,* 39**,** 1589-1596.

NGIAM, M., LIAO, S. S., PATIL, A. J., CHENG, Z. Y., CHAN, C. K. & RAMAKRISHNA, S. (2009) The fabrication of nano-hydroxyapatite on PLGA and PLGA/collagen nanofibrous composite scaffolds and their effects in osteoblastic behavior for bone tissue engineering. *Bone,* 45**,** 4-16.

OLABISI, O., ROBESON, L. M. & SHAW, M. T. (1979) *Polymer-Polymer Miscibility,* New York, Academic Press, Inc.

OLIVIER, V., FAUCHEUX, N. & HARDOUIN, P. (2004) Biomaterial challenges and approaches to stem cell use in bone reconstructive surgery. *Drug Discovery Today,* 9**,** 803-811.

ORLOVSKII, V. P., KOMLEV, V. S. & BARINOV, S. M. (2002) Hydroxyapatite and hydroxyapatite-based ceramics. *Inorganic Materials,* 38**,** 973-984.

OTA, Y., IWASHITA, T., KASUGA, T. & ABE, Y. (1998) Novel preparation method of hydroxyapatite fibers. *Journal of the American Ceramic Society,* 81**,** 1665-1668.

PACHENCE, J. M., BOHRER, M. P. & KOHN, J. (2007) Biodegradable Polymers. IN LANZA, R., LANGER, R. & VACANTI, J. (Eds.) *Principles of Tissue Engineering.* 3rd ed. Burlington, Elsevier Academic Press.

PARK, J. B. & LAKES, R. S. (1992) *Biomaterials: An Introduction,* New York, Plenum Press.

PARK, K., JU, Y. M., SON, J. S., AHN, K. D. & HAN, D. K. (2007) Surface modification of biodegradable electrospun nanofiber scaffolds and their interaction with fibroblasts. *Journal of Biomaterials Science-Polymer Edition,* 18**,** 369-382.

PATLOLLA, A., COLLINS, G. & ARINZEH, T. L. (2010) Solvent-dependent properties of electrospun fibrous composites for bone tissue regeneration. *Acta Biomaterialia,* 6**,** 90-101.

PENG, F., YU, X. H. & WEI, M. (2011) In vitro cell performance on hydroxyapatite particles/poly(L-lactic acid) nanofibrous scaffolds with an excellent particle along nanofiber orientation. *Acta Biomaterialia,* 7**,** 2585-2592.

PETREACA, M. & MARTINS-GREEN, M. (2007) The Dynamics of Cell-ECM Interactions. IN LANZA, R., LANGER, R. & VACANTI, J. (Eds.) *Principles of Tissue Engineering.* 3rd ed. Burlington, Elsevier Academic Press.

PIEKARSK, K. (1973) Analysis of Bone as a Composite-Material. *International Journal of Engineering Science,* 11**,** 557-558.

PITT, C. G., GRATZL, M. M., KIMMEL, G. L., SURLES, J. & SCHINDLER, A. (1981) Aliphatic Polyesters .2. The Degradation of Poly(Dl-Lactide), Poly(Epsilon-Caprolactone), and Their Copolymers Invivo. *Biomaterials,* 2**,** 215-220.

PRABHAKARAN, M. P., VENUGOPAL, J. & RAMAKRISHNA, S. (2009) Electrospun nanostructured scaffolds for bone tissue engineering. *Acta Biomater,* 5**,** 2884-93.

PRAMANIK, N., TARAFDAR, A. & PRAMANIK, P. (2007) Capping agent-assisted synthesis of nanosized hydroxyapatite: Comparative studies of their physicochemical properties. *Journal of Materials Processing Technology,* 184**,** 131-138.

PRILUTSKY, S., ZUSSMAN, E. & COHEN, Y. (2008) The effect of embedded carbon nanotubes on the morphological evolution during the carbonization of poly(acrylonitrile) nanofibers. *Nanotechnology,* 19.

PUPPI, D., CHIELLINI, F., PIRAS, A. M. & CHIELLINI, E. (2010) Polymeric materials for bone and cartilage repair. *Progress in Polymer Science,* 35**,** 403-440.

RAGHUVANSHI, R. S., SINGH, M. & TALWAR, G. P. (1993) Biodegradable Delivery System for Single-Step Immunization with Tetanus Toxoid. *International Journal of Pharmaceutics,* 93**,** R1-R5.

RAMAKRISHNA, S., FUJIHARA, K., TEO, W., LIM, T. & MA, Z. (2005) *An Introduction to Electrospinning and Nanofibres,* Singapore, World Scientific Publishing Co. Ltd.

RAMAKRISHNA, S., FUJIHARA, K., TEO, W. E., YONG, T., MA, Z. W. & RAMASESHAN, R. (2006) Electrospun nanofibers: solving global issues. *Materials Today,* 9**,** 40-50.

RAMAKRISHNA, S., JOSE, R., ARCHANA, P. S., NAIR, A. S., BALAMURUGAN, R., VENUGOPAL, J. & TEO, W. E. (2010) Science and engineering of electrospun nanofibers for advances

in clean energy, water filtration, and regenerative medicine. *Journal of Materials Science,* 45**,** 6283-6312.

RAMDHANIE, L. I., AUBUCHON, S. R., BOLAND, E. D., KNAPP, D. C., BARNES, C. P., SIMPSON, D. G., WNEK, G. E. & BOWLIN, G. L. (2006) Thermal and mechanical characterization of electrospun blends of poly(lactic acid) and poly(glycolic acid). *Polymer Journal,* 38**,** 1137-1145.

RASAL, R. M., JANORKAR, A. V. & HIRT, D. E. (2010) Poly(lactic acid) modifications. *Progress in Polymer Science,* 35**,** 338-356.

REED, A. M. & GILDING, D. K. (1981) Biodegradable Polymers for Use in Surgery Em Dash Poly(Glycolic)/Poly(Lactic Acid) Homo and Copolymers Em Dash 2. In Vitro Degradation. *Polymer,* 22**,** 494-498.

RENEKER, D. H. & CHUN, I. (1996a) Nanometre diameter fibres of polymer, produced by electrospinning. *Nanotechnology,* 7**,** 216-223.

RENEKER, D. H., YARIN, A. L., FONG, H. & KOOMBHONGSE, S. (2000) Bending instability of electrically charged liquid jets of polymer solutions in electrospinning. *Journal of Applied Physics,* 87**,** 4531-4547.

RENEKER, H. D. & CHUN, I. (1996b) Nanometre diameter fibres of polymer, produced by electrospinning. *Nanotechnology,* 7**,** 216.

REZWAN, K., CHEN, Q. Z., BLAKER, J. J. & BOCCACCINI, A. R. (2006) Biodegradable and bioactive porous polymer/inorganic composite scaffolds for bone tissue engineering. *Biomaterials,* 27**,** 3413-3431.

RHO, J. Y., KUHN-SPEARING, L. & ZIOUPOS, P. (1998) Mechanical properties and the hierarchical structure of bone. *Medical Engineering & Physics,* 20**,** 92-102.

SANDERS, J. E., LAMONT, S. E., MITCHELL, S. B. & MALCOLM, S. G. (2005) Small fiber diameter fibro-porous meshes: Tissue response sensitivity to fiber spacing. *Journal of Biomedical Materials Research Part A,* 72A**,** 335-342.

SARAF, A., LOZIER, G., HAESSLEIN, A., KASPER, F. K., RAPHAEL, R. M., BAGGETT, L. S. & MIKOS, A. G. (2009) Fabrication of Nonwoven Coaxial Fiber Meshes by Electrospinning. *Tissue Engineering Part C-Methods,* 15**,** 333-344.

SATO, T., CHEN, G. P., USHIDA, T., ISHII, T., OCHIAI, N., TATEISHI, T. & TANAKA, J. (2004) Evaluation of PLLA-collagen hybrid sponge as a scaffold for cartilage tissue engineering. *Materials Science & Engineering C-Biomimetic and Supramolecular Systems,* 24**,** 365-372.

SCHOFER, M. D., BOUDRIOT, U., LEIFELD, I., SUTTERLIN, R. I., RUDISILE, M., WENDORFF, J. H., GREINER, A., PALETTA, J. R. J. & FUCHS-WINKELMANN, S. (2009) Characterization of a PLLA-Collagen I Blend Nanofiber Scaffold with Respect to Growth and Osteogenic Differentiation of Human Mesenchymal Stem Cells. *Thescientificworldjournal,* 9**,** 118-129.

SHASTRI, V. P., MARTIN, I. & LANGER, R. (2000) Macroporous polymer foams by hydrocarbon templating. *Proceedings of the National Academy of Sciences of the United States of America,* 97**,** 1970-1975.

SHEA, L. D., WANG, D., FRANCESCHI, R. T. & MOONEY, D. J. (2000) Engineered bone development from a pre-osteoblast cell line on three-dimensional scaffolds. *Tissue Engineering,* 6**,** 605-617.

SHENOY, S. L., BATES, W. D., FRISCH, H. L. & WNEK, G. E. (2005) Role of chain entanglements on fiber formation during electrospinning of polymer solutions: good solvent, non-specific polymer-polymer interaction limit. *Polymer,* 46**,** 3372-84.

SHIN, Y. M., HOHMAN, M. M., BRENNER, M. P. & RUTLEDGE, G. C. (2001) Electrospinning: A whipping fluid jet generates submicron polymer fibers. *Applied Physics Letters,* 78**,** 1149-1151.

SICHINA, W. J. (2000) DSC as Problem Solving Tool: Measurement of Percent Crystallinity of Thermoplastics. http://www.perkinelmer.com/Content/applicationnotes/app_thermalcrystallinitythermoplastics.pdf. Accessed 18 July, 2011.

SIDDHARTHAN, A., SESHADRI, S. K. & KUMAR, T. S. S. (2004) Microwave accelerated synthesis of nanosized calcium deficient hydroxyapatite. *Journal of Materials Science-Materials in Medicine,* 15**,** 1279-1284.

SILL, T. J. & VON RECUM, H. A. (2008) Electro spinning: Applications in drug delivery and tissue engineering. *Biomaterials,* 29**,** 1989-2006.

SILVA, S. S., MANO, J. F. & REIS, R. L. (2010) Potential applications of natural origin polymer-based systems in soft tissue regeneration. *Critical Reviews in Biotechnology,* 30**,** 200-221.

SILVESTRE, C. & CIMMINO, S. (2003) Crystallisation, Morphology and Melting in Polymer Blends. IN KULSHRESHTHA, A. K. & VASILE, C. (Eds.) *Handbook of Polymer Blends and Composites.* Shawbury, United Kingdom, Rapra Technology Limited.

SIMSKE, S. J., AYERS, R. A. & BATEMAN, T. A. (1997) Porous materials for bone engineering. *Porous Materials for Tissue Engineering.* Zurich-Uetikon, Transtec Publications Ltd.

SISSON, K., ZHANG, C., FARACH-CARSON, M. C., CHASE, D. B. & RABOLT, J. F. (2010) Fiber diameters control osteoblastic cell migration and differentiation in electrospun gelatin. *Journal of Biomedical Materials Research Part A,* 94A**,** 1312-1320.

SMITH, L. A. & MA, P. X. (2004) Nano-fibrous scaffolds for tissue engineering. *Colloids and Surfaces B: Biointerfaces,* 39**,** 125-131.

SONGCHOTIKUNPAN, P., TATTIYAKUL, J. & SUPAPHOL, P. (2008) Extraction and electrospinning of gelatin from fish skin. *International Journal of Biological Macromolecules,* 42**,** 247-255.

ST. PIERRE, T. & CHIELLINI, E. (1986) Biodegradability of Synthetic Polymers Used for Medical and Pharmaceutical Applications: Part 1 - Principles of Hydrolysis Mechanisms. *Journal of Bioactive and Compatible Polymers,* 1.

STEPHENS, J. S., CHASE, D. B. & RABOLT, J. F. (2004) Effect of the electrospinning process on polymer crystallization chain conformation in nylon-6 and nylon-12. *Macromolecules,* 37**,** 877-881.

SU, Y., LI, X. Q., LIU, S. P., WANG, H. S. & HE, C. L. (2010) Fabrication and Properties of PLLA-Gelatin Nanofibers by Electrospinning. *Journal of Applied Polymer Science,* 117**,** 542-547.

SUI, G., YANG, X. P., MEI, F., HU, X. Y., CHEN, G. Q., DENG, X. L. & RYU, S. (2007) Poly-L-lactic acid/hydroxyapatite hybrid membrane for bone tissue regeneration. *Journal of Biomedical Materials Research Part A,* 82A**,** 445-454.

SUKIGARA, S., GANDHI, M., AYUTSEDE, J., MICKLUS, M. & KO, F. (2003) Regeneration of Bombyx mori silk by electrospinning - part 1: processing parameters and geometric properties. *Polymer,* 44**,** 5721-5727.

SUN, Z. C., ZUSSMAN, E., YARIN, A. L., WENDORFF, J. H. & GREINER, A. (2003) Compound core-shell polymer nanofibers by co-electrospinning. *Advanced Materials,* 15**,** 1929-+.

SUPOVA, M. (2009) Problem of hydroxyapatite dispersion in polymer matrices: a review. *J Mater Sci Mater Med,* 20**,** 1201-13.

SWETHA, M., SAHITHI, K., MOORTHI, A., SRINIVASAN, N., RAMASAMY, K. & SELVAMURUGAN, N. (2010) Biocomposites containing natural polymers and hydroxyapatite for bone tissue engineering. *International Journal of Biological Macromolecules,* 47**,** 1-4.

TABATA, Y. & IKADA, Y. (1998) Protein release from gelatin matrices. *Advanced Drug Delivery Reviews,* 31**,** 287-301.

TAKAHASHI, T., TANASE, S. & YAMAMOTO, O. (1978) Electrical-Conductivity of Some Hydroxyapatites. *Electrochimica Acta,* 23**,** 369-373.

TAMADA, J. A. & LANGER, R. (1993) Erosion Kinetics of Hydrolytically Degradable Polymers. *Proceedings of the National Academy of Sciences of the United States of America,* 90**,** 552-556.

TAN, H. Y., WIDJAJA, E., BOEY, F. & LOO, S. C. J. (2009) Spectroscopy Techniques for Analyzing the Hydrolysis of PLGA and PLLA. *Journal Of Biomedical Materials Research Part B-Applied Biomaterials,* 91B**,** 433-440.

TAN, S. H., INAI, R., KOTAKI, M. & RAMAKRISHNA, S. (2005) Systematic parameter study for ultra-fine fiber fabrication via electrospinning process. *Polymer,* 46**,** 6128-6134.

TAS, A. C. (2000) Synthesis of biomimetic Ca-hydroxyapatite powders at 37 degrees C in synthetic body fluids. *Biomaterials,* 21**,** 1429-1438.

TEO, W. E. & RAMAKRISHNA, S. (2006) A review on electrospinning design and nanofibre assemblies. *Nanotechnology,* 17**,** R89-R106.

THAPA, A., WEBSTER, T. J. & HABERSTROH, K. M. (2003) Polymers with nano-dimensional surface features enhance bladder smooth muscle cell adhesion. *Journal of Biomedical Materials Research Part A,* 67A**,** 1374-1383.

THERIN, M., CHRISTEL, P., LI, S. M., GARREAU, H. & VERT, M. (1992) Invivo Degradation of Massive Poly(Alpha-Hydroxy Acids) - Validation of Invitro Findings. *Biomaterials,* 13**,** 594-600.

THERON, S. A., ZUSSMAN, E. & YARIN, A. L. (2004) Experimental investigation of the governing parameters in the electrospinning of polymer solutions. *Polymer,* 45**,** 2017-2030.

THOMAS, V., JAGANI, S., JOHNSON, K., JOSE, M. V., DEAN, D. R., VOHRA, Y. K. & NYAIRO, E. (2006) Electrospun bioactive nanocomposite scaffolds of polycaprolactone and nanohydroxyapatite for bone tissue engineering. *Journal of Nanoscience and Nanotechnology,* 6**,** 487-493.

THOMSON, R. C., WAKE, M. C., YASZEMSKI, M. J. & MIKOS, A. G. (1995) Biodegradable polymer scaffolds to regenerate organs. IN PEPPAS, N. A. & LANGER, R. S. (Eds.) *Biopolymers II.* Berlin, Springer-Verlag GmbH & Company KG.

THOMSON, R. C., YASZEMSKI, M. J., POWERS, J. M. & MIKOS, A. G. (1998) Hydroxyapatite fiber reinforced poly([alpha]-hydroxy ester) foams for bone regeneration. *Biomaterials,* 19**,** 1935-1943.

TONG, H. W. & WANG, M. (2011) An Investigation into the Influence of Electrospinning Parameters on the Diameter and Alignment of Poly(hydroxybutyrate-co-hydroxyvalerate) Fibers. *Journal of Applied Polymer Science,* 120**,** 1694-1706.

TSIOPTSIAS, C. & PANAYIOTOU, C. (2008) Preparation of cellulose-nanohydroxyapatite composite scaffolds from ionic liquid solutions. *Carbohydrate Polymers,* 74**,** 99-105.

TURCO, G., MARSICH, E., BELLOMO, F., SEMERARO, S., DONATI, I., BRUN, F., GRANDOLFO, M., ACCARDO, A. & PAOLETTI, S. (2009) Alginate/Hydroxyapatite Biocomposite For Bone Ingrowth: A Trabecular Structure With High And Isotropic Connectivity. *Biomacromolecules,* 10**,** 1575-1583.

UYAR, T. & BESENBACHER, F. (2008) Electrospinning of uniform polystyrene fibers: The effect of solvent conductivity. *Polymer,* 49**,** 5336-5343.

VACANTI, J. & VACANTI, C. A. (2007) The History and Scope of Tissue Engineering. IN LANZA, R., LANGER, R. & VACANTI, J. (Eds.) *Principles of Tissue Engineering.* 3rd ed. Burlington, Elsevier Academic Press.

VAN DIJKHUIZEN-RADERSMA, R., MORONI, L., VAN APELDOORN, A., ZHANG, Z. & GRIJPMA, D. (2008) Degradable polymers for tissue engineering. IN VAN BLITTERSWIJK, C., THOMSEN, P., LINDAHL, A., HUBBELL, J., WILLIAMS, D. F., CANCEDDA, R., DE BRUIJN, J. D. & SOHIER, J. (Eds.) *Tissue Engineering.* Amsterdam, Elsevier Inc.

VAN GAALEN, S., KRUYT, M., MEIJER, G., MISTRY, A., MIKOS, A., VAN DEN BEUCKEN, J., JANSEN, J., DE GROOT, K., CANCEDDA, R., OLIVO, C., YASZEMSKI, M. & DHERT, W. (2008) Tissue Engineering of bone. IN VAN BLITTERSWIJK, C., THOMSEN, P., LINDAHL, A., HUBBELL, J., WILLIAMS, D. F., CANCEDDA, R., DE BRUIJN, J. D. & SOHIER, J. (Eds.) *Tissue Engineering.* Amsterdam, Elsevier Inc.

VENUGOPAL, J., LOW, S., CHOON, A. T., KUMAR, A. B. & RAMAKRISHNA, S. (2008a) Electrospun-modified nanofibrous scaffolds for the mineralization of osteoblast cells. *Journal of Biomedical Materials Research Part A,* 85A**,** 408-417.

VENUGOPAL, J., LOW, S., CHOON, A. T., KUMAR, T. S. S. & RAMAKRISHNA, S. (2008b) Mineralization of osteoblasts with electrospun collagen/hydroxyapatite nanofibers. *Journal of Materials Science-Materials in Medicine,* 19**,** 2039-2046.

VENUGOPAL, J., PRABHAKARAN, M. P., LOW, S., CHOON, A. T., ZHANG, Y. Z., DEEPIKA, G. & RAMAKRISHNA, S. (2008c) Nanotechnology for nanomedicine and delivery of drugs. *Current Pharmaceutical Design,* 14**,** 2184-2200.

VENUGOPAL, J., PRABHAKARAN, M. P., ZHANG, Y. Z., LOW, S., CHOON, A. T. & RAMAKRISHNA, S. (2010) Biomimetic hydroxyapatite-containing composite nanofibrous substrates for bone tissue engineering. *Philosophical Transactions of the Royal Society a-Mathematical Physical and Engineering Sciences,* 368**,** 2065-2081.

VENUGOPAL, J., VADGAMA, P., KUMAR, T. S. S. & RAMAKRISHNA, S. (2007) Biocomposite nanofibres and osteoblasts for bone tissue engineering. *Nanotechnology,* 18.

VENUGOPAL, J. R., LOW, S., CHOON, A. T., KUMAR, A. B. & RAMAKRISHNA, S. (2008d) Nanobioengineered electrospun composite nanofibers and osteoblasts for bone regeneration. *Artificial Organs,* 32**,** 388-397.

VERT, M. (2005) Aliphatic polyesters: Great degradable polymers that cannot do everything. *Biomacromolecules,* 6**,** 538-546.

VERT, M., MAUDUIT, J. & LI, S. M. (1994) Biodegradation of Pla/Ga Polymers - Increasing Complexity. *Biomaterials,* 15**,** 1209-1213.

VOLPATO, F. Z., RAMOS, S. L. F., MOTTA, A. & MIGLIARESI, C. (2011) Physical and in vitro biological evaluation of a PA 6/MWCNT electrospun composite for biomedical applications. *Journal of Bioactive and Compatible Polymers,* 26**,** 35-47.

WANG, X. J., SONG, G. J. & LOU, T. (2010) Fabrication and characterization of nano composite scaffold of poly(l-lactic acid)/hydroxyapatite. *Journal of Materials Science-Materials in Medicine,* 21**,** 183-188.

WEI, G. & MA, P. X. (2004) Structure and properties of nano-hydroxyapatite/polymer composite scaffolds for bone tissue engineering. *Biomaterials,* 25**,** 4749-4757.

WEI, K., LI, Y., KIM, K. O., NAKAGAWA, Y., KIM, B. S., ABE, K., CHEN, G. Q. & KIM, I. S. (2011) Fabrication of nano-hydroxyapatite on electrospun silk fibroin nanofiber and their effects in osteoblastic behavior. *Journal of Biomedical Materials Research Part A,* 97A**,** 272-280.

WHELAN, T. (1994) *Polymer Technology Dictionary,* London, Chapman & Hall.

WONG, S. C., BAJI, A. & LENG, S. W. (2008) Effect of fiber diameter on tensile properties of electrospun poly(epsilon-caprolactone). *Polymer,* 49**,** 4713-4722.

WOZNIAK, P. & JEL HAJ, A. (2007) Bone Regeneration and Repair using Tissue Engineering. IN BOCCACCINI, A. R. & GOUGH, J. E. (Eds.) *Tissue Engineering using Ceramics and Polymers.* Cambridge, Woodhead Publishing Limited.

WUNDERLICH, B. (2005) *Thermal Analysis of Polymeric Materials,* Berlin, Springer.

XINSONG, L., CHEN, Y., FUQIAN, S., TANGYING, S., YUNHUI, L. & YUEPU, P. (2008) Conjugate electrospinning of continuous nanofiber yarn of poly(L-lactide)/nanotricalcium phosphate nanocomposite. *Journal of Applied Polymer Science,* 107**,** 3756-64.

XU, C. Y., YANG, F., WANG, S. & RAMAKRISHNA, S. (2004) In vitro study of human vascular endothelial cell function on materials with various surface roughness. *Journal of Biomedical Materials Research Part A,* 71A**,** 154-161.

XU, X., CHEN, X., LIU, A., HONG, Z. & JING, X. (2007) Electrospun poly(L-lactide)-grafted hydroxyapatite/poly(L-lactide) nanocomposite fibers. *European Polymer Journal,* 43**,** 3187-3196.

YAMASHITA, J., LI, X., FURMAN, B. R., RAWLS, H. R., WANG, X. & AGRAWAL, C. M. (2002) Collagen and bone viscoelasticity: A dynamic mechanical analysis. *Journal of Biomedical Materials Research,* 63**,** 31-36.

YANG, F., MURUGAN, R., WANG, S. & RAMAKRISHNA, S. (2005) Electrospinning of nano/micro scale poly(L-lactic acid) aligned fibers and their potential in neural tissue engineering. *Biomaterials,* 26**,** 2603-2610.

YANG, F., WOLKE, J. G. C. & JANSEN, J. A. (2008) Biomimetic calcium phosphate coating on electrospun poly(epsilon-caprolactone) scaffolds for bone tissue engineering. *Chemical Engineering Journal,* 137**,** 154-161.

YANG, J., WAN, Y. Q., TU, C. F., CAI, Q., BEI, J. Z. & WANG, S. G. (2003) Enhancing the cell affinity of macroporous poly(L-lactide) cell scaffold by a convenient surface modification method. *Polymer International,* 52**,** 1892-1899.

YEE, W. A., NGUYEN, A. C., LEE, P. S., KOTAKI, M., LIU, Y., TAN, B. T., MHAISALKAR, S. & LU, X. (2008) Stress-induced structural changes in electrospun polyvinylidene difluoride nanofibers collected using a modified rotating disk. *Polymer,* 49**,** 4196-4203.

YEONG, K. C. B., WANG, J. & NG, S. C. (2001) Mechanochemical synthesis of nanocrystalline hydroxyapatite from CaO and CaHPO4. *Biomaterials,* 22**,** 2705-2712.

YOSHIMOTO, H., SHIN, Y. M., TERAI, H. & VACANTI, J. P. (2003) A biodegradable nanofiber scaffold by electrospinning and its potential for bone tissue engineering. *Biomaterials,* 24**,** 2077-2082.

YOU, Y., MIN, B. M., LEE, S. J., LEE, T. S. & PARK, W. H. (2005) In vitro degradation behavior of electrospun polyglycolide, polylactide, and poly(lactide-co-glycolide). *Journal of Applied Polymer Science,* 95**,** 193-200.

YOU, Y., YOUK, J. H., LEE, S. W., MIN, B. M., LEE, S. J. & PARK, W. H. (2006) Preparation of porous ultrafine PGA fibers via selective dissolution of electrospun PGA/PLA blend fibers. *Materials Letters,* 60**,** 757-760.

YOUNG, R. J. (1981) *Introduction to Polymers,* New York, Chapman and Hall.

YU, J. H., FRIDRIKH, S. V. & RUTLEDGE, G. C. (2004) Production of submicrometer diameter fibers by two-fluid electrospinning. *Advanced Materials,* 16**,** 1562-+.

ZABOROWSKA, M., BODIN, A., BACKDAHL, H., POPP, J., GOLDSTEIN, A. & GATENHOLM, P. (2010) Microporous bacterial cellulose as a potential scaffold for bone regeneration. *Acta Biomaterialia,* 6**,** 2540-2547.

ZENG, J., CHEN, X. S., LIANG, Q. Z., XU, X. L. & JING, X. B. (2004) Enzymatic degradation of poly(L-lactide) and poly (epsilon-caprolactone) electrospun fibers. *Macromolecular Bioscience,* 4**,** 1118-1125.

ZHANG, N., NICHOLS, H. L., TYLOR, S. & WEN, X. (2007a) Fabrication of nanocrystalline hydroxyapatite doped degradable composite hollow fiber for guided and biomimetic bone tissue engineering. *Materials Science & Engineering C-Biomimetic and Supramolecular Systems,* 27**,** 599-606.

ZHANG, N., NICHOLS, H. L., TYLOR, S. & WEN, X. J. (2007b) Fabrication of nanocrystalline hydroxyapatite doped degradable composite hollow fiber for guided and biomimetic bone tissue engineering. *Materials Science & Engineering C-Biomimetic and Supramolecular Systems,* 27**,** 599-606.

ZHANG, R. & MA, P. X. (1999a) Porous poly(L-lactic acid)/apatite composites created by biomimetic process. *Journal of Biomedical Materials Research,* 45**,** 285-293.

ZHANG, R. Y. & MA, P. X. (1999b) Poly(alpha-hydroxyl acids) hydroxyapatite porous composites for bone-tissue engineering. I. Preparation and morphology. *Journal of Biomedical Materials Research,* 44**,** 446-455.

ZHANG, S. (2003) Fabrication of novel biomaterials through molecular self-assembly. *Nature Biotechnology,* 21**,** 1171-1178.

ZHANG, S. & GONSALVES, K. E. (1997) Preparation and characterization of thermally stable nanohydroxyapatite. *Journal of Materials Science-Materials in Medicine,* 8**,** 25-28.

ZHANG, Y., VENUGOPAL, J. R., EL-TURKI, A., RAMAKRISHNA, S., SU, B. & LIM, C. T. (2008) Electrospun biomimetic nanocomposite nanofibers of hydroxyapatite/chitosan for bone tissue engineering. *Biomaterials,* 29**,** 4314-4322.

ZHANG, Y. Z. & LIM, C. T. (2008) The Development of Biocomposite Nanofibres for Tissue Scaffolding Applications. *JOM Journal of The Minerals, Metals and Materials Society,* 60**,** 45-48.

ZHANG, Y. Z., OUYANG, H. W., LIM, C. T., RAMAKRISHNA, S. & HUANG, Z. M. (2005) Electrospinning of gelatin fibers and gelatin/PCL composite fibrous scaffolds. *Journal Of Biomedical Materials Research Part B-Applied Biomaterials,* 72B**,** 156-165.

ZHANG, Y. Z., SU, B., VENUGOPAL, J., RAMAKRISHNA, S. & LIM, C. T. (2007c) Biomimetic and bioactive nanofibrous scaffolds from electrospun composite nanofibers. *International Journal of Nanomedicine,* 2**,** 623-638.

ZHANG, Y. Z., VENUGOPAL, J., HUANG, Z. M., LIM, C. T. & RAMAKRISHNA, S. (2006) Crosslinking of the electrospun gelatin nanofibers. *Polymer,* 47**,** 2911-2917.

ZHAO, S., WU, X., WANG, L. & HUANG, Y. (2004) Electrospinning of ethyl-cyanoethyl cellulose/tetrahydrofuran solutions. *Journal of Applied Polymer Science,* 91**,** 242-246.

ZHOU, H., GREEN, T. B. & JOO, Y. L. (2006) The thermal effects on electrospinning of polylactic acid melts. *Polymer,* 47**,** 7497-7505.

ZONG, X. H., KIM, K., FANG, D. F., RAN, S. F., HSIAO, B. S. & CHU, B. (2002) Structure and process relationship of electrospun bioabsorbable nanofiber membranes. *Polymer,* 43**,** 4403-4412.

ZONG, X. H., RAN, S. F., KIM, K. S., FANG, D. F., HSIAO, B. S. & CHU, B. (2003) Structure and morphology changes during in vitro degradation of electrospun poly(glycolide-co-lactide) nanofiber membrane. *Biomacromolecules,* 4**,** 416-423.

ZONG, X. H., WANG, Z. G., HSIAO, B. S., CHU, B., ZHOU, J. J., JAMIOLKOWSKI, D. D., MUSE, E. & DORMIER, E. (1999) Structure and morphology changes in absorbable poly(glycolide) and poly(glycolide-co-lactide) during in vitro degradation. *Macromolecules,* 32**,** 8107-8114.